General Distribution
OCDE/GD(96)19
GRS - 120
FZKA 5711

NEA/CSNI/R(95)20

International Standard Problem ISP36

CORA-W2 EXPERIMENT ON SEVERE FUEL DAMAGE FOR A RUSSIAN TYPE PWR

COMPARISON REPORT

COMMITTEE ON THE SAFETY OF NUCLEAR INSTALLATIONS
OECD NUCLEAR ENERGY AGENCY
Le Seine Saint-Germain – 12, boulevard des Îles
F-92130 Issy-les-Moulineaux (France)
Tel. (33-1) 45 24 82 00 Fax (33-1) 45 24 11 10

Gesellschaft für Anlagen-
und Reaktorsicherheit
(GRS) mbH

OECD/NEA-CSNI International Standard Problem ISP36

CORA-W2 Experiment on Severe Fuel Damage for a Russian Type PWR

Comparison Report

M. Firnhaber[1)]
S. Yegorova[2)]
U. Brockmeier[3)]
S. Hagen[4)]
P. Hofmann[4)]
K. Trambauer[1)]

1) Gesellschaft für Anlagen- und Reaktorsicherheit, Köln und München, Germany
2) Nuclear Safety Institute of Russian Research Center "Kurchatov-Institute", Mo scow, Russia
3) University of Bochum, Bo chum, Germany
4) Forschungszentrum Karlsru he, Karlsruhe, Germany

February 1996

GRS - 120
FZKA 5711
OCDE/GD(96)19
ISBN 3-923875-81-9

This report is a reproduction of OECD/NEA-CSNI-report No. OCDE/GD(96)19

Deskriptors:

Pressurized Water Reactor, International Standard Problem ISP36, CORA-VVER Severe Fuel Damage, Core Degradation, Melt Relocation, Zirconium Oxidation, Hydrogen Generation, Uranium Dioxide, Liquefaction, Material Interaction

ORGANISATION FOR ECONOMIC CO-OPERATION AND DEVELOPMENT

Pursuant to Article 1 of the Convention signed in Paris on 14th December 1960, and which came into force on 30th September 1961, the Organisation for Economic Co-operation and Development (OECD) shall promote policies designed:

- to achieve the highest sustainable economic growth and employment and a rising standard of living in Member countries, while maintaining financial stability, and thus to contribute to the development of the world economy;
- to contribute to sound economic expansion in Member as well as non-member countries in the process of economic development; and
- to contribute to the expansion of world trade on a multilateral, non-discriminatory basis in accordance with international obligations.

The original Member countries of the OECD are Austria, Belgium,Canada, Denmark, France, Germany, Greece, Iceland, Ireland, Italy, Luxembourg, the Netherlands, Norway, Portugal, Spain, Sweden, Switzerland, Turkey, the United Kingdom and the United States. The following countries became Members subsequently through accession at the dates indicated hereafter: Japan (28th April 1964), Finland (28th January 1969), Australia (7th June 1971), New Zealand (29th May 1973), Mexico (18th May 1994) and the Czech Republic (21st December 1995). The Commission of the European Communities takes part in the work of the OECD (Article 13 of the OECD Convention).

NUCLEAR ENERGY AGENCY

The OECD Nuclear Energy Agency (NEA) was established on 1st February 1958 under the name of the OEEC European Nuclear Energy Agency. It received its present designation on 20th April 1972, when Japan became its first non-European full Member. NEA membership today consists of all European Member countries of OECD as well as Australia, Canada, Japan, Republic of Korea, Mexico and the United States. The Commission of the European Communities takes part in the work of the Agency.

The primary objective of NEA is to promote co-operation among the governments of its participating countries in furthering the development of nuclear power as a safe, environmentally acceptable and economic energy source.

This is achieved by:

- *encouraging harmonization of national regulatory policies and practices, with particular reference to the safety of nuclear installations, protection of man against ionising radiation and preservation of the environment, radioactive waste management, and nuclear third party liability and insurance;*
- *assessing the contribution of nuclear power to the overall energy supply by keeping under review the technical and economic aspects of nuclear power growth and forecasting demand and supply for the different phases of the nuclear fuel cycle;*
- *developing exchanges of scientific and technical information particularly through participation in common services;*
- *setting up international research and development programmes and joint undertakings.*

In these and related tasks, NEA works in close collaboration with the International Atomic Energy Agency in Vienna, with which it has concluded a Co-operation Agreement, as well as with other international organisations in the nuclear field.

COMMITTEE ON THE SAFETY OF NUCLEAR INSTALLATIONS

The Committee on the Safety of Nuclear Installations (CSNI) of the OECD Nuclear Energy Agency (NEA), is an international committee made up of senior scientists and engineers. It was set up in 1973 to develop and coordinate the activities of the Nuclear Energy Agency concerning the technical aspects of the design, construction and operation of nuclear installations insofar as they affect the safety of such installations. The Committee's purpose is to foster international cooperation in nuclear safety among the OECD Member countries.

The CSNI constitutes a forum for the exchange of technical information and for collaboration between organisations which can contribute, from their respective backgrounds in research, development, engineering or regulation, to these activities and to the definition of its programme of work. It also reviews the state of knowledge on selected topics of nuclear safety technology and safety assessment, including operating experience. It initiates and conducts programmes identified by these reviews and assessments in order to overcome discrepancies, develop improvements and reach international consensus on technical issues of common interest. It promotes the coordination of work in different Member countries including the establishment of cooperative research projects and assists in the feedback of the results to participating organisations. Full use is also made of traditional methods of cooperation, such as information exchanges, establishment of working groups, and organisation of conferences and specialist meetings.

The greater part of the CSNI's current programme of work is concerned with safety technology of water reactors. The principal areas covered are operating experience and the human factor, reactor coolant system behaviour, various aspects of reactor component integrity, the phenomenology of radioactive releases in reactor accidents and their confinement, containment performance, risk assessment, and severe accidents. The Committee also studies the safety of the nuclear fuel cycle, conducts periodic surveys of the reactor safety research programmes and operates an international mechanism for exchanging reports on safety related nuclear power plant accidents.

In implementing its programme, the CSNI establishes cooperative mechanisms with NEA's Committee of Nuclear Regulatory Activities (CNRA), responsible for the activities of the Agency concerning the regulation, licensing and inspection of nuclear installations with regard to safety. It also cooperates with NEA's Committee on Radiation Protection and Public Health and NEA's Radioactive Waste Management Committee on matters of common interest.

* * * * * * * * * * *

Requests for additional copies of this report should be addressed to:

Nuclear Safety Division
OECD Nuclear Energy Agency
12 Boulevard des Iles
92130 Issy les Moulineaux
France

Abstract

An OECD/NEA-CSNI International Standard Problem (ISP) has been performed on the experimental comparison basis of the severe fuel damage experiment CORA-W2. The out-of-pile experiment CORA-W2 was executed in February 1993 at the Forschungszentrum Karlsruhe. The objective of this experiment was the investigation of the behavior of a Russian type PWR fuel element (VVER-1000) during early core degradation. The main difference between a Western type and a Russian type PWR bundle is the B_4C absorber rod instead of AgInCd. Measured quantities are boundary conditions, bundle temperature, hydrogen generation and the final bundle configurations after cooldown. The ISP was conducted as a blind exercise. Boundary conditions (axial power profile, shroud insulation temperature) which could not be measured but which are necessary for test simulations were estimated using ATHLET-CD. Results to the ISP were submitted by 22 participants from OECD and non-OECD countries, using six different severe accident codes: ATHLET-CD, ICARE2, KESS-III, MELCOR, RAPTA and SCDAP/RELAP5.

Due to the large number of participants the comparisons between experimental and analytical results could be grouped by codes and examined separately. The thermal behavior up to significant oxidation has been predicted quite well by most of the participants and all codes. Larger deviations have been observed for the oxidation-induced temperature escalation, both time of onset and maximum temperature as well. The bundle behavior is greatly influenced by chemical interactions involving B_4C absorber rod material, which failed relatively early at low temperature due to eutectic interaction between B_4C and SS cladding as well as the SS guide tube. Regarding the complex material interaction larger differences can be recognized between calculated and measured results because of inappropriate models for material relocation and solidification processes and the lack of models describing the interactions of absorber rod materials with the fuel rods. For the total amount of H_2 generated, acceptable agreement could be achieved, if the total of oxidized zirconium was calculated correctly. Most codes did not treat the oxidation of stainless steel components and none of them modelled the B_4C oxidation.

In general the confidence in code predictions decreases with progressing core damage. Four categories of remaining main uncertainties have been detected: user effects regarding nodalization and selection of parameters, misinterpretation of existing

models, weak modelling basis requiring large numbers of parameters and some lack of modelling of certain phenomena.

The ISP36 provided a forum for the international community enhancing the experience in performing severe fuel damage calculations. It may have a great impact on further code development in conjunction with independent peer reviews of individual codes.

Аннотация

Международная стандартная проблема OECD/NEA-CSNI (ISP) была выполнена на основе экспериментальных данных по тяжелому разрушению топлива CORA-W2. Внереакторный эксперимент CORA-W2 был подготовлен совместными усилиями немецких и российских специалистов и проведен в феврале 1993 г. в исследовательском центре Карлсруэ. Целью этого эксперимента было исследование поведения твэлов российского реактора типа ВВЭР-1000 на начальной стадии разрушения активной зоны. Основное различие между ТВС в реакторах PWR западного образца и ВВЭР российского реактора типа ВВЭР - 1000 является наличие стержней поглотителей из B_4C вместо AgInCd. В ходе эксперимента измерялись такие параметры, как граничные условия, температура ТВС, выход водорода и конечная конфигурация ТВС после захолаживания. Международная стандартная проблема была проведена как "слепой" опыт. Граничные параметры (аксиальный профиль энерговыделения, температура чехла сборки, которые не могли быть измерены, но которые необходимы для моделирования испытаний, оценивались при использовании кода ATHLET-CD. Результаты ISP (Международная стандартная проблема) были разосланы 22 участникам стран OECD и стран, не входящих в OECD с использованием шести кодов по оценке тяжелых аварий: ATHLET-CD, ICARE 2, KESS-III, MELCOR, RAPTA, SCDAP/RELAP 5.

Благодаря тому, что ISP-36 собрала большое количество участников, экспериментальные и расчетные результаты смогли быть сгруппированы и исследованы отдельно для каждого кода. Температурное поведение, вплоть до начала значительного окисления, было достаточно хорошо рассчитано большинством участников и с помощью всех кодов. Более значительные отклонения наблюдались в процессе повышения температуры вследствие окисления как для значений температуры, характеризующей начало экзотермической реакции окисления оболочек твэлов, так и для достижимого максимума температуры. Обнаружено, что поведение ТВС в большей степени зависит от химических взаимодействий с материалом стержня-поглотителя B_4C, который разрушился сравнительно рано и при низкой температуре вследствие эвтектического взаимодействия между B_4C и оболочкой из нержавеющей стали, а также направляющей трубы из нержавеющей стали.

Значительные расхождения, которые были обнаружены между расчетными и экспериментальными результатами, характеризующими процесс взаимодействия материалов ТВС, могли быть вызваны вследствие затвердевания материалов вследствие использования неподходящих моделей для описания перемещения и затвердевания материалов, а также отсутствия моделей, описывающих взаимодействие материала поглощающего стержня с твэлами. Расчет общего количества образования H_2 может быть произведен корректно, если общее количество окиси циркония было расчитано правильно. Следует отметить, что большинство кодов не рассматривают окисление компонентов из нержавеющей стали и ни один код не моделирует окисление B_4C.

В целом точность оценки с использованием кодов снижается при возрастании степени повреждения активной зоны. Были выделены четыре основные категории неопределенности:

- эффекты, связанные с выбором расчетной схемы и заданием начальных и граничных условий экспериментов;
- ошибочное применение тех или иных моделей для описания физических процессов;
- слабость существующих моделей, которая выражается в том, что пользователю нужно выбирать и задавать большое количество специфических параметров внутри отдельных моделей;
- наличие пробелов в моделировании отдельных явлений.

В завершение следует сквазать, что ISP-36 представил собой форум международного научного сообщества, который позволил обогатить опыт расчетов в области тяжелого разрушения топлива. Анализ результатов ISP-36 может оказать большое влияние на дальнейшее развитие кодов и их независимое рецензирование.

Contents

1 Introduction

An International Standard Problem (ISP) Exercise is defined as a comparative exercise in which predictions of different computer codes for a given physical problem are compared with each other and with the results of a carefully controlled experimental study. The main goal of ISP is increasing confidence in the validity and accuracy in assessing the safety of nuclear installations [1]. In addition, it enables code users to gain experience and to improve their competence. International Standard Problems (ISP) are performed as "open" and "blind" exercises. In an open ISP the experimental results are available to the participants before their calculations and in a blind ISP the experimental results are locked until the delivery of the calculated results. Preferably, ISPs should be blind.

Accepting a suggestion by the Federal Republic of Germany, the Principal Working Group (PWG) No. 2 of OECD-CSNI[1] agreed on its meeting on September 28-30, 1993 to offer the experiment CORA-W2 on severe fuel damage for a Russian type PWR (VVER) as International Standard Problem No. 36 (ISP36) to its member countries and in addition to some non OECD countries. The experiment CORA-W2 is one out of a large number of severe fuel damage (SFD) experiments conducted at Forschungszentrum Karlsruhe [2]. Two of the experiments (W1 and W2) were performed with a Russian type VVER fuel element bundle. The experiment and the performance of the ISP were sponsored by the German Ministry for Education, Science, Research and Technology, the performance of the Russian part of the work was sponsored by the Minister of Nuclear Power of the Russian Federation. The fuel bundle manufacture and post test investigation was carried out in a joint effort by Forschungszentrum Karlsruhe, Karlsruhe (formerly Kernforschungszentrum, KfK), Nuclear Safety Institute of the Russian Research Center "Kurchatov-Institute", Moscow, Russian Research Institute of Atomic Reactors, Dimitrovgrad, Research Institute "Luch" Scientific and Industrial Association, Podolsk and Bochvar Research Institute of Inorganic Materials, Moscow. The ISP was conducted as a blind exercise, i.e. only the initial and boundary conditions were given to the participants prior to performing the calculation. Only for the GRS calculation the temperature measurements were given, since this calculation was used to determine unknown, but necessary boundary conditions.

[1] Organization for Economic Cooperation and Development - Committee on the Safety of Nuclear Installations

The severe fuel damage experiment CORA-W2 was executed on February 18, 1993 by the Project of Reactor Safety Research at Kernforschungszentrum Karlsruhe in cooperation with the Nuclear Safety Institute of the Russian Research Center "Kurchatov-Institute". The major objectives of this experiment were to investigate the behavior of VVER fuel elements with B_4C absorber rods under severe fuel damage accident conditions, including liquefaction, melting and relocation. The VVER is a Russian type PWR.

After the preparatory meeting, held at Gesellschaft für Anlagen- und Reaktorsicherheit (GRS) mbH, Cologne on February 17-18, 1994 [3], organizations from 8 countries, including 3 non OECD countries, submitted 22 contributions to the ISP, some organizations used more than one code.

The International Standard Problem No. 36 is the third ISP on severe fuel damage aspects. The first one (ISP28 [4]) was performed in 1990/91 using the PHEBUS-SFD B9+ experiment as the basis for the data comparison [5], and the second one (ISP31 [6]) using CORA-13 [7].

Compared with ISP31 the main differences are the VVER test bundle (VVER-specific materials, hexagonal rod array, B_4C absorber rod) and the termination of the experiment by slow cooldown instead of quenching. The presence of a B_4C absorber rod in CORA-W2 makes the results of ISP36 also useful for Western BWR's.

2 Objectives of the Standard Problem

During an unmitigated severe LWR accident the core material reaches temperatures significantly higher than 1200° C. This causes core damage in many ways, i.e. by chemical interactions of the different materials, melting, relocation, blockage formation, embrittlement and fragmentation of the cladding on cooldown and quenching, and hydrogen generation. At the early stage of the accident the core is still coolable and for mitigating the accident a detailed knowledge of the core meltdown behavior and a method to predict the course of the accident are necessary. Experimental results and code predictions can be used to quantify the safety margins presently existing in the safety systems of operating reactors, and to explore possibilities of ending a high temperature transient before it can lead to an uncontrolled core meltdown. For

demonstrating the capability of current computer codes to model and to calculate the core meltdown phase of a severe accident with sufficient accuracy, the OECD-CSNI decided to propose fuel element meltdown standard problems.

The general objectives of International Standard Problem No. 36 (ISP36) are to analyze the heatup and meltdown phase of a CORA VVER-type fuel element experiment and to examine the reliability and accuracy of the severe accident computer codes used.

In more detail the objectives of ISP36 are the comparison and investigation of the following physical variables and phenomena:

- Temperature of selected fuel and absorber rods,
- Onset of temperature escalation as a result of the exothermal zirconium/steam interaction,
- Extent of zirconium cladding oxidation,
- Liquefaction temperatures of stainless steel spacers and B_4C-absorber rods,
- Relocation temperatures of liquid phases,
- Extent of UO_2 and ZrO_2 dissolution by molten zirconium,
- Oxidation of metallic melt containing zirconium,
- Formation of blockages, extent and location,
- Timing and magnitude of hydrogen generation,
- Fragmentation of embrittled fuel rods.

The major relevant differences between the Russian VVER reactor compared with Western type PWR's are B_4C absorber rods (instead of Ag, In, Cd), the rod array (hexagonal instead of rectangular) and the cladding material (Zr1%Nb instead of Zry-4). In

addition absorber rod cladding, guide tubes and spacer grid consist of stainless steel which results in different material interactions.

3 Description and Results of Experiment CORA-W2

Detailed descriptions of the CORA facility and the experimental arrangement are presented in [2]. This chapter concentrates on the main characteristics of the facility and specific features of CORA-W2 experiment.

3.1 Description of the CORA Test Facility

The CORA out-of-pile facility is designed to investigate the behavior of LWR fuel assemblies under severe fuel damage accident conditions. In the experiments the decay heat is simulated by electrical heating. Great emphasis is placed on the fact that the test bundle contains the original materials used in light-water reactor fuel elements to investigate the different material interactions.

Pellets, cladding, grid spacers, absorber rods and channel box walls are typical of those of the investigated LWR type with respect to their compositions and radial dimensions. In test CORA-W2 original UO_2-pellets, Zr1%Nb-cladding, SS-spacers, B_4C absorber inside stainless steel cladding and stainless steel guide tube and Zr1%Nb channel box walls are used.

A general view of the CORA facility is presented in Fig. 3.1 and its connection to the main supply components is given in Fig. 3.2. The central part of the facility is the fuel rod bundle. The bundle is enclosed in a Zr1%Nb shroud with ZrO_2 fibre insulation. A high temperature radiation shield surrounds the bundle and shroud assembly. The massive insulation provides a realistic flat radial temperature gradient. The bundle is connected to the power supply system at the upper and lower ends. The water-filled quench cylinder provides the cooling of the lower end bundle electrodes. The bundle upper end is fixed in the bundle head plate.

The steam is produced in the steam generator. Together with the additional argon it is superheated and guided to the lower end of the bundle. The steam not consumed

within the bundle is condensed in two parallel condensers and the remaining hydrogen argon mixture is fed into the off-gas system after dilution by air to a low hydrogen concentration.

- Bundle design

The bundle and its surroundings are shown in Fig. 3.3 to 3.5. Heated, unheated and absorber rods are illustrated in Fig. 3.6 and 3.7.

Test bundle CORA-W2 consisted of 19 fuel rod simulators. The test rods were arranged within the bundle as shown in Fig. 3.5. Thirteen of the 19 fuel rods were electrically heated by central tungsten heating elements (Fig. 3.6). Five rods were unheated (Fig. 3.6) and one position within the bundle was filled with an absorber rod and its pertinent guide tube (Fig. 3.7). The heated rods as well as the unheated rods were filled with annular UO2 pellets of the same outer diameter but with different sized central holes (4.2 mm + 2.4 mm). The rod cladding is made of zirconium - 1 % niobium alloy (Zr1%Nb). Three stainless steel grid spacers of 20 mm depth were mounted into the bundle at -5 mm, 210 mm and 610 mm elevations (upper edge).

The shroud surrounding the bundle is also made of Zr1%Nb and insulated with a 20 mm thick layer of ZrO_2 fiber material to guarantee a uniform radial temperature distribution. Two videoscopes, at 600 mm and 800 mm (120° orientation) were used in test CORA-W2 to observe the materials behavior and the relocation of material during transient testing. The windows in the shroud and insulation are closed by quartz windows.

The hydrogen produced during the test by the steam/zirconium reaction was measured by a two mass spectrometer system in the mixing chamber after the gas had passed the condenser.

3.2 Power Supply

Thirteen rods were electrically heated in the W2 assembly. The input power was the same for all heated fuel rods. The time dependence of the power input was controlled

by the computer and was monitored during the experiment by current and voltage measurements.

3.3 Test Conduct and Initial Boundary Conditions

The experiment scenario can be separated into the following phases (Fig 3.8).

1. 0 - 3000 s: pre heating

2. 3000 - 4500 s: heating phase

3. > 4500 s: cool down phase.

The pressure in the system is controlled to 0.22 MPa (0.2 MPa overpressure).

During the preheat phase there is a flow of 8 g/s preheated argon through the bundle and a low constant electric power input about 0.52 kW. In consequence the temperature in the insulation reaches a level which is high enough to avoid steam condensation. At 2760 s the argon flow is changed to 6 g/s. The "steam flow" of 4 g/s was started at 3300 s.

During the heatup phase the initial temperature increase of about 1 K/s is produced by raising the electric power input from 2 to 14 kW. The test was terminated by reducing the electric power at 4500 s to 0.52 kW (slow cooldown by heat losses). At the same time the steam supply was terminated.

To keep the videoscope windows clear, a flow of 0.6 g/s argon is directed to the front of the windows. For the protection of the bundle head plate, 5.4 g/s of argon flows below the plate. The 6 g/s flow from the videoscopes and bundle head plate does not move through the bundle and is marked with the label "videoscopes" in the second graph of Fig. 3.8.

The steam for the CORA experiments is produced by introducing the foreseen amount of water into the secondary side of a heat exchanger (4 g/s), so that the water is completely turned into steam. The measured amount of water is given in the forth graph of Fig. 3.8. The uncertainty of the input with a calibrated volumetric pump was $\pm$ 1 %.

The buildup of steam flow through the bundle must be determined. The time behavior used by the different code users is given in Fig. 4.02a - 4.02d of chapter 4.

Fig. 3.9 gives the temperature at the steam inlet. The increase of the temperature after 3300 s is connected to the additional heat capacity of the steam, which increases the temperature of the walls of the connecting line from steam superheater to the inlet, resulting in a higher steam temperature.

For the uncertainty estimates we can give the following values: The measurement of the system pressure has an uncertainty of $\pm$ 2 % and the Argon flow is measured with an uncertainty of $\pm$ 3 %. The power is determined with an uncertainty of $\pm$ 1 %. The power determined experimentally is the integral power over the length of the fuel rod simulators, measured at the ends of the electrodes. The axial power distribution of the heated rod is dependent on the axial resistance distribution, which is determined by the temperature distribution and the temperature distribution is calculated by the relevant code.

The temperature at the steam inlet is measured by two thermocouples. The deviation between their readings is $\leq$ 1 % based on the reading in °C. This temperature is the reading of the thermocouple and the assumption is made that the thin thermocouple (0.5 mm) is at the temperature of the by-passing steam.

At higher temperatures the uncertainty of the temperature measurement is much larger. Just before failure of the thermocouples an uncertainty of about $\pm$ 100 K is reached.

3.4 Temperature Response

The following temperature measurements that characterize the temperature field in the assembly were performed:

- coolant temperature;
- fuel rod simulator cladding temperature;
- fuel temperature in unheated fuel rod simulators;
- temperature in the gap between the guide tube and the absorber rod cladding;

- spacer grid temperature;
- shroud temperature;
- high-temperature insulation temperature.

The analysis of the temperature measurements leads to the conclusions below.

Within the heated length of the bundle the temperature difference in the horizontal cross-sections does not exceed about 100 K. The main contribution to the difference is caused by the shroud in which the temperature in the heating phase is, as a rule, 50-100 K lower than the temperature of the fuel rod simulators. Beyond the escalation phase the temperature measurements are less reliable due to increasing failure of thermocouples. The massive melt formation in the bundle also attacks the thermocouples. Formation of new thermocouple junctions must be assumed, so that the location of measurements may change.

Fig. 3.10 illustrates the temperature response at 1050 mm and 650 mm elevation. It should be noted that the temperature difference at 1050 mm exceeds 200 K in the cooling phase, which is related to the absence of the shroud insulation at this elevation.

The complete list of initial temperature measurements is given in [2]. By taking into account all measurements at a special elevation we have determined a representative temperature as function of time for different elevation. The representative temperatures are given in Fig. 3.11 and 3.12.

The curves given in Fig. 52 of [2] represents for the beyond escalation range the lower limit of the uncertainty band as the thermocouple signal used in the evaluation could possible originate from thermocouples which have formed junctions at positions of lower temperature.

3.5 Hydrogen Generation

The initial hydrogen measurements were taken in the mixing chamber. In accordance with the calibration experiments performed in CORA-7 test the initial data set was mathematically processed using an experimentally determined transfer function which

allows to obtain a corrected data set characterizing the hydrogen generation directly at the assembly outlet. The characteristics obtained in the form of the hydrogen generation rate and integral hydrogen production are presented in Fig. 3.13. The uncertainty of the corrected production rate amounts to $\pm$ 10%. According to calculation assessments, the total amount of hydrogen of about 75 g might have been generated as a result of the oxidation of about 32 % (wt) of the total zirconium present (including the shroud); About 42 % of the total steam flow rate participated in the chemical reaction of zirconium oxidation during 400 s of intensive steam-zirconium reaction. Detailed data on hydrogen generation are presented in [2].

3.6 Gas Pressure in Simulators

The simulator rods and the absorber rod were to be filled with a small excess pressure of argon by the beginning of the heating phase. The analysis of the pressure measurement shows that by 3000 s three of the six rods turned out not to be gas-tight and their pressure corresponded to the ambient pressure. The absolute gas pressure in the other three rods which were intact was from 0.265 to 0.301 MPa. The nature of pressure changes in the assembly heating phase for these rods is shown in Fig. 3.14. The absorber rod failed first.

3.7 Post-test Appearance of the Bundle and of Cross Sections

The appearance of W2-bundle after the test is shown in Fig. 3.15. Below 300 mm the shroud preserved its geometric form with increasing oxidation above 200 mm elevation. From 300 mm to 700 mm the shroud is deformed and contains many cracks and holes. Up to about 1100 mm elevation the shroud was attacked so much, that it disappeared during dismantling of the insulation.

The test bundle is fairly intact up to an elevation of about 200 mm. The severely oxidized part of the bundle lies above 400 mm. The upper grid spacer has completely molten away due to chemical interactions with the Zr1%Nb cladding and by reaching the melting point, while the central grid spacer has survived in accordance with the axial temperature profile. The absorber rod failed at about 210 mm (i.e. above this elevation the absorber rod has disappeared. A blockage has formed at about 200 mm. Interaction of the melt with the UO_2-pellets can be recognized. The radial

deformation of the cladding, the so-called "flowering" is evident from about 400 mm upward. In general, the material behavior of this VVER 1000-type bundle is comparable to that of a PWR of Western design.

For post-test investigations the bundle was filled with epoxy and then cut in the cross-sectional direction. Fig. 3.16 shows photos of several cross-sections. In accordance with the results of the post-test examinations of [8] a number of conclusions can be drawn regarding oxidation and material interactions in test W2.

3.7.1 Zirconium Oxidation

From the evaluation of the measurements two groups of data were obtained that characterize the zirconium oxidation process in CORA-W2:

- total weight percentage of the zirconium oxidized before the beginning of the zirconium melting (Fig. 3.17);

- total weight percentage of the oxidized zirconium indicating the oxidized part of the relocated melt (Fig. 3.18).

The measurement was performed by single metallurgical probes assuming that the zirconium oxidized before melting stayed in place.

In a similar way, data were obtained that characterize the total mass of Zr and Zr(0) that remained after the experiment from the assembly (Fig. 3.19) and from the shroud (Fig. 3.20).

The analysis of the results obtained demonstrates the following:

- The maximum percentage of the oxidized zirconium in the assembly before the beginning of the melting was at the level of 270 mm and was equal to 54 %. The top two-thirds of the assembly (350 - 1050 mm) has a relatively smooth profile of oxidation (25 - 30 %). There was practically no oxidation of the lower third of the assembly (-150 to 150 mm).

- Based on the final status of the experiment, there was practically no oxidation of rod cladding in the interval from -150 to 200 mm. In the interval 327 to 726 mm the zirconium was oxidized (84 - 99 %). The oxidation percentage is slightly lower in cross-sections 845 to 910 mm (70 - 80 %).

- The zirconium was not oxidized below 141 mm elevation. From 208 mm to 607 mm elevation the shroud oxidation increases continuously from 26 % to 100 %. After the experiment no shroud could be found above 607 mm.

3.7.2 UO_2 Dissolution

Fig. 3.21 characterizes the UO_2 mass distribution with elevation after the test.

The data demonstrate that below 141 mm there was no chemical interaction of UO_2 with assembly materials. The dissolution of uranium dioxide between 208 - 1098 mm corresponds to the temperature field changes and is characterized by a gradual increase of the dissolved UO_2 from 6 % in cross-section 208 mm to 17 % in cross-section 1098 mm.

3.7.3 Behavior of Spacer Grids

The post-test investigation shows the disappearance of the grid spacer at 610 mm elevation. The lowermost grid at -5 mm did not change much during the experiment. The middle grid spacer was oxidized in locations of contact with relocating melt, however no melting or interactions of the grid with assembly materials was found (Fig. 3.22).

3.7.4 Behavior of the Absorber Rod

To describe the absorber rod behavior during the experiment the following data were obtained:

- remaining SS of the absorber rod (Fig 3.23);
- remaining B_4C of the absorber rod (Fig. 3.24); the results are applicable for comparison with B_4C dissolved by stainless steel.

- B_4C Total mass (Fig. 3.25).

The data obtained demonstrate that the steel elements of the structure retained their integrity only in the bottom part of the rods (-150 - +50 mm). Starting from elevation 150 mm the melting of steel elements is noted, and they practically disappear at elevation 250 mm. Sintered B_4C columns survive till 450 mm (34 % of the initial amount). Above 550 mm B_4C has disappeared.

3.8 Blockage Formation and Mass Distribution

Data on the blockage formation were obtained by direct measurement of the area occupied by materials at all bundle cross-sections [8]. Remnants of the shroud were not taken into account. For calculation of the flow area the measured areas were referred to the initial cross-section of the inner side of shroud.

Results are presented in Fig. 3.26. The flow area increased in the upper half of the bundle from 550 to 1150 elevation. A core blockage formed between 50 and 350 mm elevation with a maximum of 28 % reduction of the flow channel at an elevation of about 200 mm.

The axial mass distribution was determined by a different method. After the test the bundle was embedded in epoxy to fix all the materials at their final position. From this process the epoxy mass filled in per centimeter elevation was determined. The bundle was then cut in segments. The mass of the structural materials was determined as the difference between the mass of the segment and the mass of the filled in epoxy. As the shroud of the axial center (hot region) was removed together with the fibre insulation of the bundle, the remnants of the shroud which were present during the filling process were excluded in the evaluation. It was assumed that there had been no shroud. The masses so obtained were referred to the initial masses of structural materials in the segment.

The results of mass distribution presented in Fig. 3.27 correspond with the results of the blockage formation. Material relocated from the upper part of the bundle (elevation > 400 mm) is refrozen at 100 to 400 mm bundle height with a maximum at about 200 mm.

4 Calculations by the Participants

4.1 Selection of Variables to be Calculated

The selection of variables to be calculated by the participants was done in order to meet the objectives of the ISP [9]. Special attention was given to consideration of the relevant design differences of the VVER. The variables comprise global parameters, temperatures at different locations and core degradation variables indicating the state of the bundle.

The global variables are needed mainly for the energy balance, e.g. heat fluxes including losses and storage, power generation by oxidation and hydrogen generation. The temperature variables indicate the thermal behavior of the bundle including shroud, shroud insulation and high temperature shield. They consist of:

- Fluid temperature
- Fuel and cladding temperature
- Absorber and guide tube temperature
- Shroud and high temperature shield (HTS) temperature

The bundle degradation variables represent the damage to the bundle and are divided into two groups: bundle degradation process and material distribution. The first group shows the degradation kinetics and does not consider any material relocation, the second shows the material distribution after relocation. The selected variables are:

- Zr oxidized
- Zr, UO_2, ZrO_2, B_4C dissolved
- Remaining absorber assembly (B_4C, SS)
- UO_2, ZrO_2, B_4C total mass
- Total mass, core blockage
- etc.

4.2 Participants and Codes

Representatives of 17 organizations from 9 countries, including 3 non OECD countries, participated in the International Standard Problem No. 36 (ISP36) based on the CORA-W2 experiment on severe fuel damage for a Russian type VVER fuel element [10-31]. They submitted a total of 22 contributions using the codes ATHLET-CD, ICARE2, KESS-III, MELCOR, RAPTA and SCDAP/RELAP5 [32-37]. Table 4.1 summarizes the analysts, the participating organizations and the codes used[2].

4.3 Codes and Computational Models Used for ISP36 Calculations

The computational models used for the ISP36 calculations are defined by both the models provided by the codes and the specific input decks defined by the participants. Descriptions of code models are given in detail in the respective documentation. The basic modeling aspects, particularly as regards the ISP36 calculations, are summarized below. The input deck reflects the way of representing the specifics of a given facility in a code. It defines the geometry, the boundary conditions of the test and the interaction between the different models in operation. The basic characteristics of the input decks for ISP36 as defined by the participants in the specific code environments are given below. Both model and input deck description are structured according to the following items:

- nodalization scheme,
- thermal hydraulics,
- structure heat-up,
- electrical heat source,
- material oxidation and hydrogen generation,
- mechanical rod behavior and cladding failure,
- chemical interactions,
- material relocation.

[2] The ATHLET-CD calculation by GRS was performed with the knowledge of the measured temperature data.

4.3.1 Nodalization Scheme

The basic constructional elements to be nodalized in the CORA bundle are the three types of rods (heated, unheated, and absorber rods), the shroud, the HTS, the flow sub channels in the bundle, the bypass flow channel and the spacer grids. In principle, the codes provide the modeling basis for the individual treatment of each element while axially subdividing it into a certain number of segments. In order to meet reasonable computing times, the codes apply the concepts of representative zones or representative components. In both concepts, certain elements are combined to representatives, with the solution of the governing equations only being required once for each representative. The concept of representative zones is basically geometry oriented, i.e. applying this concept to the CORA-W2 bundle leads to a radial subdivision into a number of concentric rings, e.g. central rod, 6 unheated rods including absorber rod, 12 heated rods, shroud, and HTS. The concept of representative components is basically structure type oriented. In principle, this concept allows the combination of all structures of a given type, e.g. all unheated rods, into one representative regardless of their individual position in the bundle. In practice, the codes under consideration apply hybrids of the two concepts. However, they may roughly be classified, with SCDAP/RELAP5 and ICARE2 tending towards the concept of representative components and ATHLET-CD, KESS-III, and MELCOR tending towards the concept of representative zones. The respective data are given in Table 4.2 together with the axial segmentation.

A further governing nodalization characteristic is the treatment of the flow channels. Despite from radiative heat transfer, the flow channels provide the only coupling between the structure representatives. For most ISP36 calculations, two flow channels have been defined, one representative channel for the bundle flow (inside the shroud) and the other for the bypass flow. For some ATHLET-CD calculations, the bundle itself has been subdivided into an inner and outer flow region, in case of ICARE2, the bypass region has not been modeled due to restrictions in the thermal hydraulics. The basic data together with other nodalization characteristics are given in Table 4.2.

4.3.2 Thermal Hydraulics

The codes uniformly apply quasi one dimensional formulations of the conservation equations coupled to constitutive equations for the modeling of heat and mass transfer between the fluid phases and between fluid and structures. True cross flow modeling is not possible in terms of momentum mixture. Instead, cross flow between parallel flow channels is modeled as mass and energy sources and sinks to the respective channels with the exchange rates governed by flow resistances and pressure drops. Some of the codes - like ICARE2 and KESS-III - act as stand alone SFD codes with their own thermal hydraulic modeling. The modeling in ICARE2 currently is restricted to the gas phase including steam and non condensables, leading to a so called 3-Equation approach; KESS-III uses a 4-Equation model with two phase flow treated below the mixture level. Others - like SCDAP/RELAP5 and ATHLET-CD - are code systems consisting out of a thermal hydraulic module and a SFD-module. In these codes, thermal hydraulics in the core are modeled by applying the full thermal hydraulic module to the core geometry. For SCDAP/RELAP5, this leads to a 6-Equation approach, for ATHLET-CD optionally to a 5-Equation (mixture momentum equation) or 4-Equation (mixture momentum and mixture energy equation) approach. Further details including the specifics of other codes used for the ISP36 action are given in Table 4.3.

One major concern besides the thermal hydraulic modeling basis itself are the interactions with other models. Geometry changes (flow area reductions) provided from the relocation and ballooning models are partially taken into account (see Table 4.3). Heat sources to the fluid provided from the radiative heat transfer models are taken into account by most of the codes at least regarding the latest versions. The impact of grid spacers on the flow is mostly accounted for by implying user defined increased flow resistances at grid spacer locations. The CORA typical cross flow situation at the coolant inlet is generally handled by applying enhanced heat transfer coefficients for the respective bundle section, partially hard wired, partially via user input.

4.3.3 Structure Heat-up

Generally, the codes provide two types of models for structure heat-up, so called heat structures for energy balances in structures maintaining their integrity during core

degradation and core structures for energy balances of degrading geometries. Heat structures are based on one dimensional heat conduction equations (with exceptions, e.g. SCDAP/RELAP5: two dimensional) with sources from oxidation and other heat sources.

Core structures generally apply two dimensional thermal energy equations including sources due to fission, fission product decay, oxidation and relocating material. Due to the coarse meshing of the structures (see Chapt. 4.3.1), most of the codes superpose the numerical finite difference solution available for discrete points in the numerical mesh with quasi-analytical solutions of the heat conduction equation yielding interpolations between mesh points.

Following the concept of representative zones or components, radiative heat transfer is defined to take place not between individual structures, but representatives. This has strong impact on the definition of view factors, which partially loose their meaning in a strong geometrical sense and appear as mean view factors between groups consisting of different individuals. Furtheron, for rod arrays radiative heat transfer is treated as apparent quasi conduction to account for single representative temperatures in coarse meshes.

In some codes (e.g. SCDAP/RELAP5), view factors are calculated by correlations based on the crossed string method (plane case), in others they are user input (MELCOR). If treated by user input, automatic view factor recalculations to account for geometry changes in degrading geometries are not possible. Most of the codes (except ATHLET-CD) take into account gas radiation and radiosity. Table 4.4 summarizes some basic characteristics of the models for structure heat-up as used for ISP36.

4.3.4 Electrical Heat Source

The out-of-pile test CORA-W2 requires models for the electrical heat input into the bundle. The models are uniformly based on serial electrical resistance approaches including the resistances of the tungsten heater rods (subdivided in axial segments according to the axial meshing of the core structures) and the resistances of the copper and molybdenum cold ends.

In case of MELCOR, an external subroutine (WOLFHE, originally designed for CORA-13) is provided which has to be adapted to the CORA-W2 bundle geometry.

4.3.5 Material Oxidation and Hydrogen Generation

Most of the calculations performed for ISP36 are based on rate equations for oxidation (some used a diffusion model). The basic correlations used in the codes are given in Table 4.5. Partially, as indicated in Table 4.5, the rate coefficients have been adapted to treat the Zr1%Nb material of the VVER-type of cladding. Most of the codes treat inside oxidation after the burst of the cladding. In some codes (e.g. SCDAP/ RELAP5), the ballooning models provide information to the oxidation model about the extension of the ballooned zones, i.e. the inner surface available for contact to steam. In others (e.g. ICARE2), the zone for inside oxidation is fixed to a certain extent in the vicinity of the cladding breach. In case of MELCOR with no ballooning model in the present versions, inside oxidation starts, when a user defined cladding rupture criteria is met.

In case of high temperatures and thin oxide layers, the oxidation rate may be governed by the mass transfer resistance in the steam-argon-hydrogen mixture against the oxygen transport to the cladding surface, rather than by the solid diffusion resistance within the material. Only SCDAP/RELAP5 and MELCOR provide models for this additional limiting factor besides steam starvation and material consumption. This advantages in the SCDAP/ RELAP5 and MELCOR modeling may only affect the oxidation of relocating melts (high temperatures and thin oxide layers).

Melt oxidation models - so far available, see Table 4.5 - are thoroughly based on rate equations for intact rods. For the rate calculation of melt mixtures consisting of UZr-O, UO_2 and ZrO_2, the mixture layers in the respective axial zones are rearranged to show a vertically stratified structure with the Zr component forming one layer in this structure. The usual rate equations are then applied to this Zr-layer, removing any new ZrO_2 instantaneously by adding it to the ZrO_2 layer. Besides Zr, most of the codes provide oxidation models for stainless steel and some (e.g. MELCOR) for B_4C too (see Table 4.5).

4.3.6 Mechanical Rod Behavior

The most important models for early phase structure mechanics are those for ballooning with subsequent cladding rupture and for the breach of oxide shells containing molten U-Zr-O mixtures and absorber materials. Except MELCOR, all codes used for ISP36 provide ballooning models, varying from highly mechanistic codes accounting for material anisotropics and circumferential temperature gradients (SCDAP/RELAP5) to more empirical (ICARE2) based on specific experiments. Although partially provided by the oxidation models, none of the models allows to account for the impact of the layer structure of the cladding consisting of ZrO_2, α-Zr(O) and β-Zry, on the mechanical rod behavior. In some models, the mean oxygen content enter the models via material properties for the stress and strain calculations. Cladding rupture occurs when certain failure criteria are met. The criteria involved differ from maximum hoop strain (ATHLET-CD, KESS-III) over maximum hoop stress (SCDAP/RELAP5) to stress dependent failure temperatures (ICARE2; "Chapman-correlation"), see Table 4.6.

The models for oxide shell breach have significant impact on the amount of liquid UZr-O mixtures and the onset of relocation of liquid materials including U-Zr-O and absorber material eutectic mixtures. The impact on the amount of U-Zr-O mixtures is due to the fact that the oxide shell keeps the mixture within the reaction zone, i.e. the chemical dissolution process (see Chap.. 4.3.7) lasts until the shell breaches and the mixture is released to outside of the fuel rod. The models for oxide shell breach depend on whether or not the codes provide models for the dissolution of the oxide shells by the liquid material they contain. In ICARE2 for instance, the model for the dissolution of ZrO_2 by liquid Zr allows for the calculation of the respective shell thickness reduction. Codes without such models (e.g. SCDAP/RELAP5 and ATHLET-CD) apply user defined criteria, mainly based on critical temperatures to trigger the cladding breach. The corresponding code specifics and user criteria applied for ISP36 calculations are given in Table 4.6.

4.3.7 Chemical Interactions

Chemical interactions important for CORA-W2 are the fuel rod UO_2-Zr-ZrO_2 and the absorber rod B_4C-Stainless Steel (SS) eutectic interactions.

New interpretations [38] of existing experiments identify two distinct stages in the dissolution of UO_2 by molten Zr with rather different reaction kinetics; a saturation and a precipitation stage. The first "saturation" stage is characterized by a very quick dissolution of UO_2 up to the saturation of the liquid phase by U and O atoms (liquidus line in ternary phase diagram). After saturation, the dissolution continues with much slower reaction kinetics obeying the well known parabolic time law. This stage is characterized by the precipitation of (U-Zr) O_{2-x} particles in the liquid phase. The kinetics in this phase are governed by the oxygen flux in the solid UO_2 (gradient UO_2 to UO_{2-x} at the solid/liquid interface). Up to now, the codes provide different models partially as alternatives to the choice of the user. Some of these models reflect the saturation stage, others (Hofmann-model) the precipitation stage corresponding to the specifics of the single effect tests they were based on. One of the specifics of these tests was the mass ratio between UO_2 and Zr. The basic conclusion in [38] is that the different models available lead to a consistent interpretation of experimental results if renormalized with respect to the UO_2/Zr mass ratios involved. Consequently, the choice of the user in applying alternative models provided in codes to a given experiment, e.g. CORA-W2 may yield misleading results (e.g. applying Hofmann's parabolic rate law together with a saturation limit defined by the liquidus line is a wrong interpretation of the underlying experiment [38]). According to this problem, Table 4.7 indicates the models used together with the saturation limits applied.

The B_4C absorber rods are a specific feature of VVER type bundles. The B_4C absorber material is surrounded by a SS cladding and a SS guide tube. Consequently, as far as the outer oxidized steel shell is intact, the chemical interactions of interest are those between B_4C and SS. Some of the codes in principle provide models for the dissolution of SS by B_4C. However they are either coupled to certain geometric situations (SCDAP/RELAP5 model for BWR absorbers) or they are rather simple by just providing an eutectic temperature leading to an instantaneous liquefaction (ATHLET-CD). Furthermore, after leaving the inside of the absorber rods, radial relocation and spreading causes contact of the B_4C-SS mixture to the ZrO_2 of oxidized fuel rod claddings and other structure materials. Both, mechanistic models for radial spreading of absorber material and for chemical interactions of B_4C-SS-ZrO_2 are presently not available in the codes. Table 4.7 summarizes some specifics of the absorber rod modeling for ISP36:

4.3.8 Material Relocation

All the codes used for ISP36 provide models for axial relocation (candling), only some (e.g. MELCOR) have simple models for radial relocation. The approaches underlying the candling models differ widely from highly mechanistic (ATHLET-CD, KESS-III) to basically parametric (MELCOR). Generally, the models are based on the assumption of a given relocation velocity (in MELCOR essentially infinitively high) and of a given arrangement of the melt leaving the rod on its outer side (film or certain number of rivulets or droplets). The data used for ISP36 are given in Table 4.8. The candling models may be subdivided into two groups: In one group, an effective conductivity (including effects from melt-to-crust heat transfer and the crust thermal conductivity) governs the heat transferred from the relocating melt to the rod (ATHLET-CD and MELCOR) and in the other a thermal shock front propagating into the surface of the rod characterizes the heat transfer. In the first group, the heat transfer coefficient has a large impact on the results. This is especially true for MELCOR with the heat transfer coefficient being user input. Table 4.8 shows the corresponding data used for the ISP36 calculations.

The models available for radial relocation require a relocation rate coefficient. So far treated in the codes for the ISP36 calculation, Table 4.8 depicts the corresponding data.

4.4 Comparison of Analytical and Experimental Results

This section compares the experimental results with the results as provided by the participants, with some additional observations and comments. From the list of variables given in the specification, only the important ones are discussed. In order to associate the different curves with the participants and the used codes, each curve is labeled with a four-letter code according to Table 4.1. For better readability of the curves, the 22 participants were divided into four plot groups with a maximum number of six curves per group (excluding the experimental data). Apart from individual comparisons, comparisons between the codes used are of special interest, so the plot groups are essentially the same as the code groups, except that the two German codes ATHLET-CD and KESS-III were combined in one plot group as well as the ICARE2 group with the single RAPTA-SFD participant. The leading three letters of the

legend labels indicate the institution, the last letter indicates the code used. Solid curves indicate experimental results.

4.4.1 Initial and Boundary Conditions

Some initial and boundary conditions measured in the test facility are compared with those actually used by the participants. This facilitates the evaluation of the calculated results.

- Bundle Power (POBU)

As shown in Fig. 4.01, a linear power increase from 1.7 to 14.3 kW between 3020 s and 4500 s was given and essentially followed by the participants of code groups ATHLET-CD, KESS-III, MELCOR, ICARE2 and RAPTA-SFD, with slight deviations only for GIDM and UBOI. Compared with this, SCDAP/RELAP5 calculations for this variable are spread over a larger range. The reason for this may be separated presentation of the thermal power of tungsten heater instead of the total power loss at assembly (RRCS) or neglect of upper and lower bundle ends due to limitation of the axial node discretization (ENES). The values for peak power, maximum voltage and maximum assembly resistance are consistent and yield an average maximum resistance of about 0.05 Ω per rod.

- Steam Inlet Flow (FIST)

Steam inlet flow (Fig. 4.02) results from the water feed flow of $4 \cdot 10^{-3}$ kg s^{-1} between 3300 s and 4500 s with a time constant of about 100 s. The time constant was estimated considering the steam temperature increase, the inertia of the fluid and the structural heat up. Apart from the ATHLET-CD and KESS-III group, most participants used the water feed flow as the steam inlet flow. The exceptions, in particular: KFIM, RRCA, OKBM, IKEK, NRII, GRSA and RASA modeled a time constant. KFIM and RRCA followed closely the ISP36 specification and used an exponential decreasing shape for the start and end of the steam inlet flow, with the specified value of 100 s as the time constant. Suitable linear approximations to this constant were chosen by OKBM, IKEK, NRII. A time constant of about 300 s was used by GRSA and RASA, leading to a lower steam flow than specified in the beginning, but to a longer duration of steam flow input. ATHLET-CD users modeled the argon gas flow by an additional

permanent steam flow without oxygen potential (inert flow) of $1.5 \cdot 10^{-3}$ kg s^{-1}, to take into account the heat capacity of this non condensable, contributing a steam flow which lies higher than the maximum water flow. KFIM has added the evaporation rate from the quench cylinder to the inlet flow. VTTS considers a linearly increasing steam flow between 3000 s and 3300 s.

Since the steam flow was not measured directly, water feed to the evaporate and superheated was taken as the experimental curve instead.

- Inlet Temperature (TEIN)

The measured inlet temperature (Fig. 4.03) was followed by most participants. Deviations occur only for AEAM, ARSR, VTTS and, in the range of 3400 s to 3800 s, for UBOI. The maximum experimental value of 910 K (637° C) is reached at 4552 s, which is consistent with the given boundary condition values (maximum value 634° C for 4580 s).

- Temperature at Bundle Top (TEBT)

For the temperature at the bundle top (Fig. 4.04) there are several choices for the experimental curve. The given boundary condition in Appendix E of the ISP36 specification [9] was a table of calculated best estimate gas temperatures above the shroud. In Fig. 4.04 these values are marked with crosses. Obviously, RRCA followed exactly the given values. For the experimental curve, the cladding temperature at 1250 mm was chosen, since the gas temperature above the shroud has a considerable time lag and may be not the same as above the bundle. Amongst all the calculations, there were three using the experimental values as boundary conditions: GRSA, NRII and RRCI. Essentially correct tendencies were calculated by AEAM, OKBM and RRCA.

4.4.2 Temperature

Fig. 4.05 to 4.14 show the thermal behavior of various locations in the assembly cross section at 5 different elevations (350, 550, 750, 950 and 1150 mm). Not all of these curves can be verified by measurements, and even the measured curves often end before the termination of the experiment because of failure of the correlated thermocouple at higher temperatures. General characteristics are:

- moderate increase due to electrical and steam heating,
- steep increase caused by exothermal zirconium reaction (temperature escalation),
- early increase at lower elevations due to melt relocation.

- Fuel Temperature (TUO2)

The fuel temperatures are plotted in Fig. 4.05 to Fig. 4.09 for the selected elevations. During the transient phase from 3000 s to approximately 4100 s the measured data show a steady increase from 750 K to 1300 K. Most of the calculated results follow this measured increase quite well with a spread of only 100 K to 150 K. The results obtained by SCDAP/RELAP5 show a larger spread of about 400 K. Between 4200 s and 4500 s the temperature increases rapidly due to the zirconium oxidation, beginning at elevation 950 mm. With one exception all calculations show this temperature escalation but they differ largely in the onset of the escalation and in the temperature maximum. Most of them lie in the expected maximum of 2250 to 2500 K. In this behavior no significant difference amongst the different codes can be seen.

For elevation 350 mm (Fig. 4.05) only three participants (GIDM, RASI and GRSA) calculated the escalation at all. For 550 mm, the participants GRSA, IKEK, RRCI and RRCS succeeded in modeling the observed second escalation due to melt relocation.

At higher elevations (750, 950 mm), temperatures are underestimated by RRCA and VTTS and overestimated by ARSR significantly. The ICARE2 group calculated smaller deviations from the real escalation time than all other groups. RASI and GRSA obtained very close agreement at all elevations. For 750 mm, the participants RASA, UBOA, ARSR, RRCS and RDIS calculated higher maximum temperatures than 2500 K.

- Cladding Temperature (TCLA)

Since the experimental radial temperature profile is very flat no great temperature difference between cladding and fuel can be expected. Also in the analytical model no large difference between heated and unheated rods was estimated. The calculated results for the cladding temperature are very similar to those of the fuel, only some spikes or the temperature escalation are more pronounced. This can be seen in Fig.

4.10 where the cladding temperature for elevation 750 mm is shown. The GIDM calculation experienced abrupt breakdowns shortly before 4500s due to overestimation of temperature and consequent complete melting of cladding even at 350 mm.

- Guide Tube, Absorber and Shroud Liner Temperature (TEGT, TAIC, TESH)

Guide tube temperatures are plotted in Fig. 4.11 and 4.12 for the elevations 350 and 750 mm. Due to the flat radial temperature profile and to the fact that the guide tube is exposed to the superheated steam and heated up by radiative heat transfer, the temperature behavior of the guide tube is very similar to that of the cladding. At 350 mm the experimental data show a temperature escalation, similar to the fuel, but with some indication of melt relocation at earlier times. From the analytical data only 3 calculations showed the temperature escalation (GIDM, GRSA and RASI). At level 750 most of the participants calculated a more or less pronounced temperature escalation. All MELCOR calculations show a complete melt away of the guide tube, when the temperature reaches 1700 K, which is supplied by input data.

An example for the absorber temperature at level 750 mm is given in Fig. 4.13. The results for the ICARE2 and RELAP5 calculations are very similar to those of the guide tube. Melting and relocation of the absorber material is not seen in the temperature history. In the MELCOR and ATHLET-CD calculations the absorber material melts and relocates between 1500 and 1700 K depending on the user supplied input data.

For the shroud liner temperature an example is given in Fig. 4.14 for elevation 750 mm. The experimental temperature escalates very rapidly at 4200 s to about 2100 K and then decreases steadily. The thermocouples in this elevations have been destroyed completely, so temperatures at higher elevations have been recorded (especially at about 1150 cm). While the ICARE2 and SCDAP/RELAP5 calculations follow this curve fairly closely, the MELCOR and ATHLET-CD calculations show a much larger spread in time for the escalation. One KESS-III calculation (IKEK) agrees very well the experimental data.

- Temperature Range Plots

It is of some interest to compare all the results of one code with all the results of other codes instead of comparing the individual calculations. For this purpose range plots

(p. 27 to 30) have been designed which comprise all the individual calculations except those which show an obvious error and except the RAPTA calculation. Each colored area represents one code group with the maximum calculated value as the upper and the minimum as the lower boundary. In addition the experimental data are plotted into the figures. The following four pages show representative examples of these range plots.

The overall impression given by the range plot is that there is no significant difference between the four codes. During the heat up phase the largest spread is shown by SCDAP/RELAP5, while during temperature escalation and cool down, depending on the location, SCDAP/RELAP5 or ATHLET-CD show the largest spread, but the upper limit of ATHLET-CD is very close to the experimental data. It can also be seen that during escalation and cool down, most results lie below the measured data. In some cases all results of one code group lie completely below the measured data. Reasons for the deviation are different code versions, different nodalizations and the heat losses to the High Temperature Shield (HTS).

The very narrow band of KESS-III is due to the fact that only two KESS-III calculations have been submitted. In the case of SCDAP/RELAP5 the results have been obtained by different code versions.

ISP 36

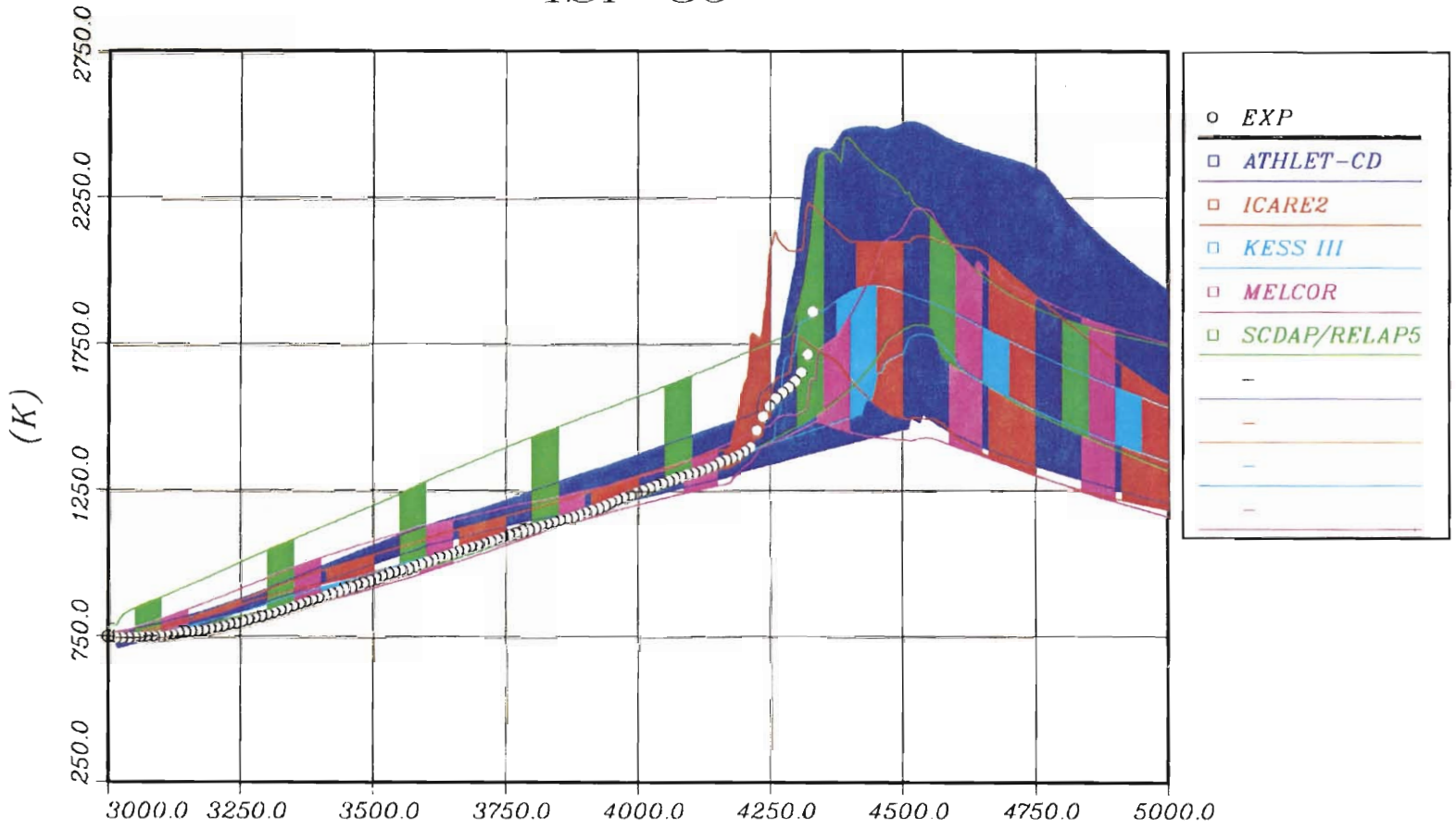

Fuel Temperature (TU02 0550)
Range Plot

ISP 36

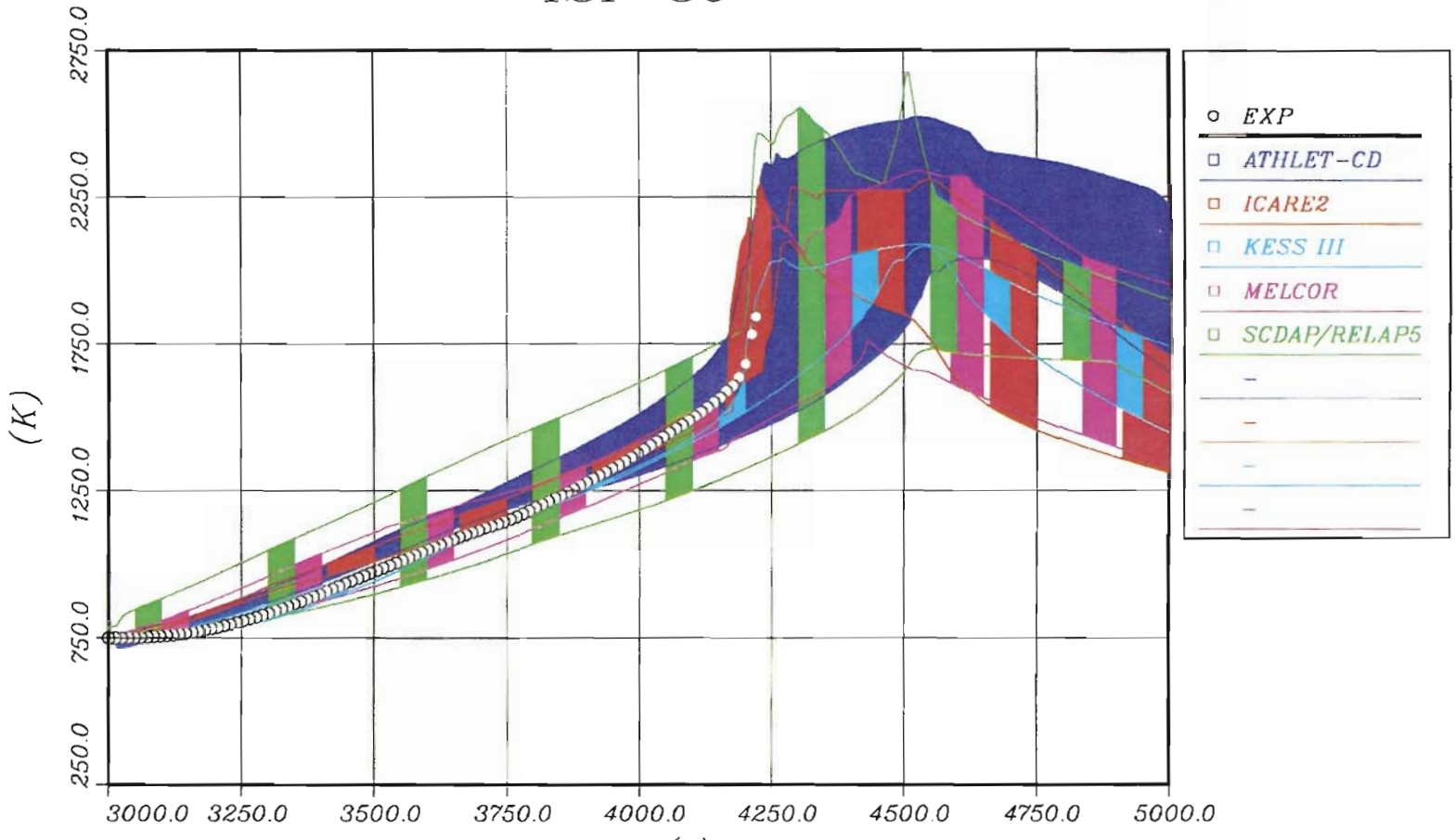

Fuel Temperature (TU02 0750)
Range Plot

ISP 36

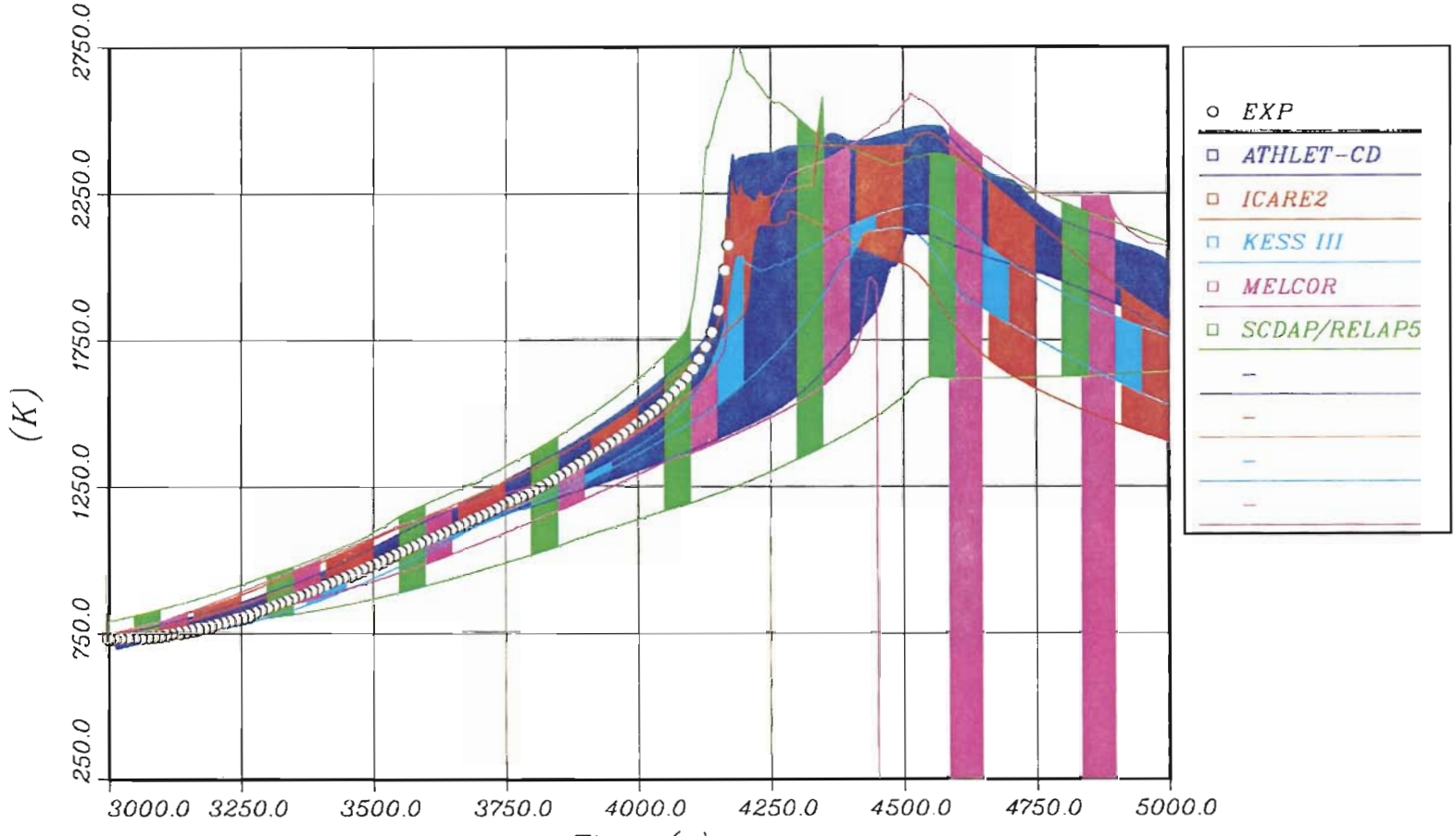

Cladding Temperature (TCLA 0950)
Range Plot

ISP 36

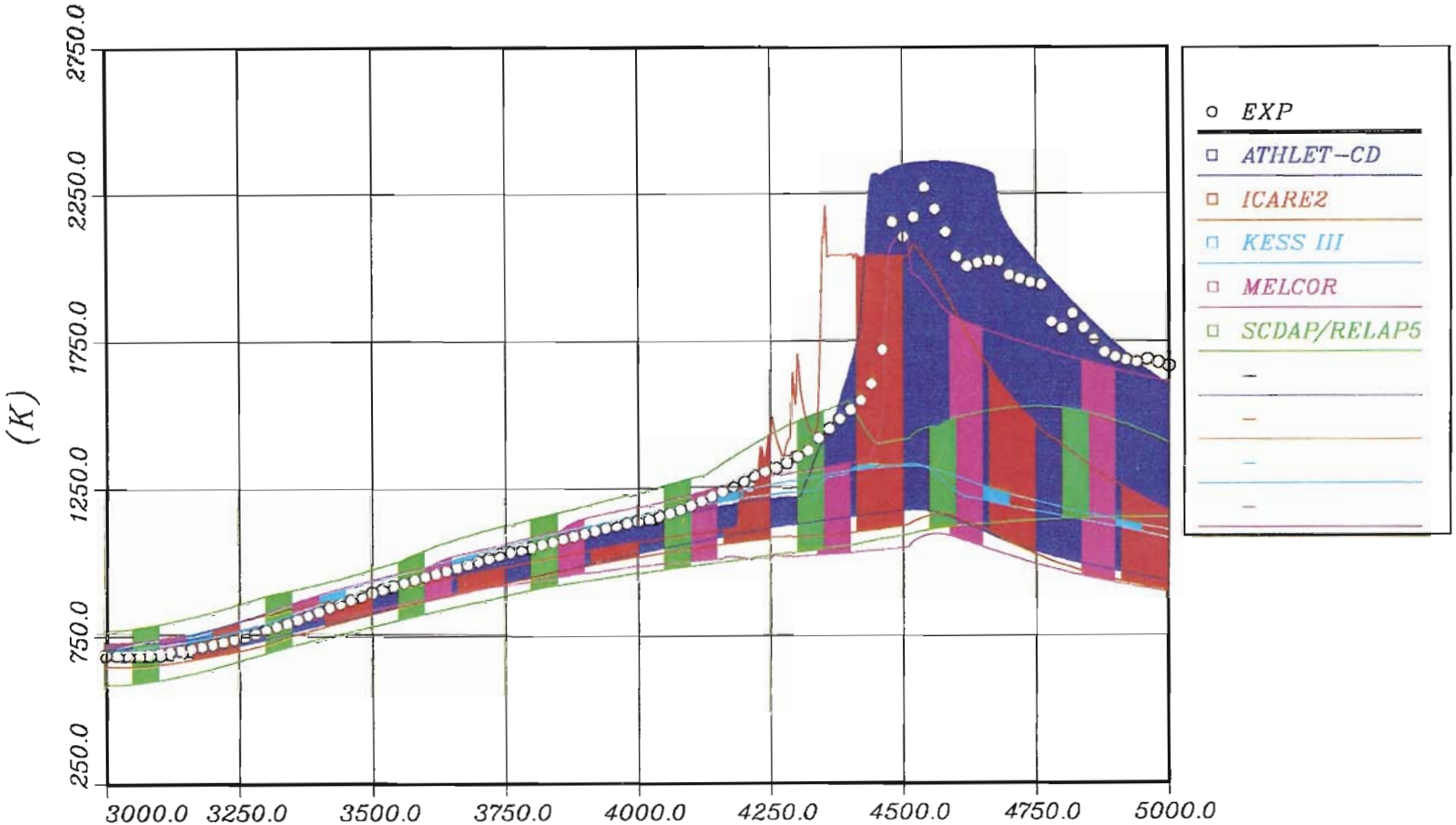

Shroud Liner Temperature (TESH 0350)
Range Plot

4.4.3 Core Degradation and Mass Distribution Variables

The core degradation variables give a picture of the core during and at the end of the experiment. The data are plotted for a given time versus the height in the test section. Since the bundle state after relocation is of special interest because of its direct comparability with the posttest analysis of the bundle, time t = 4900 s is used to get essentially the final state of the core, i.e. temperature has then lowered enough to prevent further melting and to slow down further oxidation. In some plots the experimental values are added, as they have been recorded by posttest preparing and analyzing of the bundle.

a) Bundle degradation

- Zirconium Oxidation (ZOBO)

The experimental zirconium oxidation of the bundle in Fig. 4.15 shows that between 300 mm and 850 mm about 30 % Zr was oxidized. A maximum value of 55 % is reached at 300 mm elevation. Below 200 mm oxidation is negligible. Most participants calculated the increase of oxidation between 250 mm and 550 mm and only few of them obtained such high oxidation amounts below 450 mm, namely AEAM, UBOM, GRSA, IKEK, RRCS and UBOS. Good matching between 450 and 1100 mm was reached by IKEK. Essentially correct rates were calculated by the groups MELCOR, ATHLET-CD and KESS-III except GIDM, OKBM, RCCA and UBOA. ICARE2 values are all below 18 %, most SCDAP/RELAP5 values are too high (above 40 %). The highest value of 80 % for 550 mm was calculated by UBOA.

- UO_2 Dissolved by Zr (UO2D)

Fig. 4.16 shows the amount of fuel dissolution by Zr. Posttest analysis revealed dissolution between 11 % and 17 % at elevations between 320 mm and 1100 mm. About 6 % UO_2 was dissolved between 210 mm and 320 mm. Except for RRCS and GRSA, all participants underestimated UO_2 dissolution below 450 mm significantly. The best results were obtained between 750 mm and 850 mm but even there large deviations can be observed for all calculated data. Reasonable values were delivered by OKBM, GRSA and ARSR.

- B_4C Dissolved by Stainless Steel (B4CD)

Among the few participants who calculated this variable (Fig. 4.17) there were two (ARSR and TUDK) who obtained a maximum value of 13 % - 14 %. The rest predicted 100 % dissolution or melting with subsequent relocation between 550 mm and 950 mm, which was measured after the experiment: total dissolution was found between 510 mm and 1250 mm. This was most closely matched by IKEK (450 mm to 1150 mm).

RASI calculated 100 % dissolution from 350 mm to 1250 mm, RRCI from 250 mm to 1250 mm, OKBM from 350 mm to 950 mm and NRII from 550 mm to 950 mm. The SCDAP/RELAP5 group delivered no calculation for this variable due to the lack of an appropriate model.

- Remaining B_4C of Absorber Assembly (B4CR)

This variable is shown in Fig. 4.18 and can be considered complementary to B_4C dissolved by stainless steel. Most participants, and the experimental data confirmed this point of view, although it is also possible to take more than two terms to complete the mass balance. This might be the reason why in the case of ARSR and TUDK the variables are not exactly complementary. The experimental data show 100 % remaining B_4C below 200 mm and no B_4C above 500 mm.

Reasonable results were obtained by GRSA, TUDK, AEAM, NUPM, OKBM, RASI and RRCI. Close approaches to the experimental curve are the calculations of IKEK, UBOM, ARSR and NRII.

b) Mass Distribution After Relocation

- UO_2 Total Mass (UO2T)

Fig. 4.19 shows the total mass distribution of UO_2 after melt relocation. Only slight UO_2 disappearance (due to dissolution or relocation) was measured compared with the initial value of 6.3 kg/m between elevation 100 and 850 mm. From the remaining pellets at this elevation a dissolution of 17 % could be inferred. The partial disappearance at 1050 mm was modeled correctly by all MELCOR participants except GIDM

(who found complete melting even at lower elevations) and by RASI, NRII, UBOI, ENES, RRCS. Complete disappearance of UO_2 was calculated by ARSR (due to overestimation of temperature) and RRCI (due to overestimation of dissolution by Zr).

Between elevations 50 mm to 950 mm, the best results (about 6 kg/m) were obtained by GRSA, RRCA, NRII, RRCI, UBOI, ARSR and ENES. Melt relocation can be seen at about 150 mm. This location was predicted by GRSA, correctly.

- Zr Total Mass (ZTBU)

Fig. 4.20 shows Zr, α-Zr (O) total mass, this means the remaining metallic zirconium which was not oxidized or dissolved. The original value was 2.2 kg/m. After the experiment, no α-Zr at all was found between 350 mm and 950 mm (the cladding remains were completely oxidized). From the calculated results, only GRSA came fairly close to the experiment, but the calculated data show some relocation including the Zr in the unoxidized Zr-U-O crust, which was not included in the measured data. The ICARE2 and SCDAP/RELAP5 group calculated the complete disappearance at metallic Zr above approximately 650 mm and the MELCOR group above 950 mm. All calculated results, which show complete disappearance, show metallic Zr relocation.

- Absorber Material Total Mass (B4CT)

Fig. 4.21 shows the B_4C total mass. Complete disappearance of B_4C Total Mass was found above 500 mm, relocation of melt was found below 300 mm (up to 0.9 kg/m, compared with the original value of 0.654 kg/m). This mass was modeled nearly perfectly by GRSA. All the other participants did not match the data either quantitatively or qualitatively.

- Core Blockage (COBL)

The core blockage is given in Fig. 4.22. The experiment shows core blockage at about -10 % above elevation 650 mm and a maximum core blockage at 30 % at elevation 200 mm. Close to the experimental data are some MELCOR calculations (UBOM, KFIM) and the ICARE2 calculations by NRII and RASI showed the correct tendency. Due to the definition of core blockage in the ISP and mass balance, negative and positive values of core blockage should be calculated. All ATHLET-CD and

SCDAP/RELAP5 participants calculated only positive values, which is related to a different definition of core blockage in the code. (The remaining oxide shell of guide tube and cladding occupies the whole fuel rod and absorber assembly area).

4.4.4 Hydrogen Generation (HRBS, HABS)

The hydrogen generation rate and the accumulated hydrogen generation for both the bundle plus shroud are given in Fig. 4.23 and 4.24 for the time from 4100 s to 4600 s (generation rate) and 3000 s to 5000 s (accumulated generation). The experimental generation rate increases between 4100 s and 4200 s up to 0,12 g/s and remains fairly steady up to 4500 s, then it decreases again. This behavior, both qualitatively and quantitatively, was not predicted by any of the calculations. The analytical results over- or underestimate the experimental data considerably. Only some calculations (e.g. OKBM, IKEK, ARSR) meet the experimental results partly.

This deviation in the generation rate results in large difference in the accumulated hydrogen generation. The experimental value increases up to 68 g during the last 1000 s. This end value is met by one calculation (RRCS), and four others (UBOM, OKBM, UBOA, IKEK) come very close to it.

5 Summary and Assessment

The objectives of the International Standard Problem (ISP) No. 36 on severe fuel damage, which has been proposed by OECD-CSNI, are to analyze and to describe the heat up and meltdown phase of a CORA VVER-type fuel element experiment and to examine the reliability and precision of the severe accident computer codes used. The experiment selected for this ISP was the CORA-W2 test conducted at the Forschungszentrum Karlsruhe (formerly Kernforschungszentrum, KfK). CORA-W2 was designed to investigate the behavior of Russian VVER-type fuel elements under severe accident conditions, including material interactions, liquefaction, melting, relocation, solidification and blockage formation. Contrary to Western-type PWR fuel bundles, the VVER-type fuel bundle contains B_4C as absorber material contained in stainless steel cladding and stainless steel guide tubes. In VVER reactors Zr1%Nb is used as fuel rod cladding material instead of Zircaloy-4.

To challenge the predictive capability of the codes in a most efficient way, the ISP was conducted as a blind exercise, i.e. only the initial and boundary conditions were provided to the participants for performing the calculation. Since some thermal hydraulic boundary condition have not been measured (axial power profile and temperatures at the outer side of shroud insulation and inner side of High Temperature Shield), an ATHLET-CD calculation, knowing the measured temperatures, was carried out to provide the necessary data. The use of these derived data depends on the modelling capability of the codes employed. For this reason the ATHLET-CD calculation (GRSA) discussed in this report was performed by GRS under knowledge of the measured temperature data contrary to the other participants.

The ISP attracted wide support. Representatives of 17 organizations from 9 countries, including 3 non-OECD countries, participated in the ISP performing a total of 22 different calculations. They used the severe accident codes ATHLET-CD, ICARE2, KESS-III, MELCOR, RAPTA and SCDAP/RELAP5. The great number of calculations enabled to group the data according the codes used and to compare the results of each code.

The physical variables compared in the report are basically temperature histories at different location in the bundle, hydrogen generation and core degradation variables of the final bundle state.

At the comparison workshop, held in Moscow, the following observations and conclusions have been drawn by the participants and the ISP organisators:

- Heat-up Phase

The heat-up phase lasted about 1200 s till the onset of oxidation. Most participants predicted the thermal behavior up to the onset of significant oxidation reasonably well, but there was a large spread (Δt = 400 s) in the calculated time of the start of the temperature excursion itself. The thermal behavior of the bundle depends on uncertain experimental conditions as radial heat losses (heat conductivity of shroud insulation) and fluid bypass flow (asymetric inflow). It is concluded that the overall heat balance in the bundle needs to be calculated more accurately.

- Material Interaction and Cladding Failure Criteria

The bundle behavior is greatly influenced by chemical interactions involving B_4C absorber rod material, and interactions between the stainless steel grid spacers and the Zr1%Nb cladding material. Relocation of UO_2 fuel-bearing melts is stronly dependent on the user-specified cladding oxide shell breach criteria. A more realistic cladding breach criteria - based on experimental results - should be developed at least for detailed mechanistic codes. For integral codes improved parametric failure criteria might be sufficient.

The B_4C absorber rod failed relatively early at low temperatures due to eutectic interactions between B_4C and SS cladding as well as the SS guide tube. Subsequently the liquefied and molten absorber rod materials attack the Zr1%Nb fuel rod cladding and chemically dissolves it below its melting point. By these processes also the UO_2 fuel dissolution starts already at lower temperatures.

Regarding the complex material interactions larger differences can be recognized between calculated and measured results because of inappropriate models for material relocation and solidification processes, and the lack of models describing the interactions of absorber rod materials with the fuel rods. In general, the material properties data base for the tested Russian materials was not sufficient in all cases, therefore, the data for Western type of reactors were used.

- Hydrogen Generation

The time dependent hydrogen generation as a result of the cladding/steam reaction is strongly influenced by local events in the bundle such as bypass flows, steam starvation and relocating metallic melts. The large differences of the calculated values for the hydrogen rate to the experimental values far above the uncertainty limits, show that the effective time dependent hydrogen release is not described correctly. Recent experimental results hint for an additional influence of hydrogen absorption by Zircaloy on the time dependent release. For the total H_2-amount, acceptable agreement could be achieved, if the total amount of oxidized zirconium was calculated correctly. Codes which underpredicted the bundle temperature due to overestimated bundle heat losses consequently underestimated the hydrogen generation. Nevertheless, most

codes did not treat the oxidation of stainless steel components and none of them modelled the B_4C oxidation.

- Core Blockage

Some calculations with ICARE2 and MELCOR calculated the axial bundle blockage reasonably well, others (ATHLET-CD and SCDAP/RELAP5) show only positive values because the cladding and pellet are assumed to remain in place following relocation of U-Zr-O melt and the enclosed space inside the remaining oxide shell is not considered to contribute to the flow area. The core blockage depends on refreezing and crust remelting processes which are in general described by simple models. Some improvement regarding oxidation and ternary phase diagrams would reduce the uncertainties. In general the feedback of blockage formation to thermal-hydraulics processes like flow deflection needs to be considered.

- Confidence in Code Prediction

In general the confidence of code predictions decreases with progressing core damage. In consistency to the amount and quality of experimental data available, code models for early phase core degradation particularly up to the onset of core-melt are adequate and verification is possible. Entering into late phase melt progression marked by the onset of substantial formation and relocation of ceramic materials, the level of uncertainty becomes larger. This includes the transition between early and late phase core degradation sequences governed by phenomena like oxidation of complex metallic material mixtures and melts.

Regarding early phase code predictions, the remaining main uncertainties may be subdivided into 4 categories:

- "User effects" in context with the nodalization of the given facility, the used time step size, the numerical treatment of the resulting mathematical system and the choice of reasonable parameters for the operation of the numerous parametric models still existing in the codes.
- Misinterpretation of existing models approaches in the code environment, e.g. wrong definition of radiative heat transfer view factors and unreasonable choice of

material solubility limits in connection with optional correlations for the fuel chemical interactions.

- Weak modelling basis with a still large number of parametric models and further modeling needs particularly as regards chemical interactions, material properties, oxidation of melts and mixtures, and quench phenomena (not covered herein).
- Lack in physical interpretation of certain phenomena (e.g. "flowering", cladding failure mode) and uncertainties and incompleteness in experimental data.

Summarizing, the state-of-the-art in code modelling reflects a high standard of knowledge regarding severe accident phenomena while bearing a high potential for further development at the same time. Consequently, code aided plant analyses will most likely continue to play an increasing role in safety assessment in nuclear and also non-nuclear areas.

- General Observation

In general the ISP showed that basically the codes calculated the overall thermal behavior of CORA-W2 sufficiently correctly. Some material interactions and relocation processes were fairly well simulated. However, for detailed mechanistic codes especially, the modelling of material interactions and component failure (of oxidized fuel rod cladding and absorber rods) needs further improvement. This assessment reflects the early phase core degradation processes only. It is obvious (though not a conclusion from this ISP per se) that further modelling effort and international code assessment exercises should be directed towards late phase core degradation phenomena.

ISP36 demonstrated the importance of assessments of this kind. It provided a forum for the international community enhancing the experience in performing severe fuel damage calculations in comparison with each other and with experimental data. It may have a great impact on further code development, in conjunction with independent peer reviews of individual codes.

6 References

[1] CSNI Standard Problem Procedure
CSNI Report No. 17, November 1989

[2] S. Hagen et al.
Behavior of a VVER-1000 Fuel Element with Boron Carbide/Steel Absorber Tested under Severe Fuel Damage Conditions in the CORA Facility; Results of Experiments CORA-W2
KfK 5363 (1994)

[3] Summary Record of the First ISP36 Workshop on CORA-VVER Test W2
NEA/SEN/SIN/WG2(94)4, March 1994

[4] B. Adroguer et al.
OECD/NEA/CSNI International Standard Problem ISP 38
PHEBUS-SFD B9+ Experiment on the Degradation of a PWR Core Type
Comparison Report, NEA/CSNI/R(92)17, December 1992

[5] C. Gonnier, G. Geoffroy, B. Adroguer
PHEBUS Severe Fuel Damage Programme
ANS Meeting, Portland, July 1991

[6] M. Firnhaber et al.
OECD/NEA/CSNI International Standard Problem No. 31
CORA-13 Experiment on Severe Fuel Damage
CSNI Report NEA/CSNI/R(93)17, July 1993

[7] S. Hagen et al.
Results of Severe Fuel Damage Experiment CORA-13
KfK 5054, February 1993

[8] L. Sepold, Herausgeber
Post-test Examination of the VVER-1000 Fuel Rod Bundle CORA W2;
FZKA 5570 (1995)

[9] M. Firnhaber et al.
Specification of International Standard Problem No. 36
CORA-VVER Experiment on Severe Fuel Damage
GRS-A-2230, January 1995

[10] B.J. Holmes
ISP36 Blind Submission (letter)
Winfrith Technology Centre, Dorchester, 09.07.1994

[11] A.V. Salatov et al.
International Standard Problem ISP36
Code RAPTA-SFD Blind Calculations of CORA-W2 Experiments
All-Russia Scientific Research Institute of Inorganic Materials, ARSRIIM, Moscow 1994

[12] G. Bandini
International Standard Problem ISP36: CORA-W2 Experiment on Severe Fuel Damage
ENEA Report, Bologna, June 1994

[13] Y. Sorokin, G. Volkov
Blind Post-Test Calculations for the CORA-W2 Experiment with MELCOR 1.8.2 Code
Experimental and Design Organisation "Gidropress", Podolsk 1994

[14] J. Bestele
Nachrechnung des Versuchs CORA-W2 mit dem Programm ATHLET-CD
Technische Notiz GRS, Garching, July 1994

[15] K. Müller
Beitrag des IKE zum ISP36 (letter)
Universität Stuttgart, Institut für Kernenergetik und Energiesysteme IKE
Stuttgart-Vaihingen, 15.07.1994

[16] G. Gyenes
ISP36 calculation results
KFKI Atomic Energy Research Institute, Budapest, 21.06.1994

[17] L. Belovsky, M. Valach
Simulation of the CORA-W2 Experiment by modified ICARE2-V2mod1 in the frame of OECD-CSNI ISP36, Results of a Blind Calculation
Nuclear Research Institute Rez, June 1994

[18] Y. Kiso
Results of ISP36 (letter)
NUPEC Nuclear Power Engineering Corporation, Tokyo, 13.07.1994

[19] A.S. Gusev, V.S. Kuul, A.A. Falkov
International Standard Problem ISP36, CORA-W2 blind calculation with MELCOR 1.8.2
OKB Mechanical Engineering (OKBM), Nizhny Novgorod 1994

[20] B. Dobrov, I. Plotnikova
Main results of simulation experiment with assembly VVER/1000 CORA-W2 on a code ATHLET-CD-01.V
Nuclear Safety Institute, Russian Academy of Sciences, Moscow 1994

[21] A. Kisselev, G. Samoilova, A. Deryugin
Main results of simulation experiment with assembly VVER/1000 CORA-W2 on a code IDARE2 mod 1.0
Nuclear Safety Institute, Russian Academy of Sciences, Moscow 1994

[22] V.E. Radkevich
International Standard Problem ISP36 Post-Test Blind Calculations for CORA-W2 Experiment
Research and Development Institute of Power Engineering (RDIPE), Moscow, June 1994

[23] M.A. Maltchevski
Blind Pretest Calculation of International Standard Problem 36 'COrA-W2' with the computer code ATHLET-CD
Institute of Nuclear Reactors of the Russian Research Center Kurchatov Institute, RRC KI, Moscow, June 1994

[24] N. Sulhanishvili, F. Jacq
International Standard Problem ISP36 Post-Test Blind Calculations with ICARE2/V2MOD1 Code for CORA-W2 Experiment on Severe Fuel Damage
Nuclear Safety Institute, RRC KI, Moscow and Institut de Protection et de Surete Nucleaire de Cadarache, CEA, June 1994

[25] S. Pylev
Results of SCDAP/RELAP5/MOD3.1 Blind Calculations on the Severe Fuel Damage CORA-W2 Experiment
Nuclear Safety Institute RRC "Kurchatov Institute", Moscow, 1994

[26] S. Kretschmer, V. Sanchez
Report for the International Standard Problem ISP36: CORA-W2 Experiment on Severe Fuel Damage Calculations with the Code KESS-Mod1.0-WWER
TU Dresden, Institute for Power Engineering, Dresden, June 1994

[27] T. Steinrötter, J. Paulus, U. Brockmeier, H. Unger
Participation in ISP36 - CORA-W2 Calculations with ATHLET/CD
Ruhr-University of Bochum, Department of Nuclear and New Energy Systems, Bochum

[28] A. Shwetsow, T. Steinrötter, J. Paulus, U. Brockmeier, H. Unger
Participation in ISP36 - CORA-W2 Calculations with ICARE2
Ruhr-University of Bochum, Department of Nuclear and New Energy Systems, Bochum

[29] N. Pohl, T. Steinrötter, J. Paulus, U. Brockmeier, H. Unger
Participation in ISP36 - CORA-W2 Calculations with MELCOR
Ruhr-University of Bochum, Department of Nuclear and New Energy Systems, Bochum

[30] T. Steinrötter, J. Paulus, U. Brockmeier, H. Unger
Participation in ISP36 - CORA-W2 Calculations with RELAP5/SCAP
Ruhr-University of Bochum, Department of Nuclear and New Energy Systems, Bochum

[31] E. Pekkarinen
ISP36 result (letter)
VTT Energy, Nuclear Energy, Espoo, 29.06.1994

[32] K. Trambauer
Entwicklung des Rechnerprogramms ATHLET-SA zur Analyse schwerer Störfälle - Abschlußbericht
GRS-A-1937, August 1992

[33] R. Gonzalez, P. Chatelard, F. Jacq
ICARE2 - A Computer Program for Severe Core Damage Analysis in LWRs
Institut de Protection et de Surete Nucleaire, Note Technique SEMAR 93/33, CEA, France 1993

[34] K.D. Hocke, M. Bürger, A. Schatz
KESS III - Ein Programmsystem zur Simulation auslegungsüberschreitender Störfälle in Leichtwasserreaktoren
Institut für Kernenergie und Energiesysteme, IKE 2-93, Universität Stuttgart, Januar 1991

[35] R.M. Summers et al.
MELCOR 1.8.3: Computer Code Manual, Vol. 2, Reference Manuals and Programmers Guides,
Sandia National Laboratories, Albuquerque, New Mexico, July 1994

[36] RAPTA
(to be published)

[37] C.M. Allison et al.
SCDAP/RELAP5/MOD3.1 Code Manual, Vol. 1-5
NUREG/CR-6150, EGG-2720, Idaho National Engineering Laboratory, Idaho, October 1993

[38] M.S. Veshchunov, P. Hofmann
Dissolution of Solid UO_2 by Molten Zircaloy
Journal of Nuclear Materials, Vol. 209, pp. 27-40, 1994

Acknowledgment

The authors would like to acknowledge the financial support of the German Ministry for Education, Science, Research and Technology (Contract No. RS 871A), the financial support of the Ministry of Nuclear Power of the Russian Federation for the analytical and experimental work performed in Russia and the technical comments of the members of the Principal Working Group No. 2 and the Task Group on "In Vessel Degraded Core Behavior" of the OECD-CSNI. The experimental work at Forschungszentrum Karlsruhe was supported by the CEC in part-fulfillment of the Contract FI3S-CT92-0001 CORE DEGRADATION.

Also the authors would like to express their gratitude to V. Noack, L. Sepold and G. Schanz from Forschungszentrum Karlsruhe, to Y. Degaltsev from Kurchatov Institute, Moscow, A. Goryachev from Reasearch Institute for Atomic Reactors, Dimitrovgrad, and to N. B. Sokolov from A. A. Bochvar Institute, Moscow, as well as to their co-workers for performing the experiment and the extensive post-test material investigations, both in Germany and Russia.

Thanks also to T. J. Haste for critically reviewing the report.

Table 4.1: Organizations, Analysts and Codes Used

Legend	Institution		Analysts	Code Used
AEAM	AEA	Winfrith, UK	B. Holmes	MELCOR 1.8.2
ARSR	ARSRIIM	Moscow, Russia	A.V. Salatov L.N. Andreeva-Andrievskaya F.Y. Vlasov O.A. Nechaeva	RAPTA-SFD
ENES	ENEA	Bologna, Italy	G. Bandini	SCDAP/RELAP5/MOD2
GIDM	Gidropress	Podolsk, Russia	Y. Sorokin G. Volkov	MELCOR 1.8.2
GRSA	GRS	Garching, Germany	J. Bestele	ATHLET-CD MOD 1.1B-0.1V
IKEK	IKE	Stuttgart, Germany	K. Müller	KESS / MOD 1.3
KFIM	KFKI	Budapest, Hungary	G. Gyenes	MELCOR 1.8.2
NRII	NRI	Rez. Czech Republic	L. Belovsky M. Valach	ICARE2 V2 MOD 1 (Dec. 93)
NUPM	NUPEC	Tokyo, Japan	Y. Kiso	MELCOR 1.8.2, COR modified
OKBM	OKB	Nizhny Novgorod, Russia	A.S. Gusev V.S. Kuul A.A. Falkov	MELCOR 1.8.2

Table 4.1: Organizations, Analysts and Codes Used (Continuation)

Legend	Institution		Analysts	Code Used
RASA	NSI RAS	Moscow, Russia	B. Dobrov I. Plotnikova	ATHLET-CD MOD 1.1B-0.1V
RASI	NSI RAS	Moscow, Russia	A. Kisselev G. Samoilova A. Deryugin	ICARE2 MOD 1.0
RDIS	RDIPE	Moscow, Russia	V.E. Radkevich	SCDAP/RELAP5/MOD 2.5
RRCA	INR RRC KI	Moscow, Russia	M.A. Maltchevski	ATHLET-CD MOD 1.1B-0.1V
RRCI	NSI RRC KI CEA	Moscow, Russia Cadarache, France	N. Sulhanishvili F. Jacq	ICARE2 V2 MOD 1.0
RRCS	NSI RRC KI	Moscow, Russia	S. Pylev	SCDAP/RELAP5/MOD 3.1
TUDK	TU	Dresden, Germany	S. Kretschmer V. Sanchez	KESS-MOD 1.0-WWER (KESS III)
UBOA UBOI UBOM UBOS	University of Bochum	Bochum, Germany	Th. Steinrötter J. Paulus	ATHLET-CD MOD 1.1B-0.1V ICARE2-V2-MOD 0 MELCOR 1.8.2 SCDAP/RELAP5/MOD 3.0 7
VTTS	VTT	Espoo, Finland	E. Pekkarinen	SCDAP/RELAP5/MOD 3 V7 af

Table 4.2a: Nodalization Characteristics for ISP36 Calculations (ATHLET and KESS)

	Participants				
Nodalization	**GRSA**	**RASA**	**UBOA**	**IKEK**	**TUDK**
Number of axial meshes	13 -200 mm up to 1250 mm	17 -200 mm up to 1470 mm	13 -200 mm up to 1470 mm	18	
Radial meshing	3 radial rings: 1 + 6 + 12 rods			3 radial rings: 3 representative segments	3 radial rings: 1 + 6 + 12 rods
Treatment of shroud ?	Yes				
Treatment of absorber rod ?	Yes		No	Yes	
Treatment of grid spacer ?	Only flow resistance modelled			Yes. Eutectic melt formation	Yes. Heat-up and melt down processes
Additional comments	HTS modelled. Bundle flow channel subdivided into two subchannels	-	HTS modelled. Bundle flow channel subdivided into two subchannels.		

Table 4.2b: Nodalization Characteristics for ISP36 Calculations (ICARE2 and RAPTA)

	Participants				
Nodalization	**NRII**	**RASI**	**RRCI**	**UBOI**	**ARSR**
Number of axial meshes	48	18	15	48 30 axial meshes in the heated region	10
Radial meshing	8 representative rods	5 representative rods		5 representative rods: 3 heated rods, 1 unheated rod, 1 absorber rod	4 representative rods
Treatment of shroud ?	Yes				
Treatment of absorber rod ?	Yes		Yes, but AIC absorber material used	Yes	
Treatment of grid spacer ?	Yes			No	Yes

Table 4.2c: Nodalization Characteristics for ISP36 Calculations (MELCOR)

	Participants					
Nodalization	**AEAM**	**GIDM**	**KFIM**	**NUPM**	**OKBM**	**UBOM**
Number of axial meshes	4 hydraulic cells in the core, 19 cells for rods, 12 hydraulic cells in the bypass	15	13	15	19	4 hydraulic cells in the core, 17 cells for rods, 1 hydraulic cell in the bypass
Radial meshing	3 radial rings	1 radial ring	3 radial rings: 1) absorber rod + 5 unheated rods 2) 13 heated rods 3) shroud	4 radial rings: 1) central rod 2) unheated rods + control rod 3) heated rods 4) shroud	3 radial rings: 1) central rod 2) unheated rods + control rod 3) heated rods	4 radial rings 4th ring is shroud
Treatment of shroud ?	Represented by BWR canister model					
Treatment of absorber rod ?	B_4C and steel masses input for each axial level. BWR control rod model activated					
Treatment of grid spacer ?	Mass added at the grid spacer positions					

Table 4.2d: Nodalization Characteristics for ISP36 Calculations (SCDAP/RELAP5)

	Participants				
Nodalization	**ENES**	**RDIS**	**RRCS**	**UBOS**	**VTTS**
Number of axial meshes	10 corresponding to the heated section		14	14 -220 mm up to 1470 mm	10 corresponding to the heated section
Radial meshing	3 SCDAP-components: 1) fuel rods 2) unheated rods 3) absorber rod		4 SCDAP- components: 1) unheated rods 2) heated rods 3) absorber rod 4) shroud + insulation	4 SCDAP-components: 1) unheated rods 2) central heated rod 3) heated rods 4) shroud + insulation	4 SCDAP-components: 1) unheated rods 2) heated rods 3) absorber rod 4) shroud + insulation
Treatment of shroud ?	Yes		Yes		Yes
Treatment of absorber rod ?	Yes		Yes. Control rod was modelled as BWR control blade box in cylindrical interpretation	No	Yes
Treatment of grid spacer ?	Only treated as a flow resistance		Thermal behaviour and flow resistance	Only treated as a flow resistance	Thermal behaviour and flow resistance

Table 4.3a: Characteristics of the Thermal Hydraulic Models Used for ISP36 Calculations (ATHLET and KESS)

	Participants				
Thermal Hydraulics	**GRSA**	**RASA**	**UBOA**	**IKEK**	**TUDK**
3-, 4-, 5- or 6-equation model used? (Equations for non-condensables not counted)	5-equation model	4-equation model	5-equation model	4-equation model	
Non-condensables treated?	No			Yes	
Feedback between geometry changes of structures and flow pathes ?	No			Yes	No
Flow resistance of grid spacers modelled ?	Yes			No	
Fluid heatup due to radiative heat transfer taken into account ?	No	Yes	No		
Heat transfer coefficients in lower bundle region adapted to an account for bundle crossflow situation at steam inlet ?	Yes Reduced hydraulic diameter	No	Yes Reduced hydraulic diameter between 0 mm and 400 mm	Yes Special correction model for calculation of the heat transfer coefficient	
Additional information	Heat capacity of Ar is taken into account by an equivalent steam flow	Quantity of non-condensables was treated for cladding oxidation	Heat capacity of Ar is taken into account by an equivalent steam flow	-	-

Table 4.3b: Characteristics of the Thermal Hydraulic Models Used for ISP36 Calculation (ICARE2 and RAPTA)

	Participants				
Thermal Hydraulics	**NRII**	**RASI**	**RRCI**	**UBOI**	**ARSR**
3-, 4-, 5- or 6-equation model used ? (Equations for non-condensables not counted)	3-equation model				
Non-condensables treated ?	Yes			Yes (only Ar)	Yes
Feedback between geometry changes of structures and flow pathes ?	Yes				
Flow resistance of grid spacers modelled ?	No		Yes	No	
Fluid heatup due to radiative heat transfer taken into account ?	Yes				No
Heat transfer coefficients in lower bundle region adapted to an account for bundle crossflow situation at steam inlet ?	Yes			No	-

Table 4.3c: Characteristics of the Thermal Hydraulic Models Used for ISP36 Calculations (MELCOR)

	Participants					
Thermal Hydraulics	**AEAM**	**GIDM**	**KFIM**	**NUPM**	**OKBM**	**UBOM**
3-, 4-, 5- or 6-equation model used? (Equations for non-condensables not counted)	6-equation model					
Non-condensables treated ?	Yes					
Feedback between geometry changes of structures and flow pathes ?	Yes. But only for relocation.					
Flow resistance of grid spacers modelled ?	No	Yes	No		Yes	No
Fluid heatup due to radiative heat transfer taken into account ?	Yes			No	Yes	
Heat transfer coefficients in lower bundle region adapted to an account for bundle crossflow situation at steam inlet	No	-	No			

Table 4.3d: Characteristics of the Thermal Hydraulic Moduls Used for ISP36 Calculations (SCDAP/RELAP5)

	Participants				
Thermal Hydraulics	**ENES**	**RDIS**	**RRCS**	**UBOS**	**VTTS**
3-, 4-, 5- or 6-equation model used ? (Equations for non-condensables not counted)	6-equation model		6-equation model		6-equation model
Non-condensables treated ?	Yes (Ar + H_2)		Yes (Ar + H_2)		Yes (Ar + H_2)
Feedback between geometry changes of structures and flow pathes ?	Yes		Yes		Yes
Flow resistance of grid spacers modelled ?	Yes		Yes		Yes
Fluid heatup due to radiative heat transfer taken into account ?	Yes		Yes		Yes
Heat transfer coefficients in lower bundle region adapted to an account for bundle crossflow situation at steam inlet ?	No		No		No

Table 4.4a: Modelling of Structure Heat-up in ISP36 (ATHLET and KESS)

	Participants				
Core Heat-up	**GRSA**	**RASA**	**UBOA**	**IKEK**	**TUDK**
Used structure models: a) Core structures b) Heat structures	a) Rods b) Shroud and HTS	a) Rod structures	a) Rods b) Shroud and HTS	a) All components except: b) Grid spacer and HTS	b) Bundle, shroud and HTS
Electrical heater rod model used ?	Yes, electrical resistance only depends on rod temperature				
Used view factors for: a) Radial between fuel rods, b) radial to shroud, c) axial to bottom/top structures	a) F = 0.52 b) F = 0.17 c) Bottom: F = 0.081 Top: F = 0.001	a) + b) + c) All calculated	a) F = 0.52 b) F = 0.17 c) Bottom: F = 0.081 Top: F = 0.001	a) + b) + c) All calculated Radiation shape factors for cylindrical assemblies "The American Society of Mech. Eng." Paper 56-17-144	a) Between radial zone 1 and 2: F = 0.26, between radial zone 2 and 3: F = 0.534, between rod and absorber rod: F = 0.714 b) F = 1 c) F = 1
Treatment of the thermal behavior of grid spacer ?	No				Yes Radiative and convective heat transfer
Other energy sources depart from electrical power considered ?	Only oxidation reactions considered				

Table 4.4b: Modelling of Structure Heat-up Used in ISP36 (ICARE2 and RAPTA)

	Participants				
Core Heat-up	**NRII**	**RASI**	**RRCI**	**UBOI**	**ARSR**
Used structure models: a) Core structures b) Heat structures	ICARE only provides so called macro components				Models used are similar to core structure models
Electrical heater rod model used ?	Yes, electrical resistance only depends on local rod temperature				
Used view factors for: a) Radial between fuel rods, b) radial to shroud, c) axial to bottom/top structures	a) Calculated b) F = 0 (no radiation) c) F = 0 (no radiation)	a) + b) Calculated c) Not modelled	a) Calculated b) + c) Not calculated	a) Calculated b) Calculated c) Not modelled	a) Calculated b) Calculated c) Not modelled
Treatment of the thermal behaviour of grid spacer ?	Yes			No	
Other energy sources depart from electrical power considered ?	Oxidations reactions and chemical material interactions				Only oxidation reactions

Table 4.4c: Modelling of Structure Heat-up in ISP36 (MELCOR)

	Participants					
Core Heat-up	**AEAM**	**GIDM**	**KFIM**	**NUPM**	**OKBM**	**UBOM**
Used structure models: a) Core components b) Heat structures	a) Rods, grid spacer b) Tungsten, molybdenum, copper, shroud insulation, HTS	a) Rods, grid spacer, shroud b) Shroud insulation, HTS	a) - b) Whole bundle structures	a) Rods, shroud b) Shroud insulation	a) Rods, grid spacer, shroud b) Shroud insulation, HTS	
Electrical heater rod model used ?	Yes Separate user routine, electrical resistance only depends on local rod temperature		Yes, but for ISP36 input of power distribution via table	Yes Separate user routine, electrical resistance only depends on local rod temperature		
Used view factors for: a) Radial between fuel rods, b) radial to shroud, c) axial to bottom/top structures ?	a) Radial: F = 0.648, axial: F = 0.6 b) F = 0.2 c) Not modelled	a) Radial: F = 0.25 axial: F = 0.25 b) F = 0.25 c) F = 0.25	a) Radial: F = 0.16 b) F = 0.25 c) F = 0.25	a) Radial: F = 0.36 b) F = 0.36 c) Not modelled	a) Radial: F = 0.7 b) F = 1.0 c) F = 0.25	a) Radial: F = 0.25 axial: F = 0.25 b) F = 0.25 c) Not modelled
Treatment of the thermal behaviour of grid spacer ?	No	Yes	No		Yes	No
Other energy sources depart from electrical power considered ?	Only oxidation reactions					

Table 4.4d: Modelling of Structure Heat-up Used in ISP36 (SCDAP/RELAP5)

	Participants				
Core Heat-up	**ENES**	**RDIS**	**RRCS**	**UBOS**	**VTTS**
Used structure models: a) Core structures b) heat structures	a) Rods and shroud (SCDAP components)		a) Rods and shroud b) HTS	a) Rods, shroud and shroud insulation (heated region) b) Rods and shroud below and above heated region, HTS	a) Rods, shrouds and shroud insulation (heated region SCDAP components)
Electrical heater rod model used ?	Yes, electrical resistance only depends on local rod temperature		Yes, electrical resistance only depends on local rod temperature		Yes
Used view factors for: a) Radial between fuel rods b) radial to shroud c) axial to bottom/top structures	a) + b) Treated c) Not modelled		a) + b) Treated c) Not modelled	a) Central rod - unheated rods: F = 0.133, central rod - heated rods: F = 0.017, heated rods - unheated rods: F = 0.744 b) Central rod - shroud: F = 0.0, unheated rods - shroud: F = 0.028, heated rods - shroud: F = 0.845 c) Not modelled	a) + b) treated c) not modelled
Treatment of the thermal behaviour of grid spacer ?	Yes		Yes	No	Yes
Other energy sources depart from electrical power considered ?	Only oxidation reactions		Only oxidation reactions		Only oxidation reactions

Table 4.5a: Details of the Oxidation Models Used in ISP36 (ATHLET and KESS)

	Participants				
Oxidation and H_2-Generation	**GRSA**	**RASA**	**UBOA**	**IKEK**	**TUDK**
Parabolic rate equations or diffusion models used ?	Parabolic rate equation by Sokolov	Parabolic rate equations	Parabolic rate equation by Cathcart and Urbanic/Heidrick	Parabolic rate equation	Parabolic rate equation measured at DRESSMAN-facility
Oxidation limitation by the following conditions: a) Steam starvation b) diffusion resistance	a) Yes b) No				
Specifics of Zr 1 % Nb considered ?	Only oxidation process	Only density, specific heat capacity and thermal conductivity	No	No	Only oxidation process
B_4C oxidation treated ?	No				
Oxidation of fragments, melt and frozen U-Zr-O mixtures considered ?	Only oxidation of refrozen U-Zr-O mixtures			Oxidation of melt and refrozen U-Zr-O mixtures	Only oxidation of melt
Double-sided oxidation calculated ?	No				
Termination of the oxidation due to relocated melt ?	No	Yes	No	Yes	No
Grid spacer and shroud oxidation calculated ?	Only shroud oxidation				Grid spacer and shroud oxidation
Additional comments	Limitation of oxidation by two channel modelling	-	-	-	-

Table 4.5b: Details of the Oxidation Models Used in ISP36 (ICARE2 and RAPTA)

	Participants				
Oxidation and H_2-Generation	**NRII**	**RASI**	**RRCI**	**UBOI**	**ARSR**
Parabolic rate equations or diffusion models used ?	Parabolic rate equations	Sophisticated diffusion equations	Parabolic rate equations		
Oxidation limitation by the following conditions: a) Steam starvation b) diffusion resistance	a) Yes b) Yes	a) Yes b) -	a) Yes b) Yes		a) Yes b) No
Specifics of Zr 1 % Nb considered ?	Only cladding oxidation	Yes			
B_4C oxidation treated ?	No				
Oxidation of fragments, melt and frozen U-Zr-O mixtures considered ?	Oxidation of fragments, melt and frozen U-Zr-O treated		Only oxidation of melt treated	Oxidation of fragments, melt and frozen U-Zr-O treated	Only oxidation of melt and frozen U-Zr-O treated
Double-sided oxidation calculated ?	Yes				No
Termination of the oxidation due to relocated melt ?	Yes. Only relocated melt can oxidize				No
Grid spacer and shroud oxidation calculated ?	Only shroud oxidation. Basic oxidation model	Only shroud oxidation. Basic diffusion module UZRO for Zr components	Yes Basic oxidation models	Only shroud oxidation. Basic oxidation model.	

Table 4.5c: Details of the Oxidation Models Used in ISP36 (MELCOR)

	Participants					
Oxidation and H_2-Generation	AEAM	GIDM	KFIM	NUPM	OKBM	UBOM
Parabolic rate equations or diffusion models used ?	Parabolic rate equations					
Oxidation limitation by the following conditions: a) Steam starvation b) diffusion resistance	a) No b) No	a) Yes b) No				
Specifics of Zr 1 % Nb considered ?	Yes			No	Yes	
B_4C oxidation treated ?	No					
Oxidation of fragments, melt and frozen U-Zr-O mixtures considered ?	Yes					
Double-sided oxidation calculated ?	No	Yes	No			
Termination of the oxidation due to relocated melt ?	Yes, but area submerged can be less than total area	-	-	Yes, but area submerged can be less than total area		
Grid spacer and shroud oxidation calculated ?	Yes. Basic oxidation models used.				Shroud oxidation with basic model, steel oxidation turned off	Yes. Basic oxidation models used

Table 4.5d: Details of the Oxidation Models Used in ISP36 (SCDAP/RELAP5)

	Participants				
Oxidation and H_2-Generation	**ENES**	**RDIS**	**RRCS**	**UBOS**	**VTTS**
Parabolic rate equations or diffusion models used ?	Parabolic rate equation		Parabolic rate equation with ARSRIIM growth rate constants	Parabolic rate equation Cathcart and Urbanic/Heidrick	Parabolic rate equation
Oxidation limitation by the following conditions: a) Steam starvation b) diffusion resistance	a) Yes b) No		a) Yes b) No		a) Yes b) No
Specifics of Zr 1 % Nb considered ?	No		Only for cladding oxidation	No	No
B_4C oxidation treated ?	No		No		No
Oxidation of fragments, melt and frozen U-Zr-O mixtures considered ?	Yes		Yes		-
Double-sided oxidation calculated ?	Yes		Yes		Yes
Termination of the oxidation due to relocated melt ?	No		Yes	No	Yes
Grid spacer and shroud oxidation calculated ?	Only shroud oxidation calculated (basic oxidation model)		Only shroud oxidation calculated (basic oxidation model)		Only shroud oxidation calculated

Table 4.6a: Models for Mechanical Rod Behaviour and Corresponding User Defined Criteria in ISP36 (ATHLET and KESS)

	Participants				
Mechanical Rod Behaviour	**GRSA**	**RASA**	**UBOA**	**IKEK**	**TUDK**
Ballooning of rods modelled ?	Yes. Internal pressure was given as function of time. Failure due to strain / stress	Yes	Yes. Separate model	Yes	Yes. ZrNb1 specific creeping equation of Solgani used
Changes of material properties due to oxidation considered ?	Yes	No		Yes	No
Criterion for fragmentation of solid core structures ?	Not modelled		Not modelled	Not calculated	

Table 4.6b: Models for Mechanical Rod Behaviour and Corresponding User Defined Criteria in ISP36 (ICARE2 and RAPTA)

	Participants				
Mechanical Rod Behaviour	**NRII**	**RASI**	**RRCI**	**UBOI**	**ARSR**
Ballooning of rods modelled ?	Yes		No	Yes	
Changes of material properties due to oxidation considered ?	No	Yes	No		
Criterion for fragmentation of solid core structures ?	No	a) ZrO2 thickness < 0.35 mm and T_{ZrO2} > 2240 K or b) T_{ZrO2} > 2500 K	No	a) ZrO2 thickness < 0.35 mm and T_{ZrO2} > 2250 K or b) T_{ZrO2} > 2500 K	No

Table 4.6c: Models for Mechanical Rod Behaviour and Corresponding User Defined Criteria Used in ISP36 (MELCOR)

	Participants					
Mechanical Rod Behaviour	**AEAM**	**GIDM**	**KFIM**	**NUPM**	**OKBM**	**UBOM**
Ballooning of rods modelled ?	No ballooning model implemented					
Changes of material properties due to oxidation considered ?						
Criterion for fragmentation of solid core structures ?	No	Minimum thickness for unoxidized Zr = 0.01 mm	Minimum thickness for unoxidized Zr = 0.0 mm, minimum thickness for SS = 0.15 mm	Critical minimum thickness of unoxidized intact material	Critical minimum thickness of unoxidized intact material: Cladding = 0 mm, other structures = 0.1 mm	Yes, but not used for ISP36

Table 4.6d: Models for Mechanical Rod Behaviour and Corresponding User Defined Criteria in ISP36 (RELAP5 / SCDAP)

	Participants				
Mechanical Rod Behaviour	**ENES**	**RDIS**	**RRCS**	**UBOS**	**VTTS**
Ballooning of rods modelled ?	Yes		No	Yes	Yes
Changes of material properties due to oxidation considered ?	No		No		No
Criterion for fragmentation of solid core structures ?	Not calculated		SCDAP default values were used	Not calculated	SCDAP default values were used

Table 4.7a: Chemical Interactions for ISP36 (ATHLET and KESS)

	Participants				
Chemical Interactions	**GRSA**	**RASA**	**UBOA**	**IKEK**	**TUDK**
List of chemical interactions calculated	UO_2 / liquid Zr	-	UO_2 / liquid Zr	UO_2 / liquid Zr, B_4C / SS, Zr / SS	UO_2 / liquid Zr, B_4C / SS, Zr / SS (grid spacer)
UO_2 dissolution by liquid Zr: a) Which kind of model ? b) Which kind of equilibrium condition ?	a) Hofmann b) Eutectic concentration (XZRMIN = 0.2)	-	a) Hofmann b) Eutectic concentration (XZRMIN = 0.2)	a) Kim & Olander b) Liquidus line	a) Hofmann b) Liquidus line
Multi material interactions considered ?	No				
Treatment of interaction between dissolution process and cladding oxidation ?	No				

Table 4.7b: Chemical Interactions for ISP36 (ICARE2 and RAPTA)

	Participants				
Chemical Interactions	**NRII**	**RASI**	**RRCI**	**UBOI**	**ARSR**
List of chemical interactions calculated	UO_2 / liquid Zr, UO_2 / solid Zr, B_4C / SS	UO_2 / liquid Zr, UO_2 / solid Zr, ZrO_2 / liquid Zr	UO_2 / liquid Zr UO_2 / solid Zr ZrO_2 / liquid Zr	UO_2 / liquid Zr, UO_2 / solid Zr ZrO_2 / liquid Zr	UO_2 / liquid Zr, UO_2 / solid Zr, B_4C / SS, Zr / SS
UO_2 dissolution by liquid Zr: a) Which kind of model ? b) Which kind of equilibrium condition ?	a) Kim & Olander b) Liquidus line	a) Module UZRO (diffusion approach) b) -	a) Kim & Olander b) Liquidus line		a) Hofmann b) -
Multi material interactions considered ?	Yes				No
Treatment of interaction between dissolution process and cladding oxidation ?	No	Yes		No	

Table 4.7c: Chemical Interactions for ISP36 (MELCOR)

	Participants					
Chemical Interactions	**AEAM**	**GIDM**	**KFIM**	**NUPM**	**OKBM**	**UBOM**
List of chemical interactions calculated	UO_2 / liquid Zr, ZrO_2 / liquid Zr	UO_2 / liquid Zr, ZrO_2 / liquid Zr, B_4C / SS, Zr / SS, B_4C / Zr		UO_2 / liquid Zr, ZrO_2 / liquid Zr, Zr / SS	UO_2 / liquid Zr, ZrO_2 / liquid Zr, B_4C / SS Zr / SS, B_4C / Zr	UO_2 / liquid Zr, ZrO_2 / liquid Zr, B_4C / SS Zr / SS (only temperature criterion)
UO_2 dissolution by liquid Zr: a) Which kind of model ? b) which kind of equilibrium condition ?	a) Hofmann, b) When mixture enthalpy falls below liquidus enthalpy	a) Eutectic model was inactive, b) -	a) Hofmann, b) Liquidus line and parabolic rate limitation	a) Sokolov, b) Liquidus line and parabolic rate limitation	a) Hofmann, b) Liquidus line	a) Hofmann (without saturation phase) b) When mixture enthalpy falls below liquidus enthalpy
Multi material interactions considered ?	Model with up to two solids able to be attacked by a liquid component	-	Model with up to two solids able to be attacked by a liquid component			
Treatment of interaction between dissolution process and cladding oxidation ?	No	-	No			

Table 4.7d: Chemical Interactions for ISP36 (SCDAP/RELAP5)

	Participants				
Chemical Interactions	**ENES**	**RDIS**	**RRCS**	**UBOS**	**VTTS**
List of chemical interactions calculated	UO_2 / liquid Zr		UO_2 / liquid Zr UO_2 / solid Zr, ZrO_2 / liquid Zr	UO_2 / liquid Zr	UO_2 / liquid Zr
UO_2 dissolution by liquid Zr: a) Which kind of model ? b) Which kind of equilibrium condition ?	a) Hofmann b) Solidus line		a) Hofmann b) Solidus line		a) Hofmann b) Solidus line
Multi material interactions considered ?	No		Yes. Simultaneous dissolution of UO_2 and ZrO_2 by liquid Zr	No	No
Treatment of interaction between dissolution process and cladding oxidation ?	No		No		No

Table 4.8a: Variables Defined for the Relocation Models Used in ISP36 (ATHLET and KESS)

	Participants				
Material Relocations	**GRSA**	**RASA**	**UBOA**	**IKEK**	**TUDK**
Which cladding failure criterion has been used ?	Temperature criterion for fuel rod (TALHIGH = 2200 K) and guide tube (CRTVER = 1523 K)	Combination of: Minimum ZrO_2 thickness and maximum ZrO_2 temperature	Combination of: Maximal ZrO_2 thickness and ZrO_2 temperature (TALLOW = 2450 K and DDTAL < 0.6 mm)	Temperature criterion: T = 2053 K	Temperature criterion: T = 2133 K
Relocation of melt: a) Relocation inside of cladding possible ? b) Film or rivulet type of outside relocation ? c) Relocation velocity ?	a) No b) Rivulets; wetted perimeter fraction: Fuel rod = 0.125, control rod = 0.25 c) Fuel rod = 0.3 m/s, control rod = 1.09 m/s	a) No b) Specific film at wetted segment; wetted perimeter increasing during time c) -	a) No b) Rivulets; wetted perimeter fraction: Fuel rod = 0.125 c) 0.01 m/s	a) No b) Rivulets; wetted perimeter fraction: Fuel rod = 0.2 c) 0.2 m/s	a) No b) Rivulets; wetted perimeter fraction: Fuel rod = 0.13 c) 0.3 m/s
Melting of refrozen melts possible ?	No				
Radial relocation in case of core blockage possible ?	No				
Relocation of solid fragments along with relocating melts possible ?	No			Separate model is available	No

Table 4.8b: Variables Defined for the Relocation Models Used in ISP36 (ICARE2 and RAPTA)

	Participants				
Material Relocations	**NRII**	**RASI**	**RRCI**	**UBOI**	**ARSR**
Which cladding failure criterion has been used ?	Minimum ZrO_2 thickiness = 0.3 mm, maximum ZrO_2 temperature = 2045 K	Combination of: Minimum ZrO_2 thickness = 0.35 mm and maximum ZrO_2 temperature = 2240 K	Combination of: Minimum ZrO_2 thickness = 0.3 mm and maximum ZrO_2 temperature > 2250 K or maximum ZrO_2 temperature > 2500 K		Melt temperature of cladding (Zr1%Nb or SS)
Relocation of melt: a) Relocation inside of cladding possible ? b) Film or rivulet type of outside relocation ? c) Relocation velocity ?	a) No b) Rivulets; wetted perimeter fractions: Cladding = 0.08, shroud = 0.10 c) 0.6 m/s	a) No b) Droplets and rivulets; wetted perimeter calculated by the code c) Calculated by the code	a) No b) Rivulets; wetted perimeter fraction: 0.3 c) 0.6 m/s		a) No b) Film c) Constant velocity
Melting of refrozen melts possible ?	Yes				
Radial relocation in case of core blockage possible ?	No		Yes	No	
Relocation of solid fragments along with relocating melts possible ?	Yes	No	Yes		Yes. Only solid B_4C

Table 4.8c: Variables Defined for the Relocation Models Used in ISP36 (MELCOR)

	Participants					
Material Relocations	**AEAM**	**GIDM**	**KFIM**	**NUPM**	**OKBM**	**UBOM**
Which cladding failure criterion has been used ?	Minimum ZrO_2 thickness = 0.5 mm, maximum ZrO_2 temperature = 2100 K	Combination of: Minimum ZrO_2 thickness and ZrO_2 temperature	Minimum ZrO_2 thickness = 0 mm, maximum ZrO_2 temperature = 2500 K	Minimum ZrO_2 thickness = 1 mm, maximum ZrO_2 temperature = 2500 K	Minimum ZrO_2 thickness = 0.65 mm, maximum ZrO_2 temperature = 2500 K	Minimum ZrO_2 thickness = 0.06 mm, maximum ZrO_2 temperature = 2100 K
Relocation of melt: a) Relocation inside of cladding possible ? b) Film or rivulet type of outside relocation ? c) Relocation velocity ?	a) No b) Rather rivulet than film; wetted perimeter fraction = 0.8 c) Quasi infinite	a) No b) - c) -	a) No b) Rather rivulet than film c) Quasi infinite			
Melting of refrozen melts possible ?	Yes					
Radial relocation in case of core blockage possible ?	Yes					
Relocation of solid fragments along with relocating melts possible ?	Solid debris relocates with melt unless eutectics model enabled					

Table 4.8d: Variables Defined for the Relocation Models Used in ISP36 (SCDAP/RELAP5)

	Participants				
Material Relocations	**ENES**	**RDIS**	**RRCS**	**UBOS**	**VTTS**
Which cladding failure criterion has been used ?	Combination of: Fraction of oxidation < 0.6 and cladding temperature > 2300 K		Minimum ZrO_2 thickness = 0.36 mm, maximum ZrO_2 temperature = 2400 K	Combination of: Fraction of oxidation < 0.6 and cladding temperature > 2500 K	Combination of: Fraction of oxidation < 0.6 and cladding temperature > 2500 K
Relocation of melt: a) Relocation inside of cladding possible ? b) Film or rivulet type of outside relocation ? c) Relocation velocity ?	a) No b) Film c) Calculated by equation of motion		a) No b) Droplets c) Constant velocity	a) No b) Film c) Calculated by equation of motion	a) No b) Film c) Calculated by equation of motion
Melting of refrozen melts possible ?	Yes		-	Yes	Yes
Radial relocation in case of core blockage possible ?	No		-	No	No
Relocation of solid fragments along with relocating melts possible ?	No		-	No	No

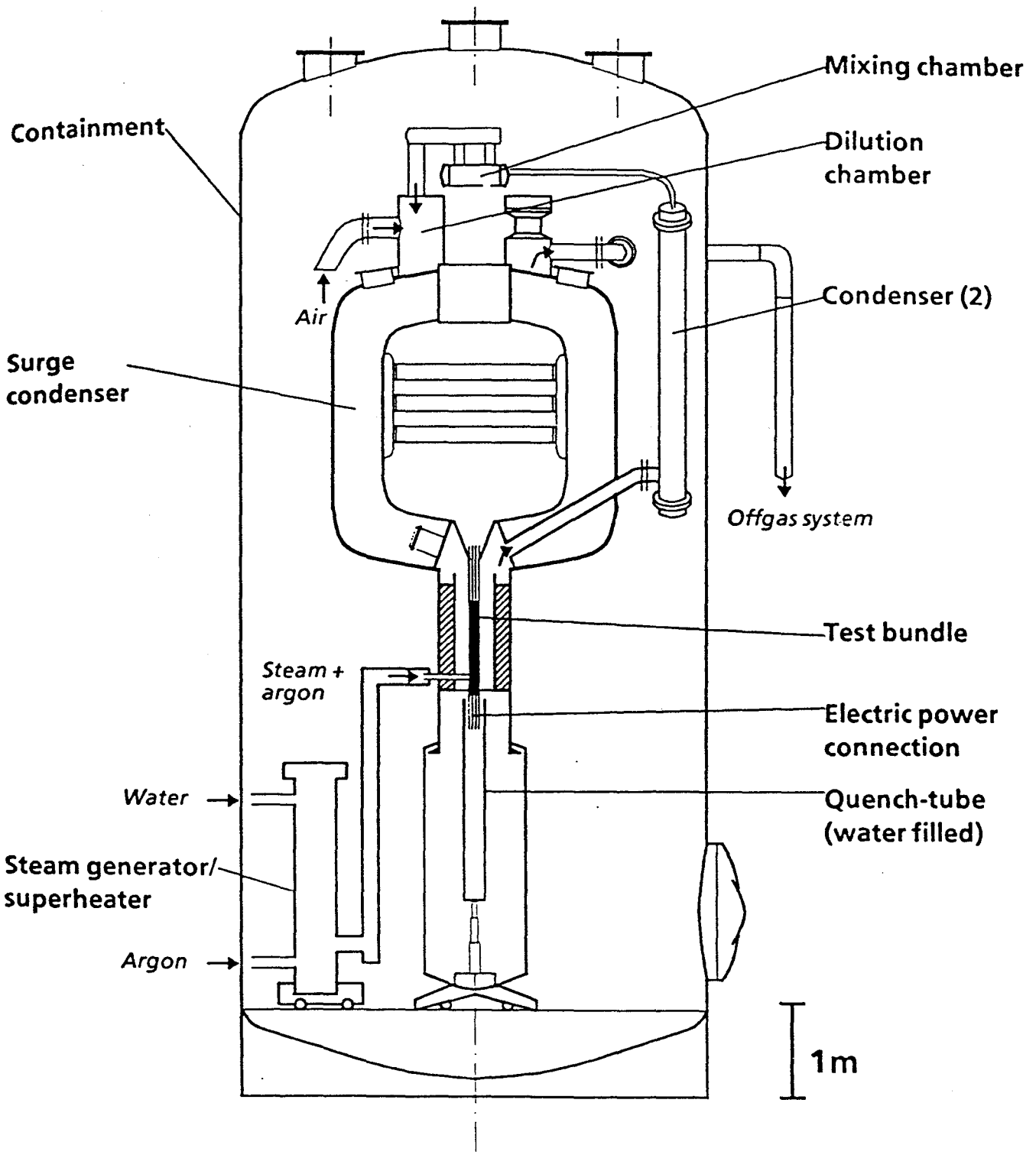

Fig. 3.1 SFD Test Facility CORA (Main components)

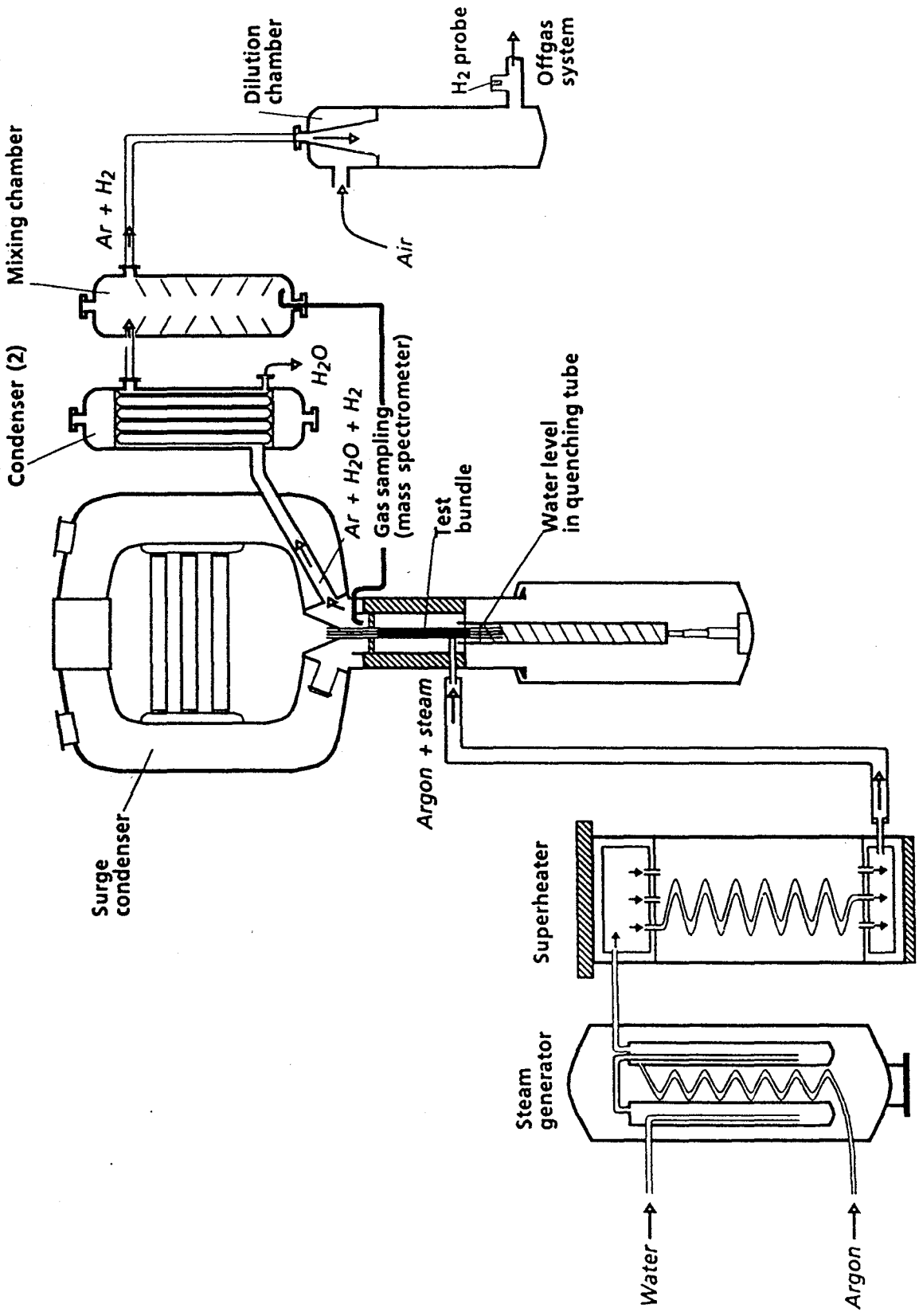

Fig. 3.2 SFD Test Facility (Simplified flow diagram)

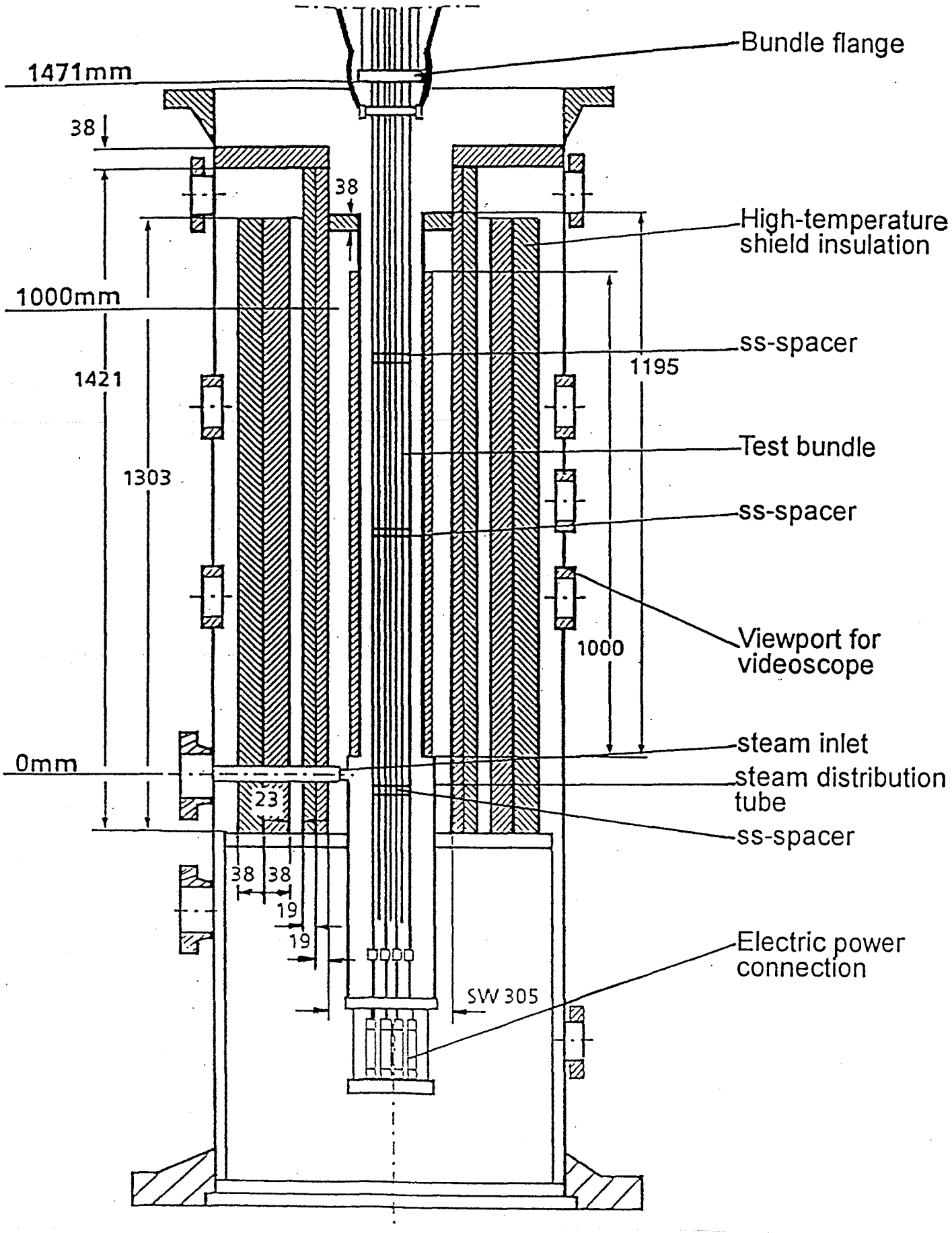

Fig. 3.3 CORA bundle arrangement

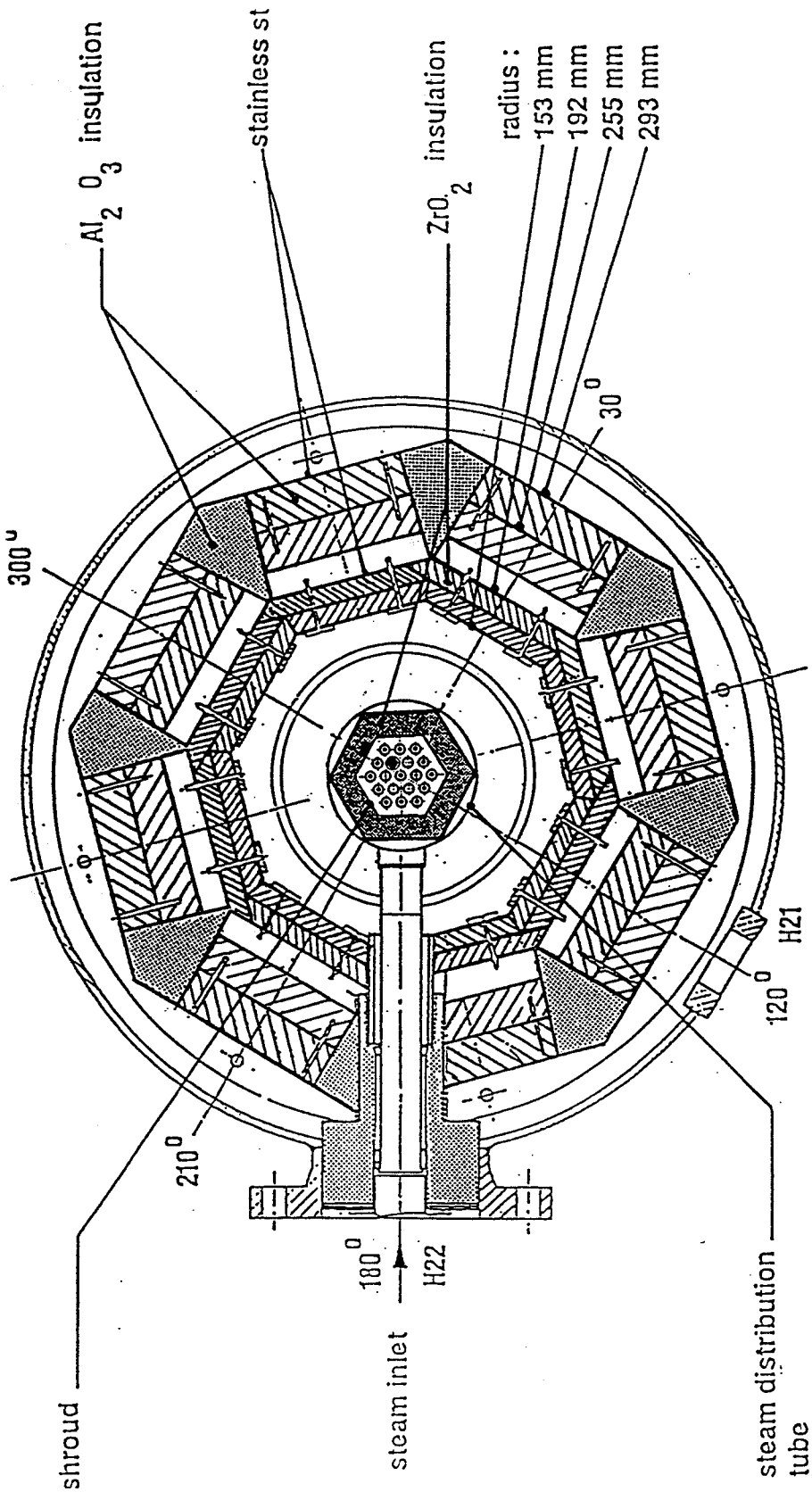

Fig. 3.4 Horizontal cross section of the high temperature shield

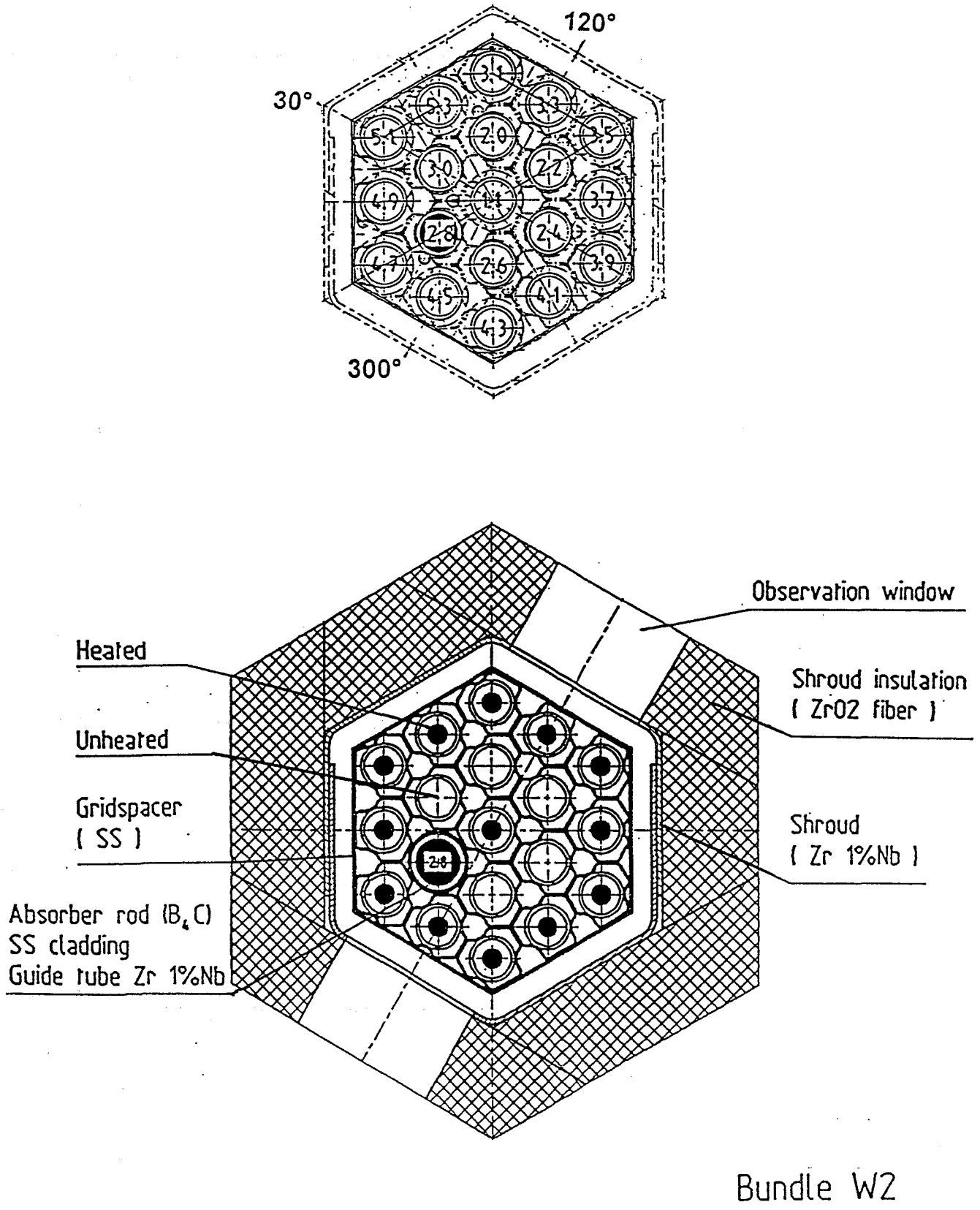

Fig. 3.5 Rod arrangement and test rod designation of bundle CORA-W2

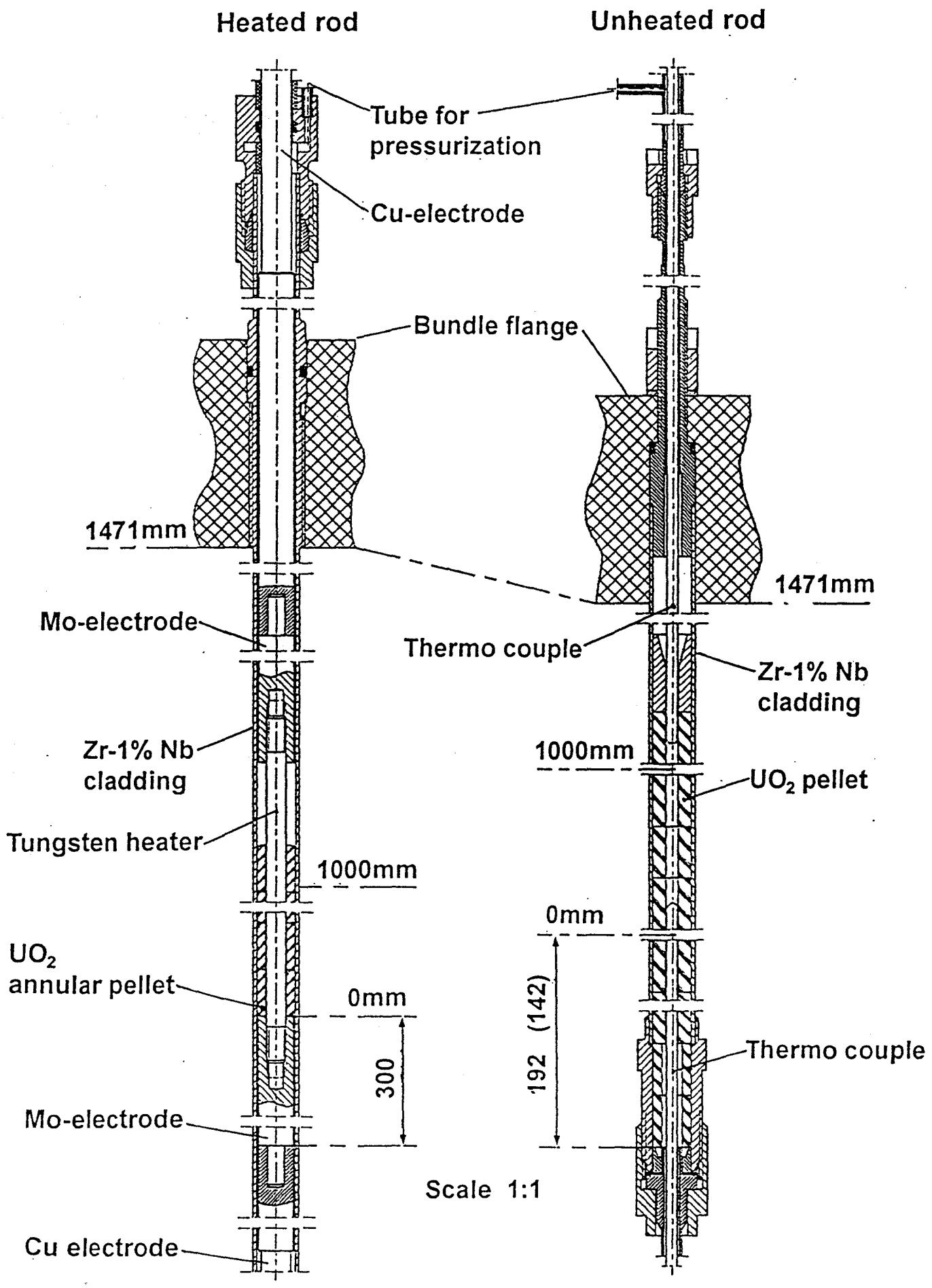

Fig. 3.6 Rod types used in the CORA / VVER experiments

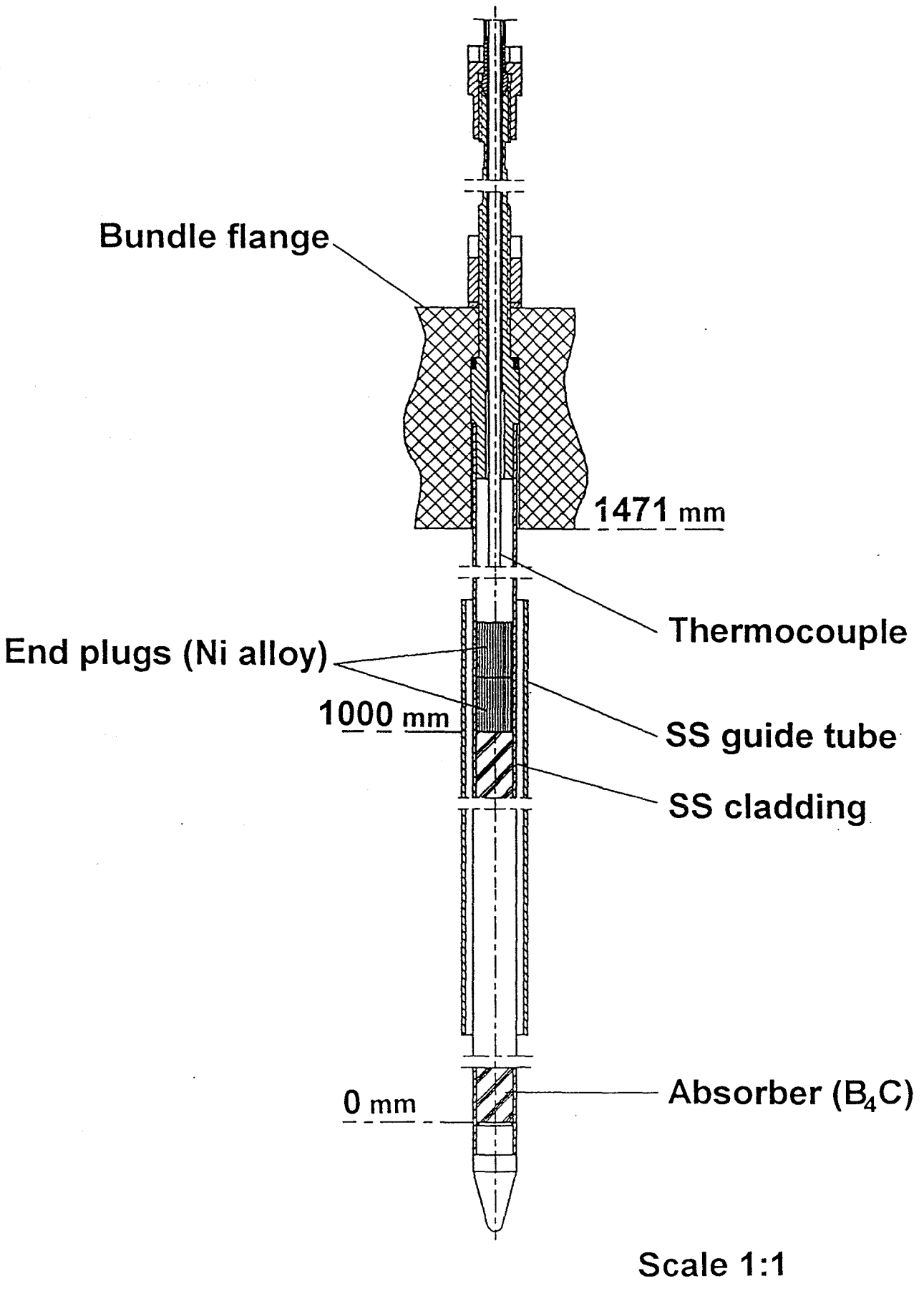

Fig. 3.7 CORA-W2; Absorber rod design

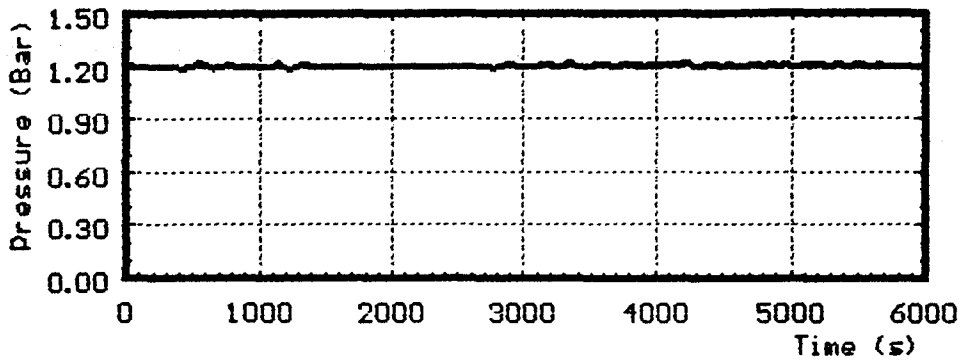

System overpressure

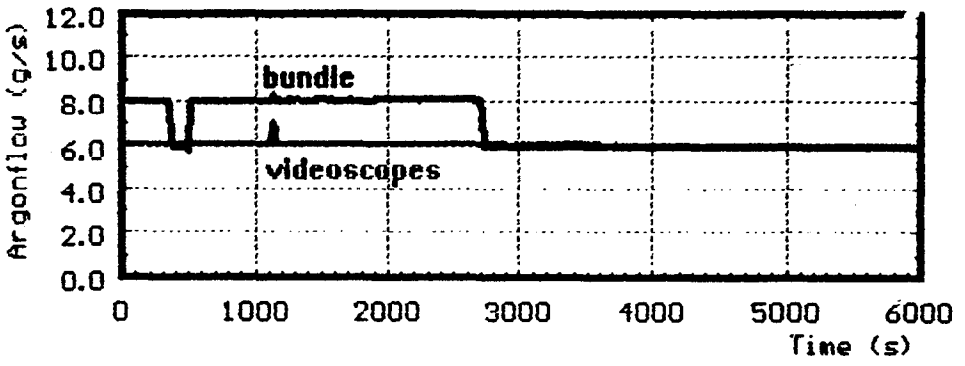

Argonflow

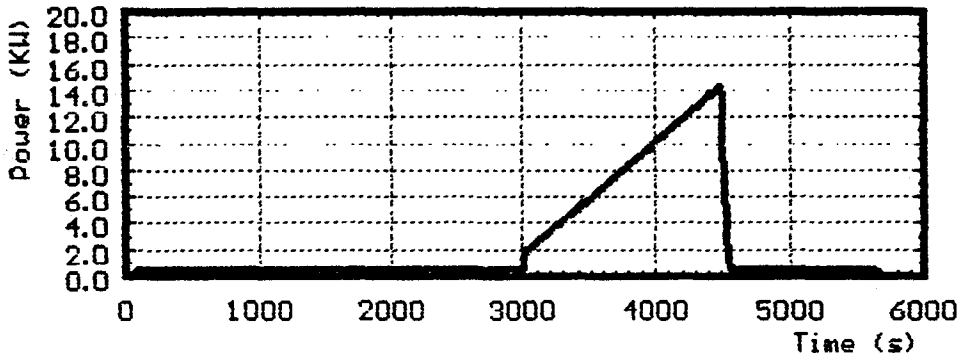

Power

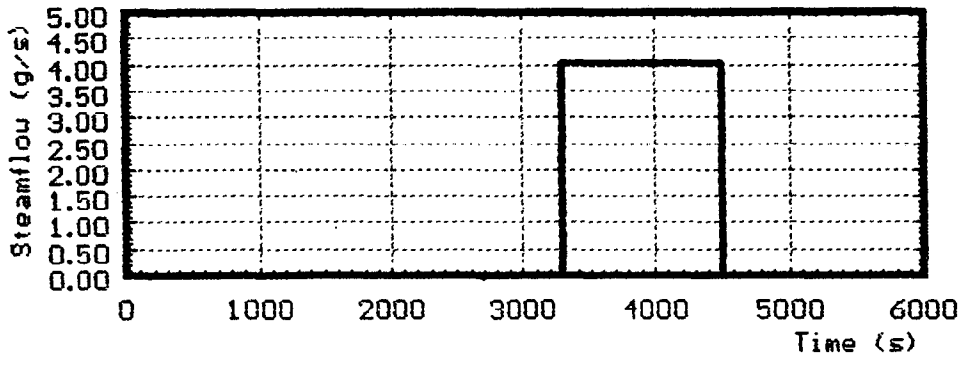

Steam input

Fig. 3.8 CORA-W2; System pressure, argon flow, steam input and power

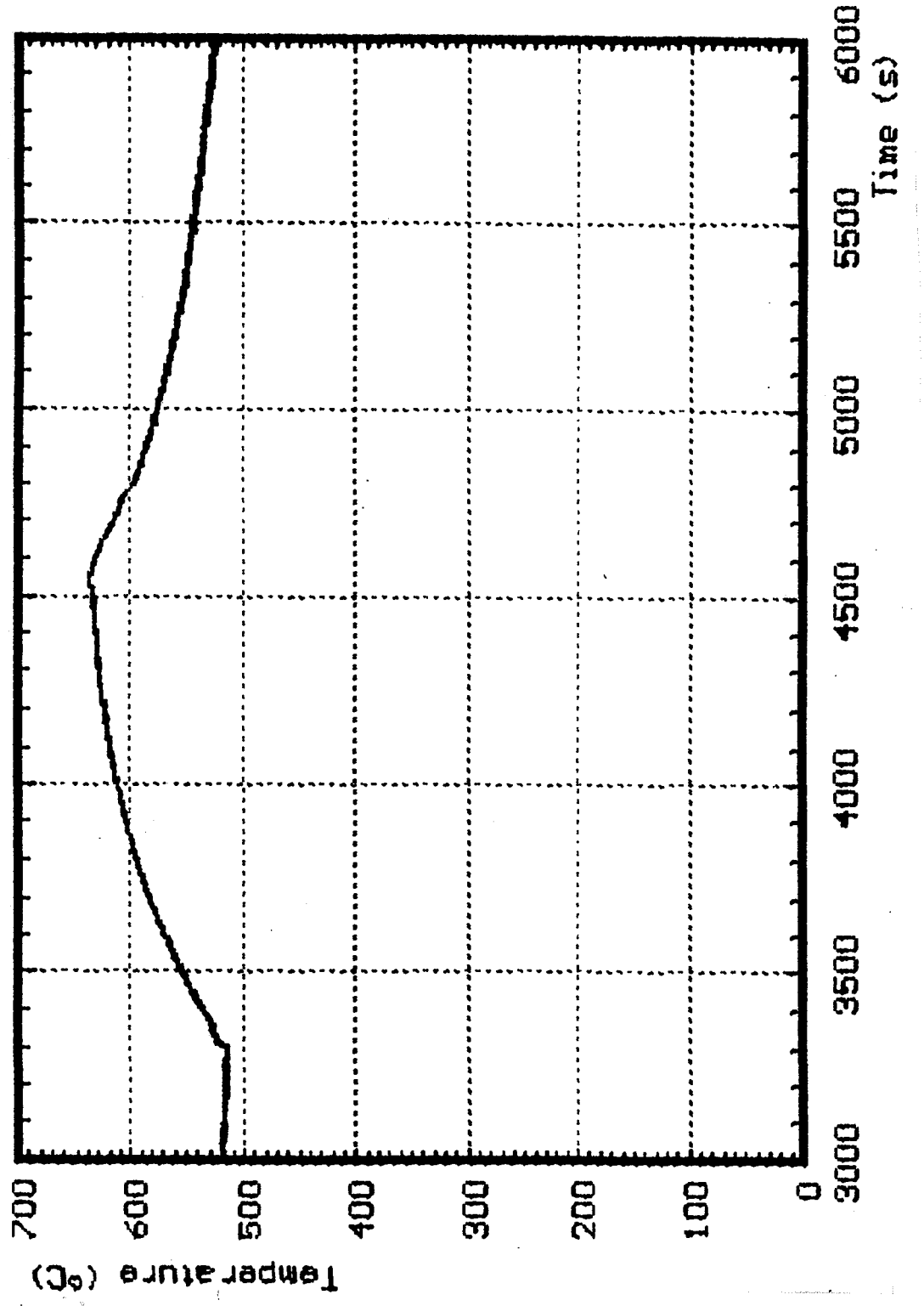

Fig. 3.9 CORA-W2; Temperature at steam inlet

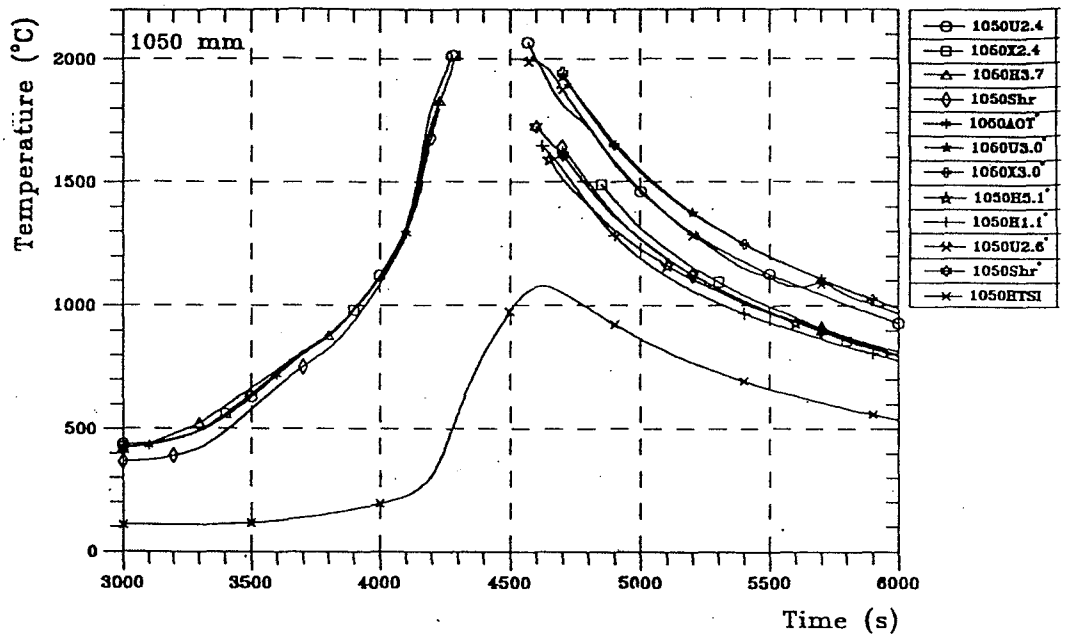

Fair temperatures curves at elevation 1050 mm

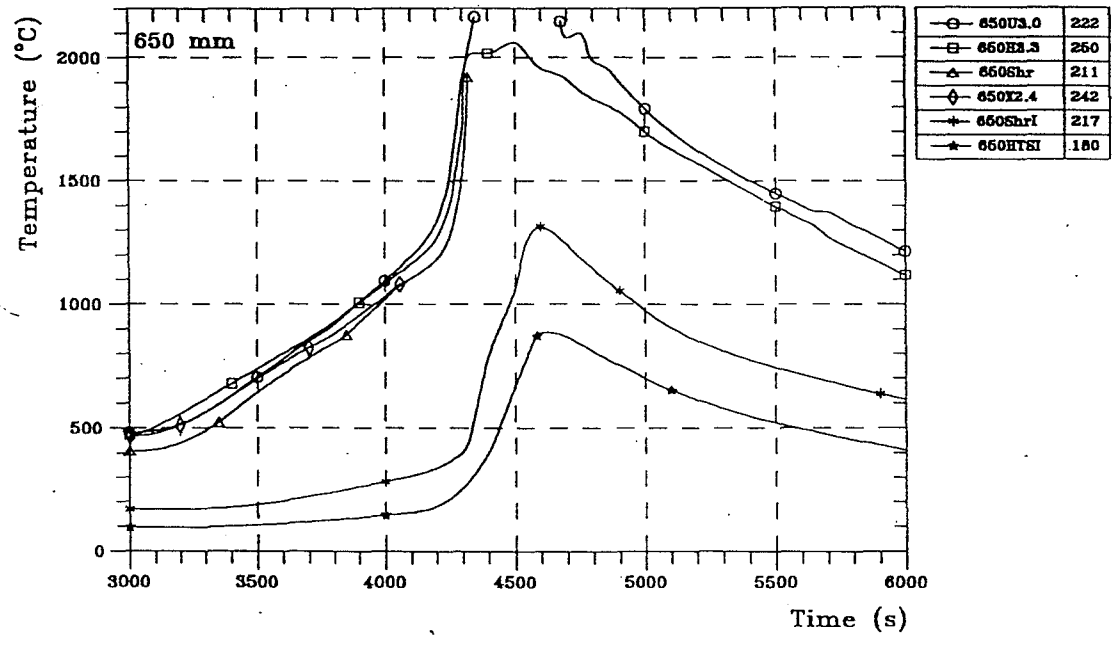

Fair temperatures curves at elevation 650 mm

Fig. 3.10 Fair temperature curves

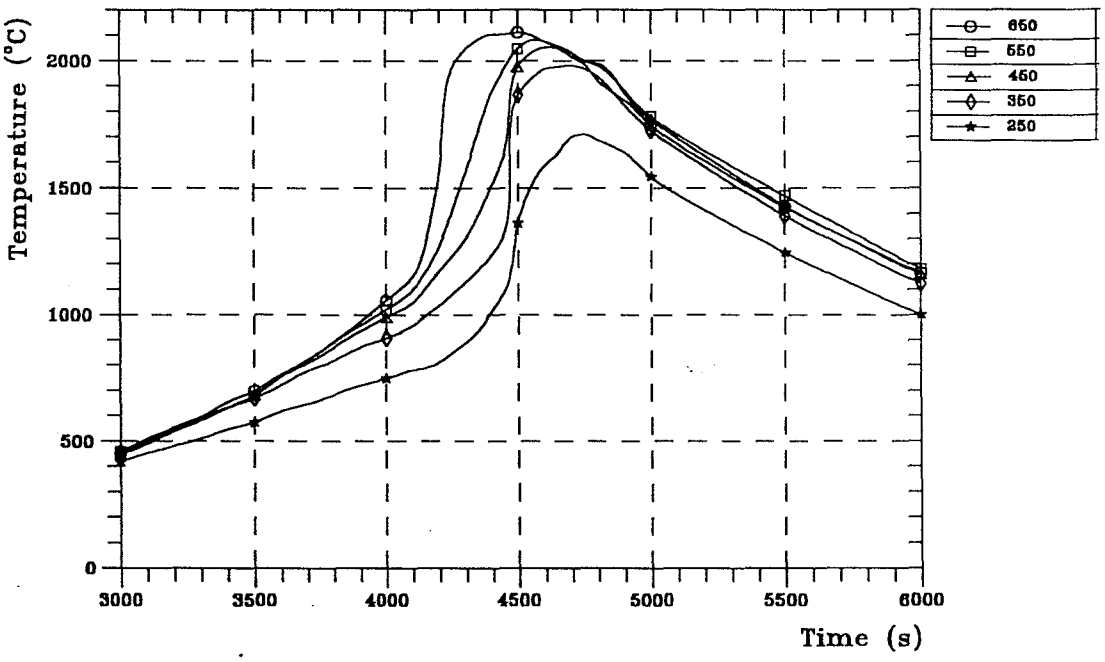

Representative temperature estimations
at elevations 250÷650 mm

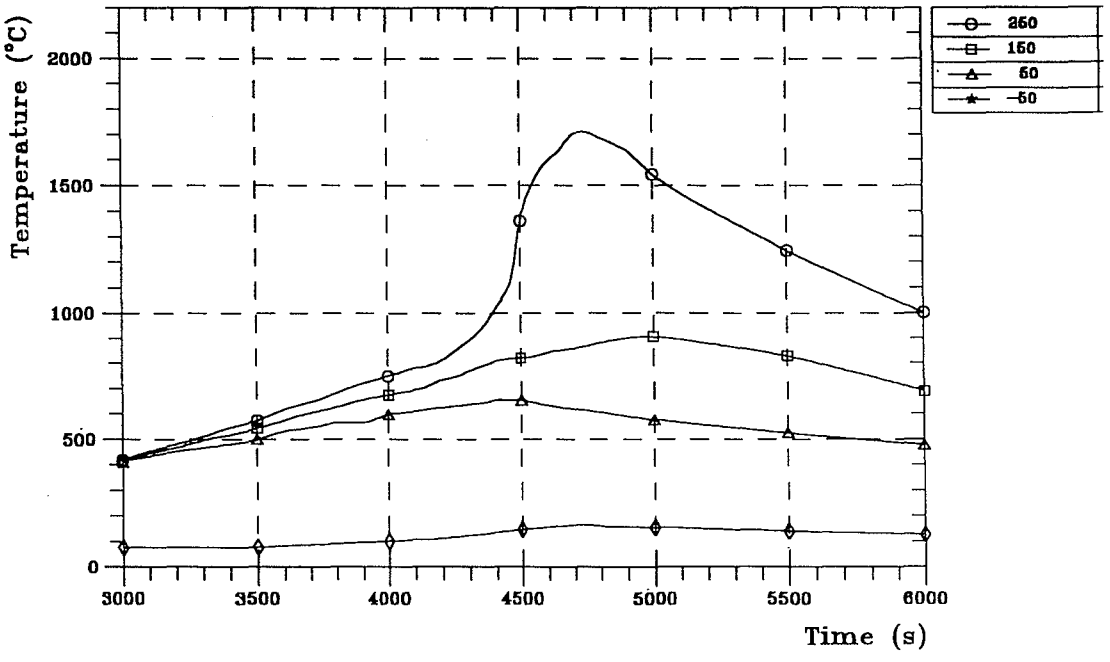

Representative temperature estimations
at elevations -50÷250 mm

Fig. 3.11 Representative temperature estimations

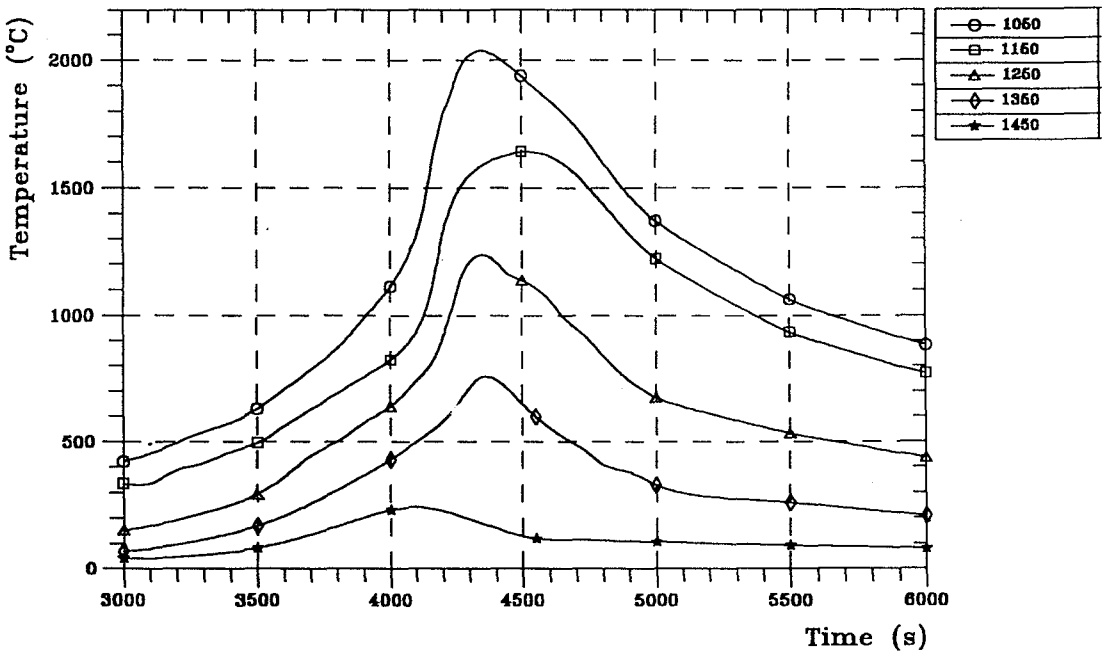

Representative temperature estimations
at elevations 1050÷1450 mm

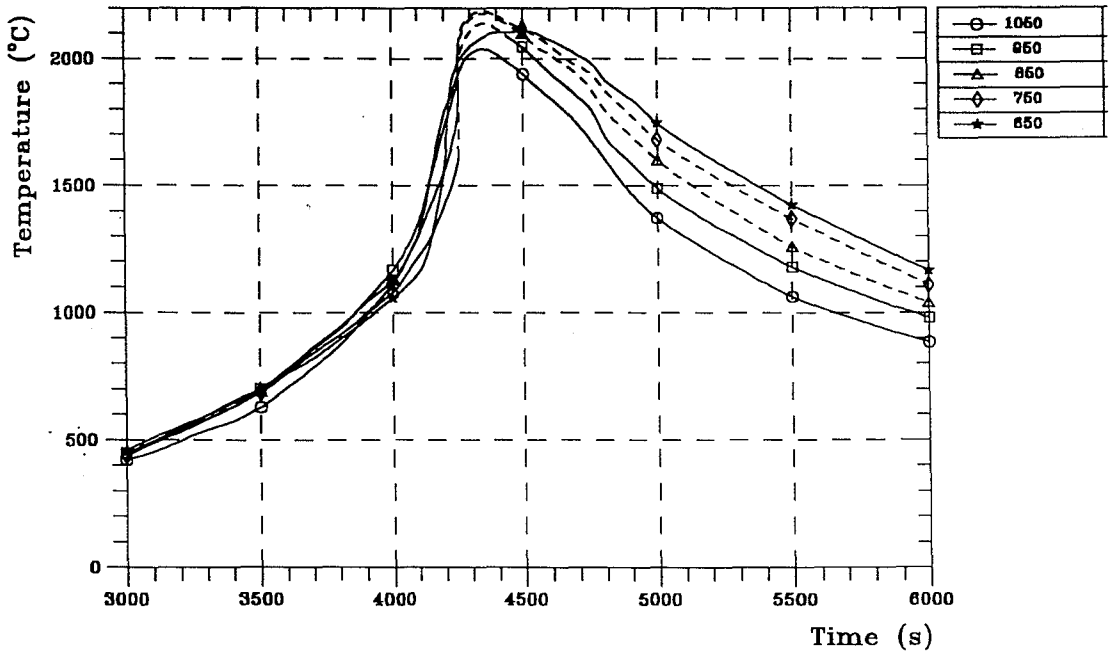

Representative temperature estimations
at elevations 650÷1050 mm

Fig. 3.12 Representative temperature estimations

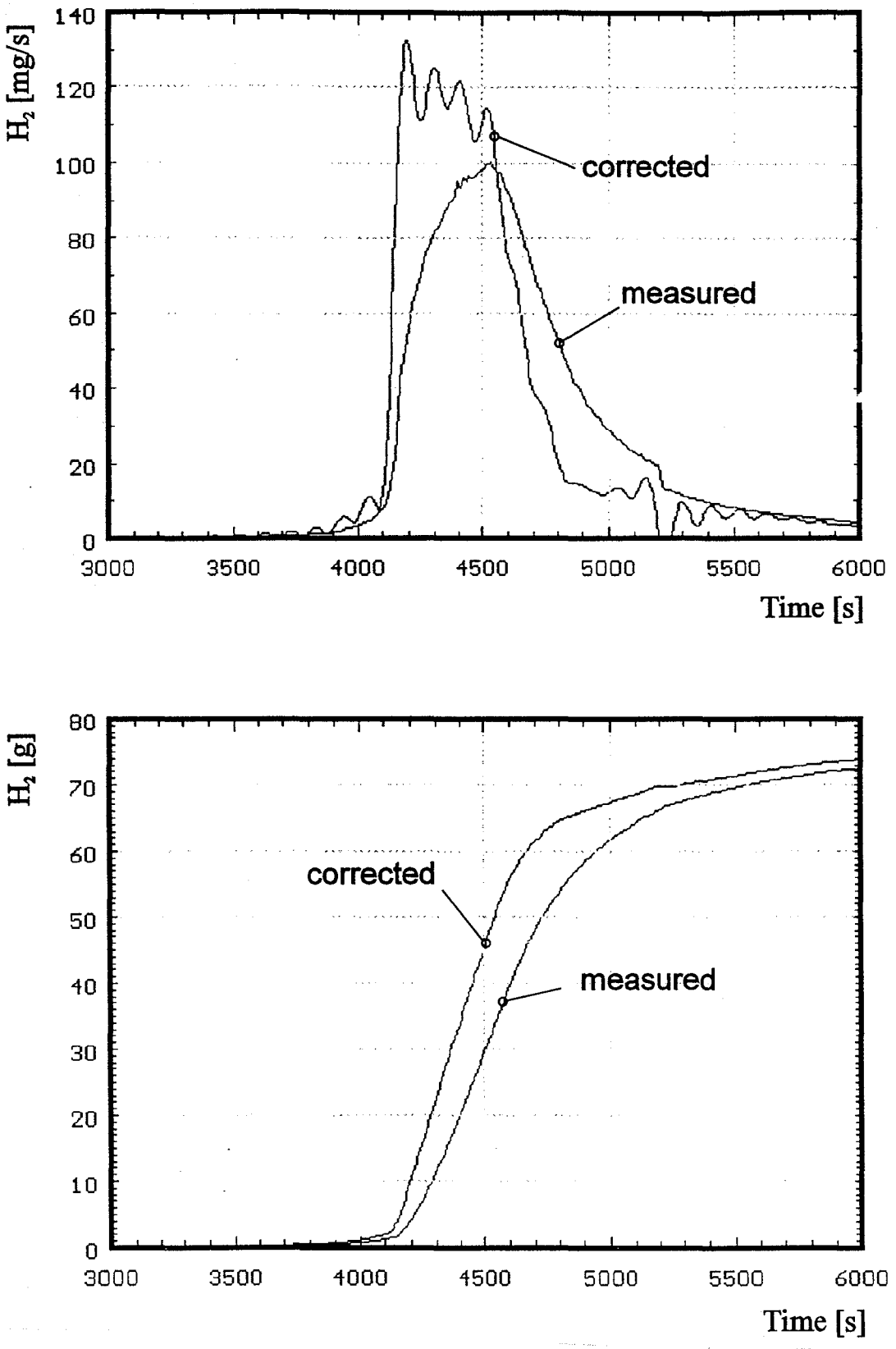

Fig. 3.13 Hydrogen production in test CORA-W2; production rate (top) and integral values (bottom)

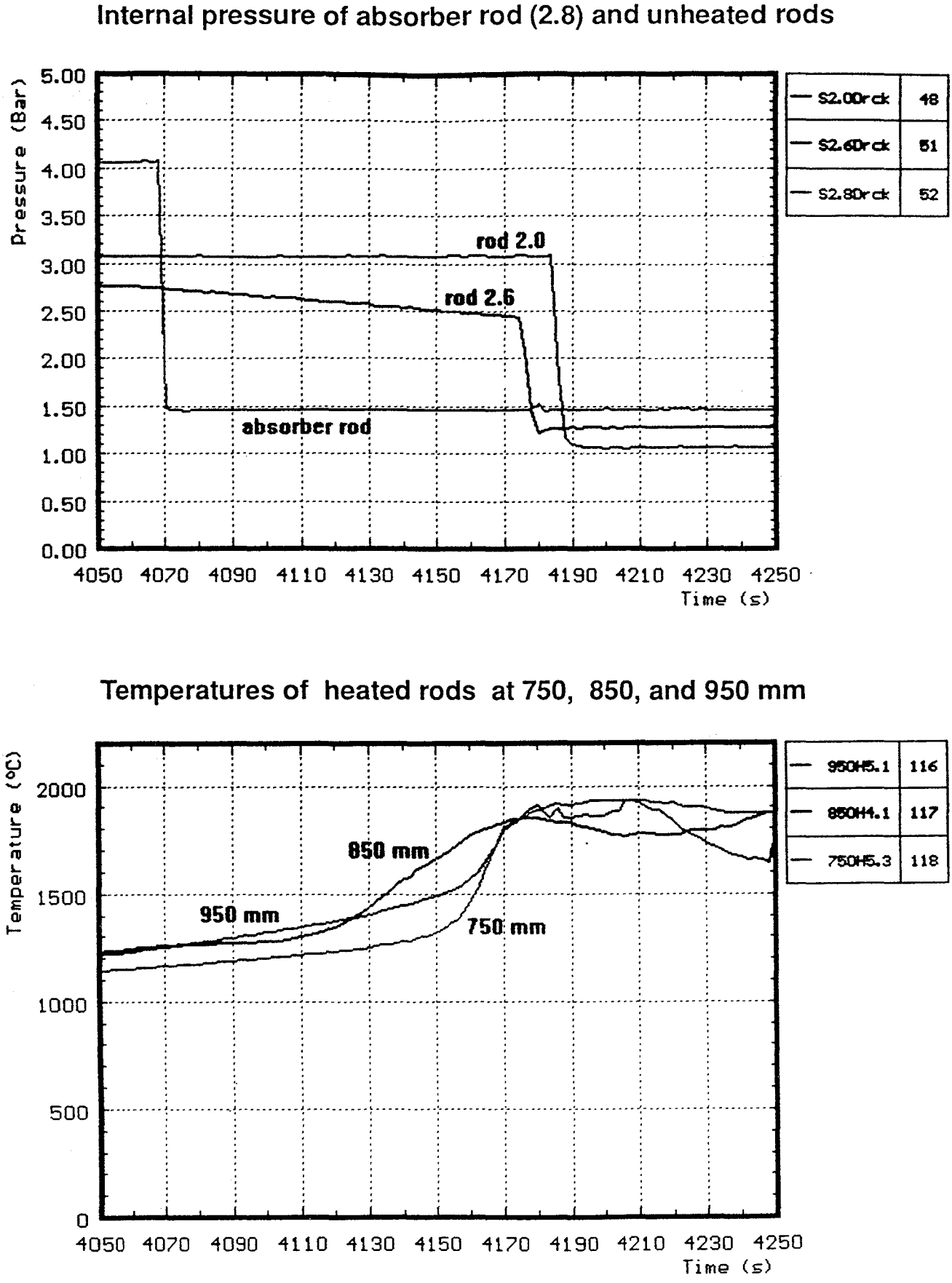

Fig. 3.14 CORA-W2: Comparison of internal pressure of absorber rod and unheated rods with temperatures of heated rods at 750, 850 and 950 mm

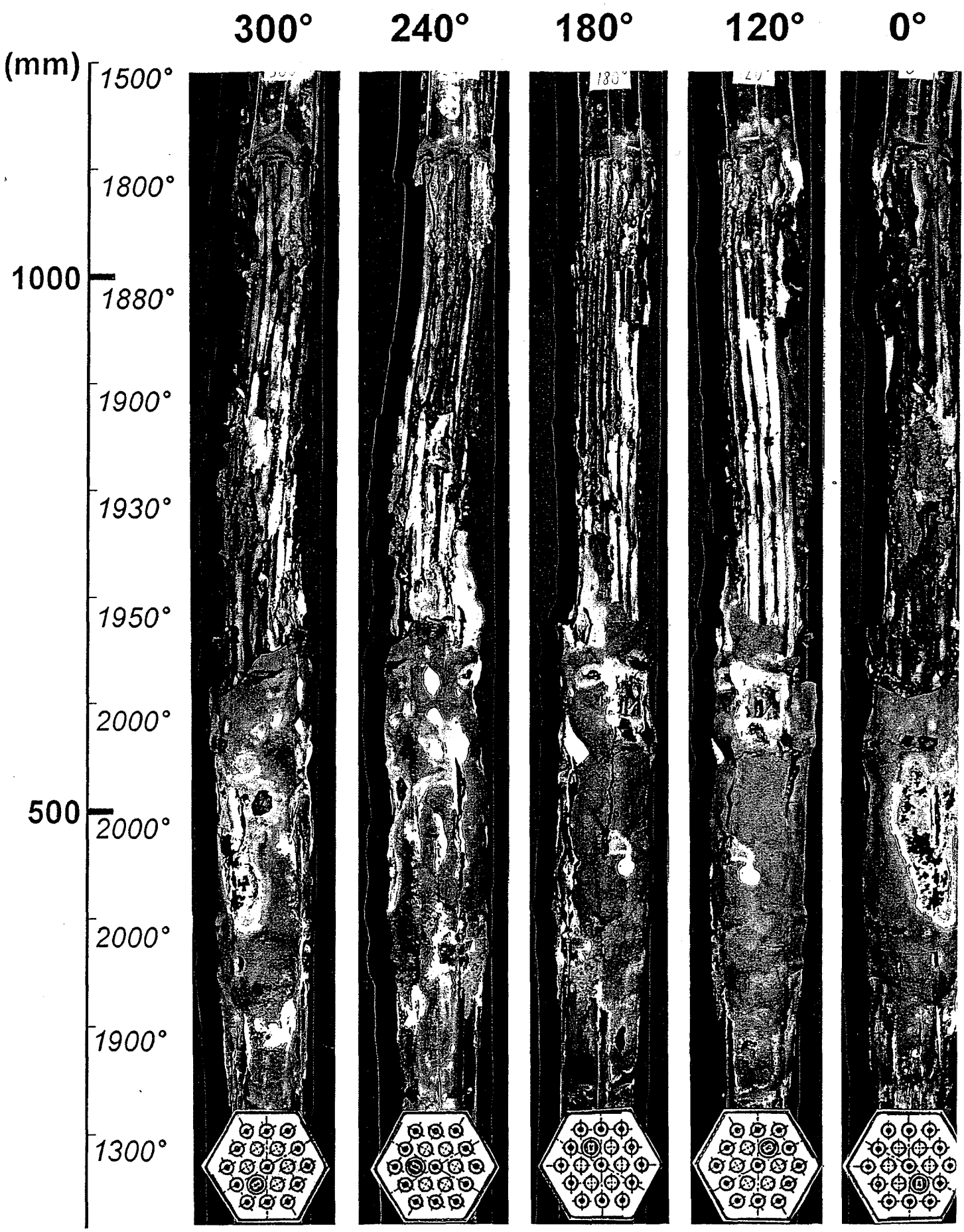

Fig. 3.15 Posttest view of bundle CORA-W2 after partial removal of shroud

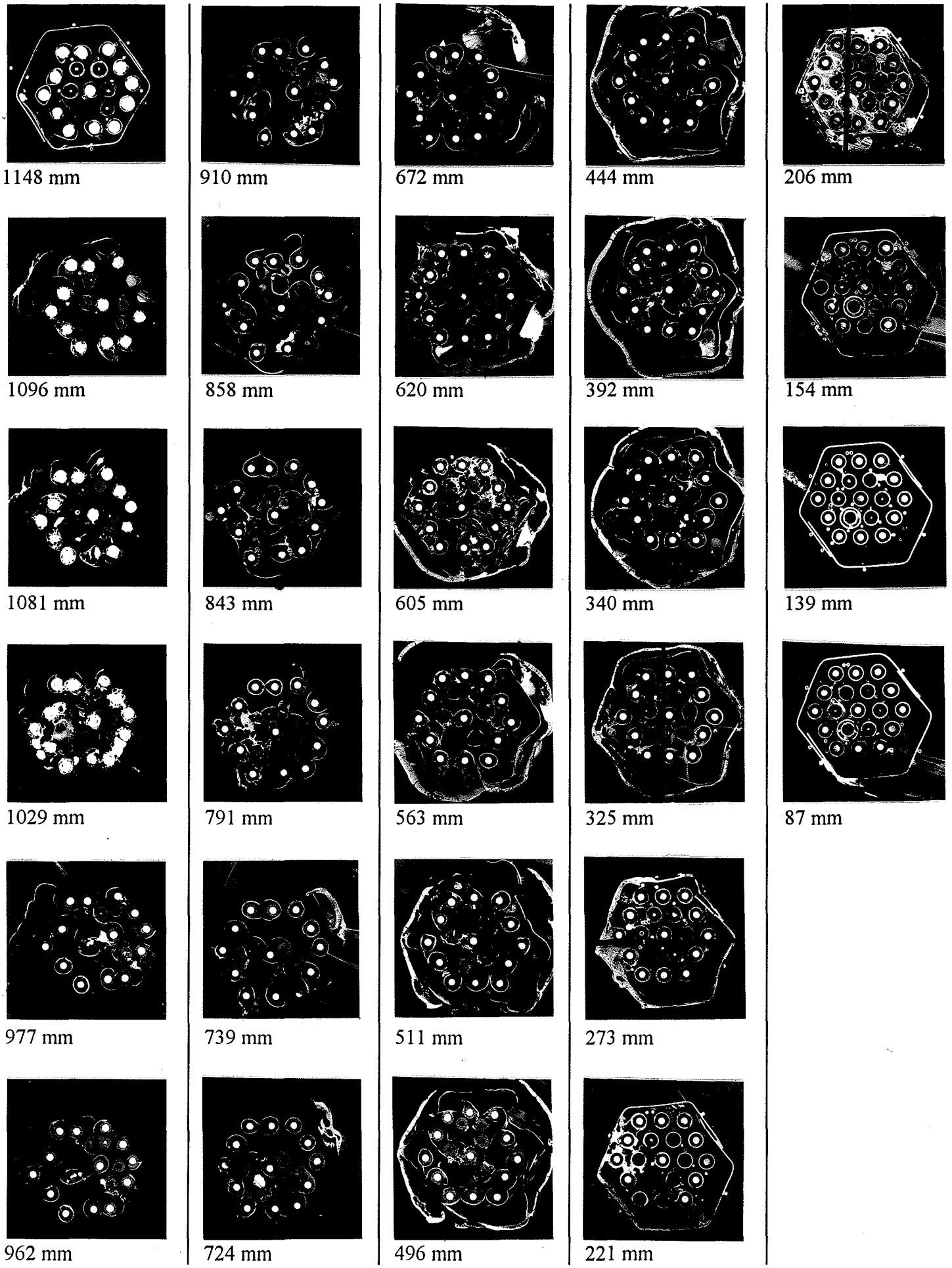

Fig. 3.16 Horizontal cross sections of bundle CORA-W2

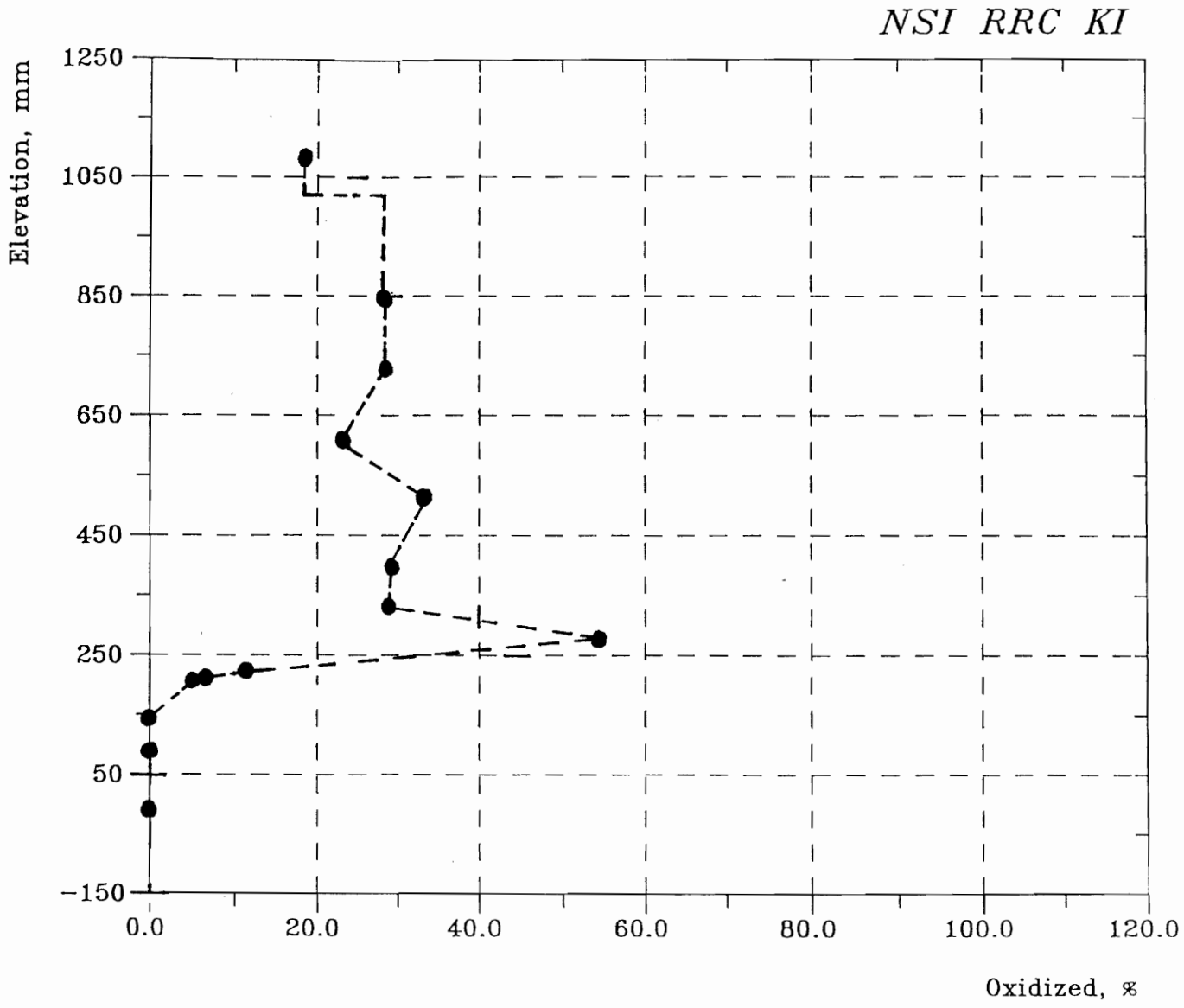

Fig. 3.17 Zr Oxidized Bundle (at original position, before melting)

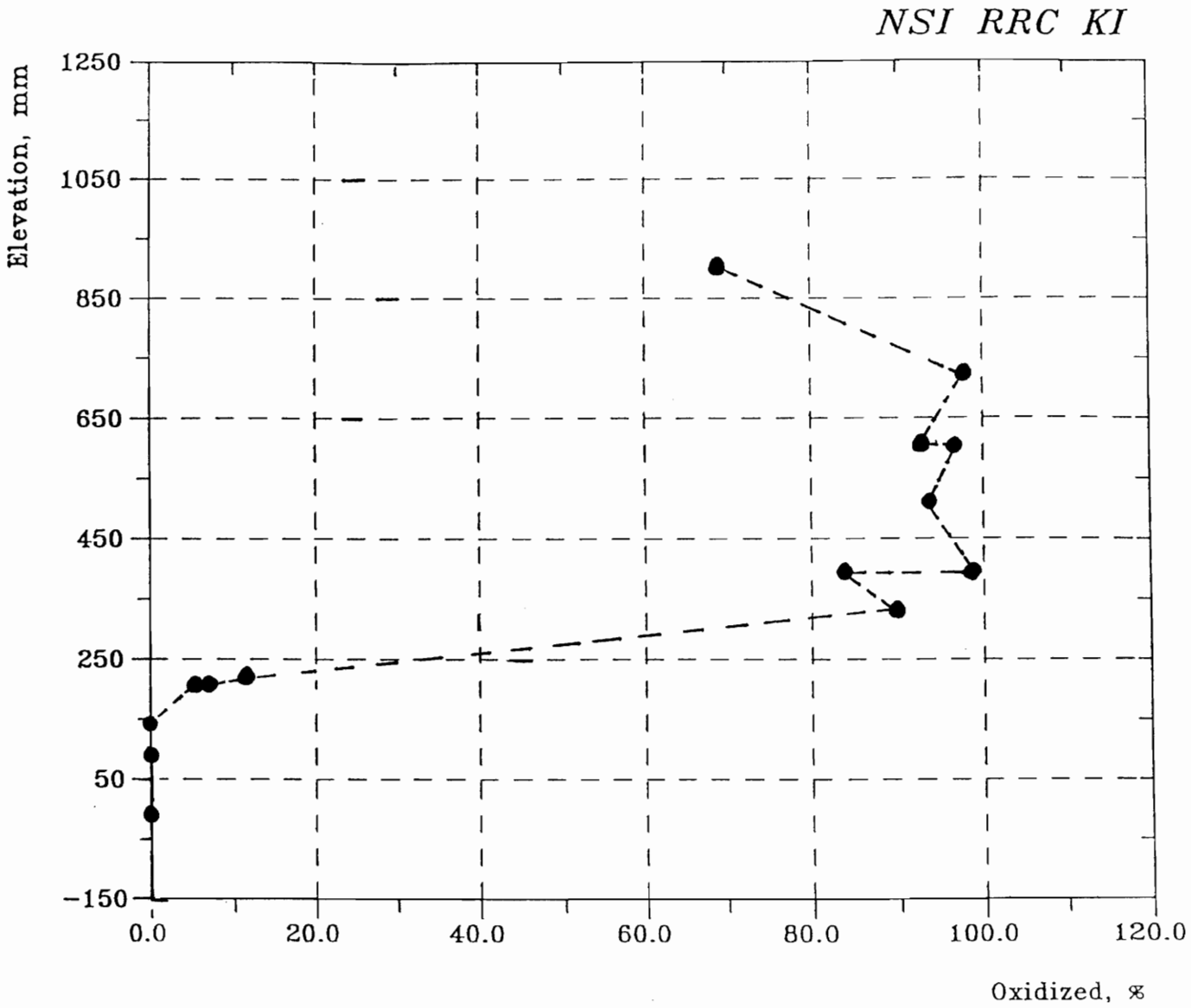

Fig. 3.18 Zr Oxidized Bundle (at original position and relocating melts)

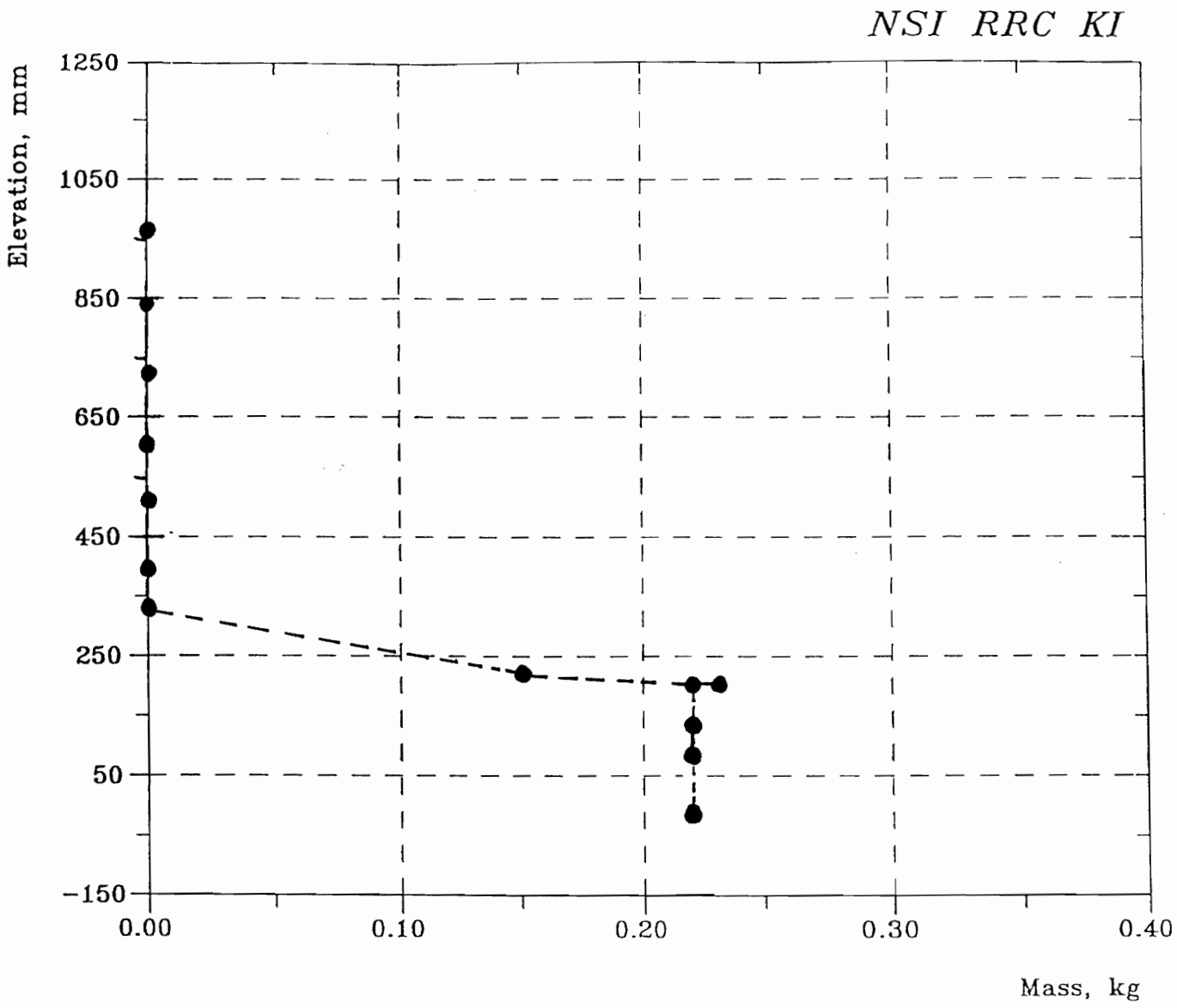

Fig. 3.19 Zr, α-Zr(0) Total Mass (Bundle)

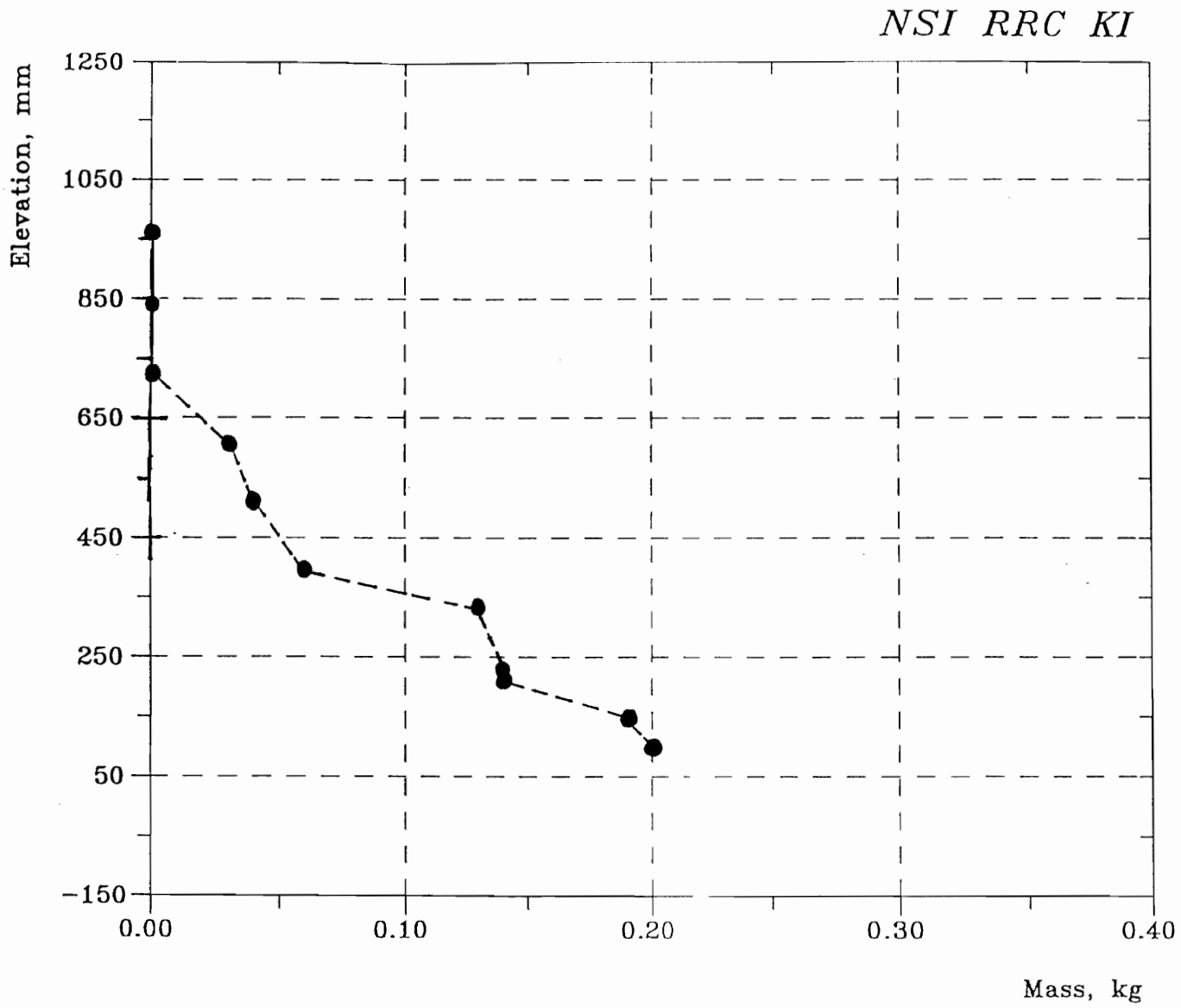

Fig. 3.20 Zr, α-Zr(0) Total Mass (Shroud)

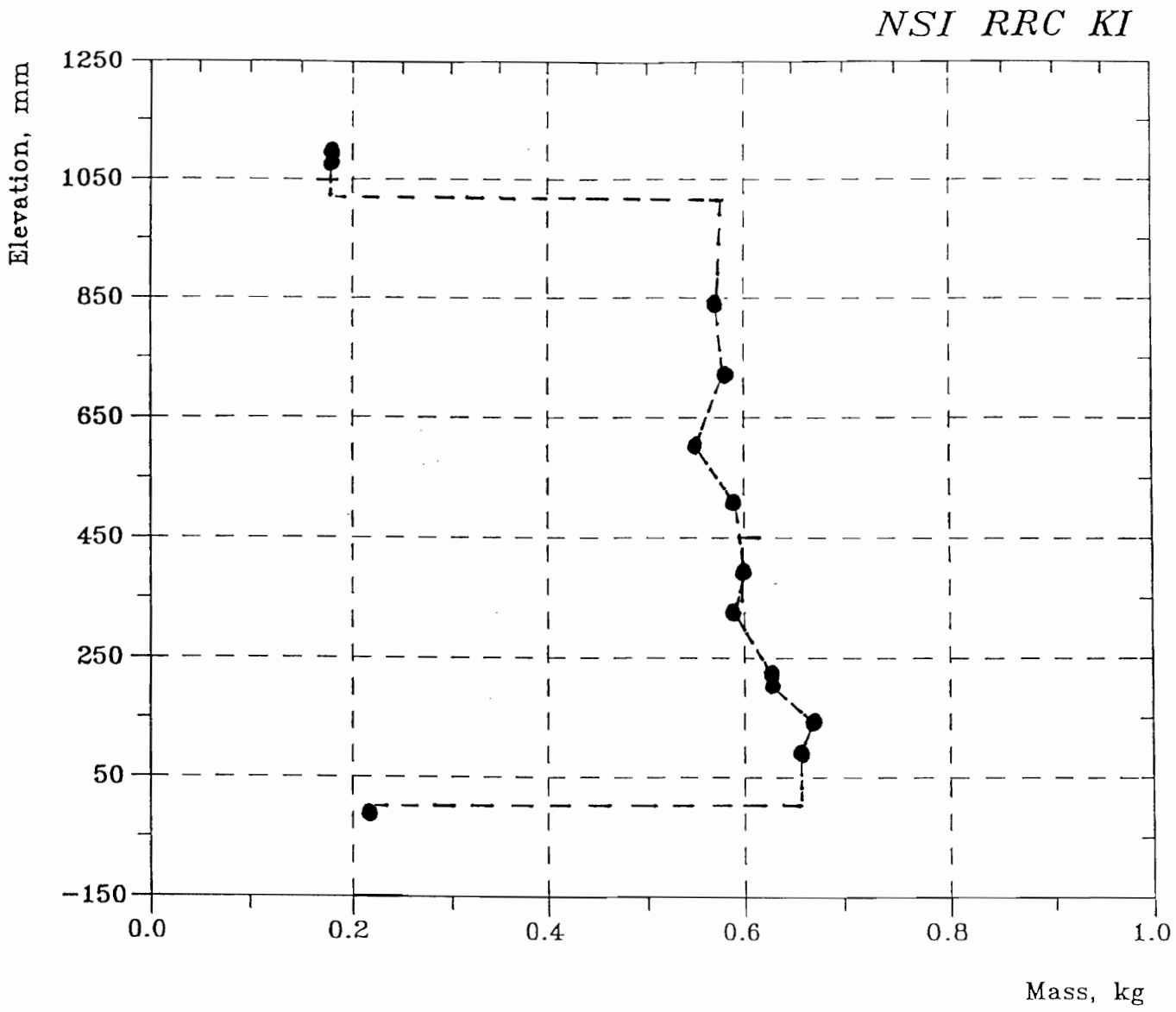

Fig. 3.21 UO_2 Total Mass

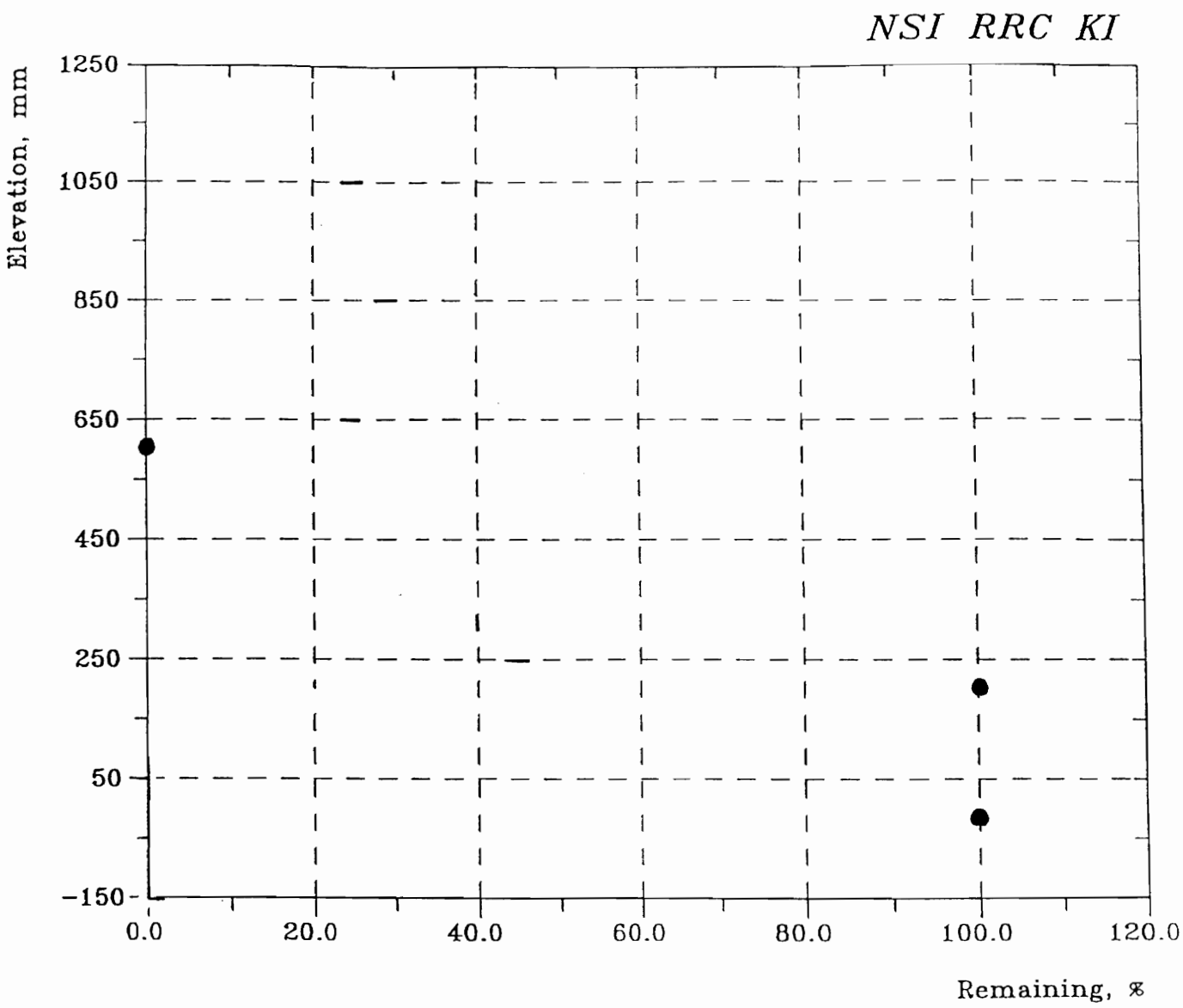

Fig. 3.22 Remaining SS of Grid Spacer

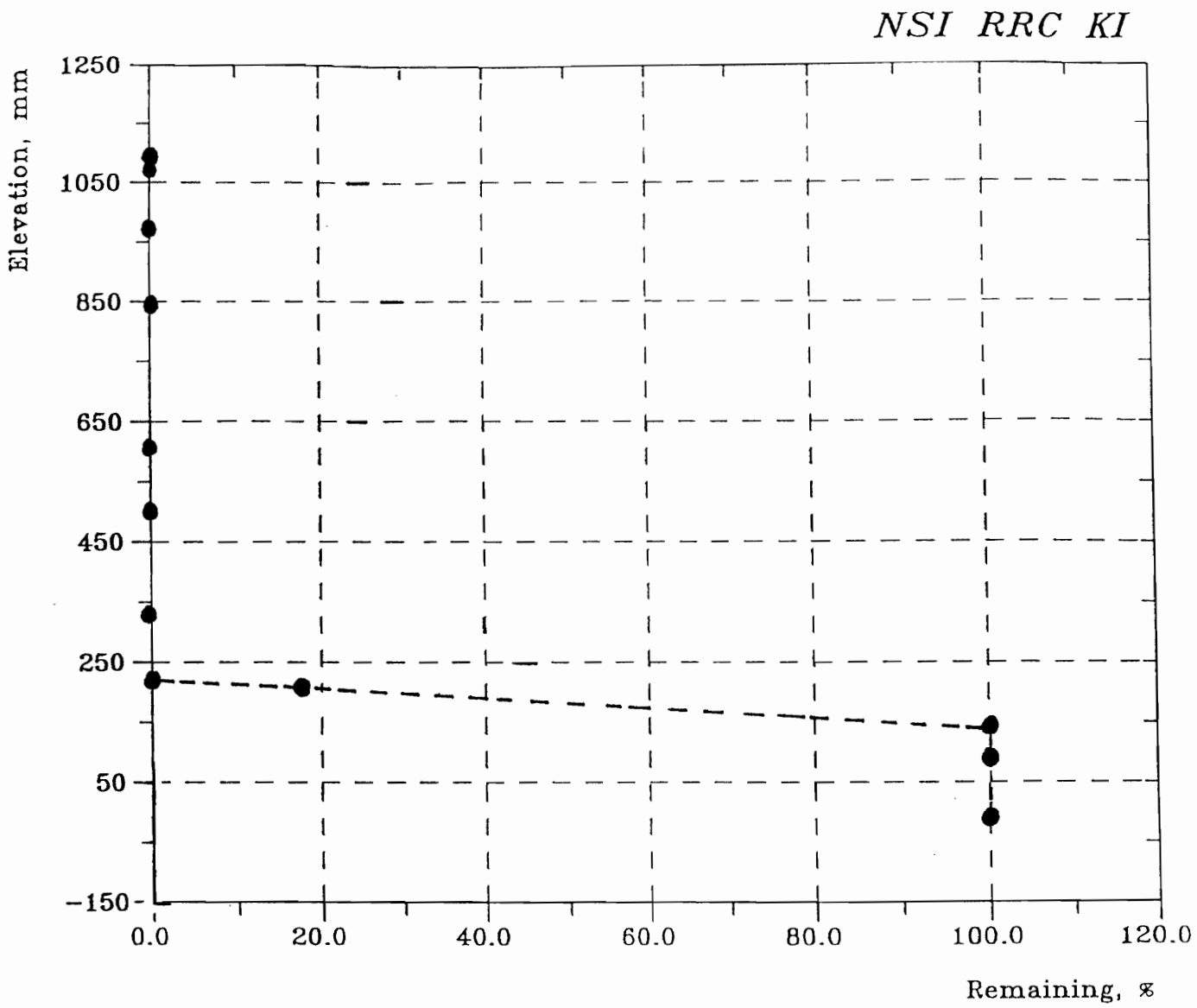

Fig. 3.23 Remaining SS of Absorber Assembly

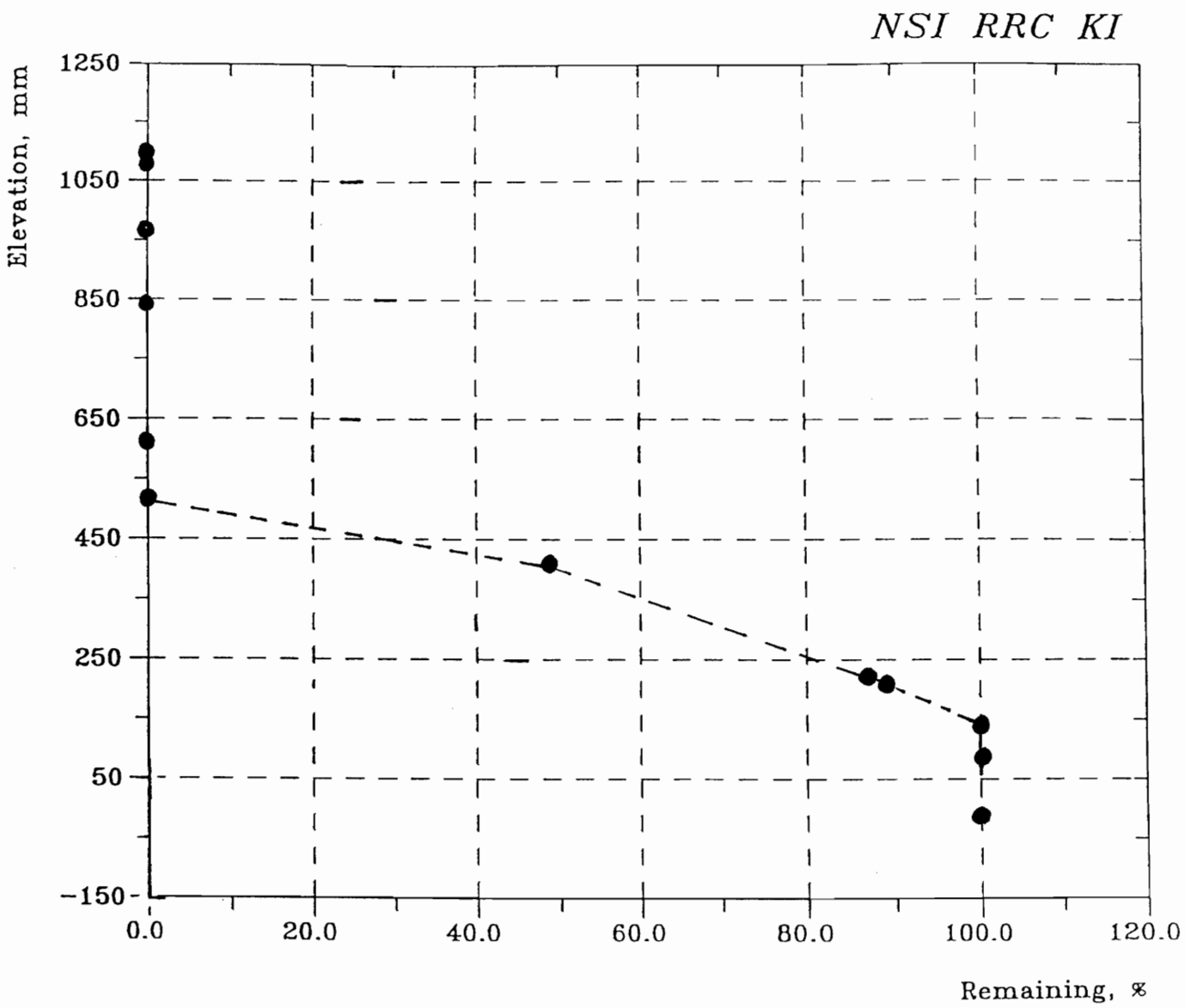

Fig. 3.24 Remaining B_4C of Absorber Assembly

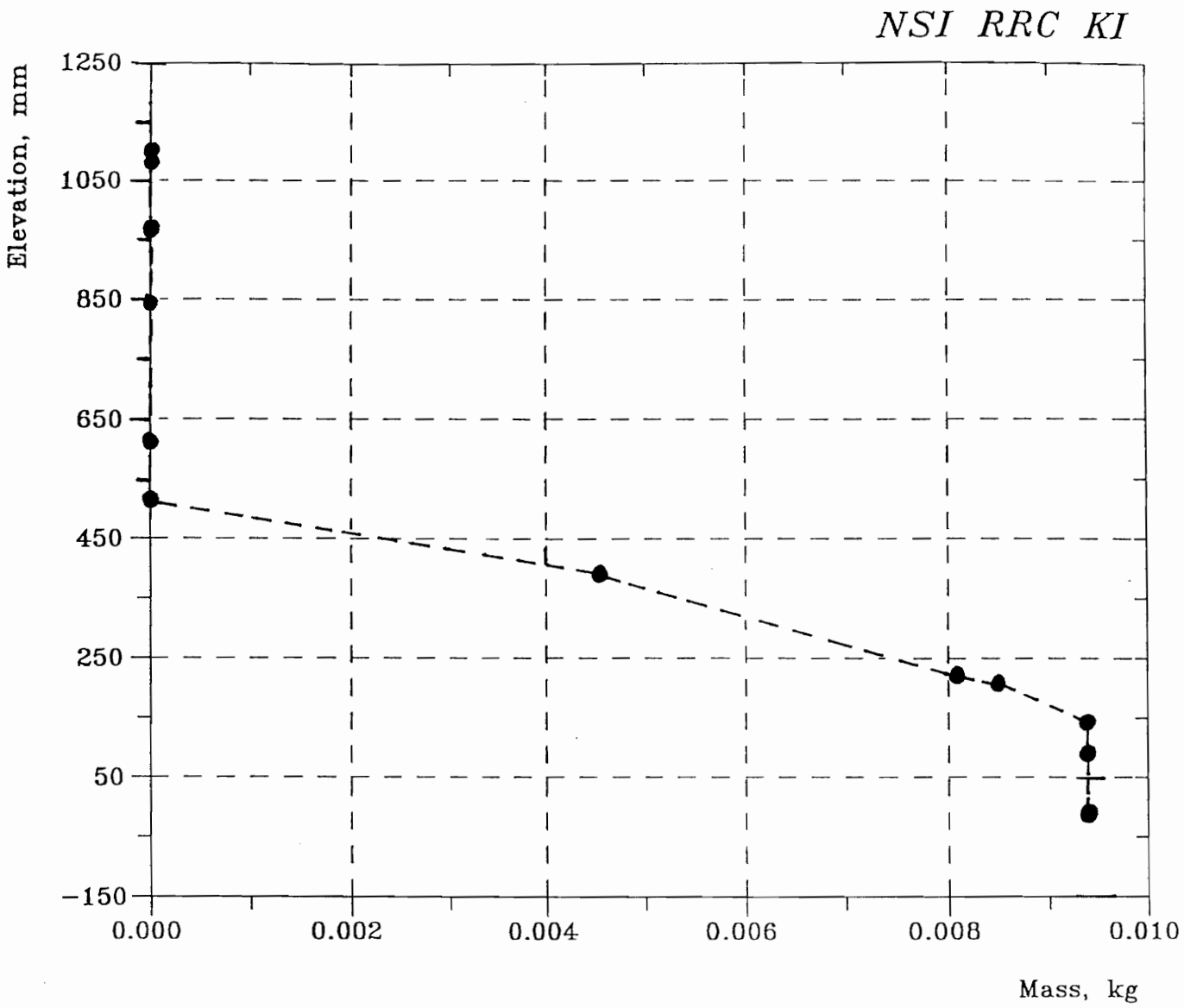

Fig. 3.25 B_4C Total Mass

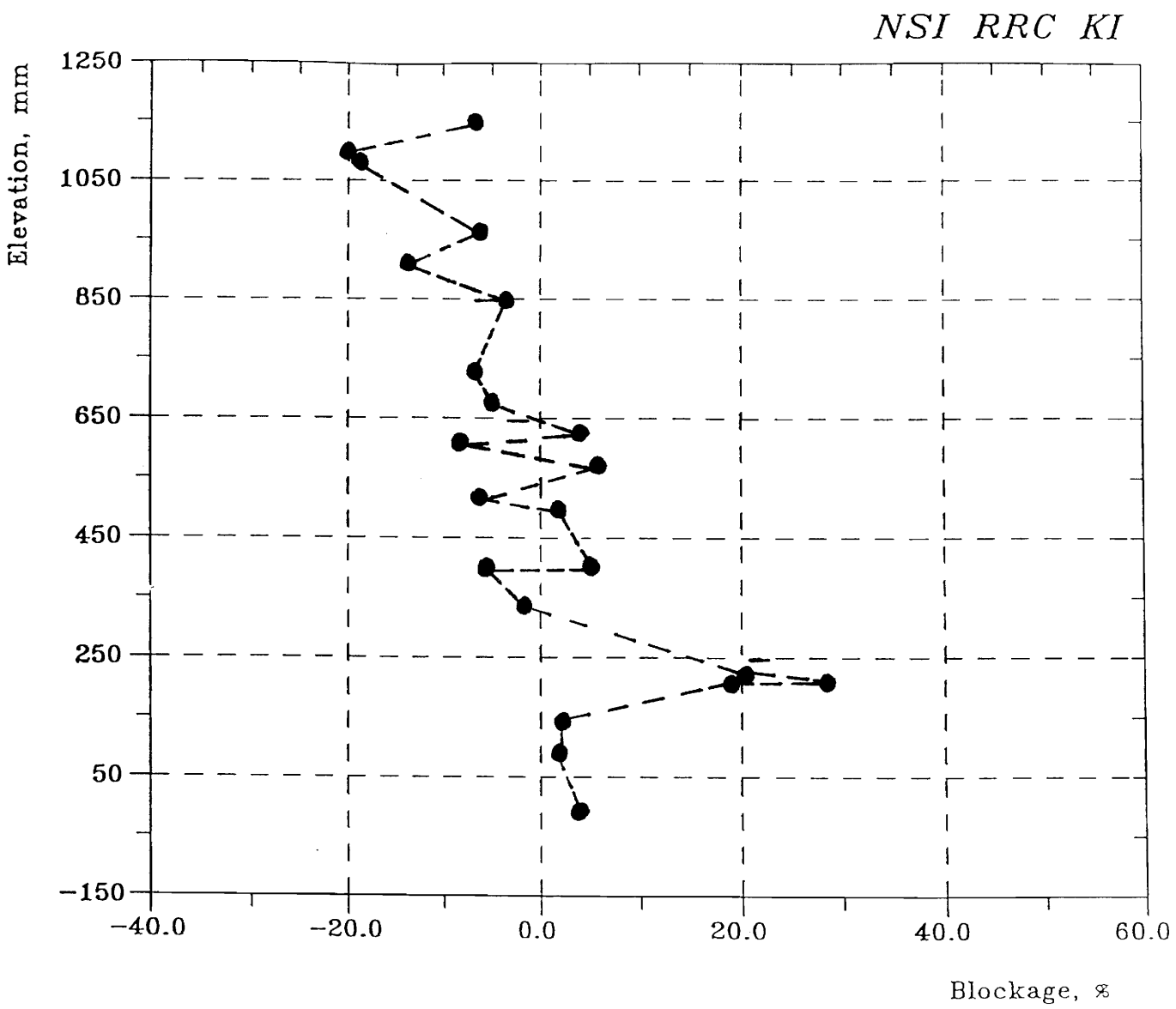

Fig. 3.26 Core Blockage

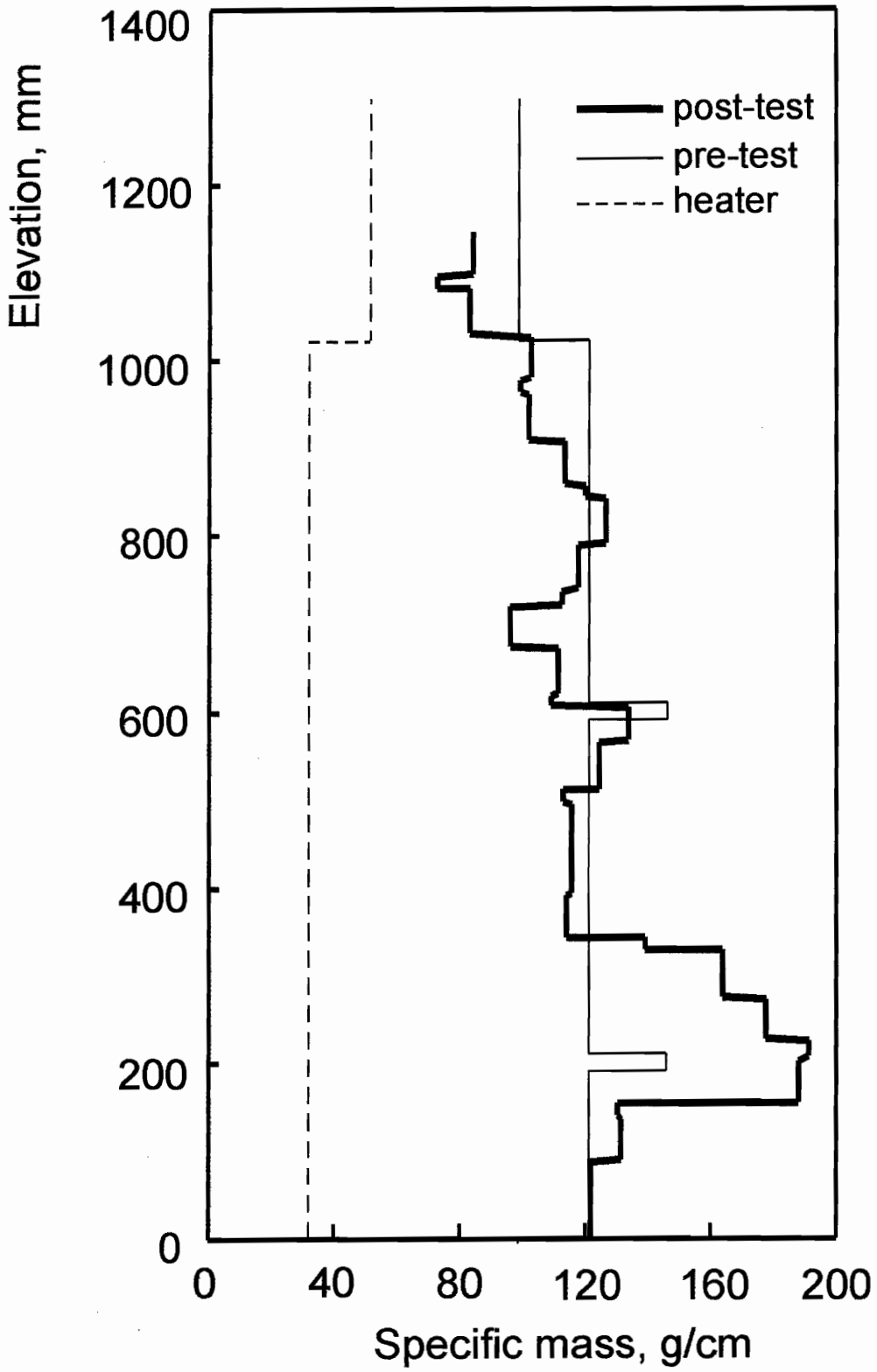

Fig. 3.27 Total Mass of Structure Materials

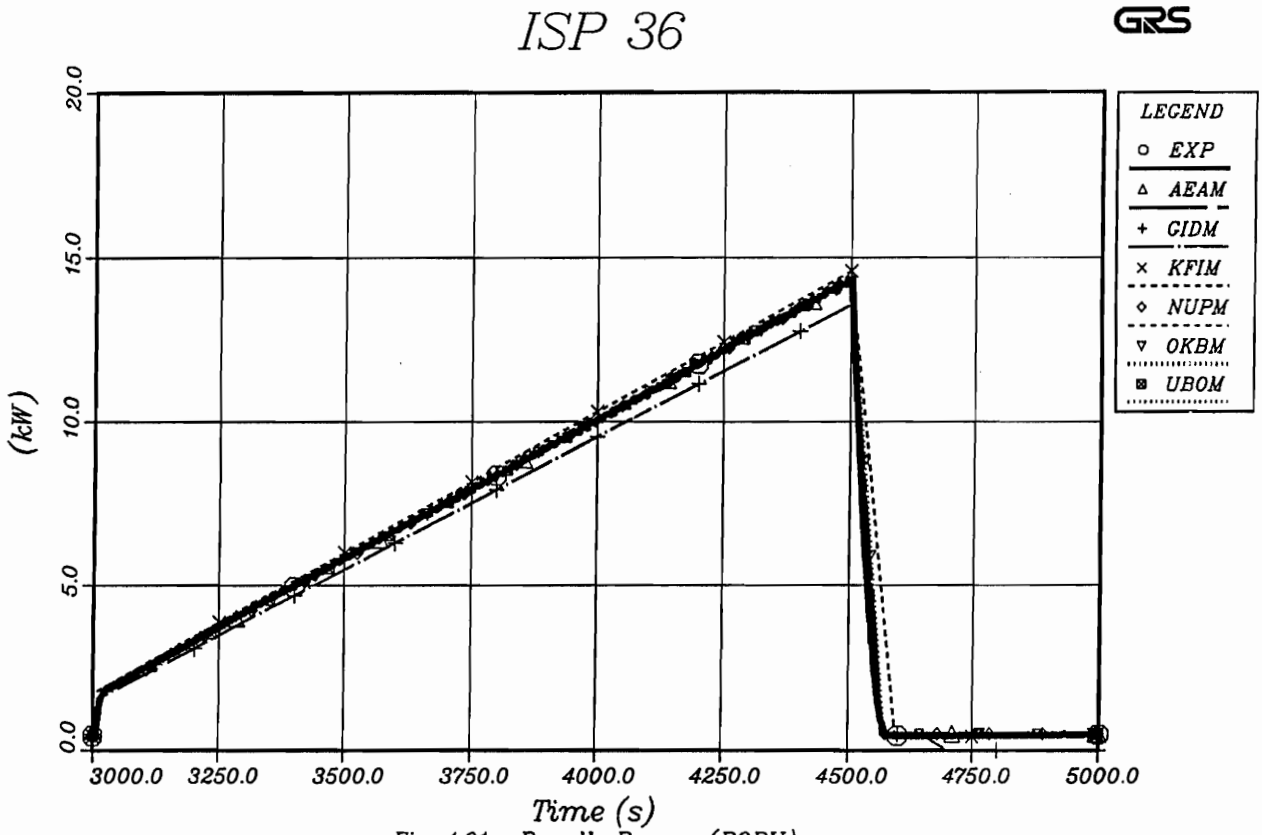

Fig. 4.01a: Bundle Power (POBU)
Code: MELCOR

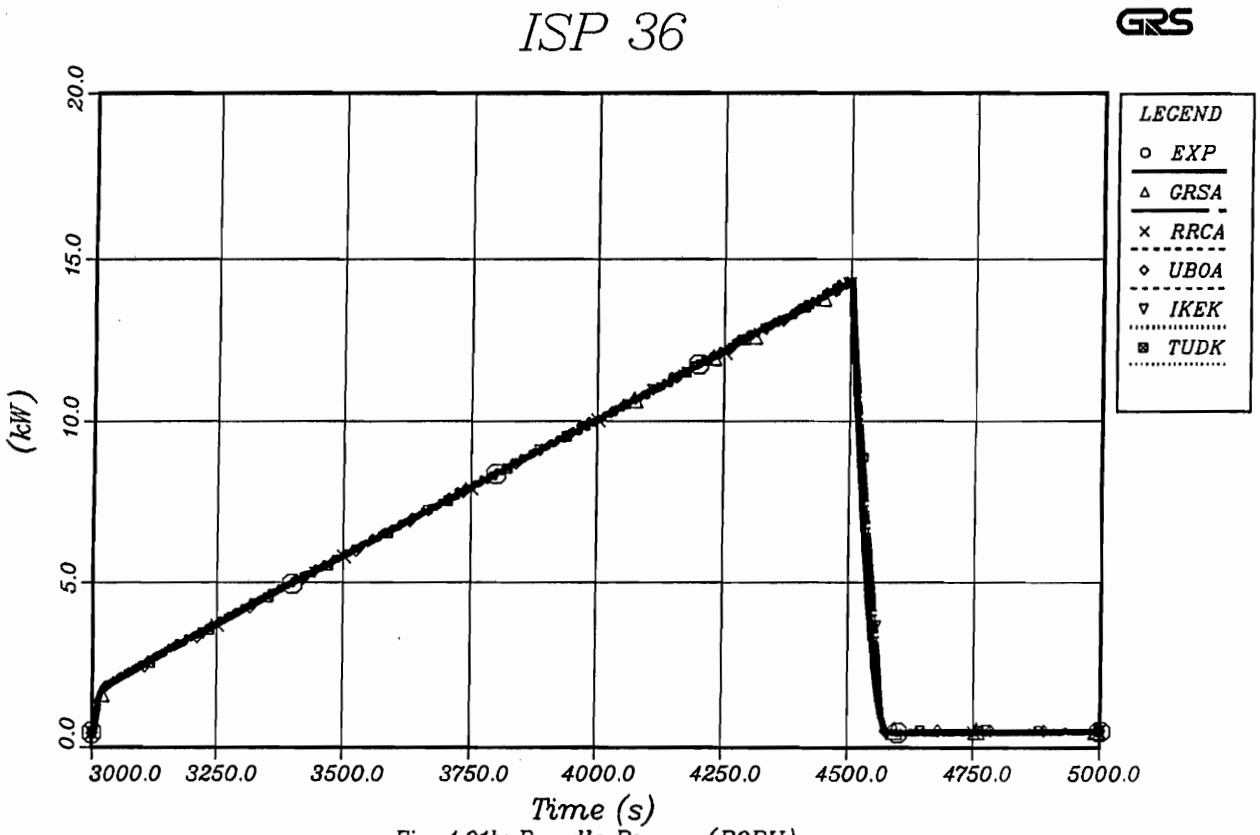

Fig. 4.01b: Bundle Power (POBU)
Codes: ATHLET-CD, KESS III

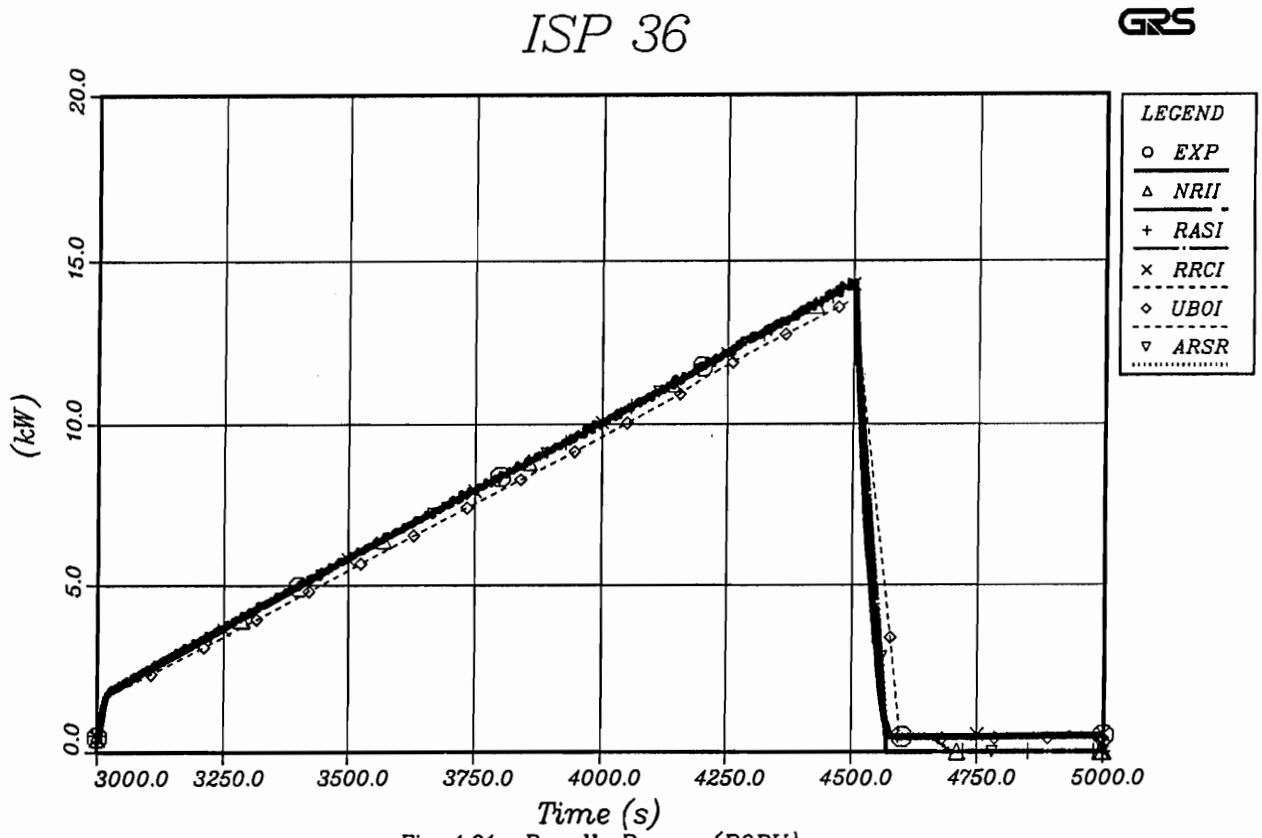

Fig. 4.01c: Bundle Power (POBU)
Codes: ICARE2, RAPTA-SFD

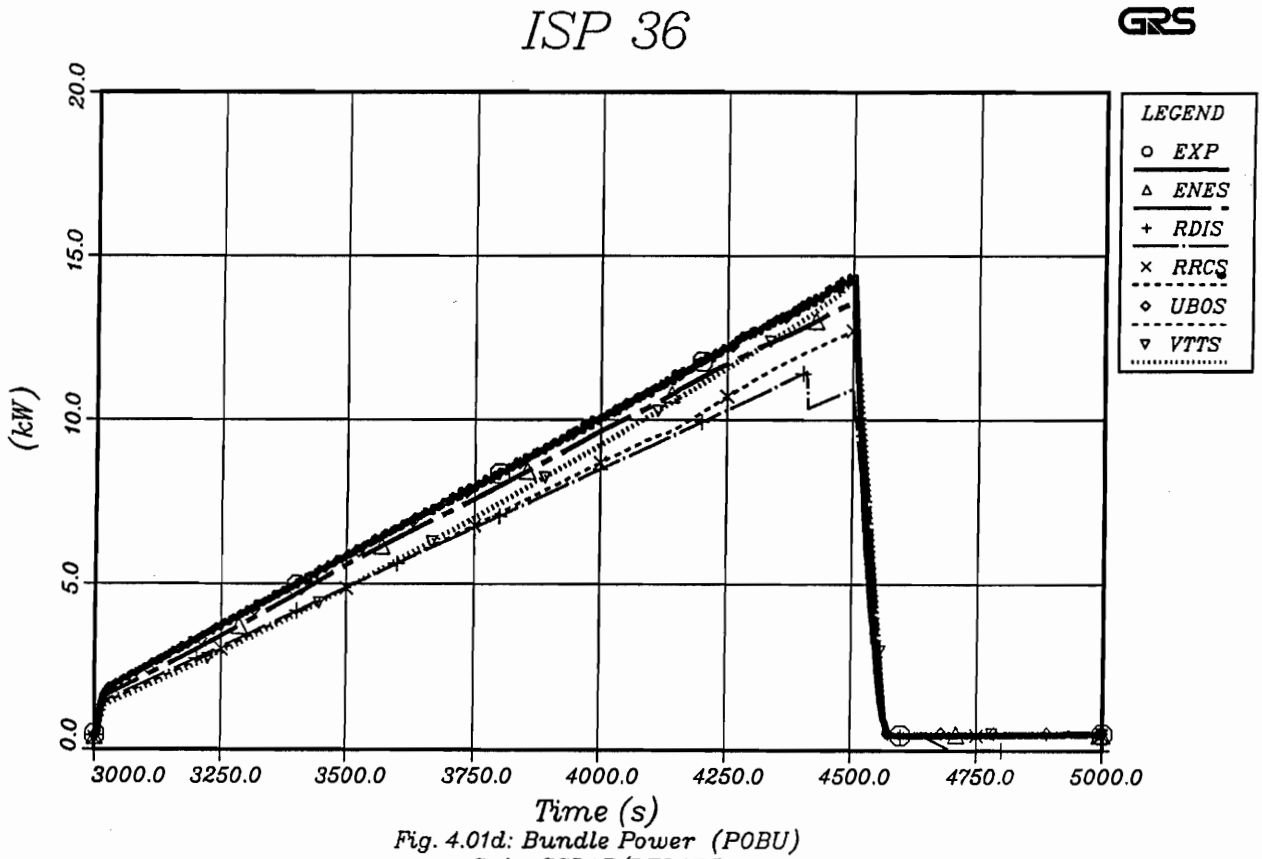

Fig. 4.01d: Bundle Power (POBU)
Code: SCDAP/RELAP5

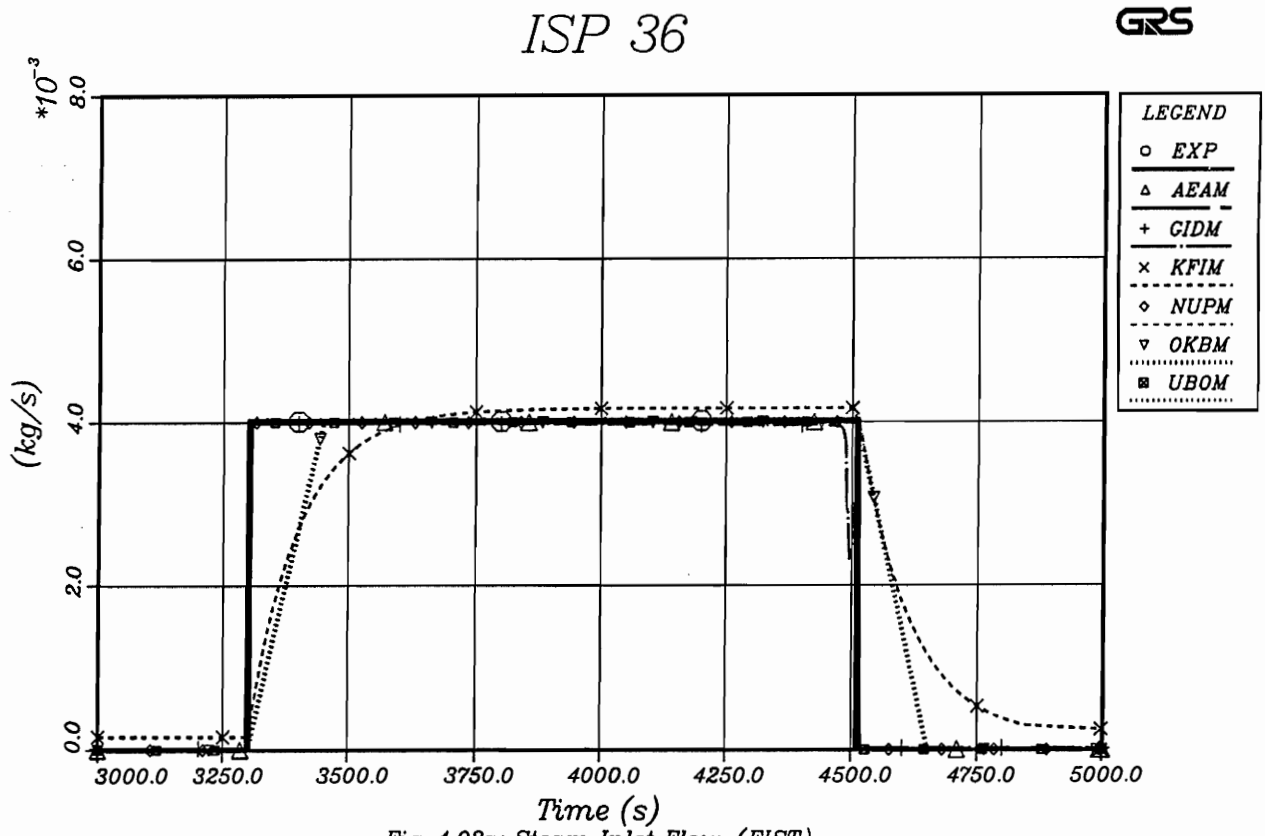

Fig. 4.02a: Steam Inlet Flow (FIST)
Code: MELCOR

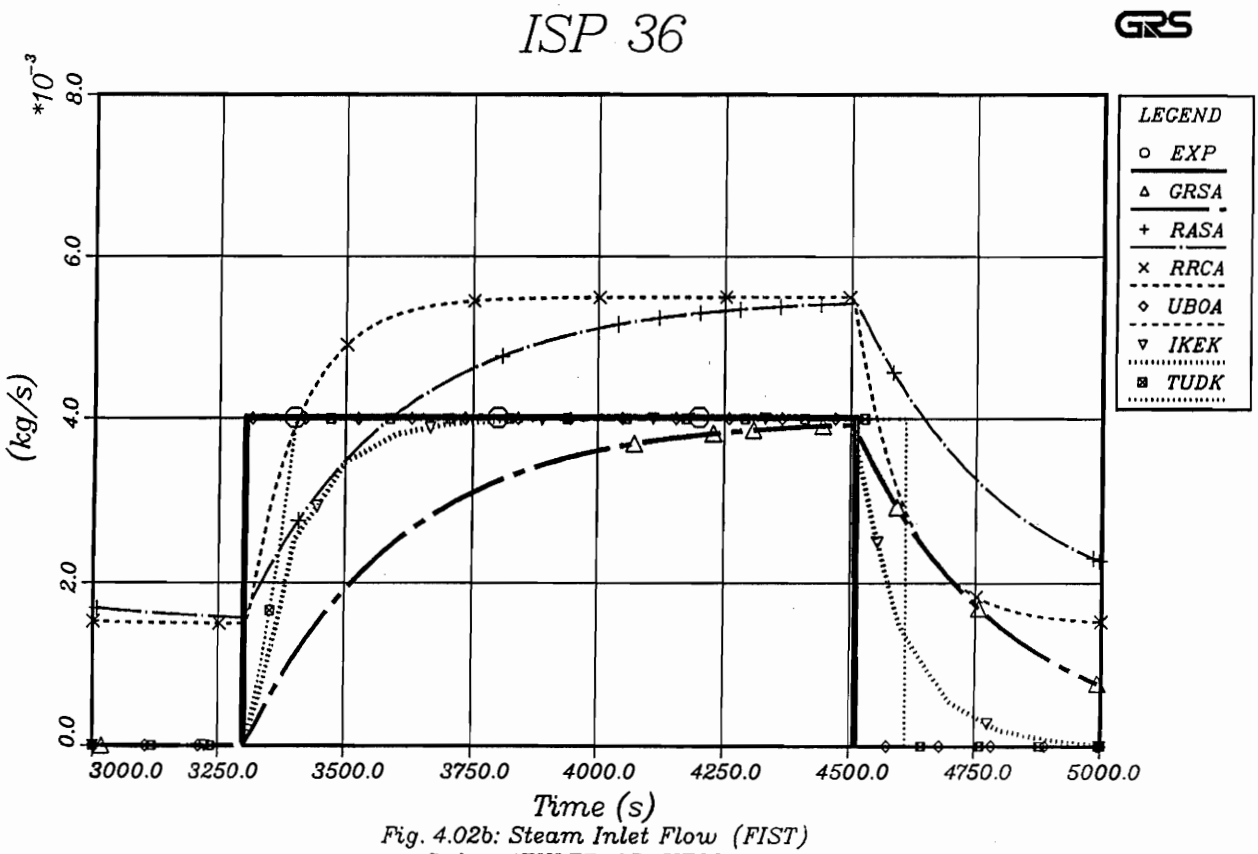

Fig. 4.02b: Steam Inlet Flow (FIST)
Codes: ATHLET-CD, KESS III

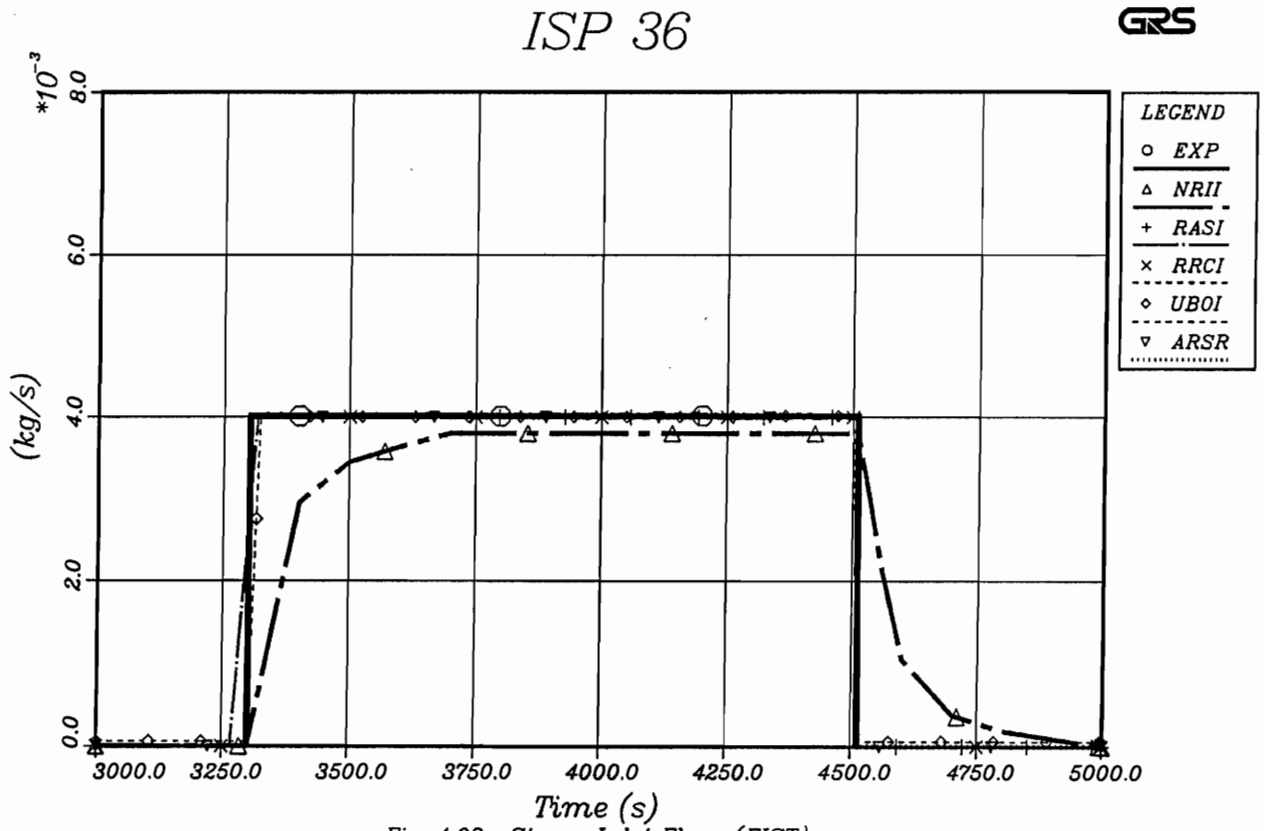

Fig. 4.02c: Steam Inlet Flow (FIST)
Codes: ICARE2, RAPTA-SFD

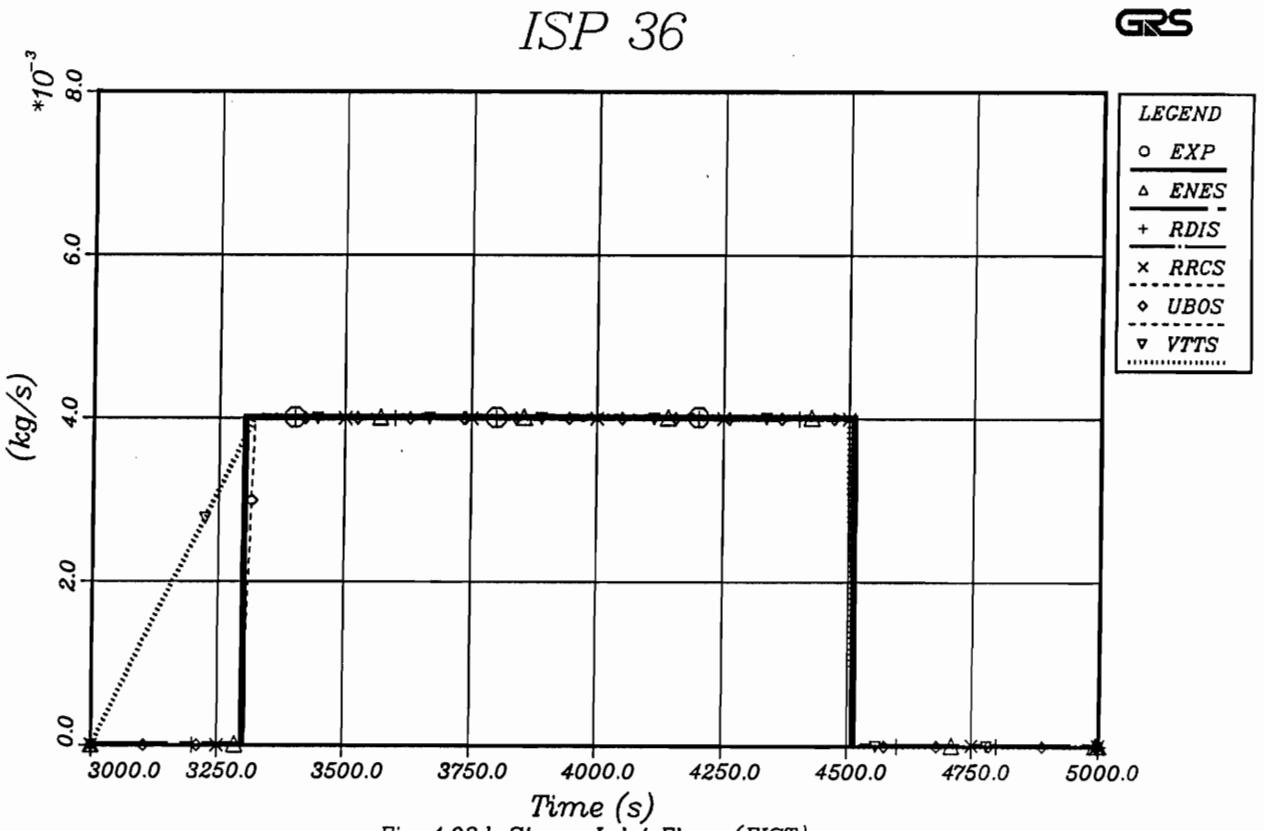

Fig. 4.02d: Steam Inlet Flow (FIST)
Code: SCDAP/RELAP5

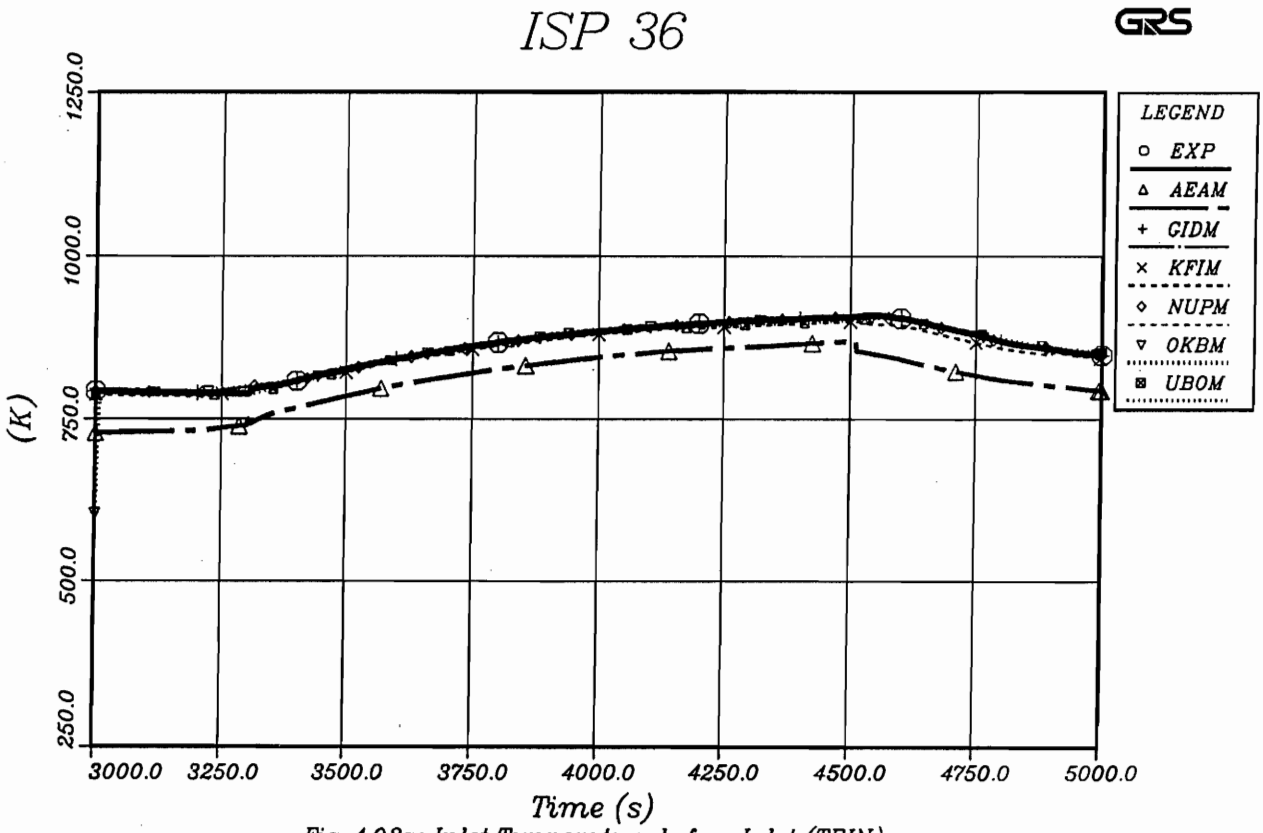

Fig. 4.03a: Inlet Temperature before Inlet (TEIN)
Code: MELCOR

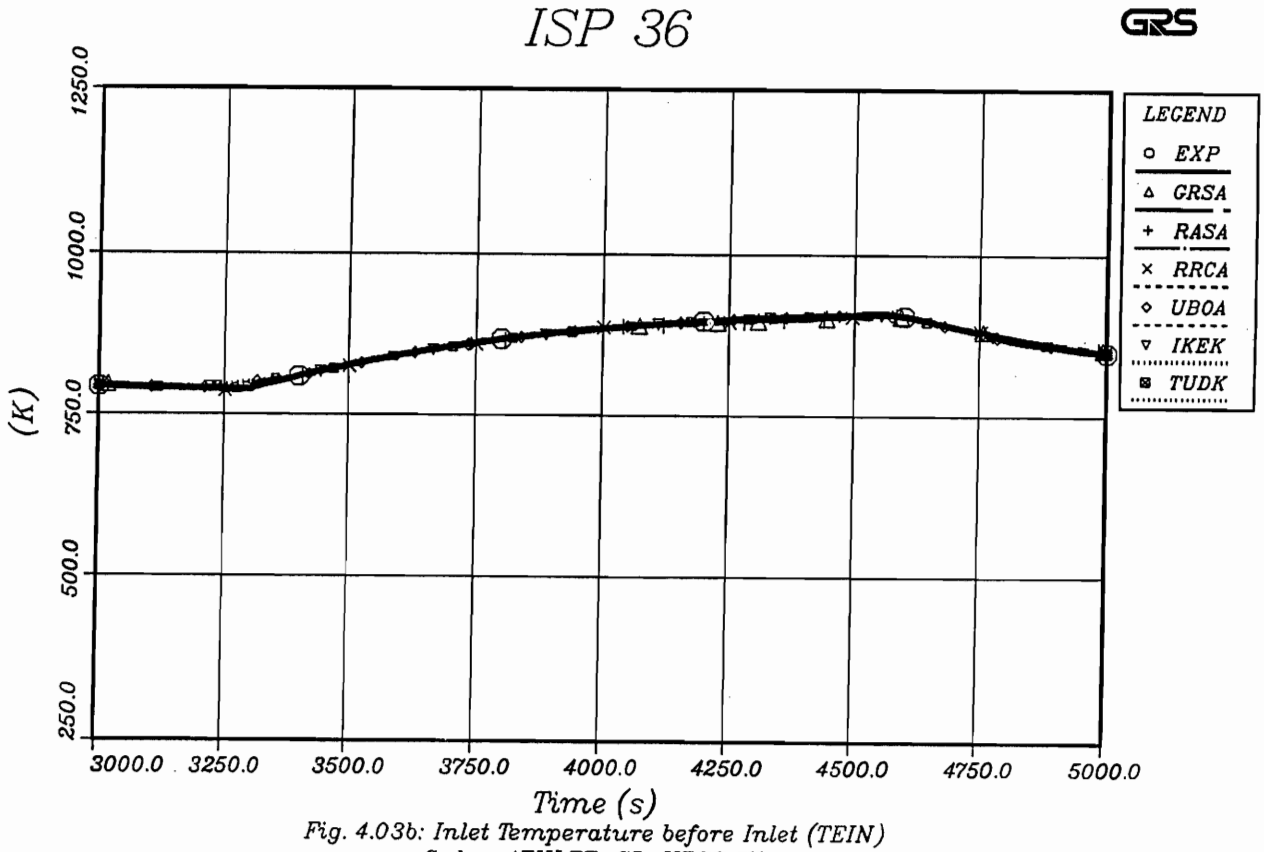

Fig. 4.03b: Inlet Temperature before Inlet (TEIN)
Codes: ATHLET-CD, KESS III

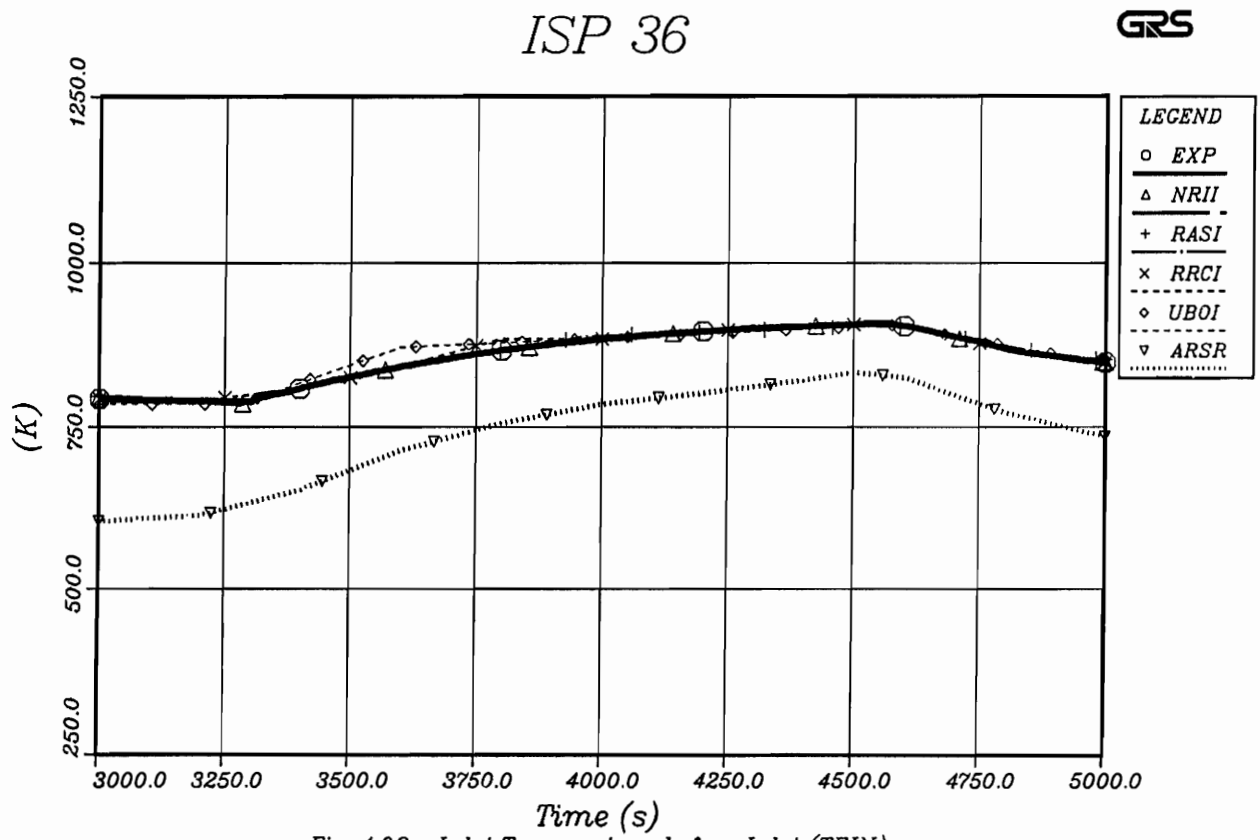

Fig. 4.03c: Inlet Temperature before Inlet (TEIN)
Codes: ICARE2, RAPTA–SFD

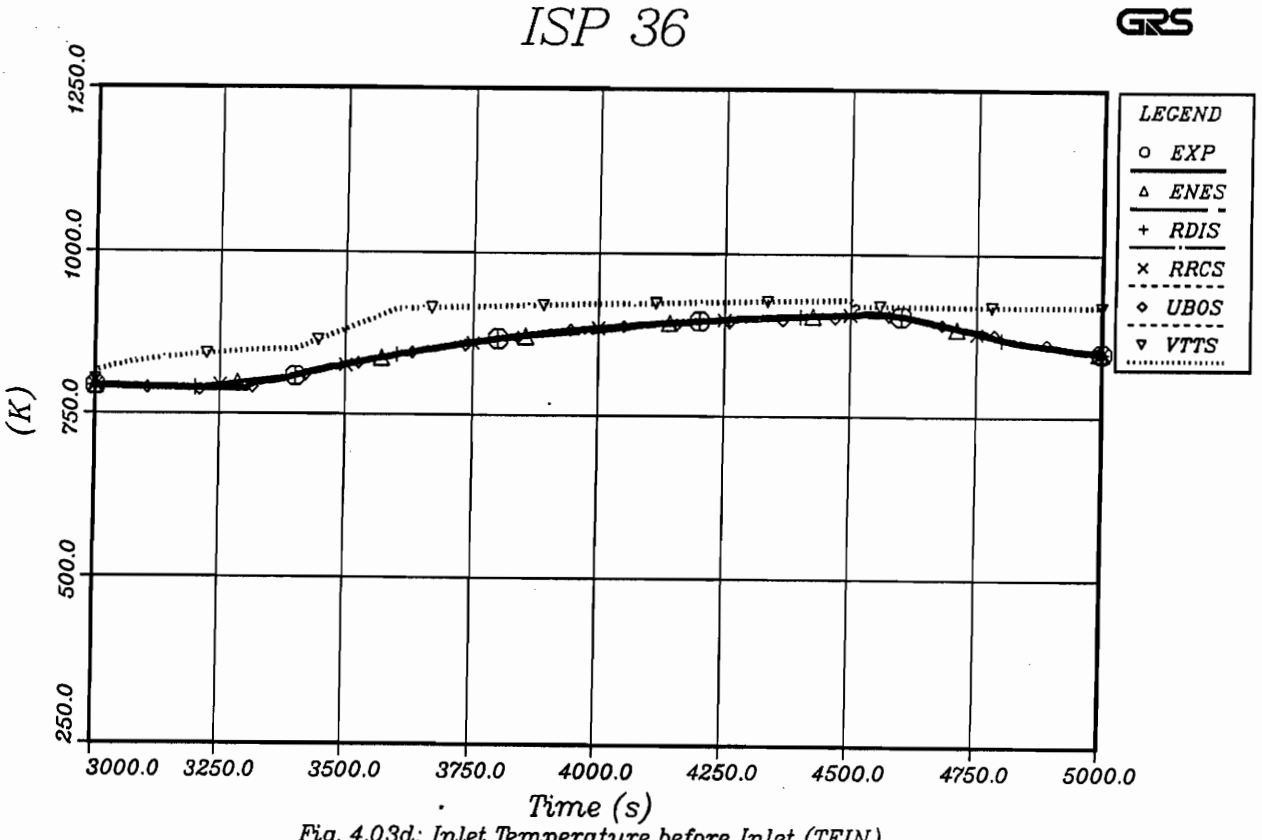

Fig. 4.03d: Inlet Temperature before Inlet (TEIN)
Code: SCDAP/RELAP5

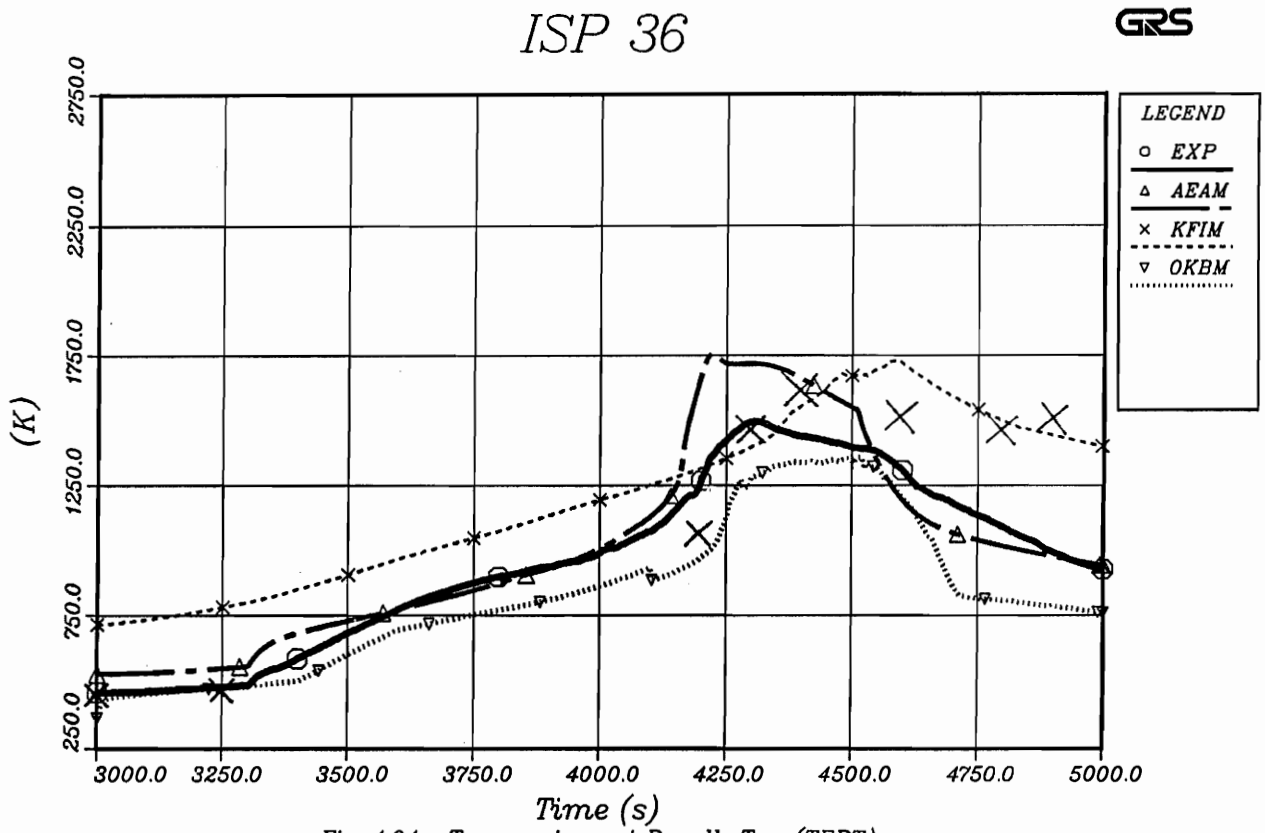

Fig. 4.04a: Temperature at Bundle Top (TEBT)
Code: MELCOR

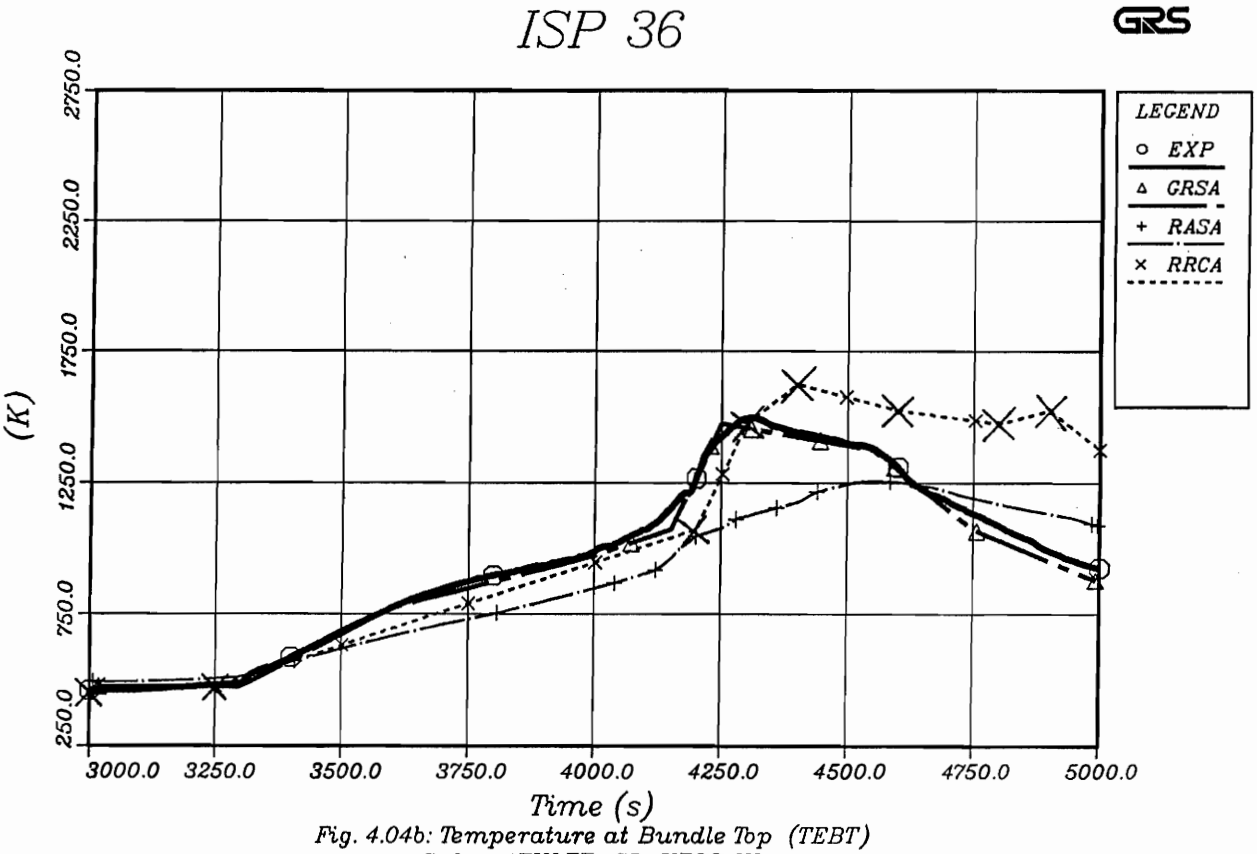

Fig. 4.04b: Temperature at Bundle Top (TEBT)
Codes: ATHLET-CD, KESS III

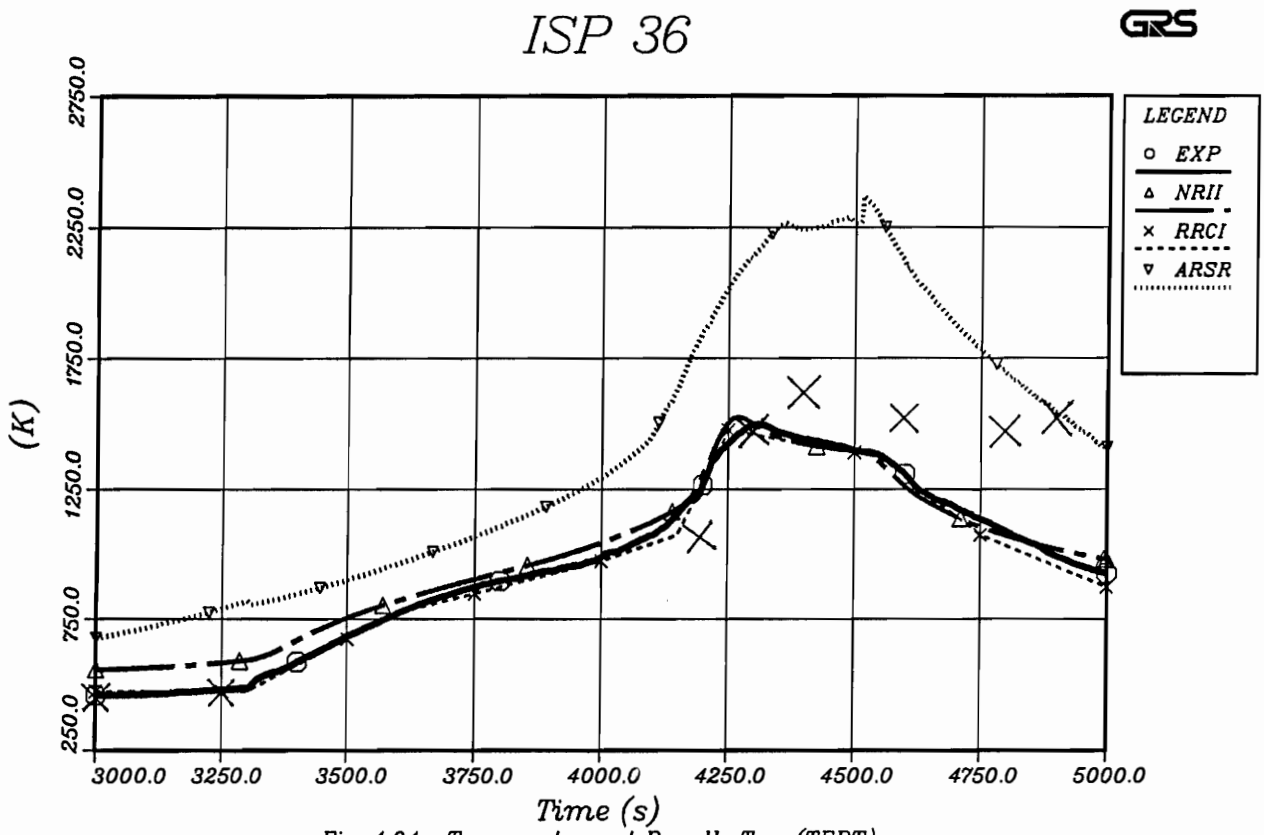

Fig. 4.04c: Temperature at Bundle Top (TEBT)
Codes: ICARE2, RAPTA–SFD

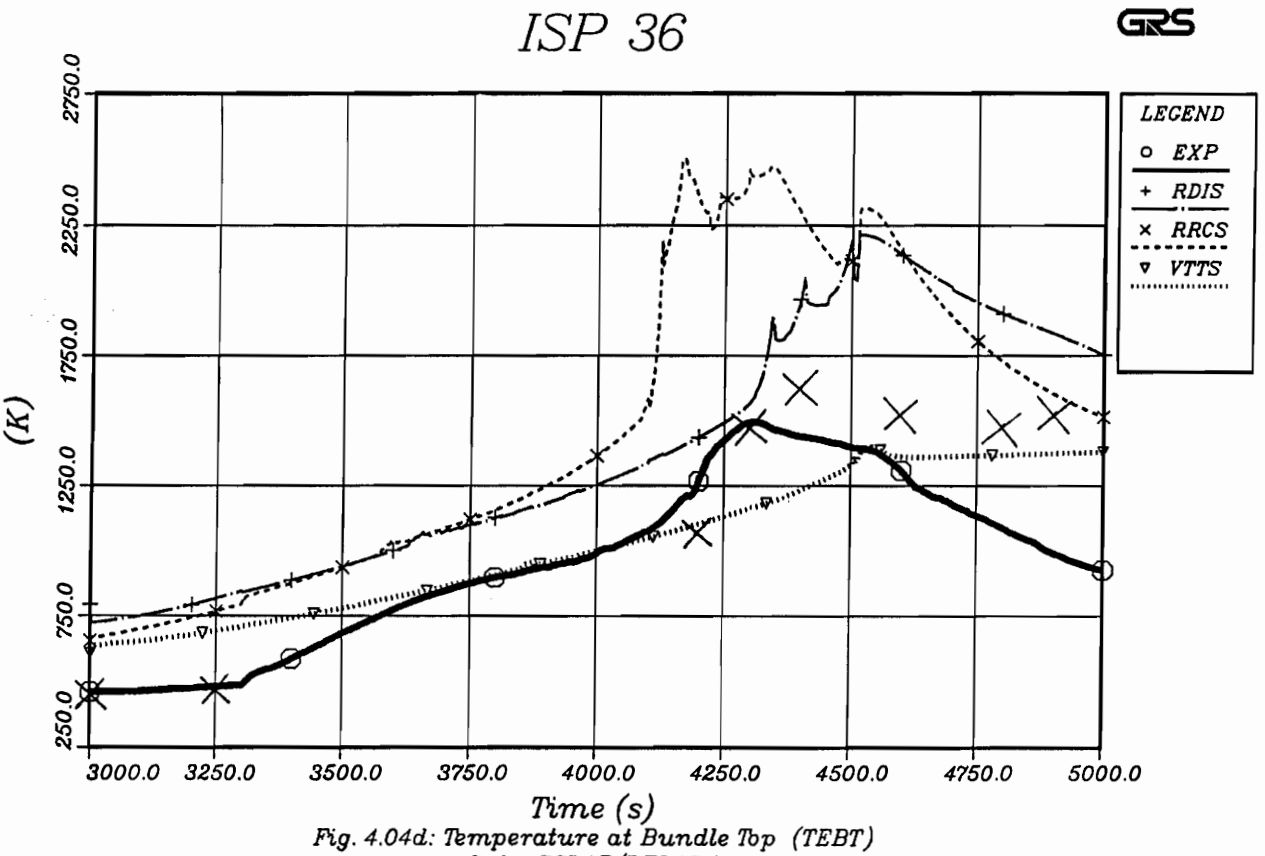

Fig. 4.04d: Temperature at Bundle Top (TEBT)
Code: SCDAP/RELAP5

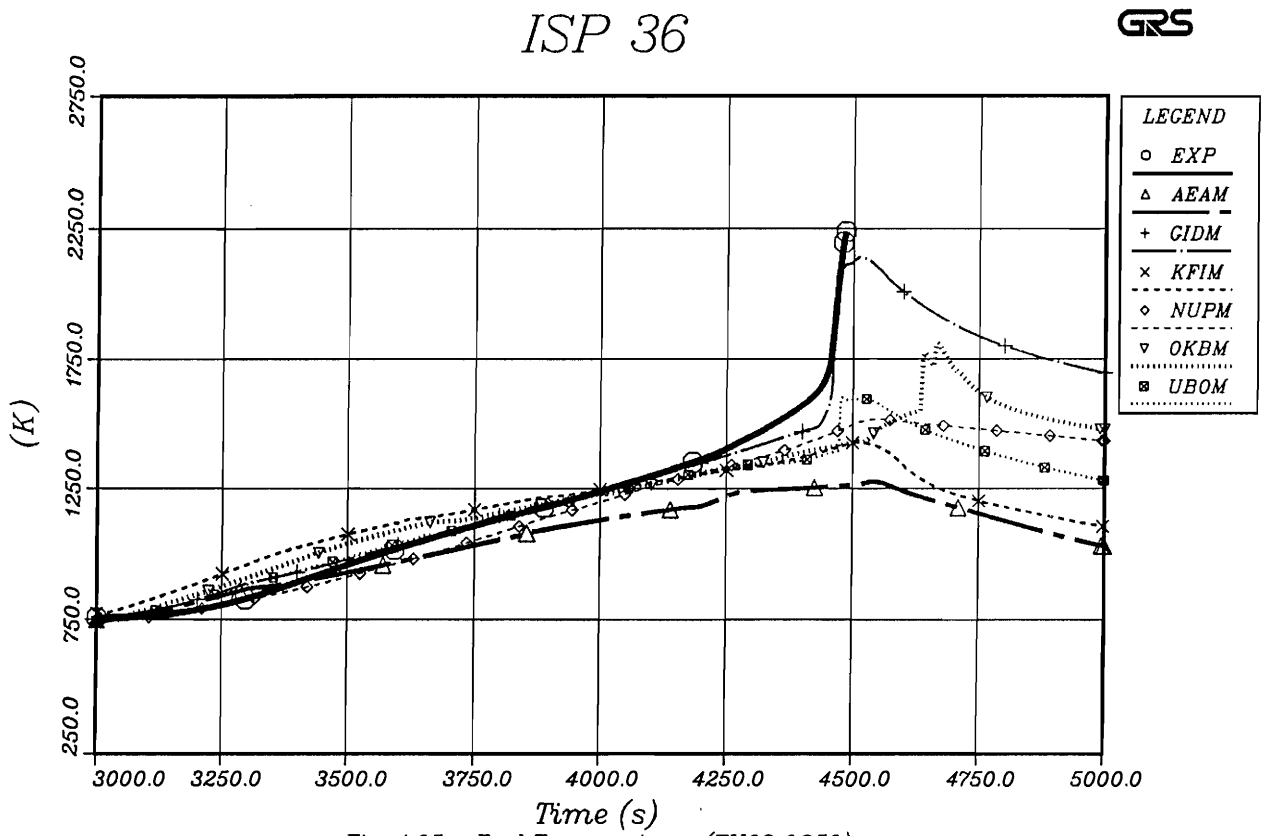

Fig. 4.05a: Fuel Temperature (TU02 0350)
Code: MELCOR

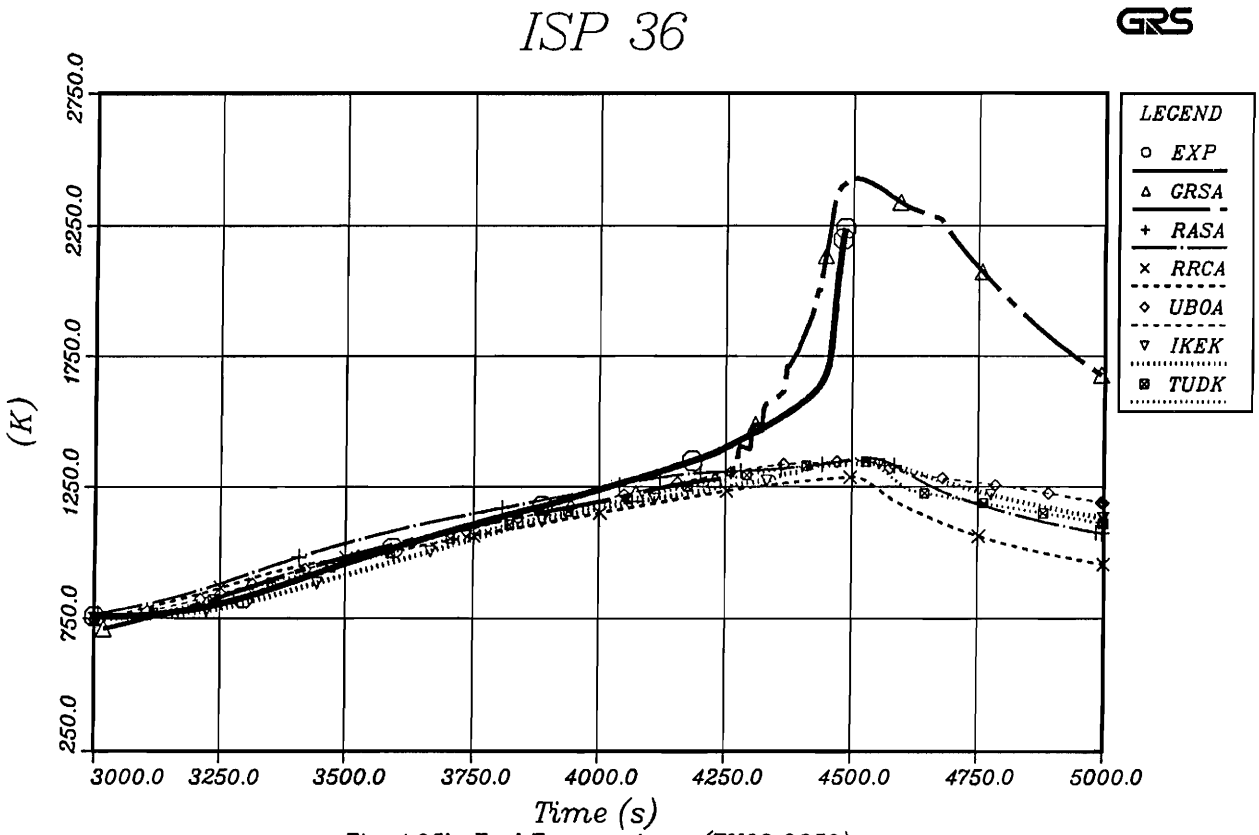

Fig. 4.05b: Fuel Temperature (TU02 0350)
Codes: ATHLET-CD, KESS III

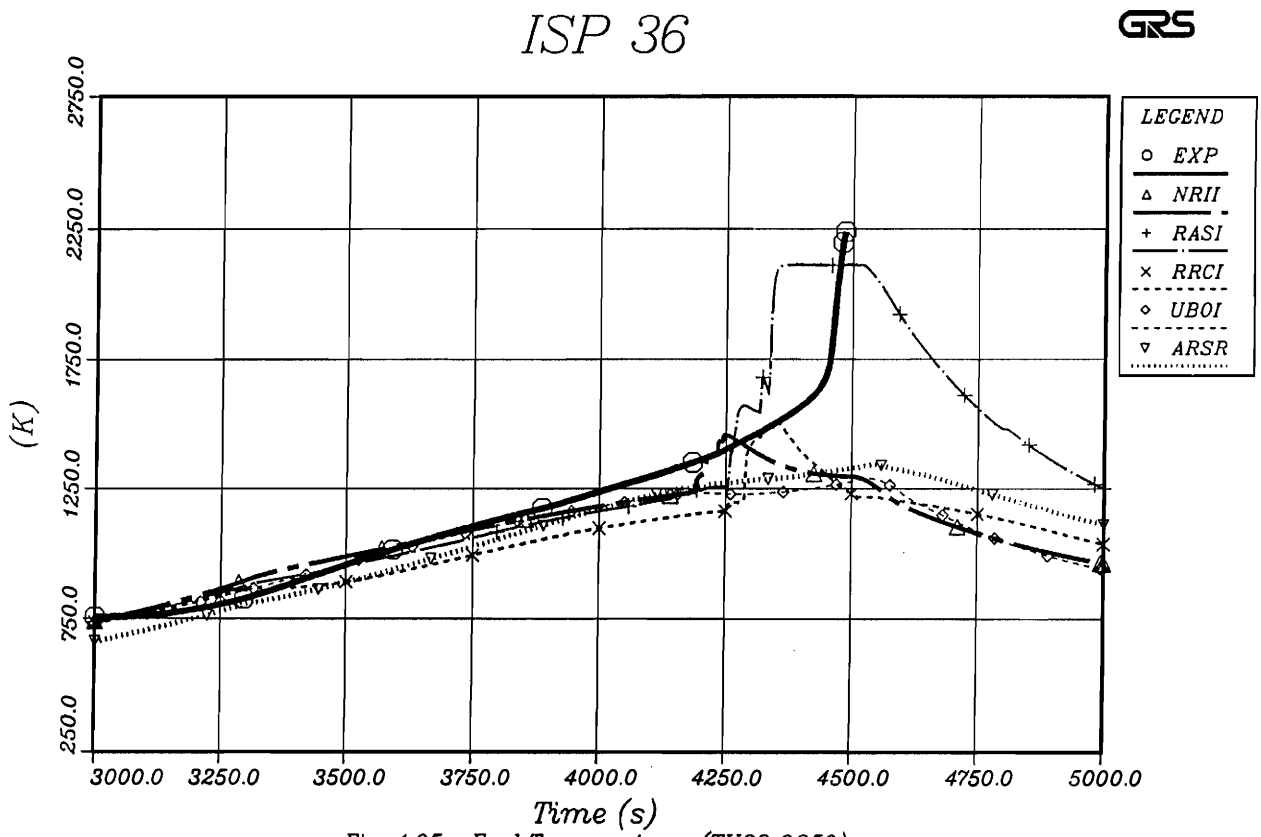

Fig. 4.05c: Fuel Temperature (TU02 0350)
Codes: ICARE2, RAPTA-SFD

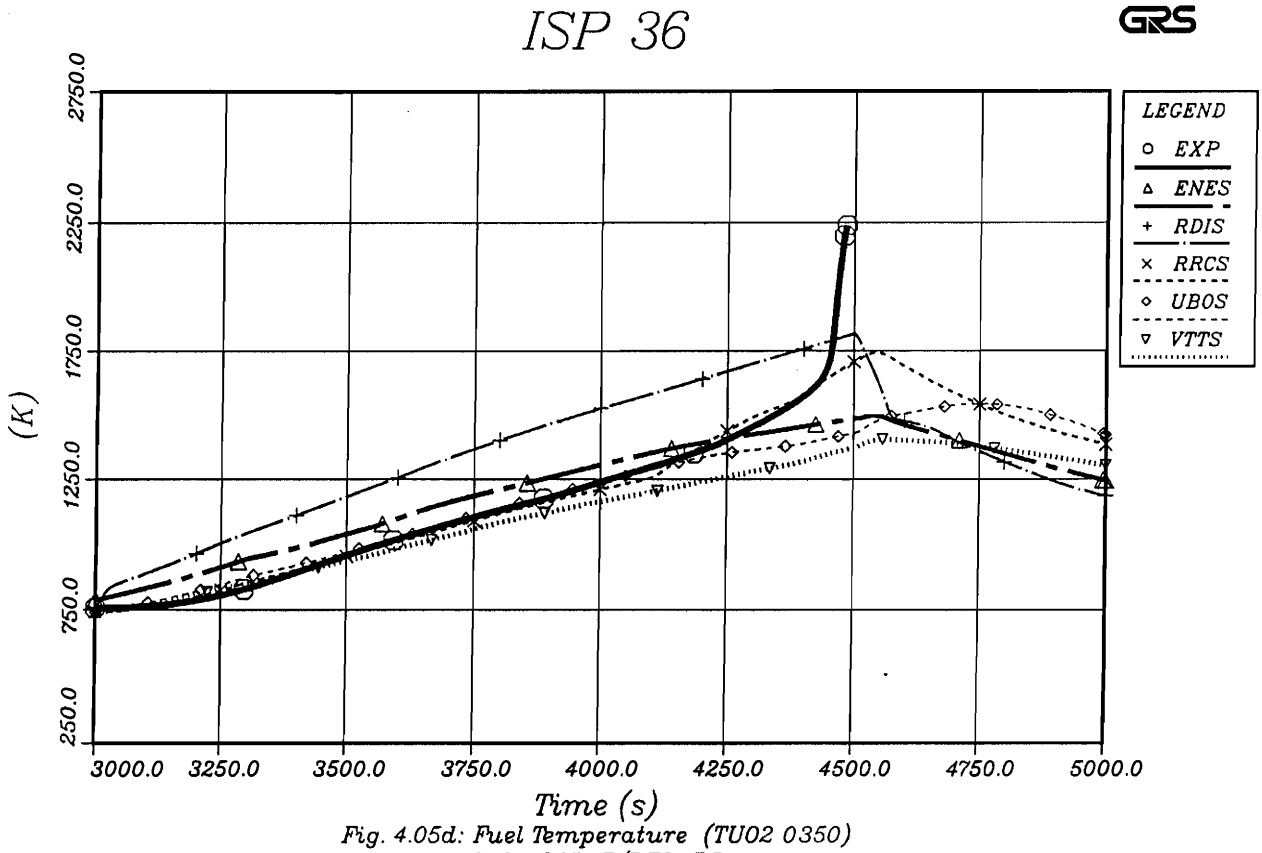

Fig. 4.05d: Fuel Temperature (TU02 0350)
Code: SCDAP/RELAP5

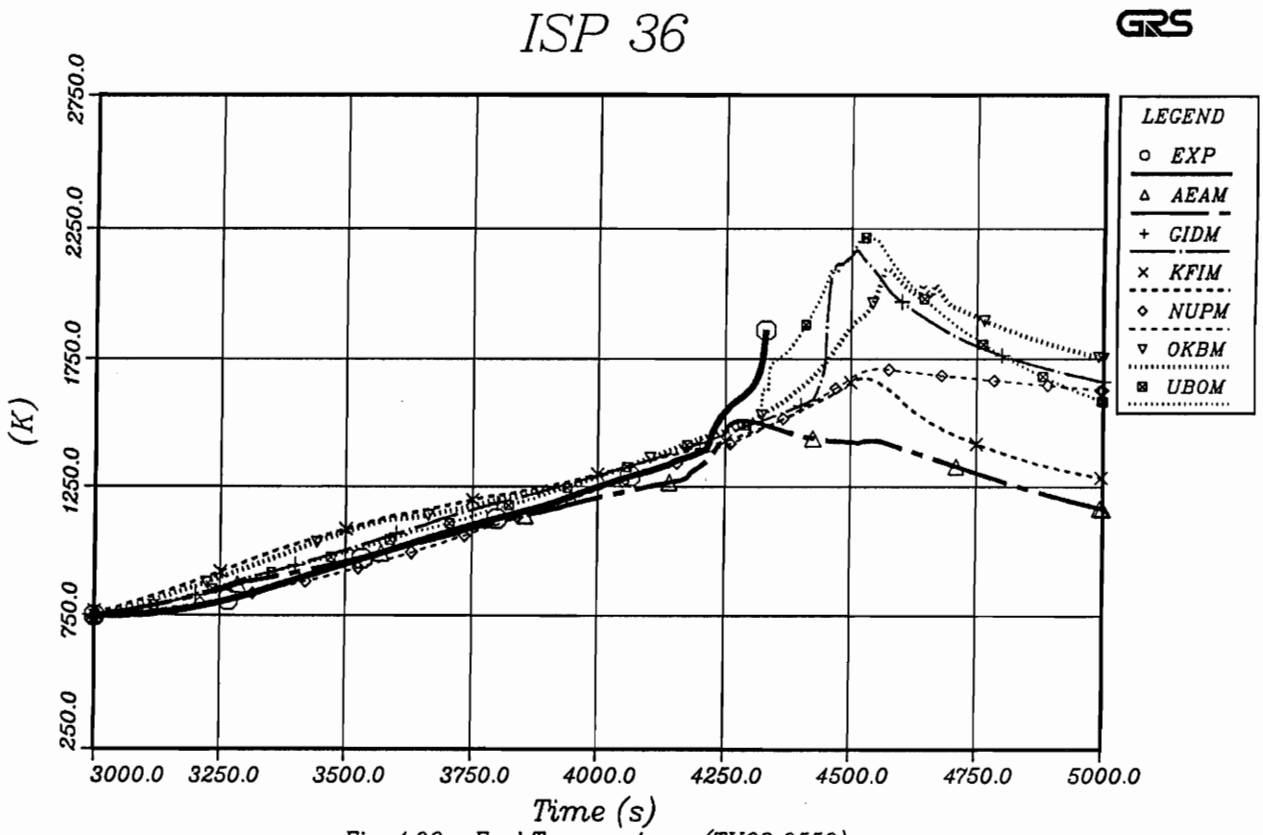

Fig. 4.06a: Fuel Temperature (TU02 0550)
Code: MELCOR

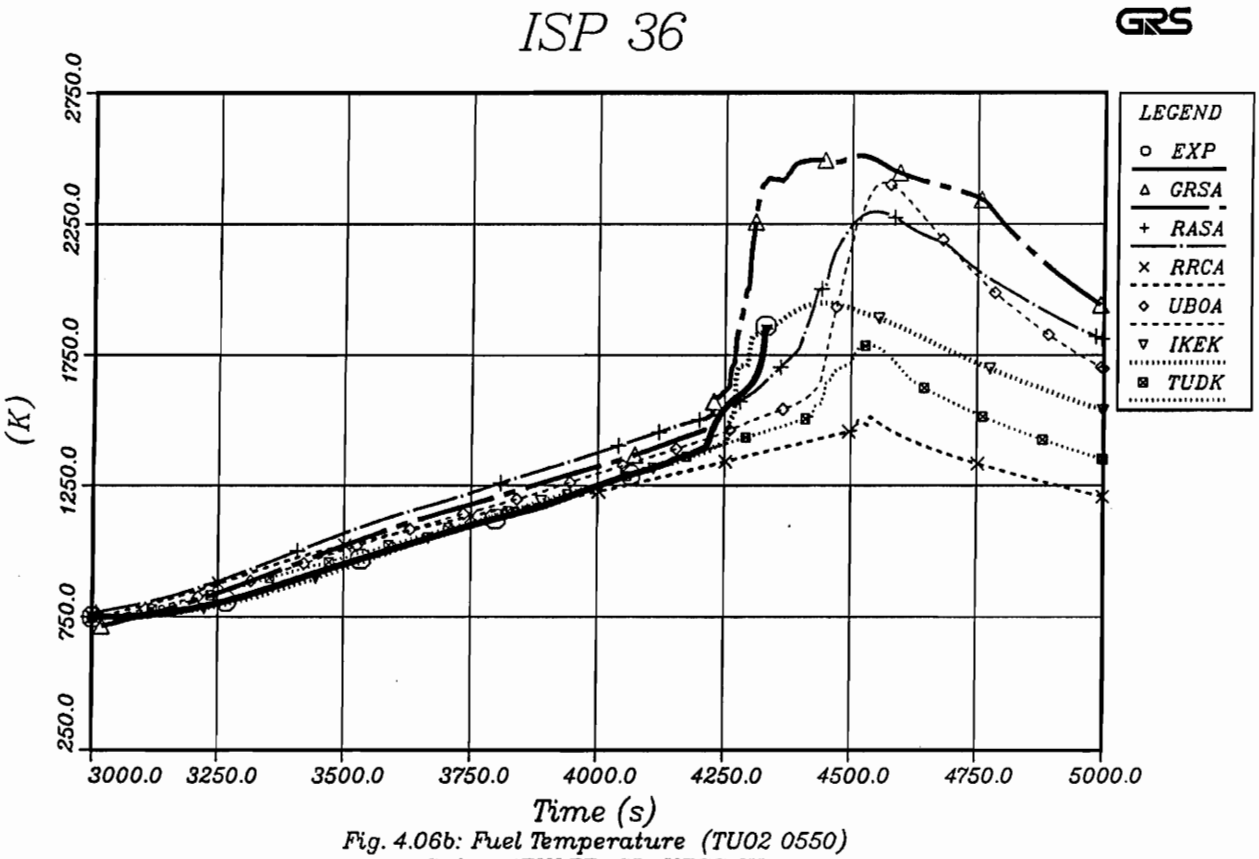

Fig. 4.06b: Fuel Temperature (TU02 0550)
Codes: ATHLET-CD, KESS III

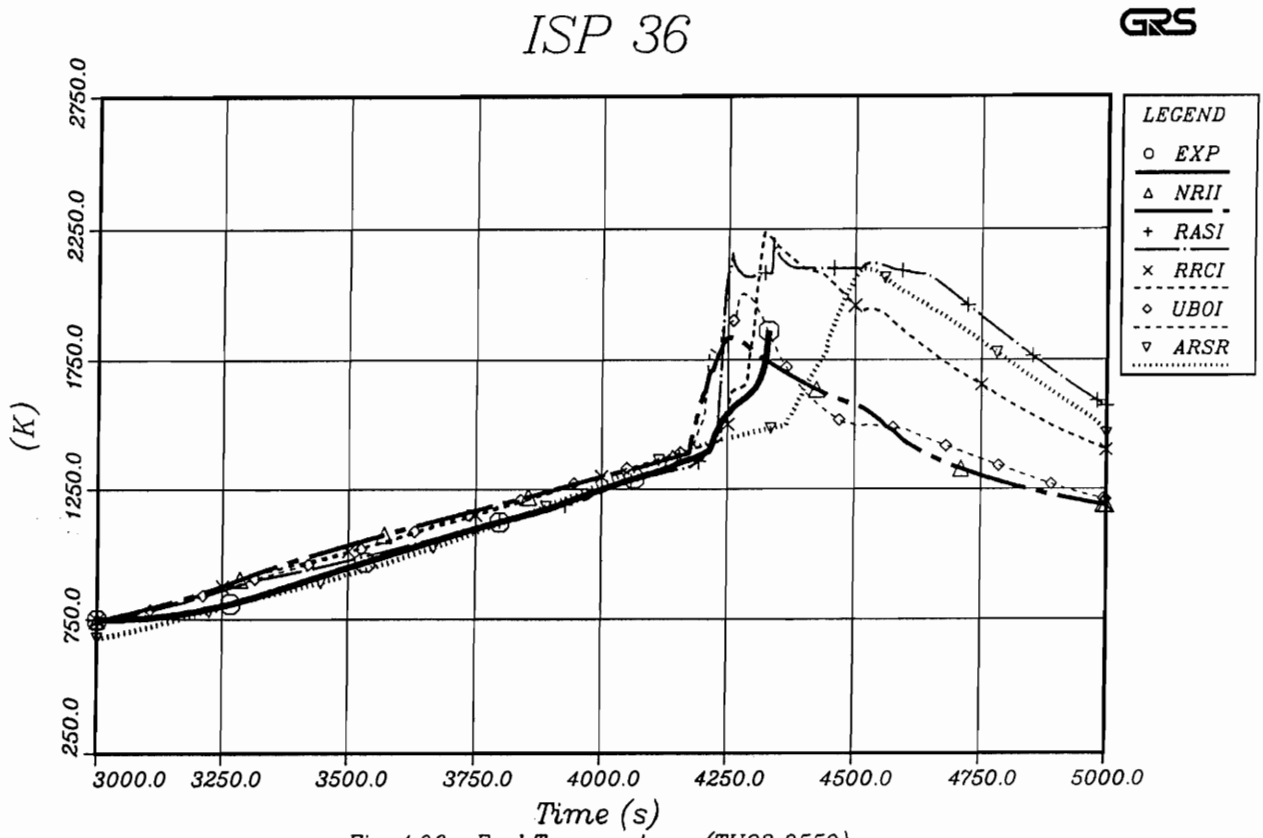

Fig. 4.06c: Fuel Temperature (TU02 0550)
Codes: ICARE2, RAPTA-SFD

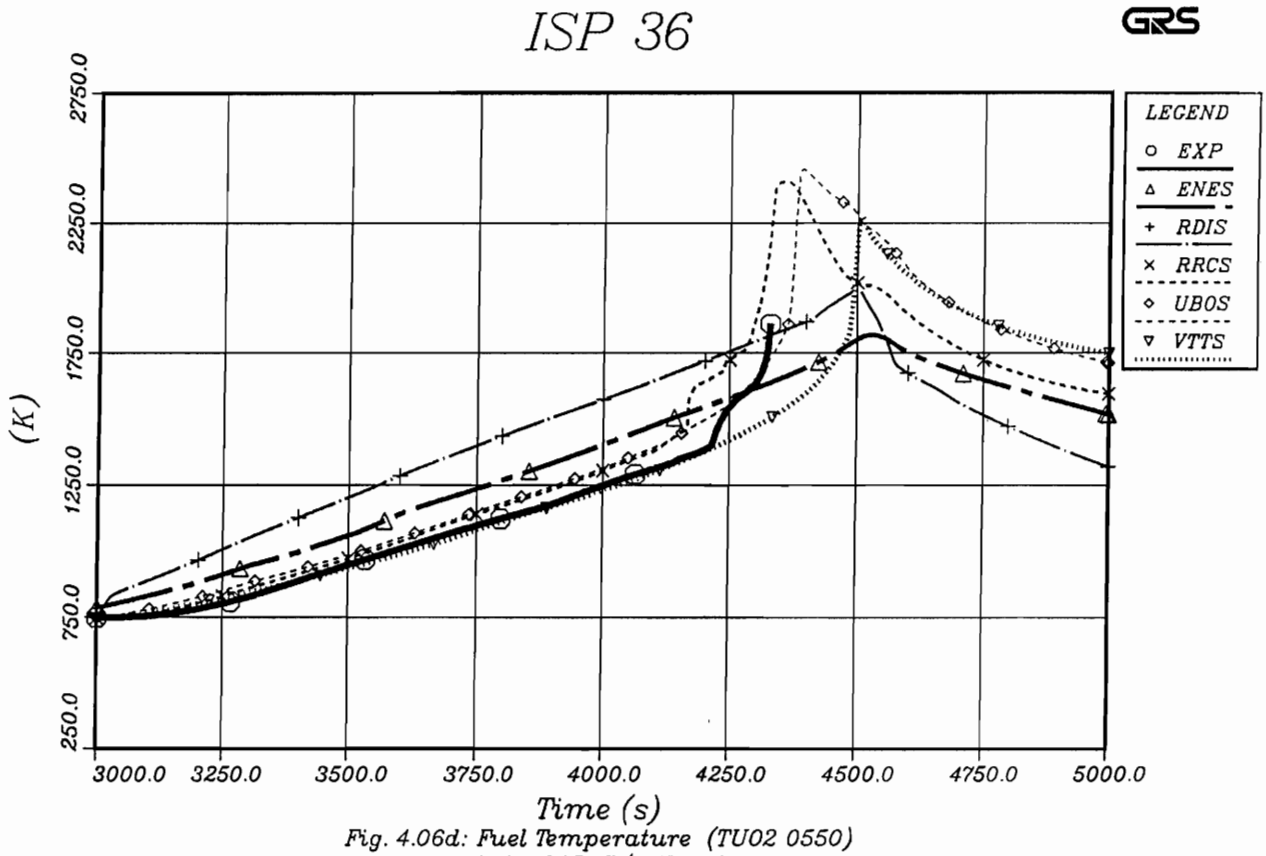

Fig. 4.06d: Fuel Temperature (TU02 0550)
Code: SCDAP/RELAP5

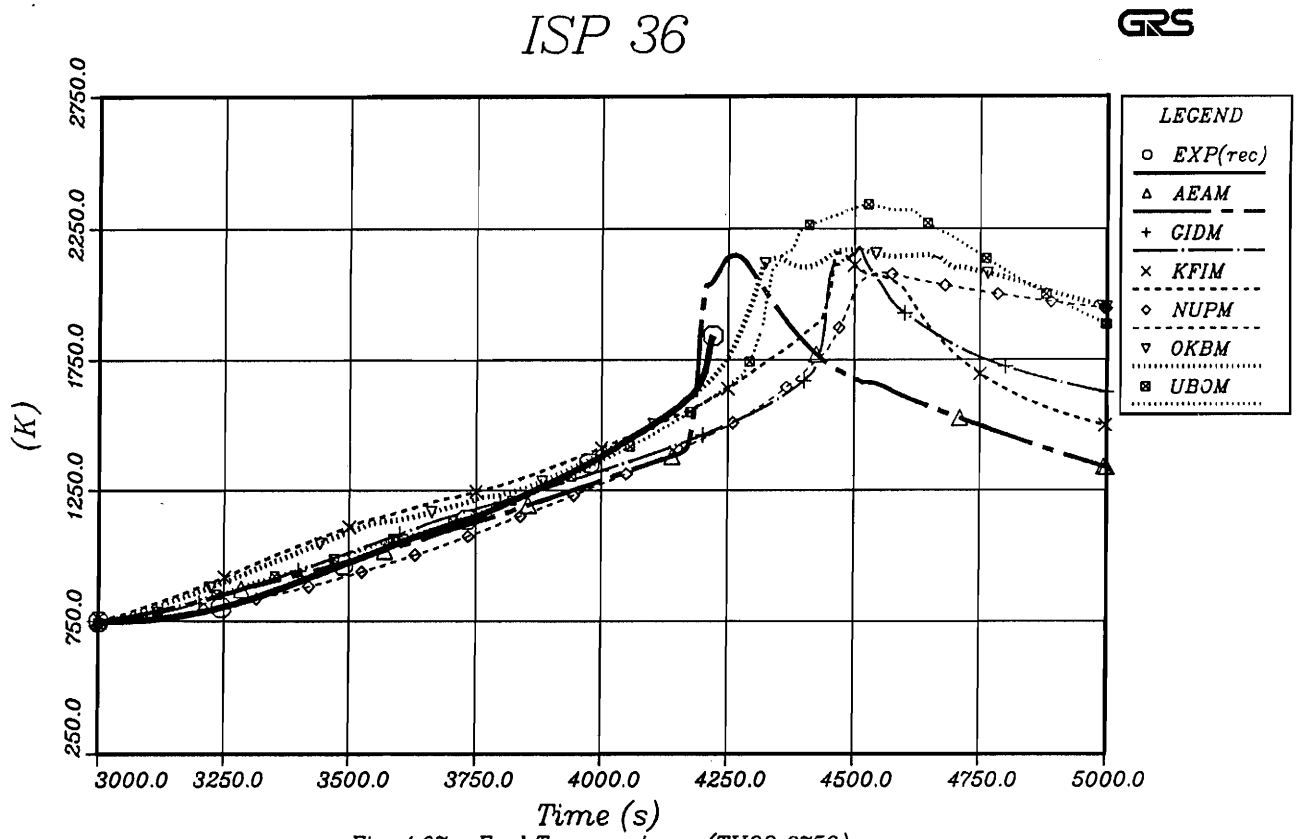

Fig. 4.07a: Fuel Temperature (TU02 0750)
Code: MELCOR

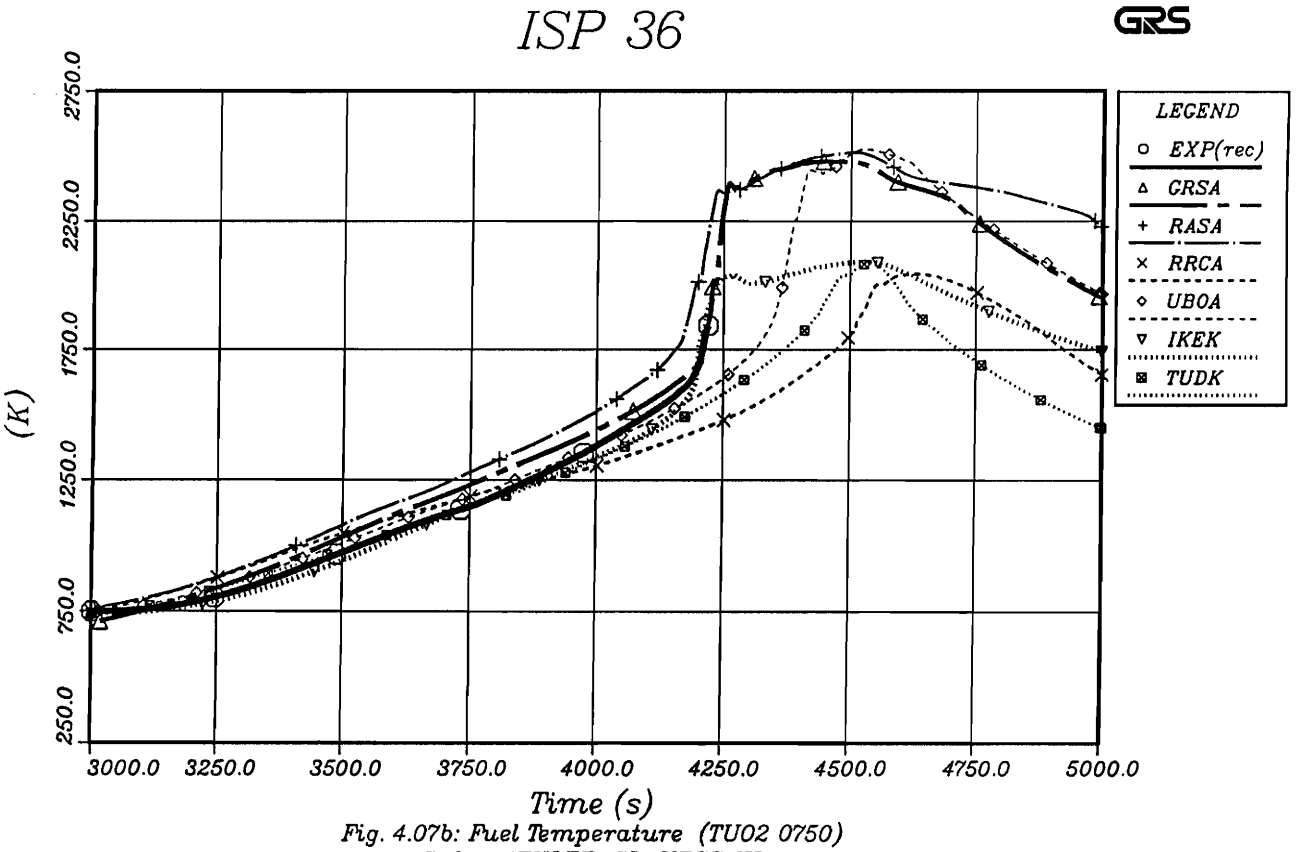

Fig. 4.07b: Fuel Temperature (TU02 0750)
Codes: ATHLET-CD, KESS III

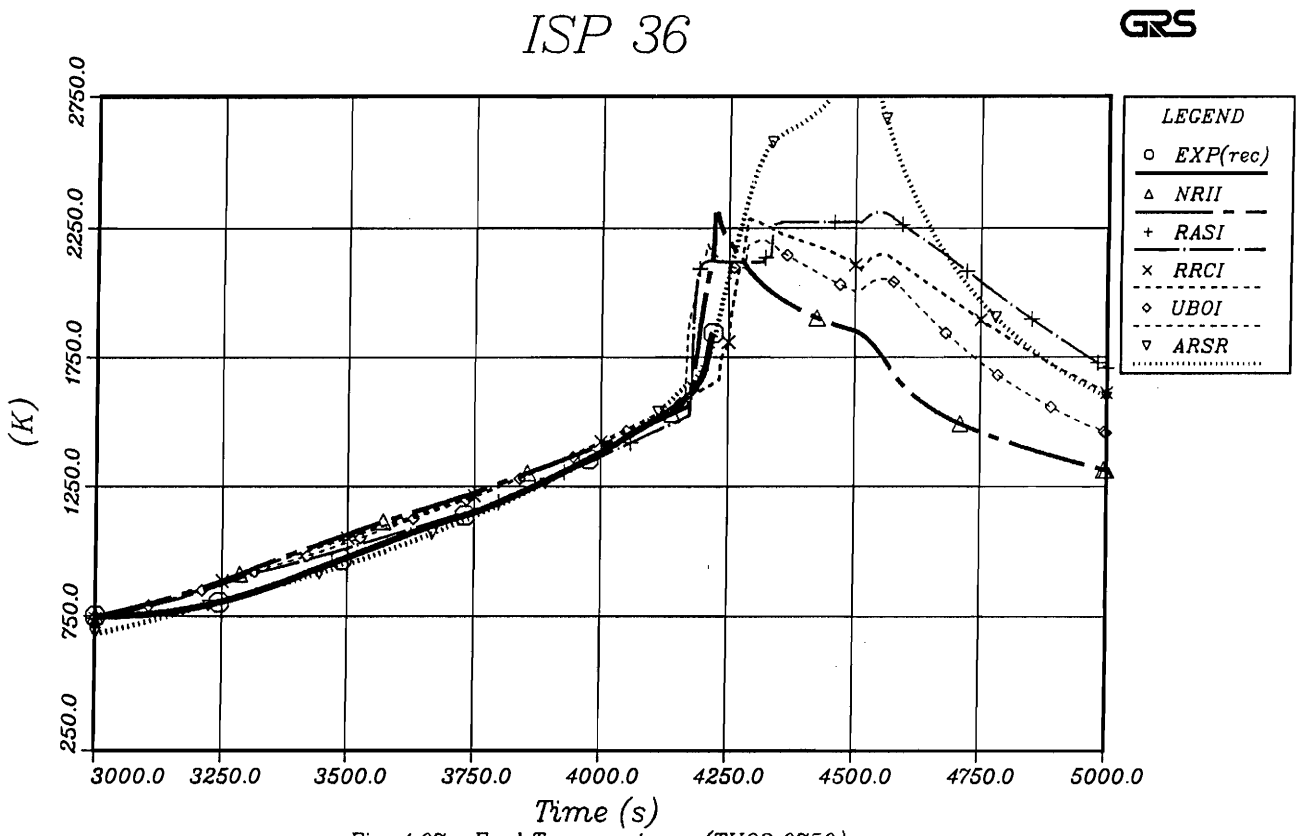

Fig. 4.07c: Fuel Temperature (TU02 0750)
Codes: ICARE2, RAPTA-SFD

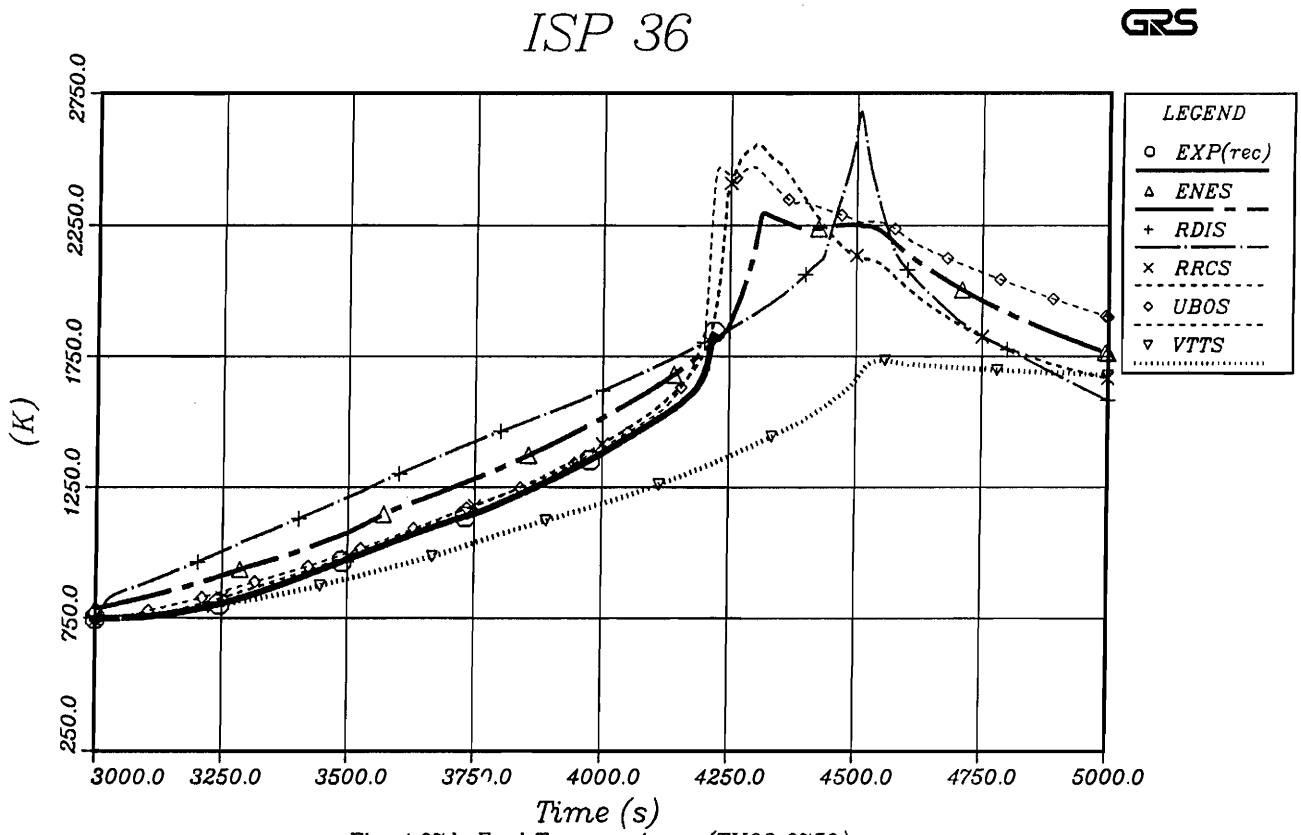

Fig. 4.07d: Fuel Temperature (TU02 0750)
Code: SCDAP/RELAP5

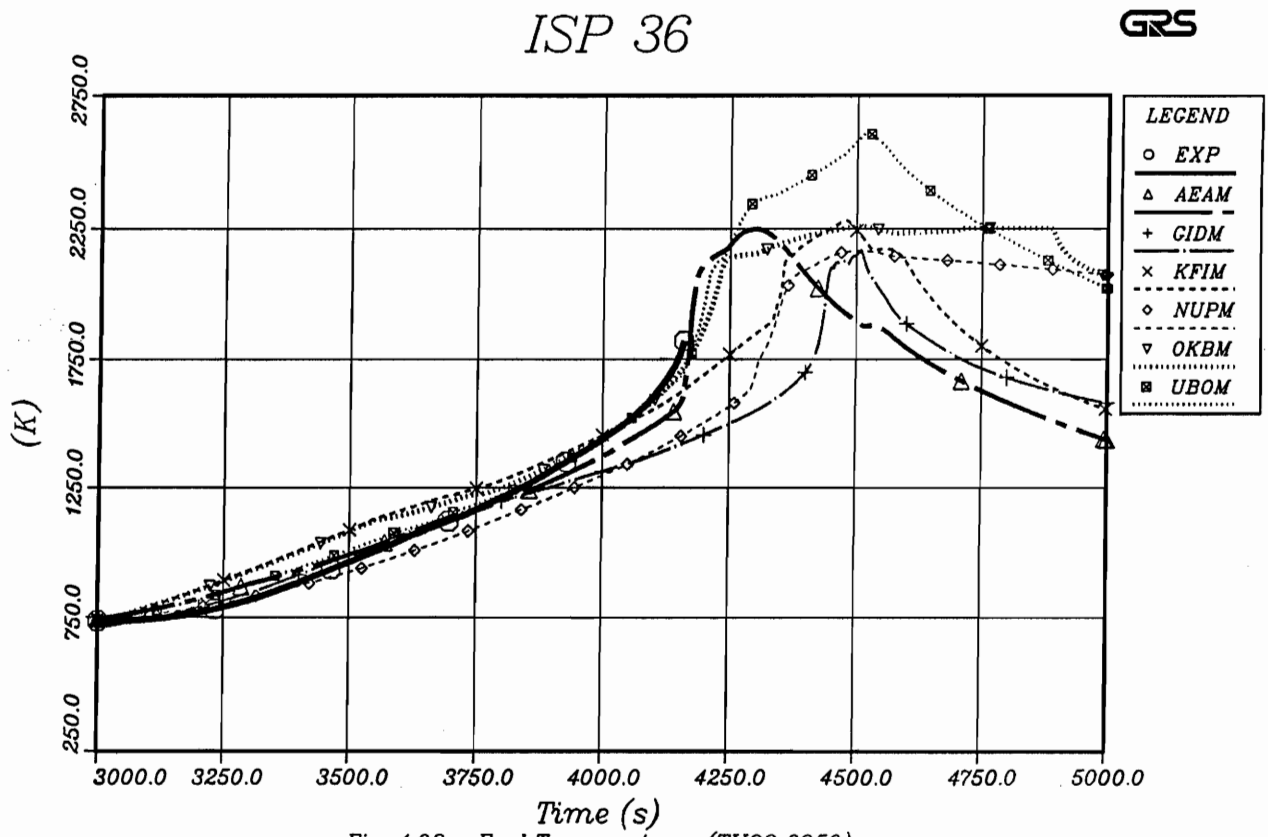

Fig. 4.08a: Fuel Temperature (TU02 0950)
Code: MELCOR

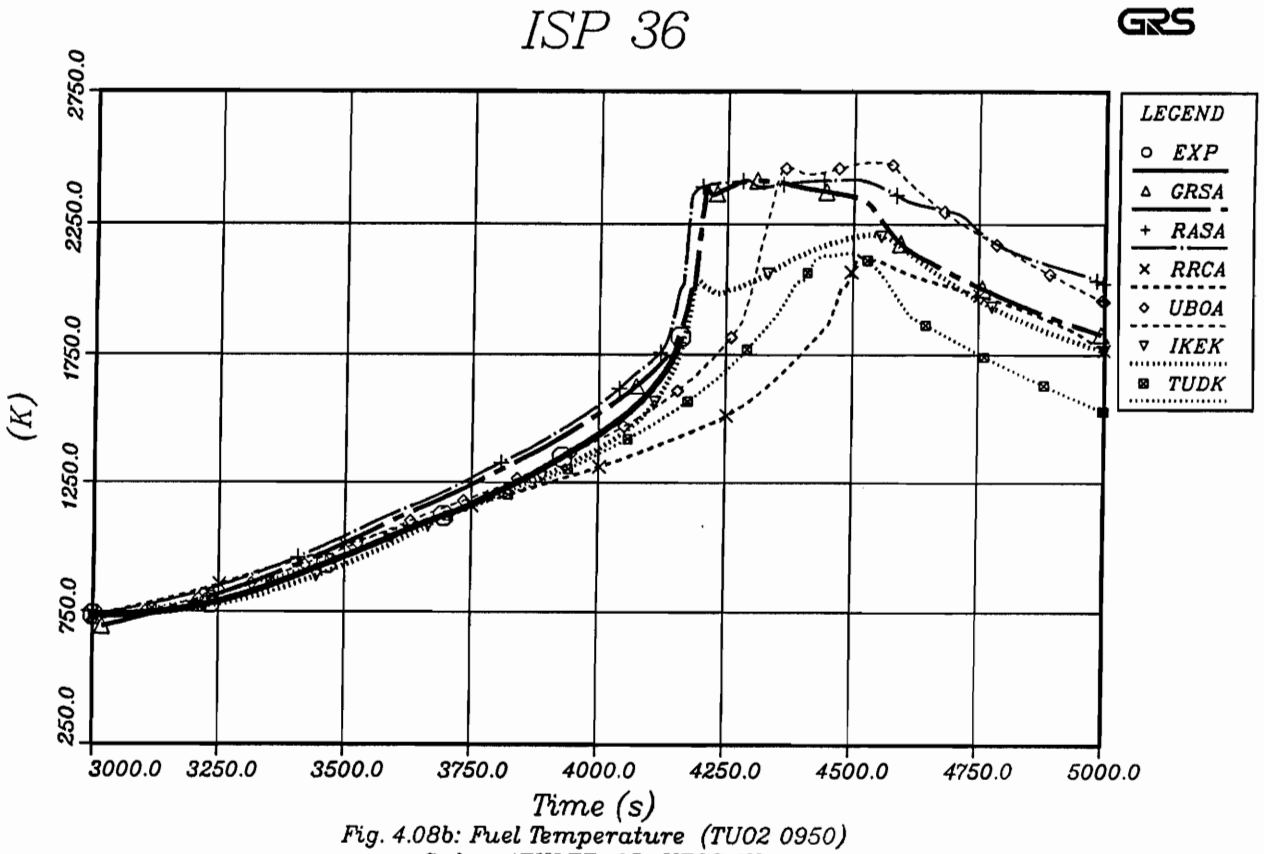

Fig. 4.08b: Fuel Temperature (TU02 0950)
Codes: ATHLET-CD, KESS III

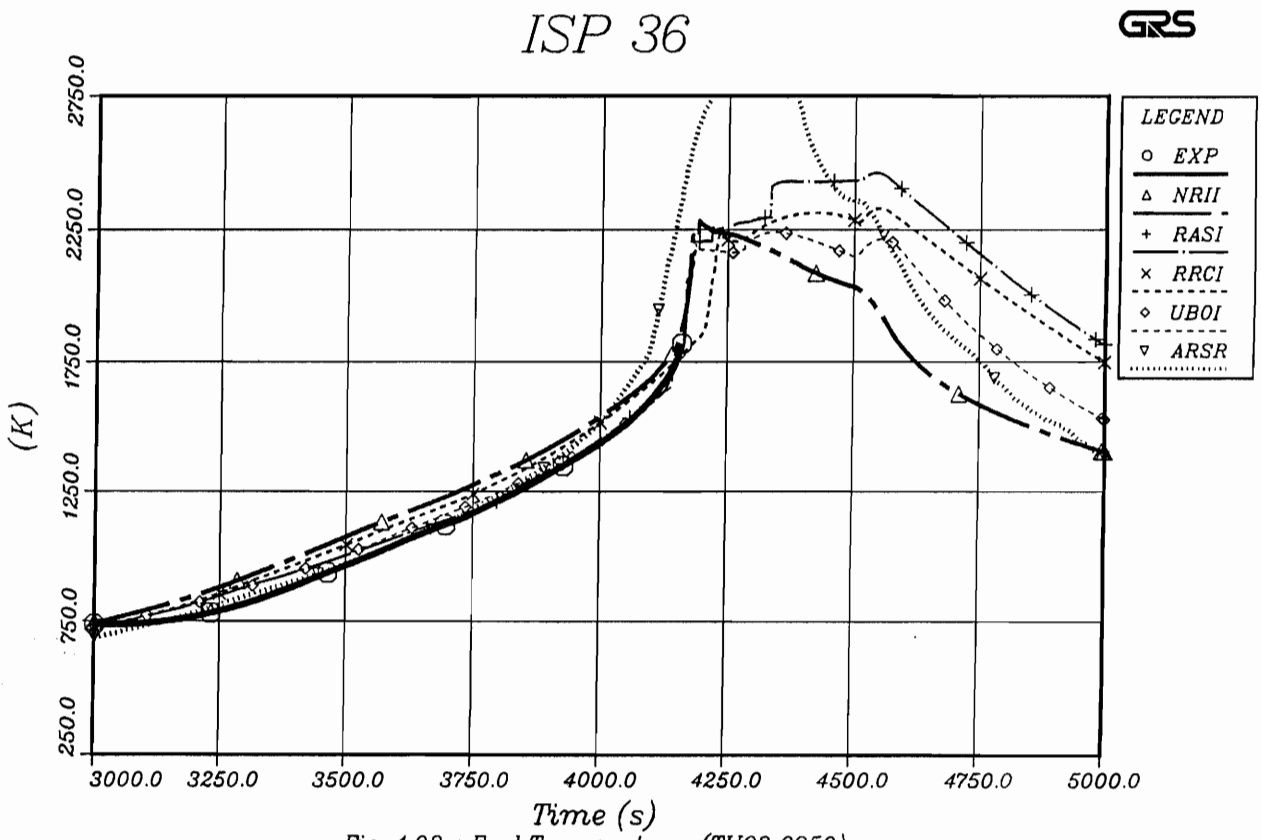

Fig. 4.08c: Fuel Temperature (TU02 0950)
Codes: ICARE2, RAPTA-SFD

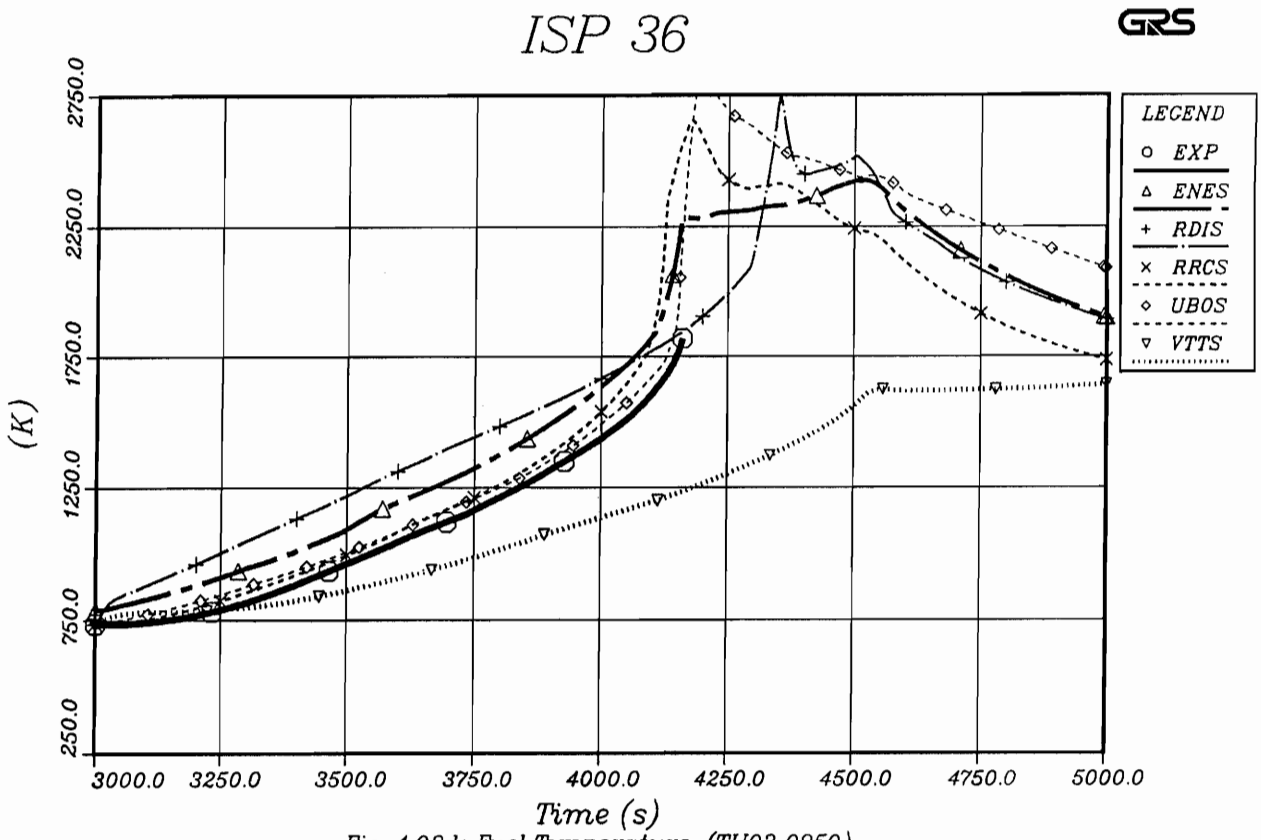

Fig. 4.08d: Fuel Temperature (TU02 0950)
Code: SCDAP/RELAP5

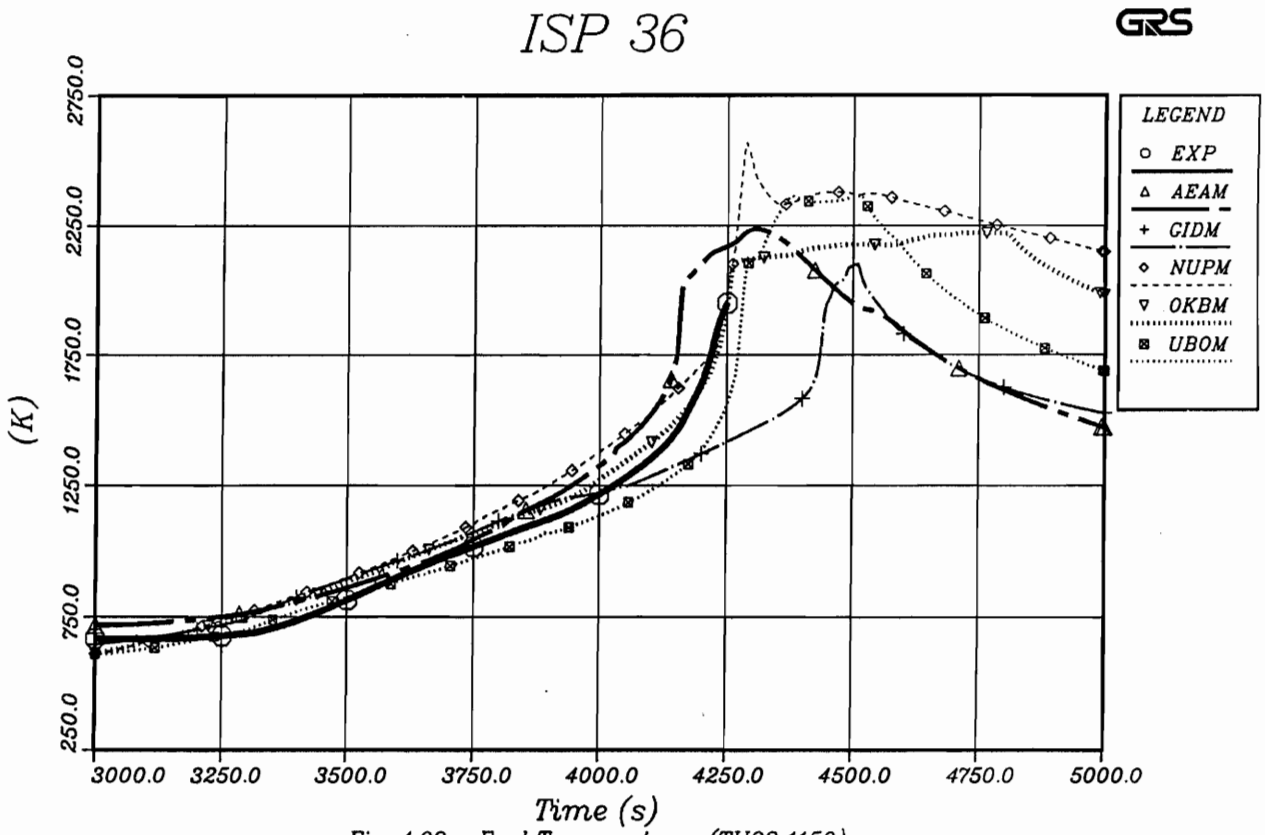

Fig. 4.09a: Fuel Temperature (TU02 1150)
Code: MELCOR

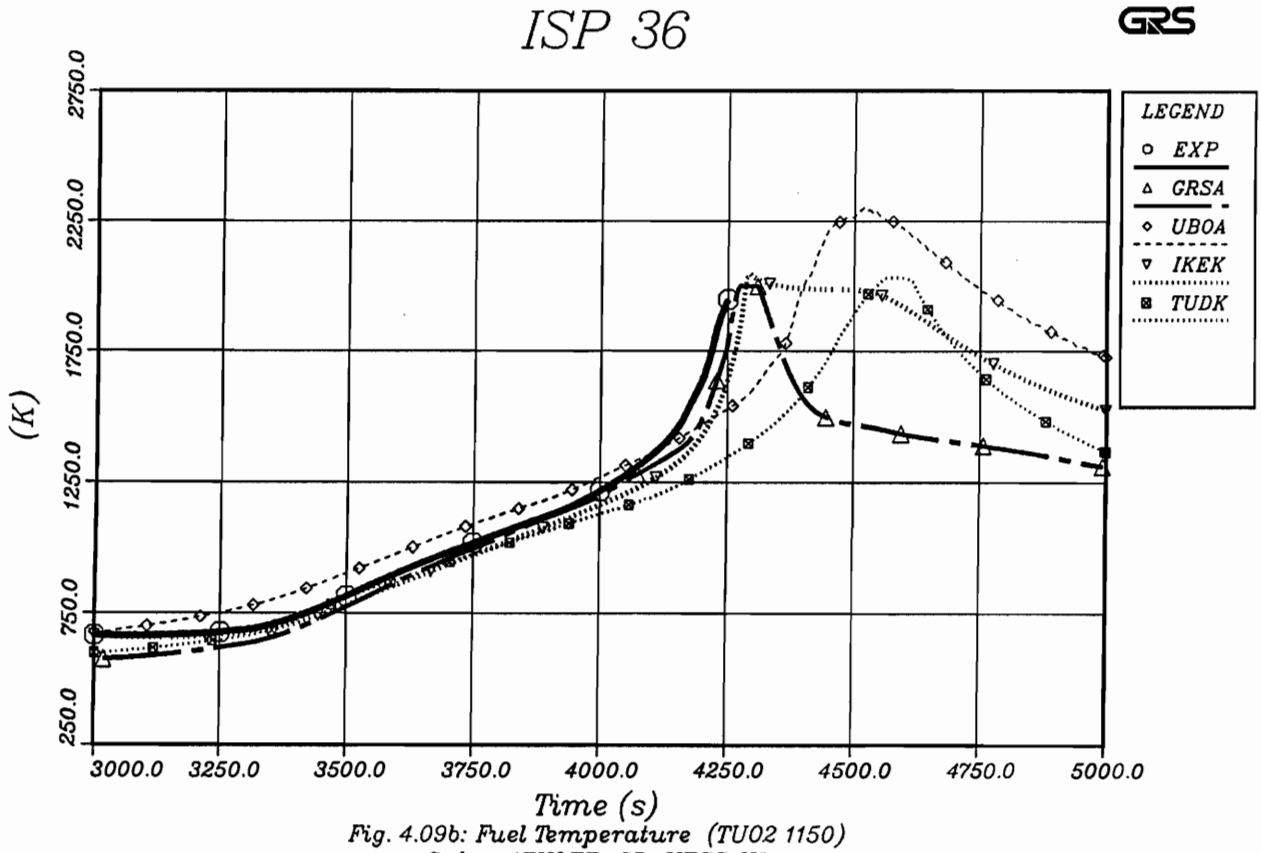

Fig. 4.09b: Fuel Temperature (TU02 1150)
Codes: ATHLET-CD, KESS III

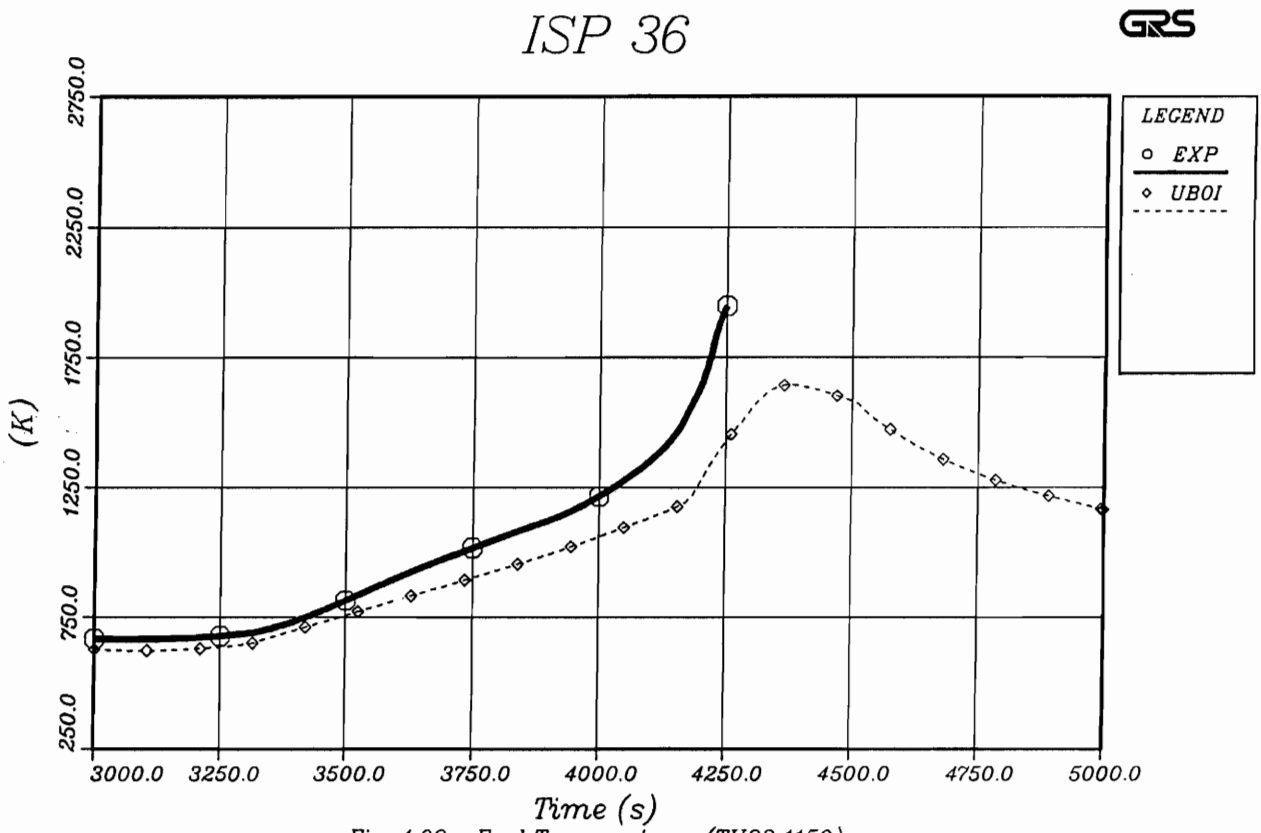

Fig. 4.09c: Fuel Temperature (TU02 1150)
Codes: ICARE2, RAPTA–SFD

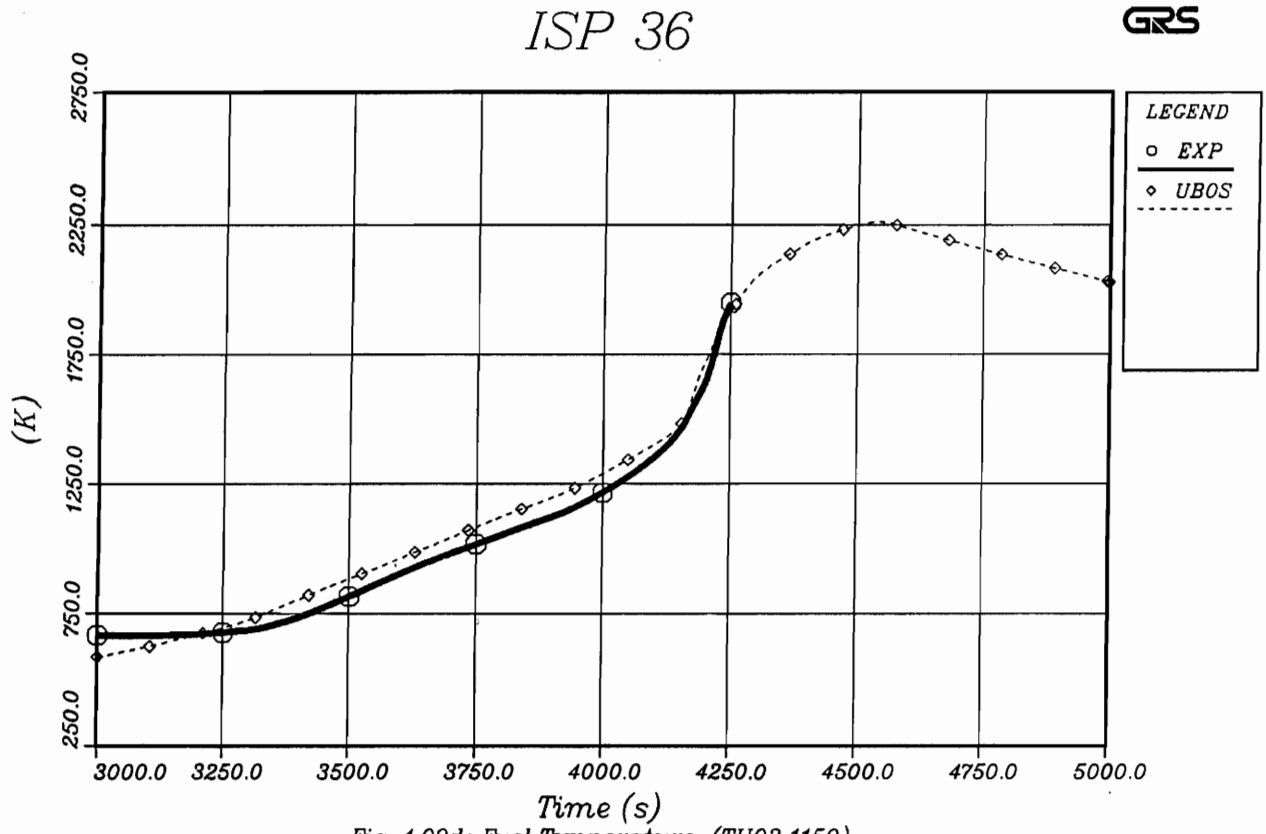

Fig. 4.09d: Fuel Temperature (TU02 1150)
Code: SCDAP/RELAP5

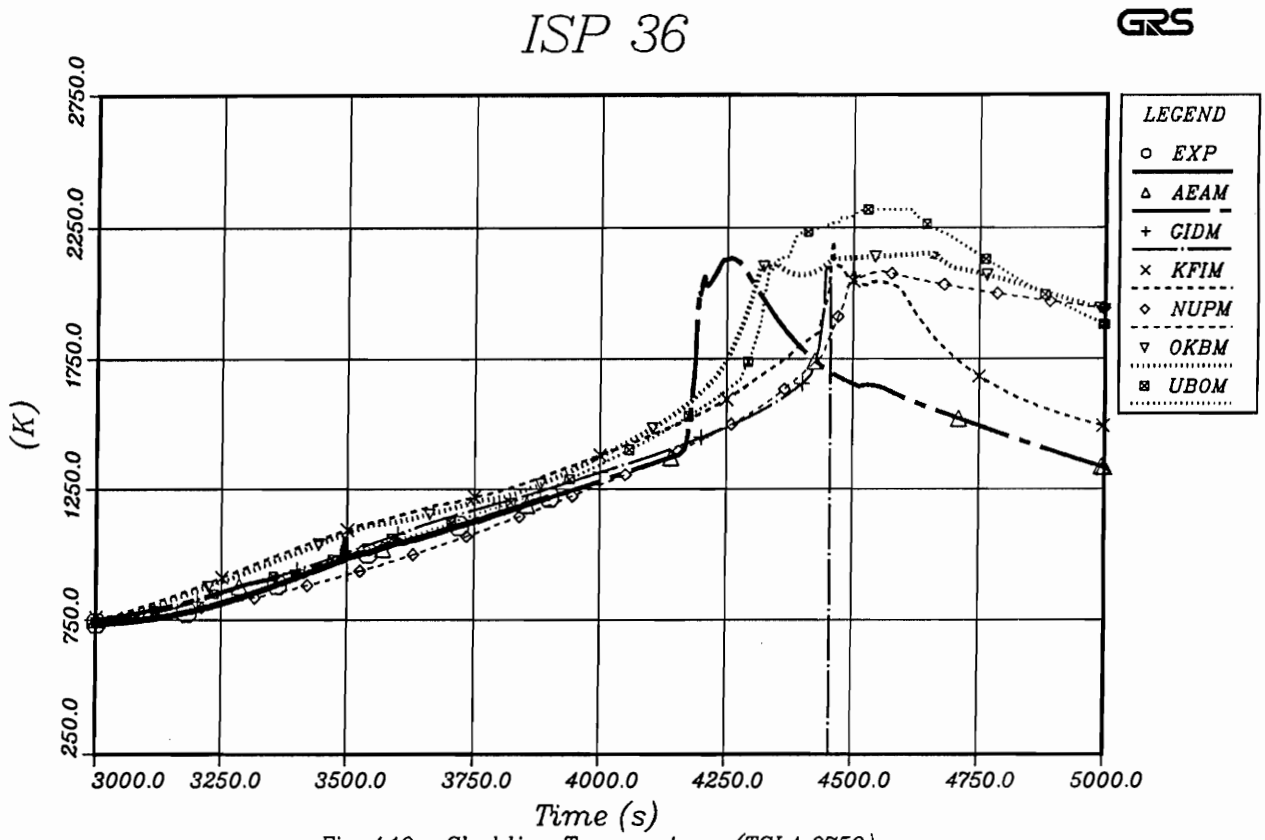

Fig. 4.10a: Cladding Temperature (TCLA 0750)
Code: MELCOR

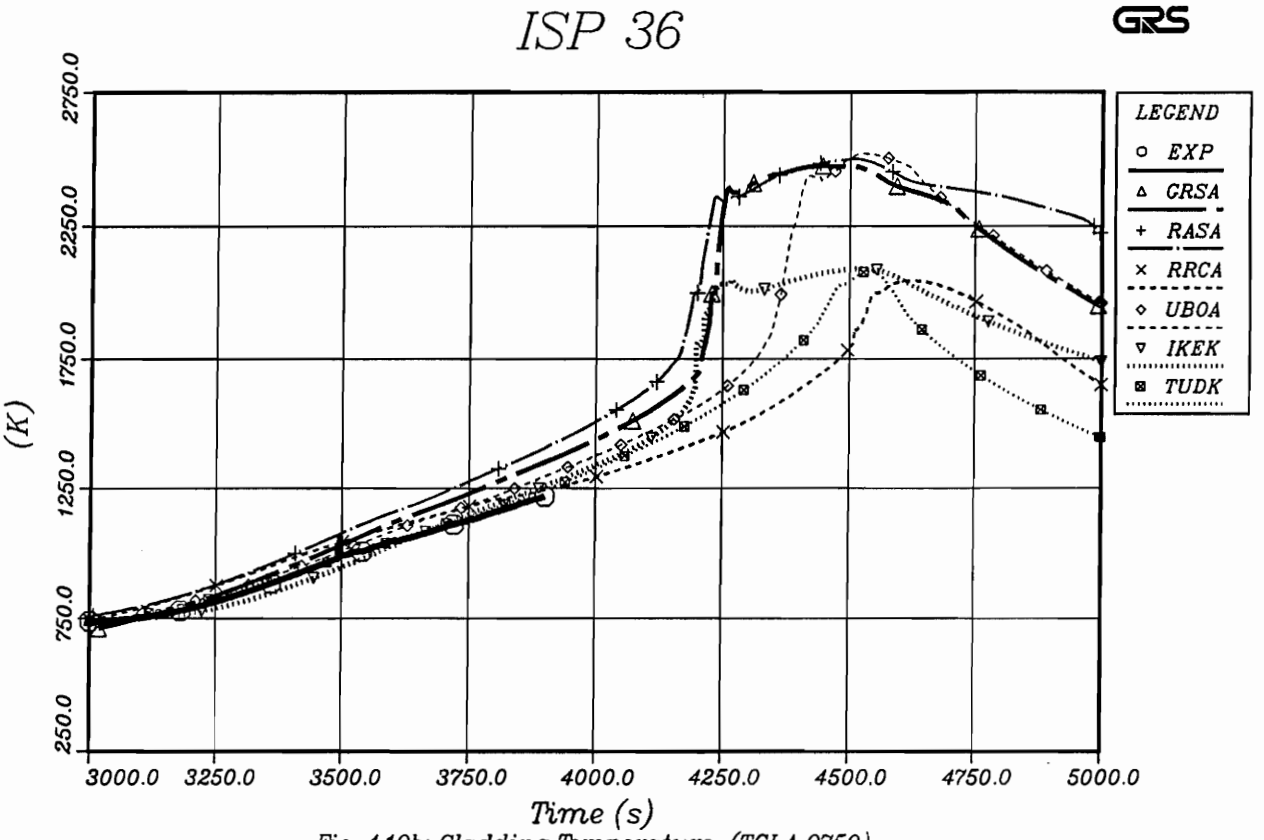

Fig. 4.10b: Cladding Temperature (TCLA 0750)
Codes: ATHLET-CD, KESS III

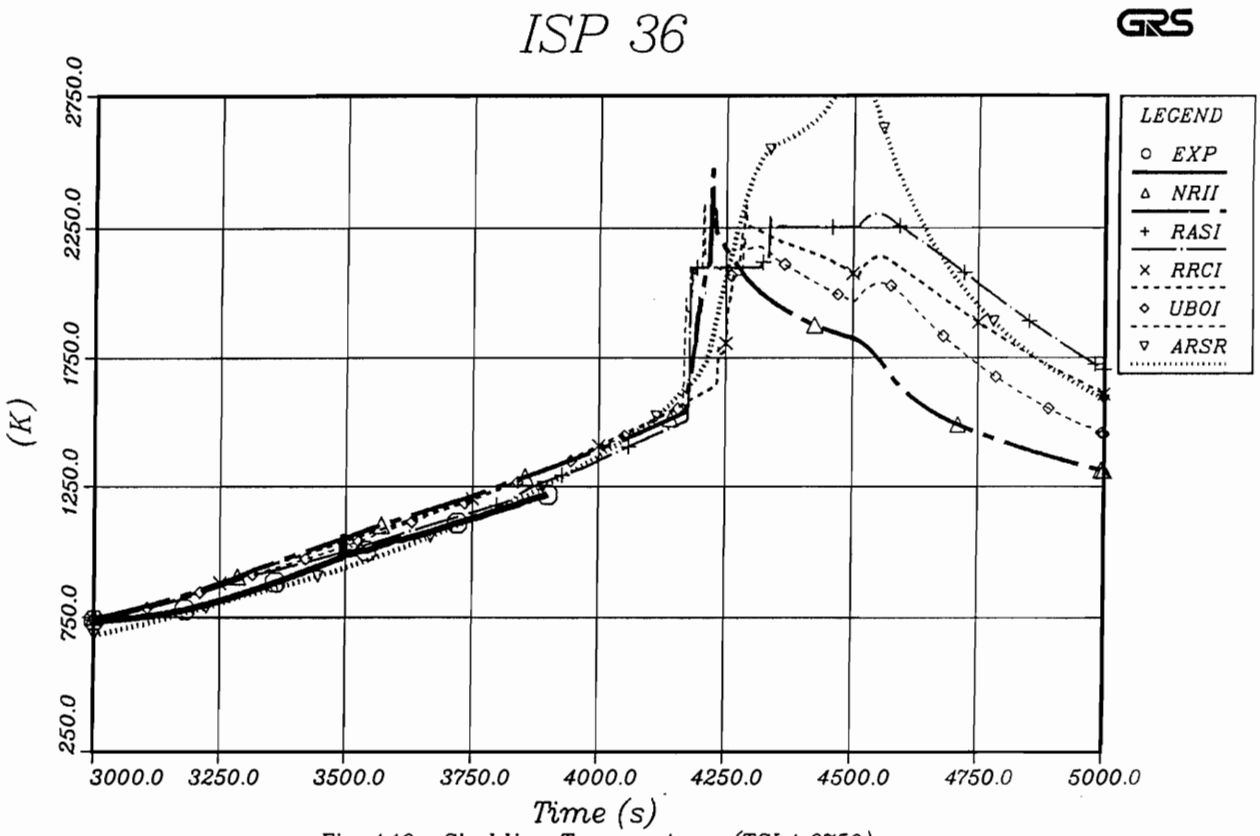

Fig. 4.10c: Cladding Temperature (TCLA 0750)
Codes: ICARE2, RAPTA-SFD

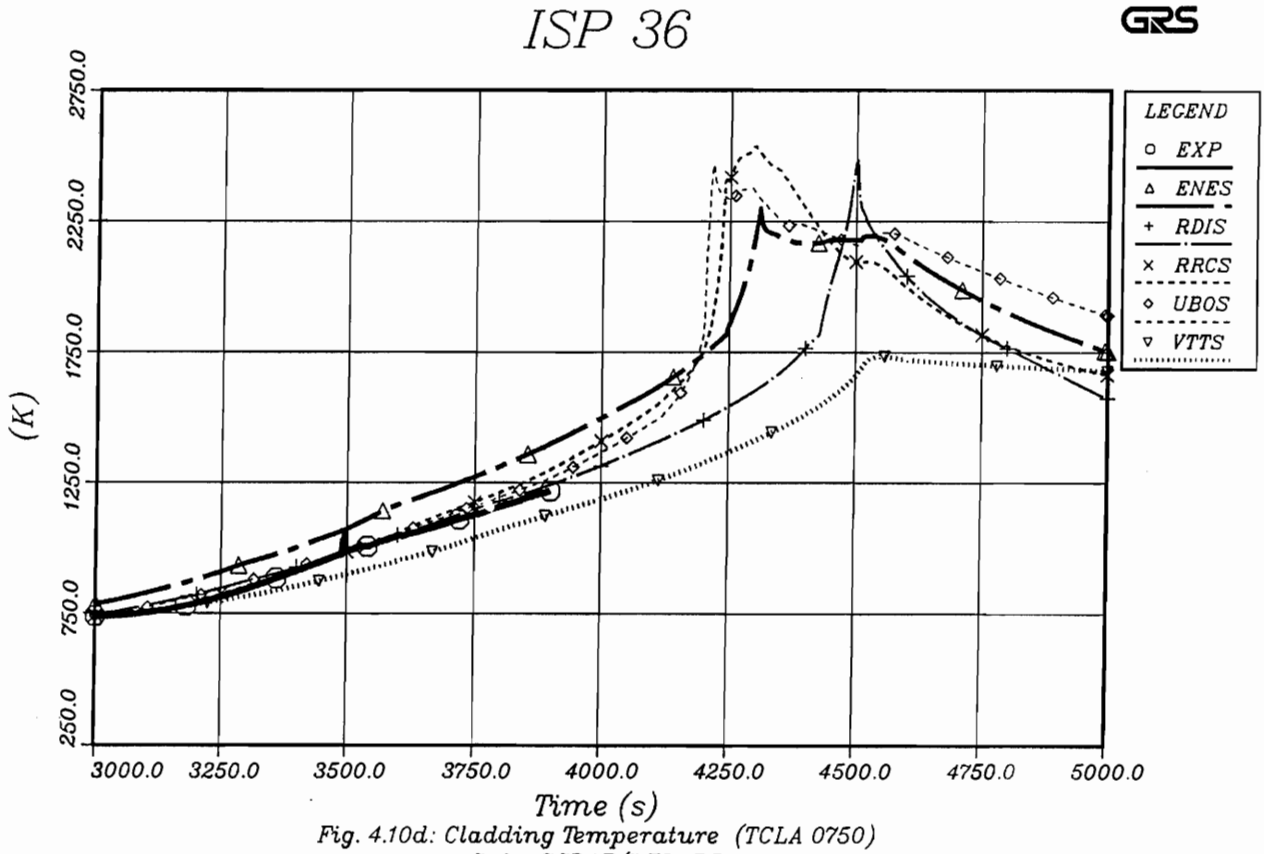

Fig. 4.10d: Cladding Temperature (TCLA 0750)
Code: SCDAP/RELAP5

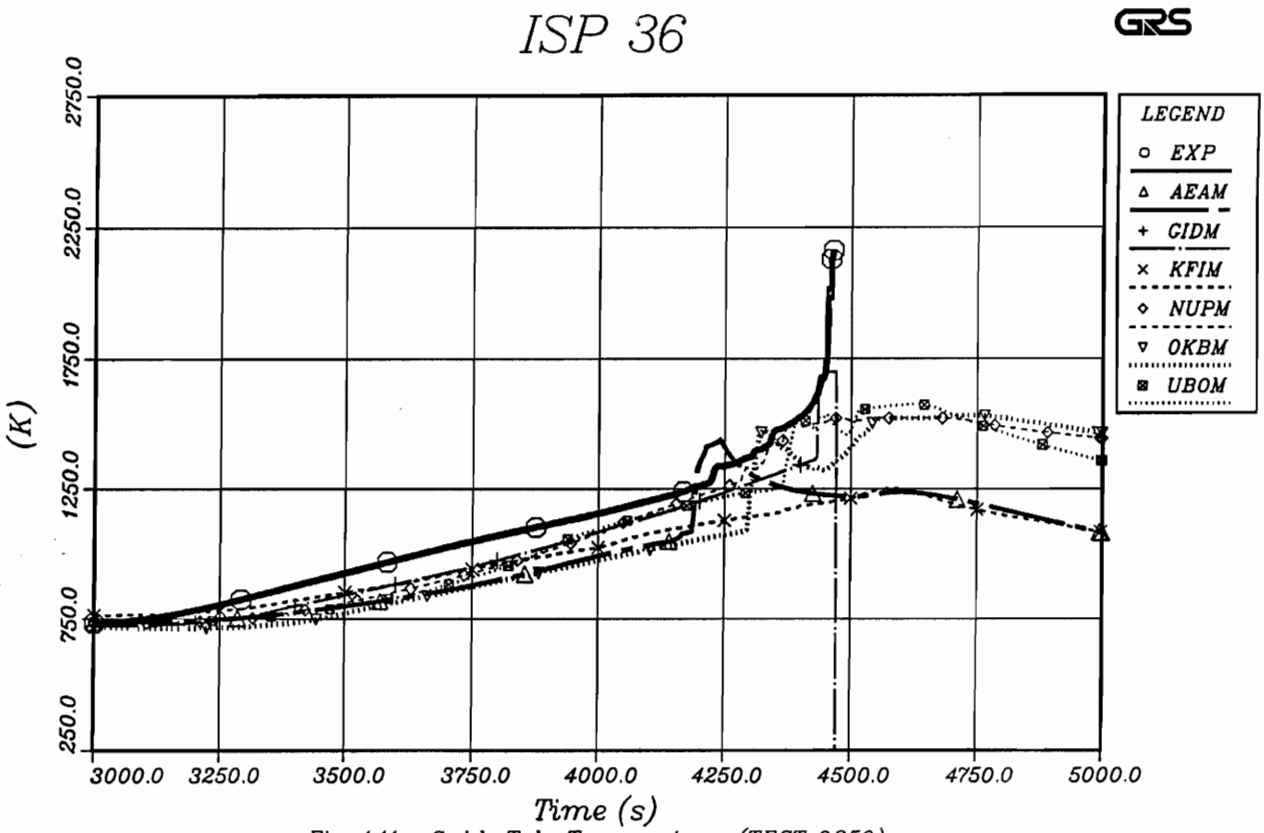

Fig. 4.11a: Guide Tube Temperature (TEGT 0350)
Code: MELCOR

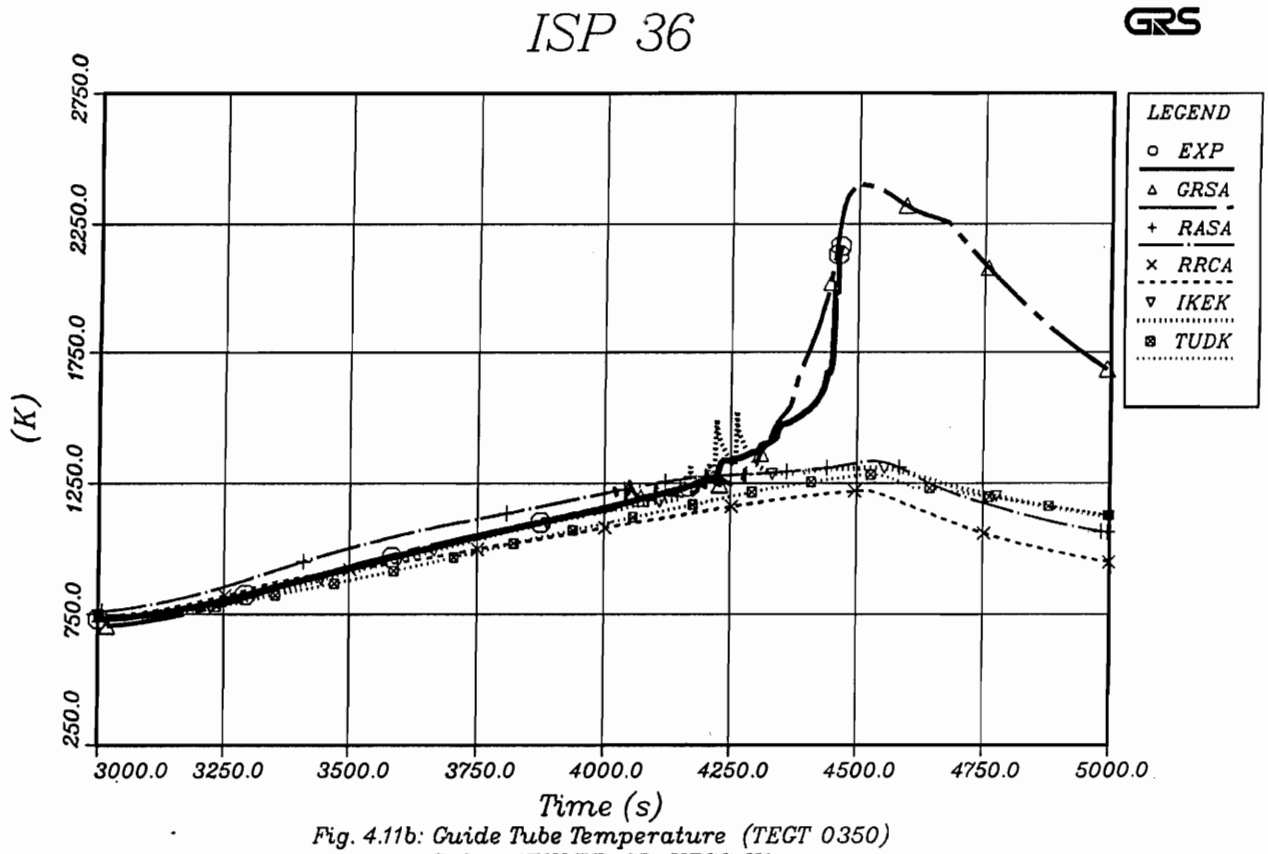

Fig. 4.11b: Guide Tube Temperature (TEGT 0350)
Codes: ATHLET-CD, KESS III

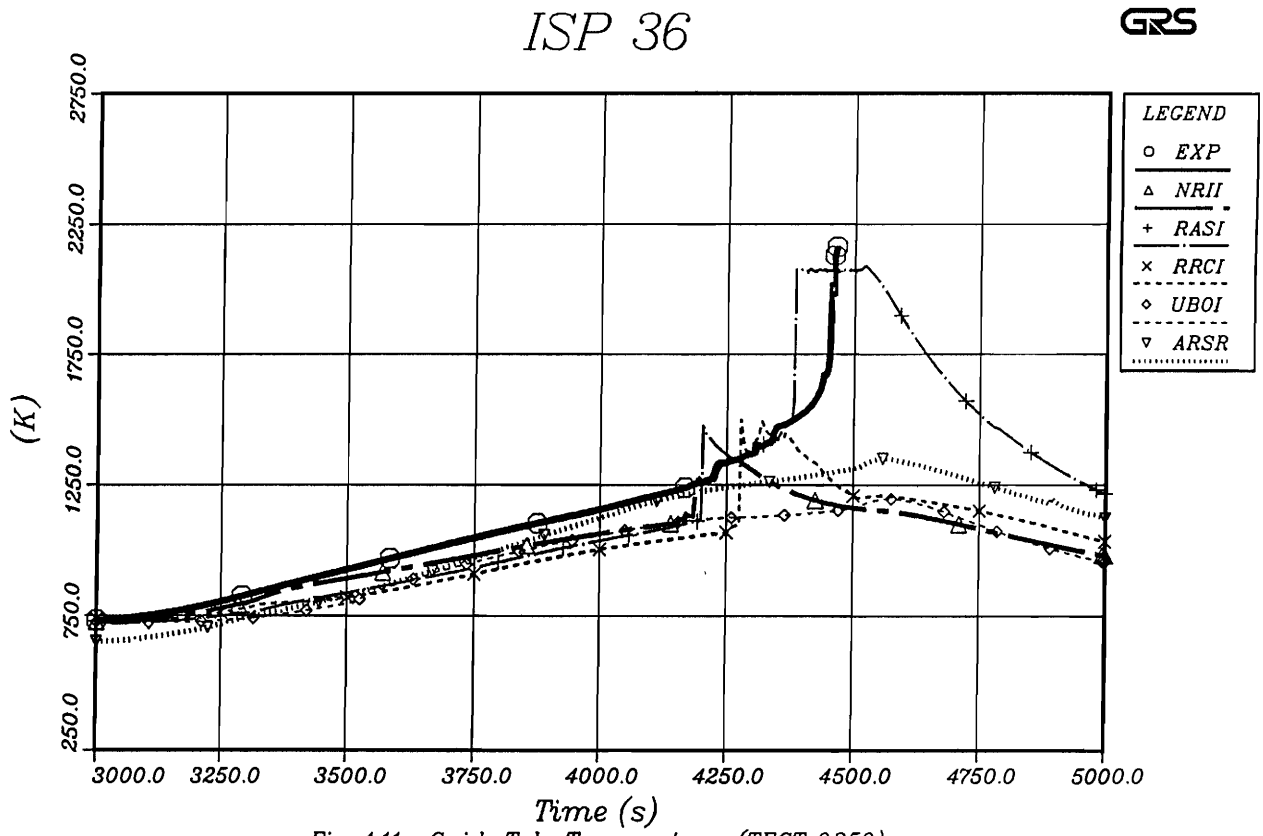

Fig. 4.11c: Guide Tube Temperature (TECT 0350)
Codes: ICARE2, RAPTA-SFD

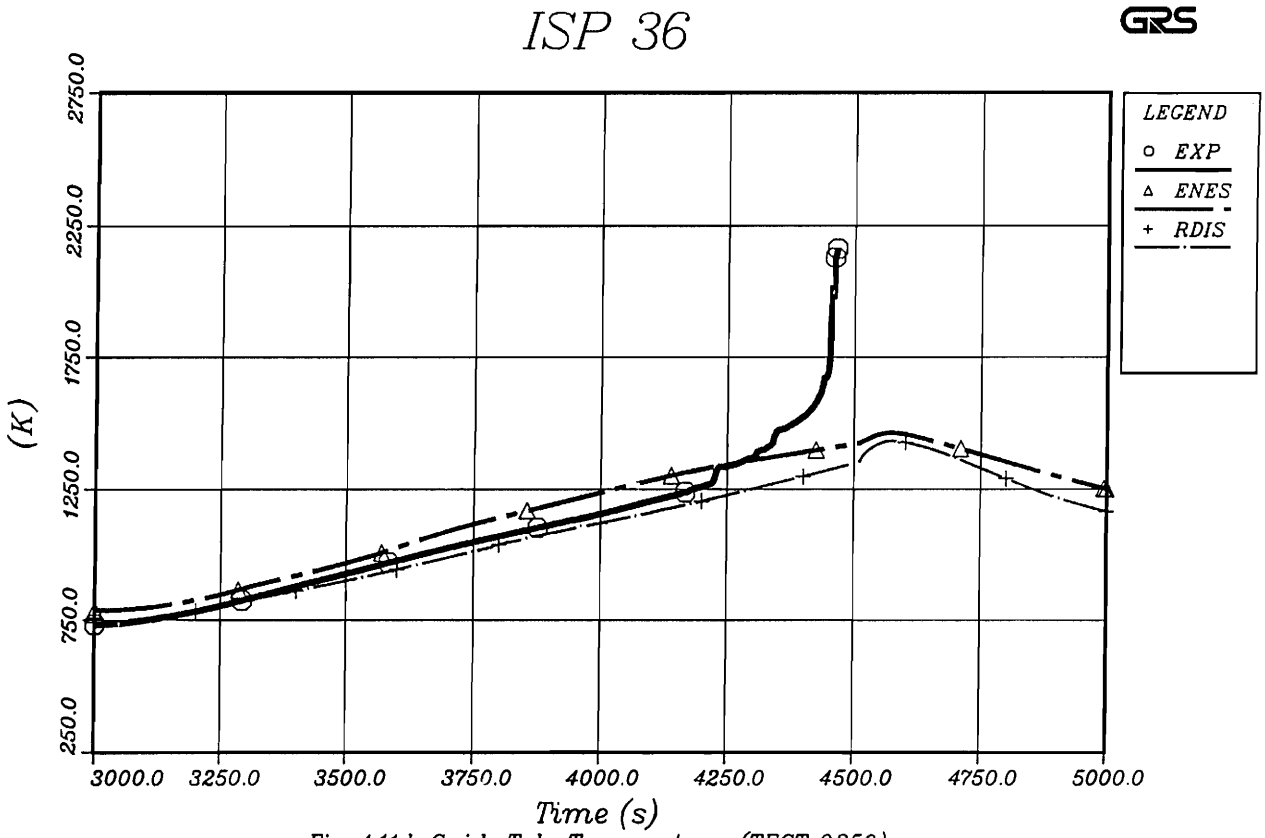

Fig. 4.11d: Guide Tube Temperature (TECT 0350)
Code: SCDAP/RELAP5

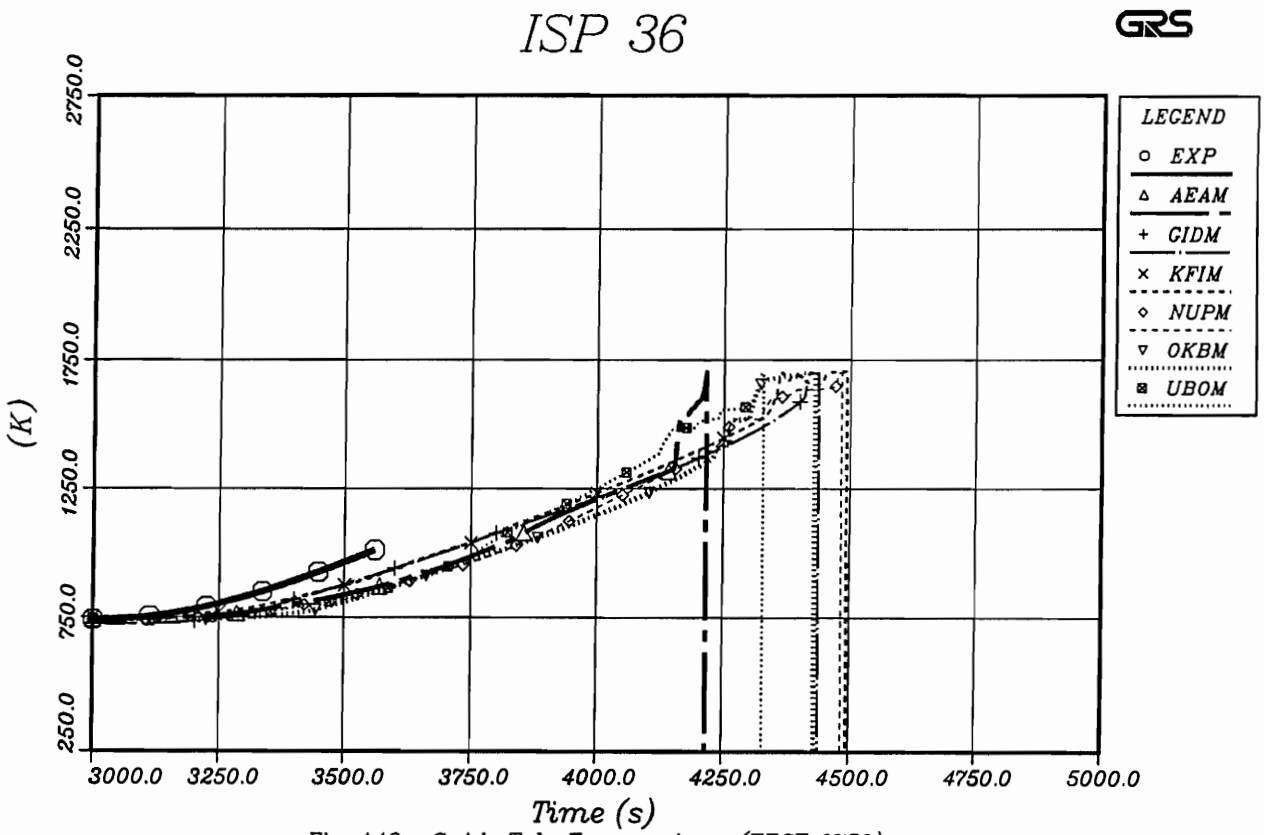

Fig. 4.12a: Guide Tube Temperature (TECT 0750)
Code: MELCOR

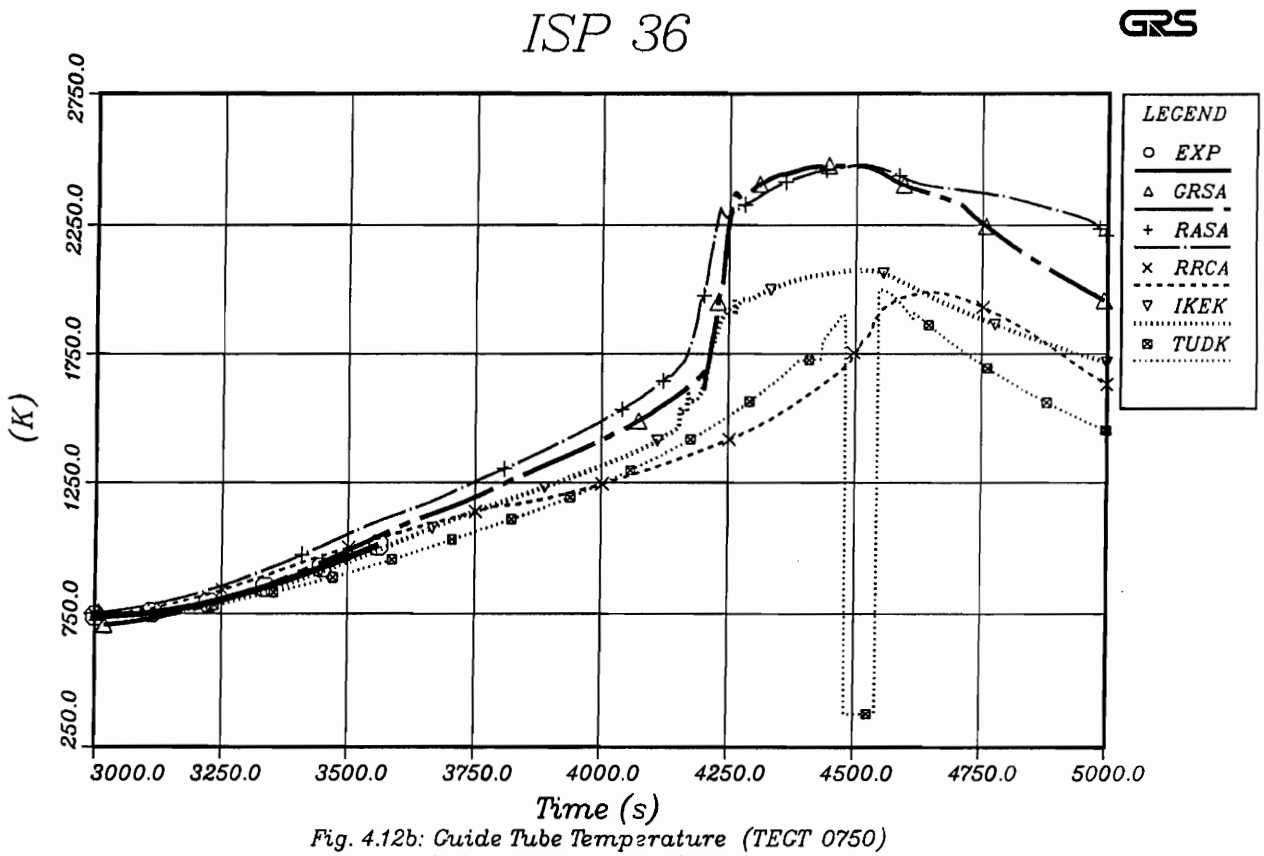

Fig. 4.12b: Guide Tube Temperature (TECT 0750)
Codes: ATHLET-CD, KESS III

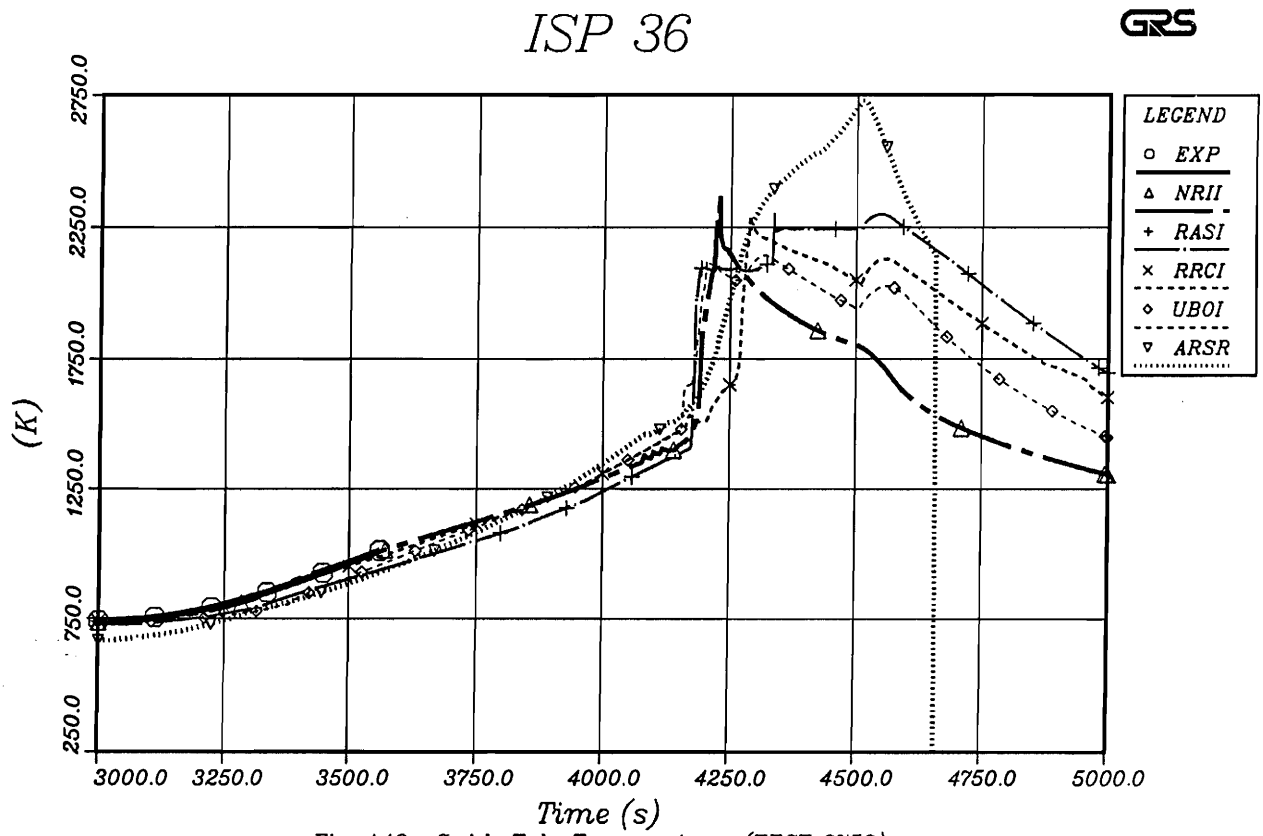

Fig. 4.12c: Guide Tube Temperature (TEGT 0750)
Codes: ICARE2, RAPTA–SFD

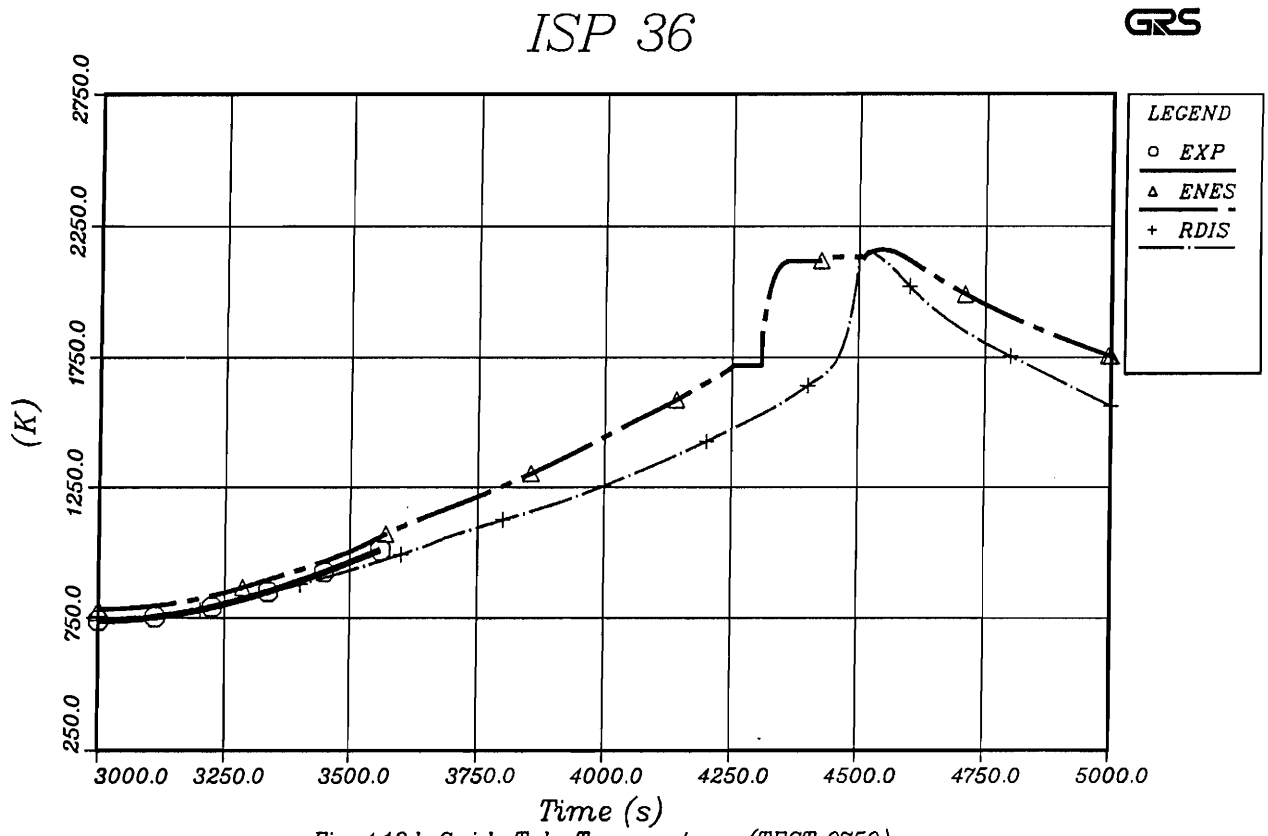

Fig. 4.12d: Guide Tube Temperature (TEGT 0750)
Code: SCDAP/RELAP5

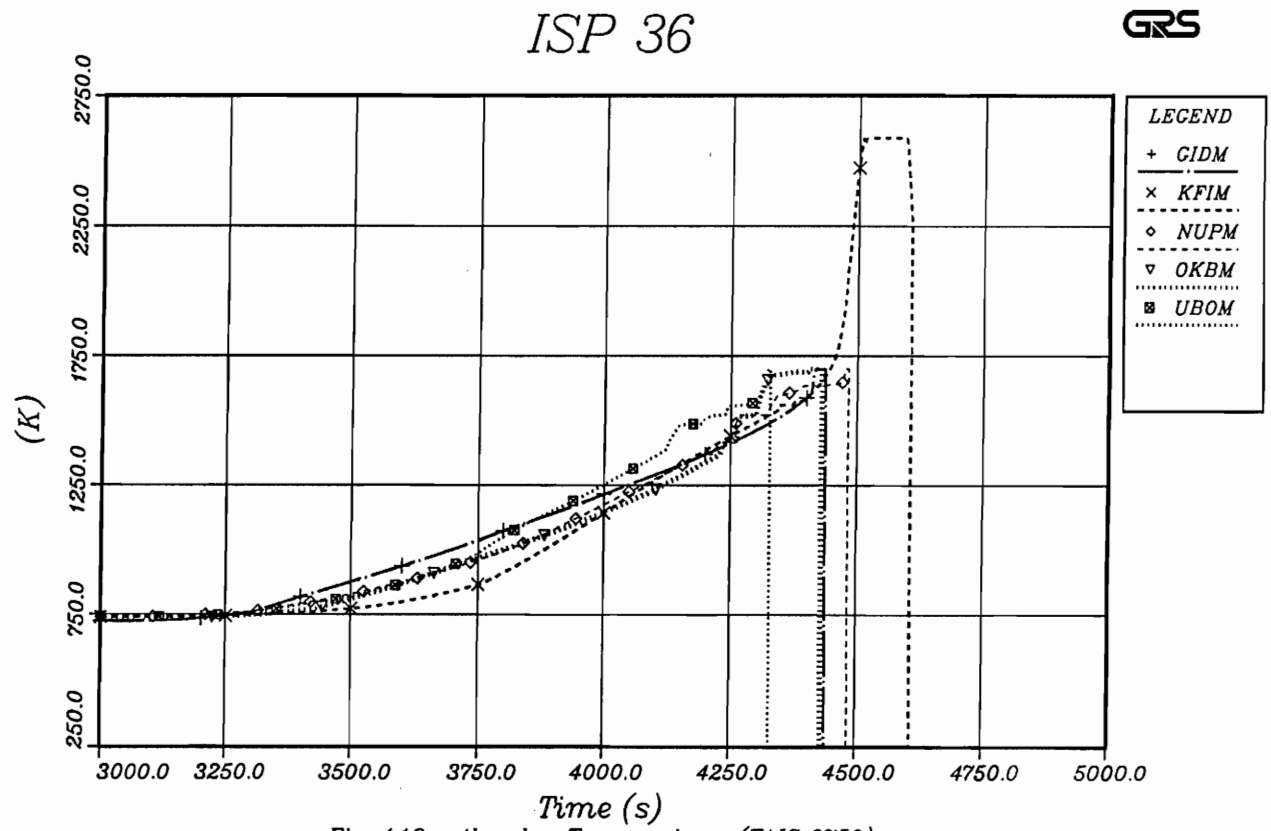

Fig. 4.13a: Absorber Temperature (TAIC 0750)
Code: MELCOR

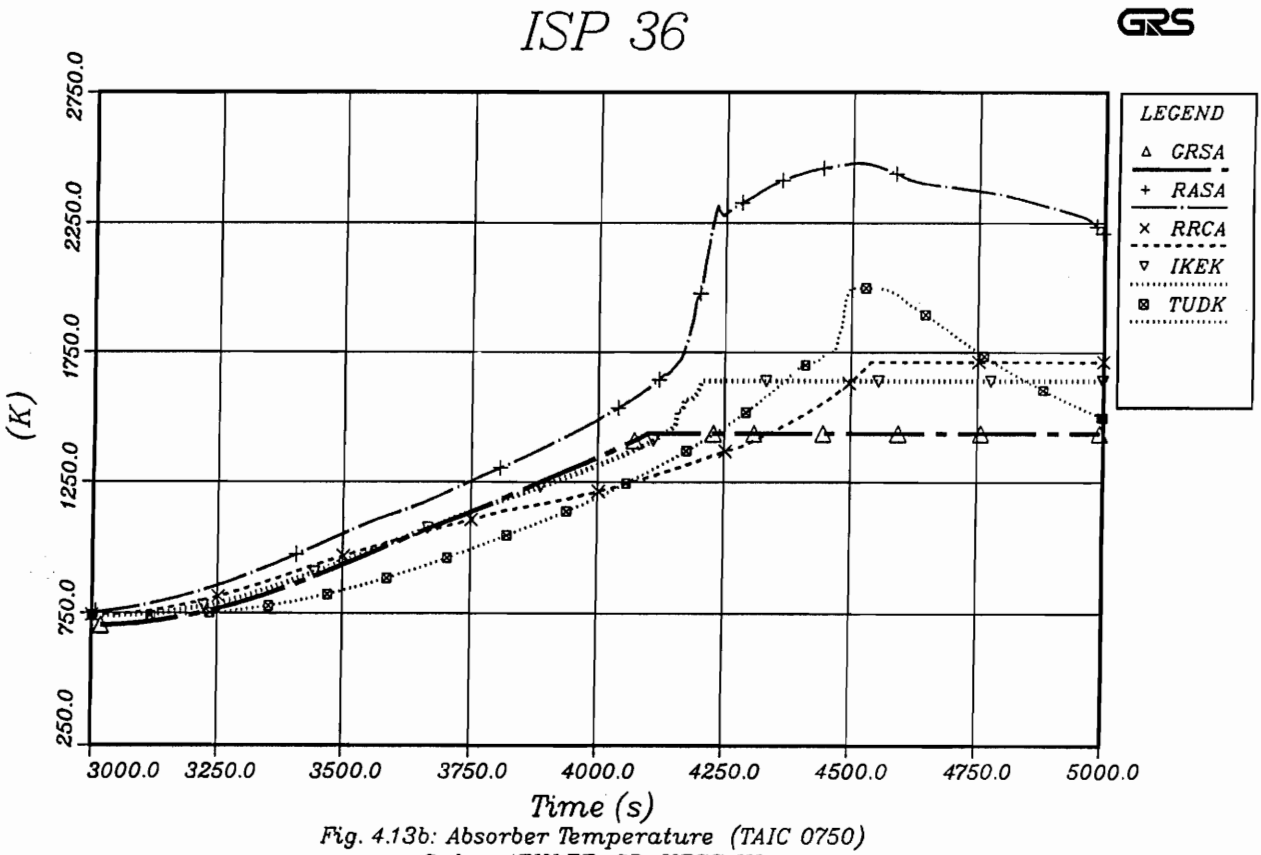

Fig. 4.13b: Absorber Temperature (TAIC 0750)
Codes: ATHLET-CD, KESS III

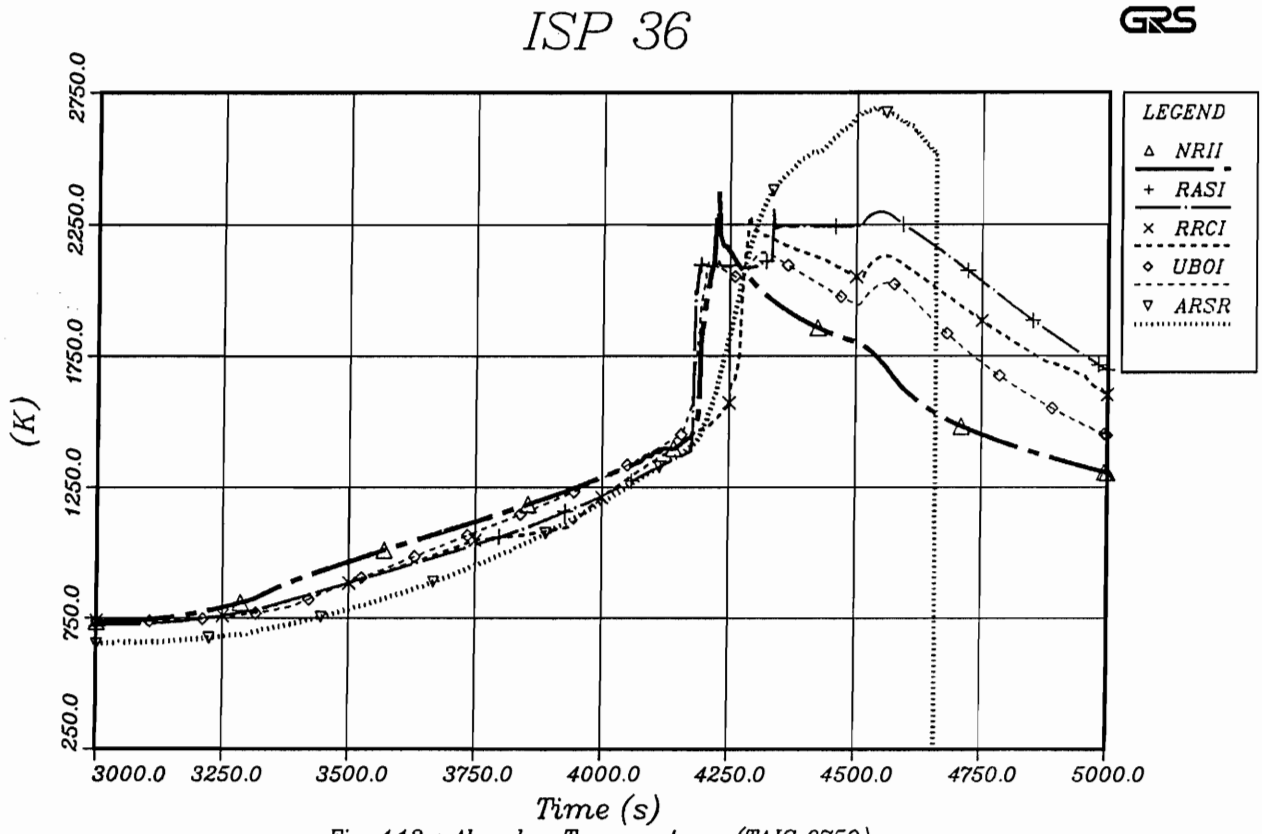

Fig. 4.13c: Absorber Temperature (TAIC 0750)
Codes: ICARE2, RAPTA–SFD

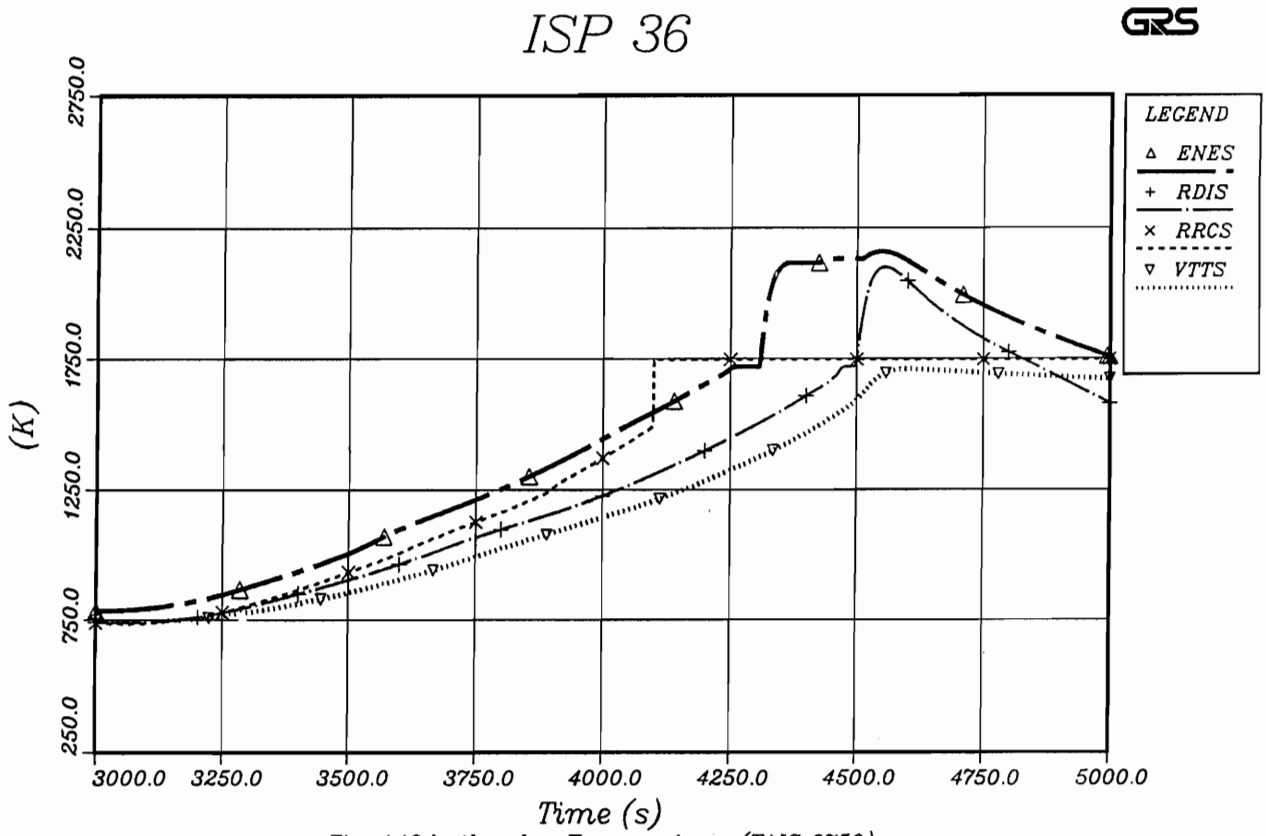

Fig. 4.13d: Absorber Temperature (TAIC 0750)
Code: SCDAP/RELAP5

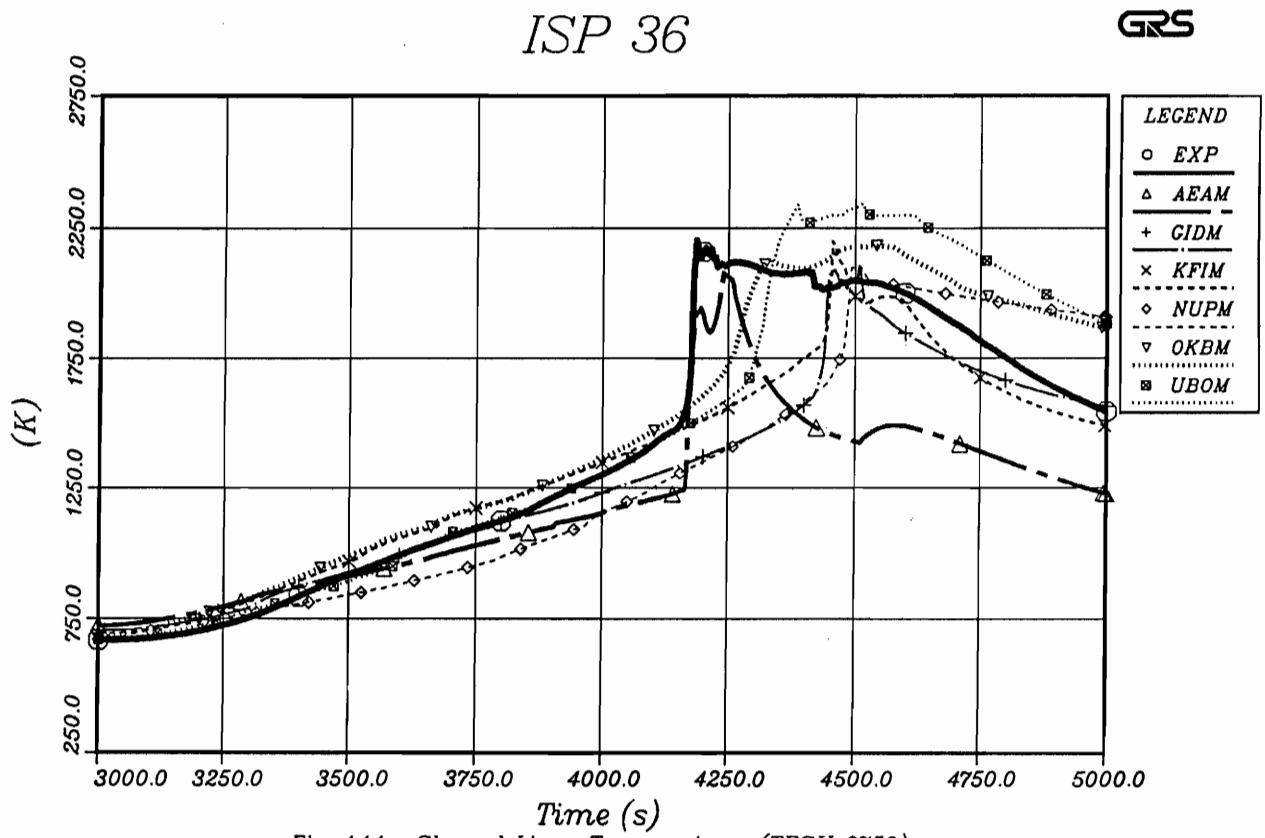

Fig. 4.14a: Shroud Liner Temperature (TESH 0750)
Code: MELCOR

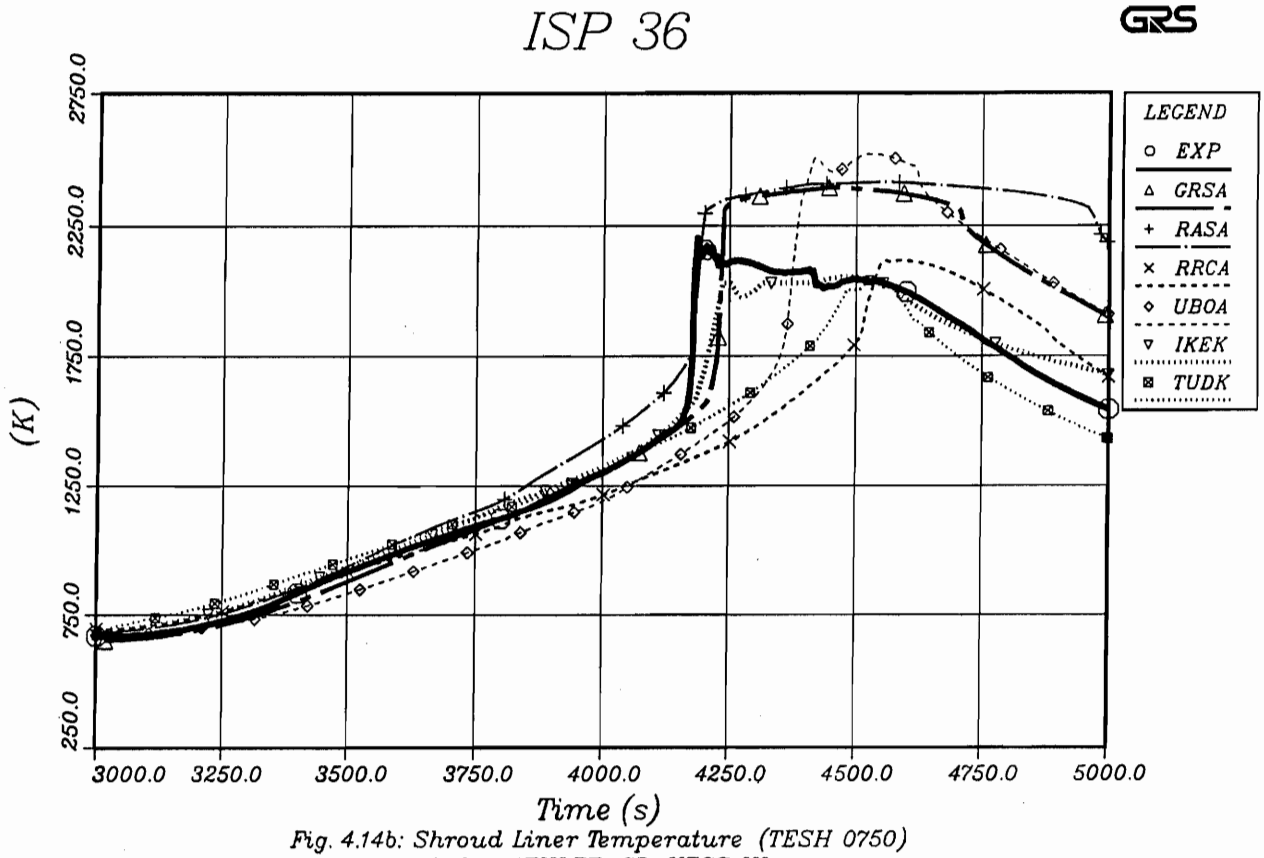

Fig. 4.14b: Shroud Liner Temperature (TESH 0750)
Codes: ATHLET-CD, KESS III

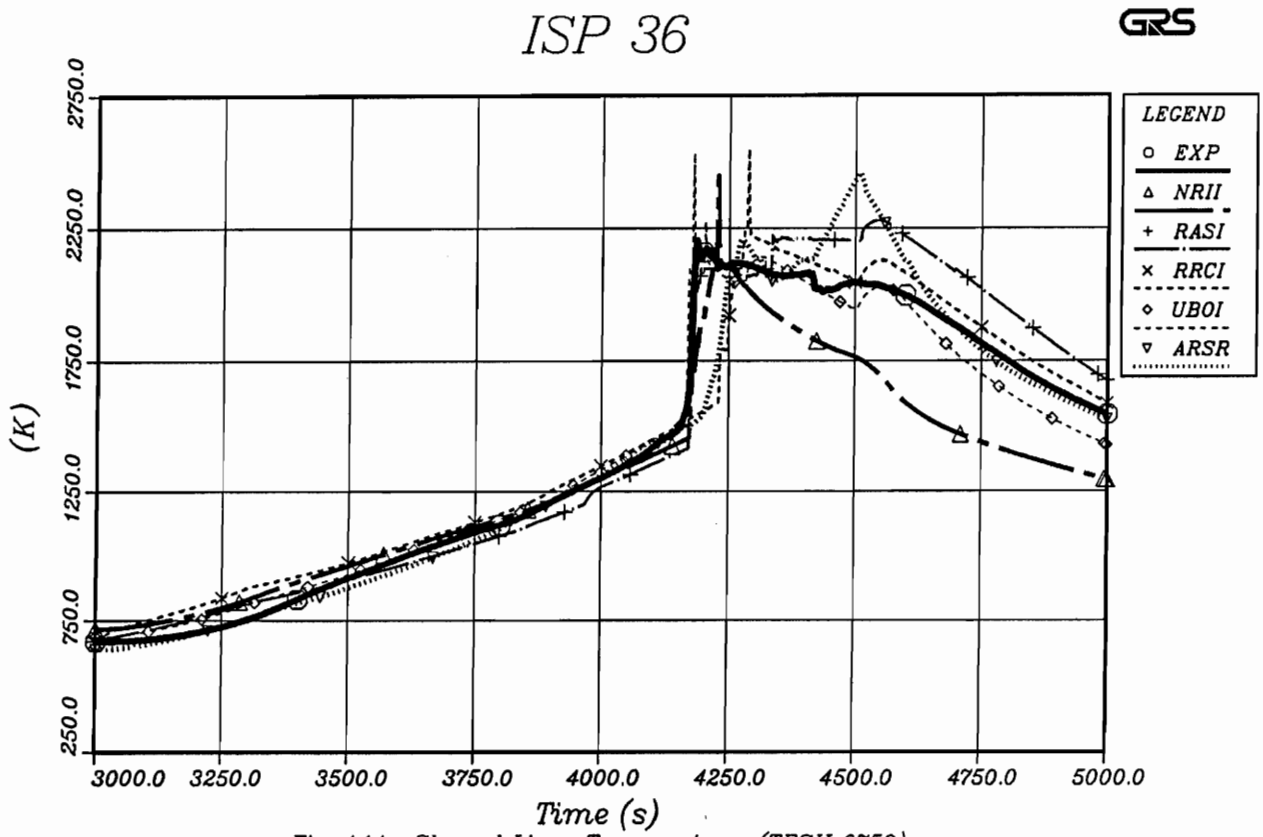

Fig. 4.14c: Shroud Liner Temperature (TESH 0750)
Codes: ICARE2, RAPTA–SFD

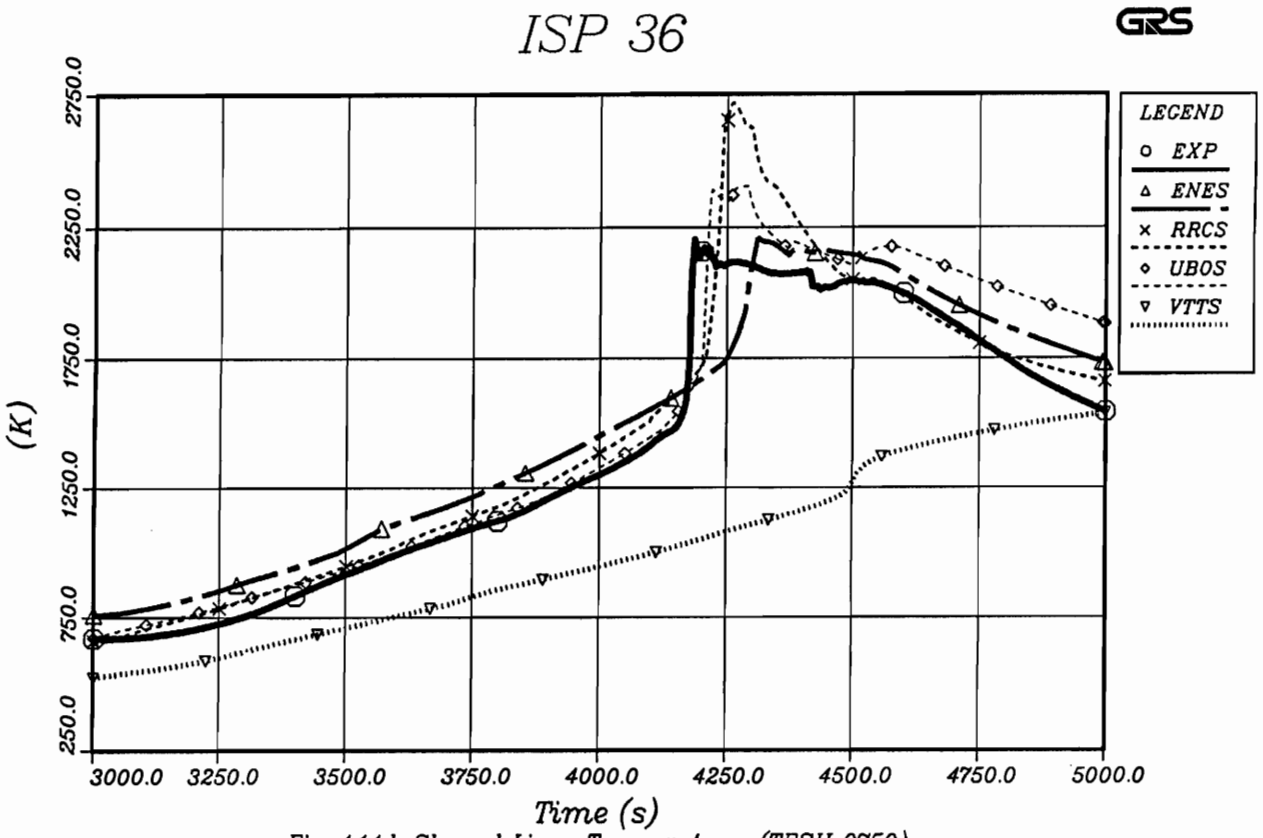

Fig. 4.14d: Shroud Liner Temperature (TESH 0750)
Code: SCDAP/RELAP5

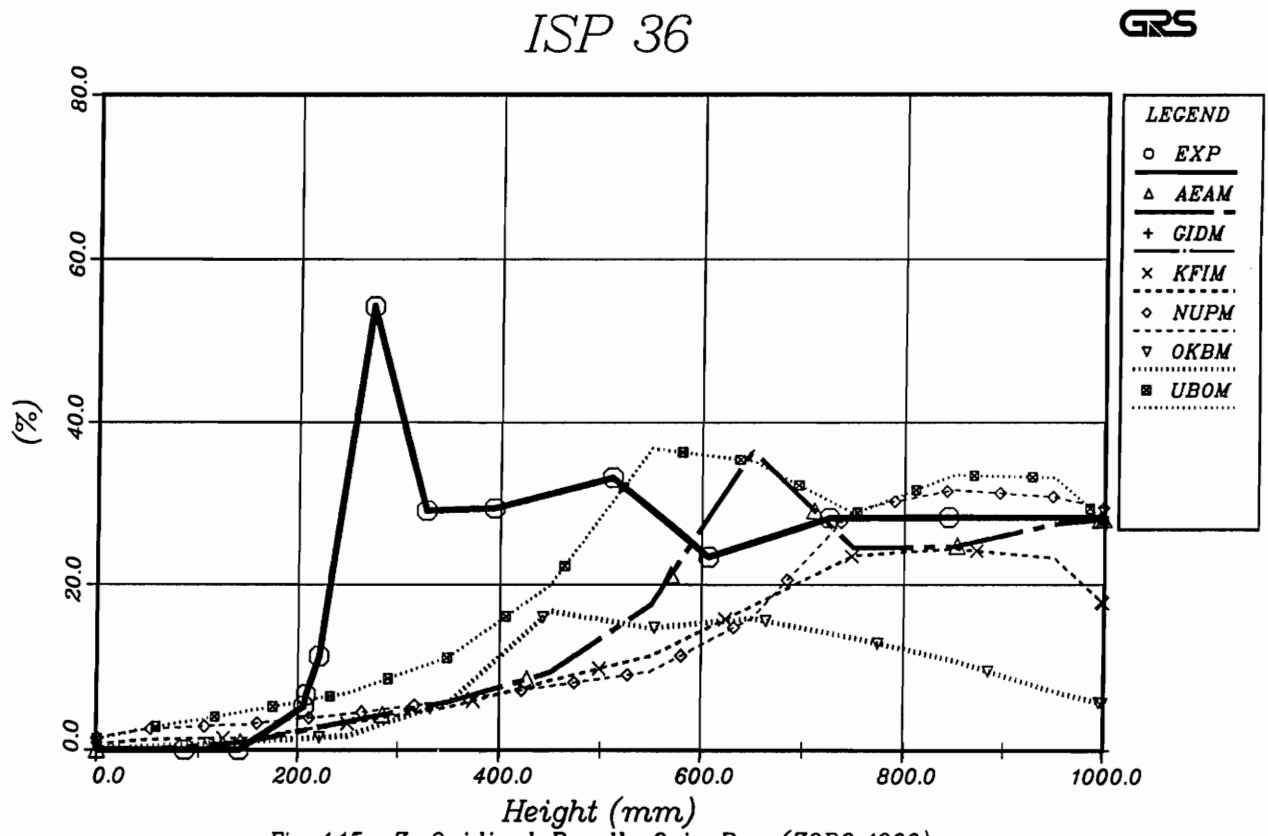

Fig. 4.15a: Zr Oxidized, Bundle, Orig. Pos. (ZOBO 4900)
Code: MELCOR

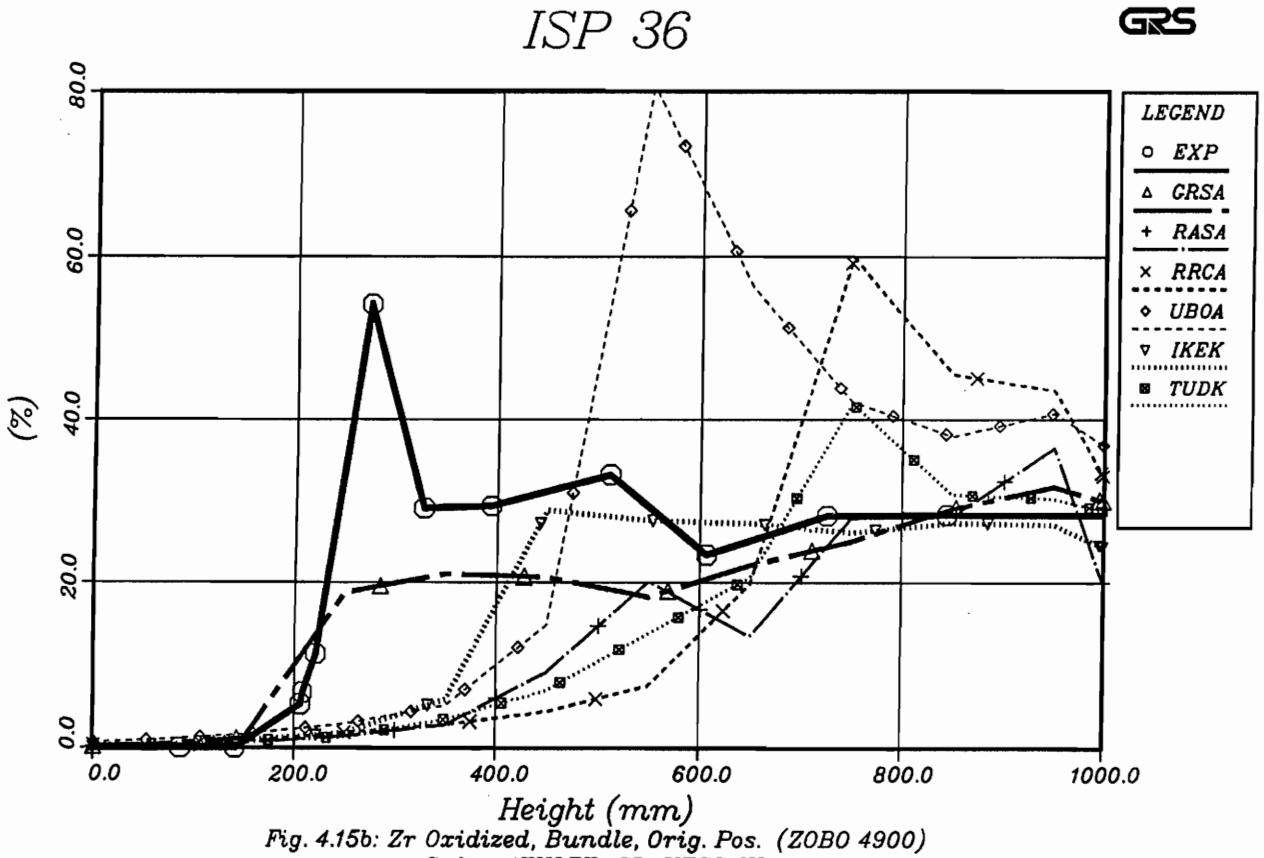

Fig. 4.15b: Zr Oxidized, Bundle, Orig. Pos. (ZOBO 4900)
Codes: ATHLET-CD, KESS III

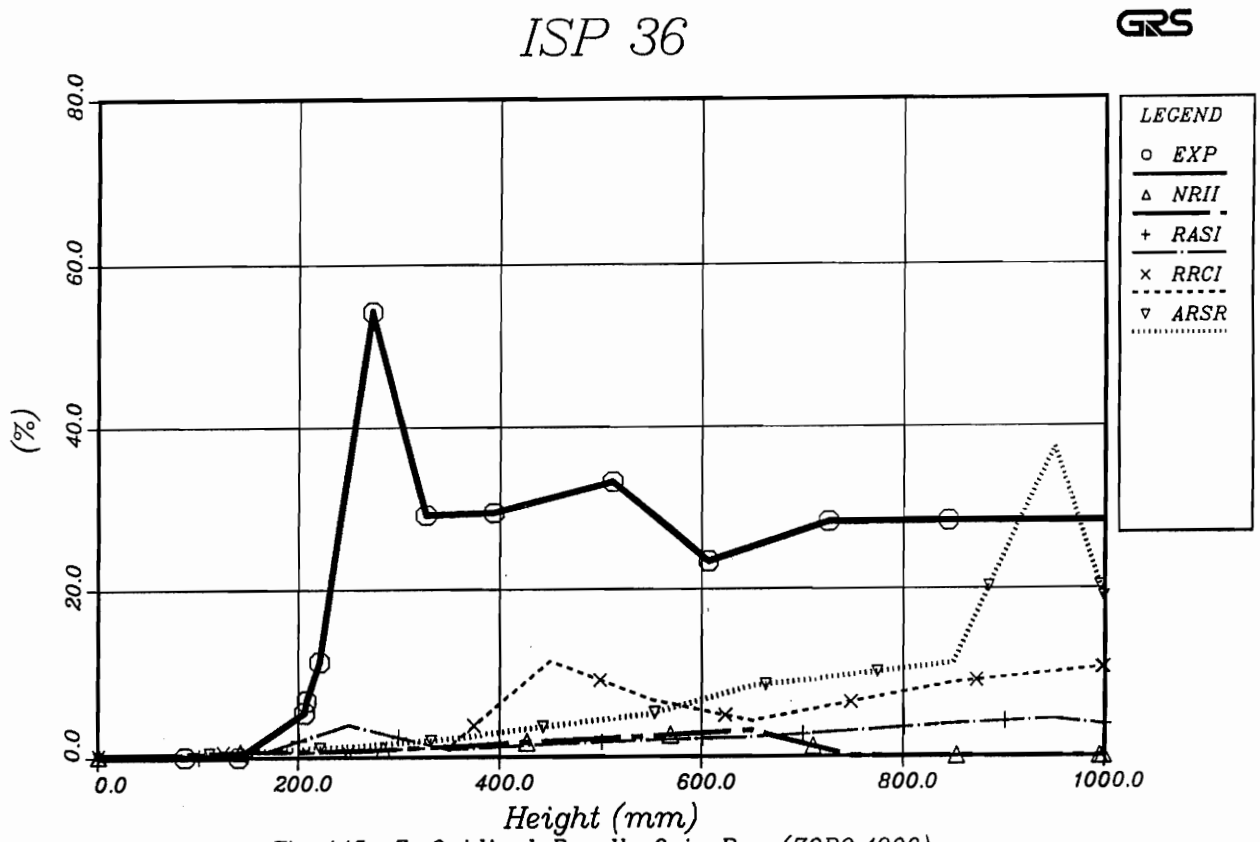

Fig. 4.15c: Zr Oxidized, Bundle, Orig. Pos. (Z0B0 4900)
Codes: ICARE2, RAPTA–SFD

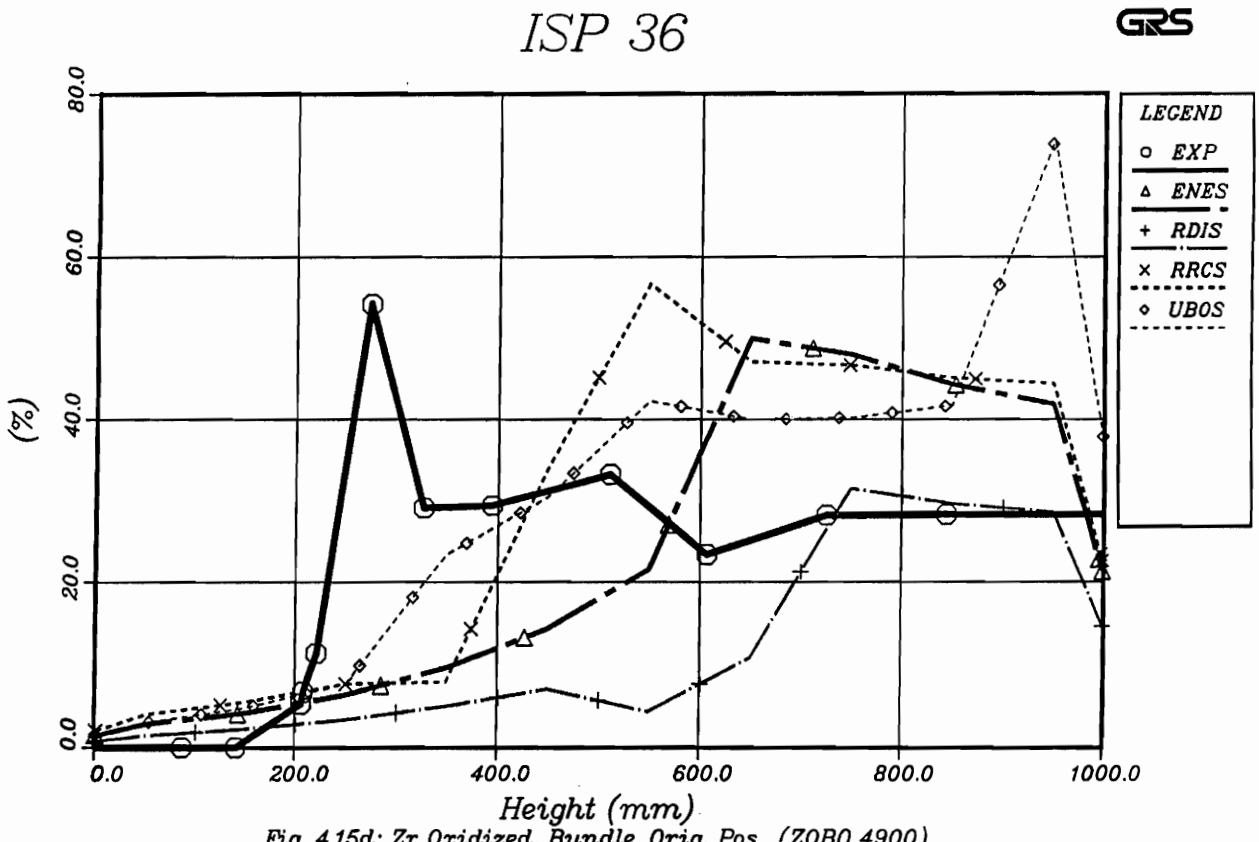

Fig. 4.15d: Zr Oxidized, Bundle, Orig. Pos. (Z0B0 4900)
Code: SCDAP/RELAP5

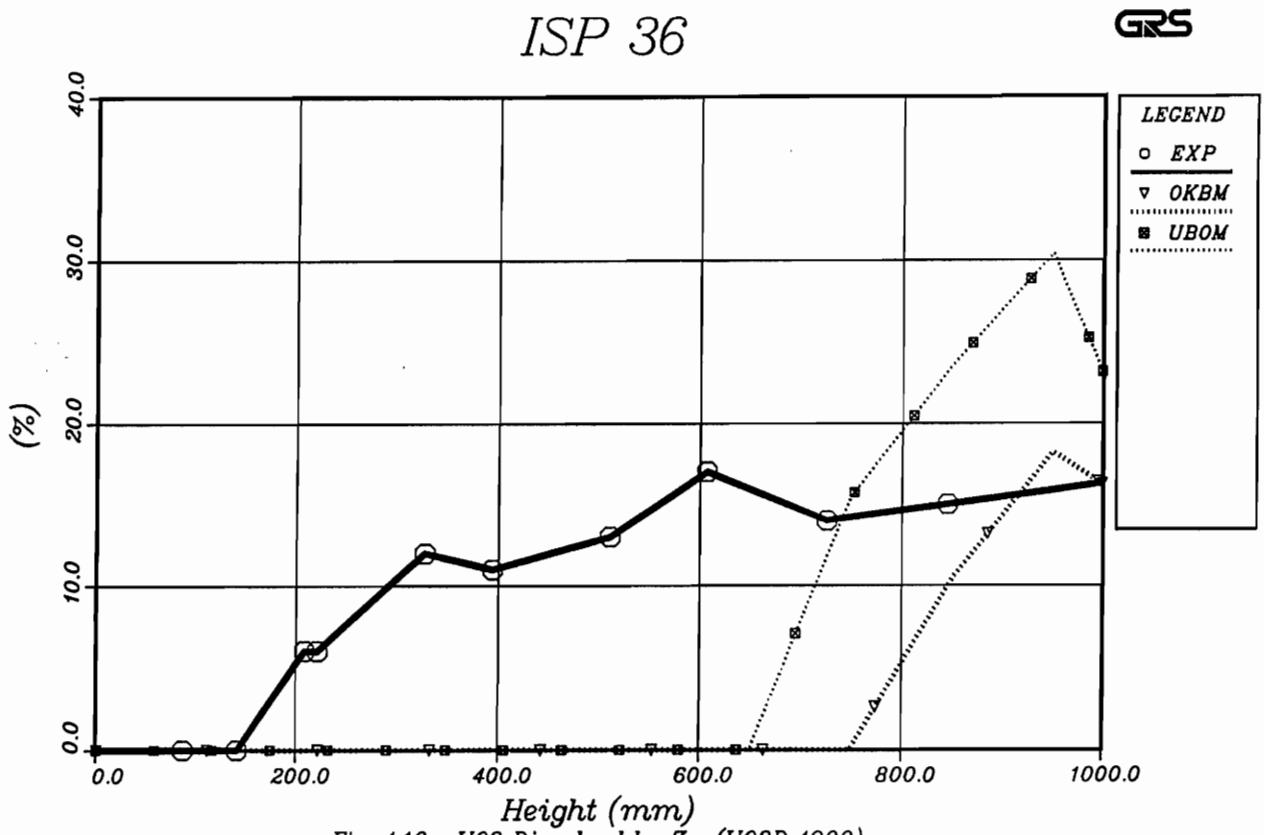

Fig. 4.16a: U02 Dissolved by Zr (U02D 4900)
Code: MELCOR

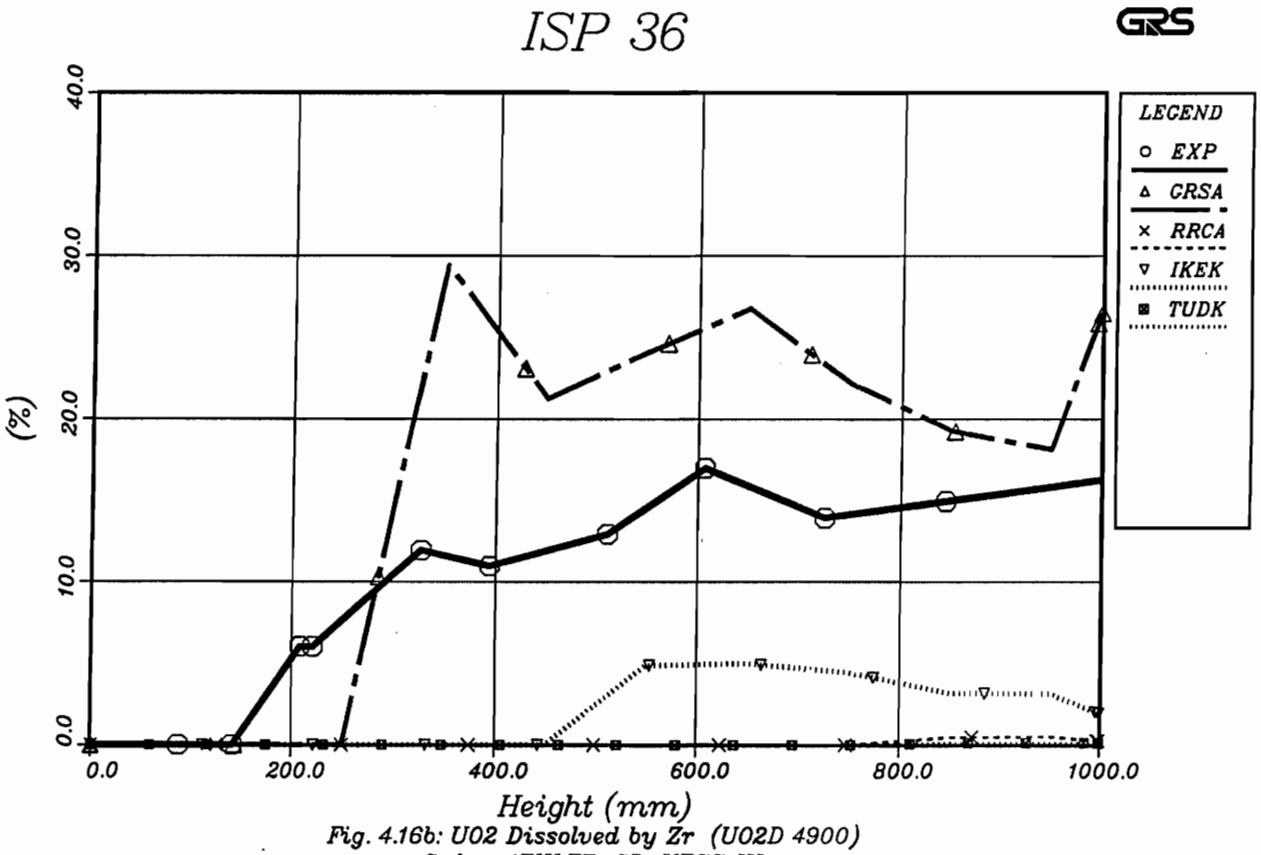

Fig. 4.16b: U02 Dissolved by Zr (U02D 4900)
Codes: ATHLET-CD, KESS III

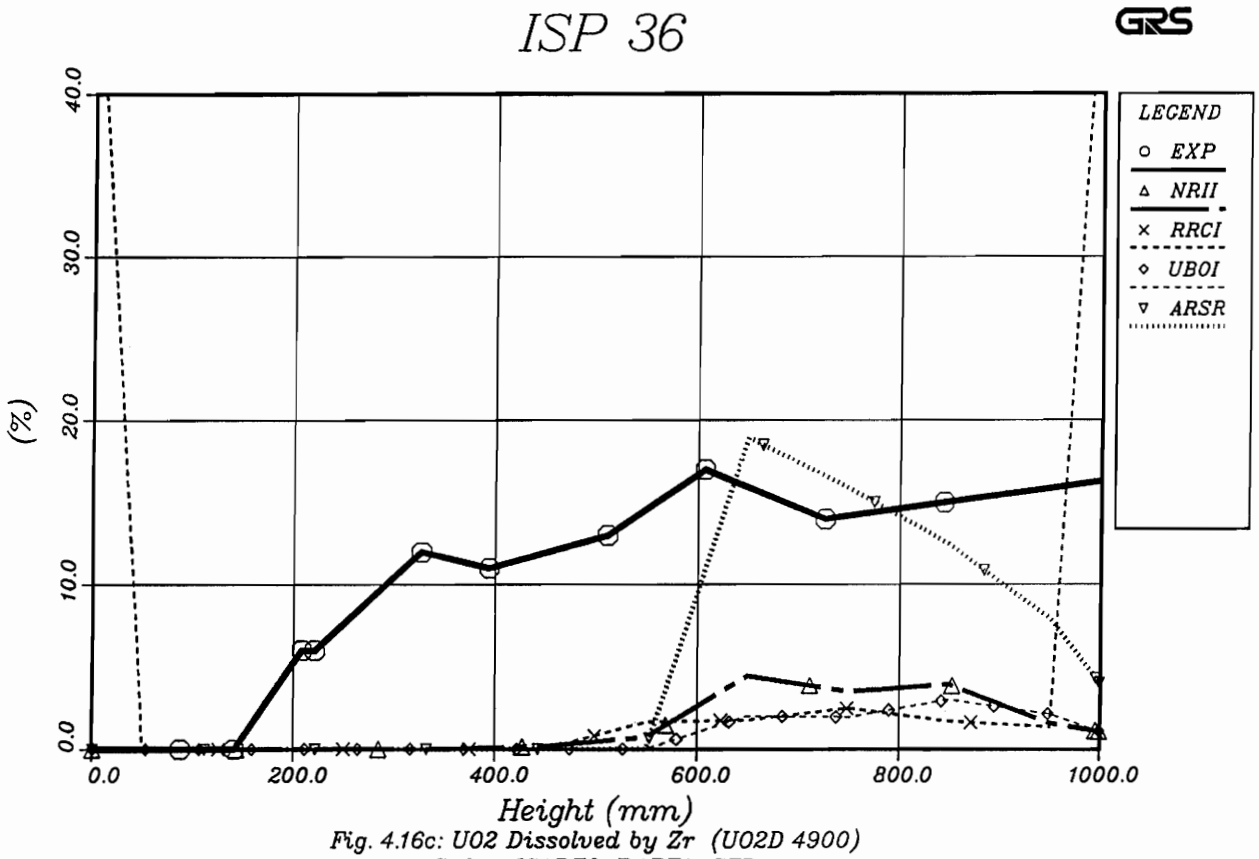

Fig. 4.16c: U02 Dissolved by Zr (U02D 4900)
Codes: ICARE2, RAPTA-SFD

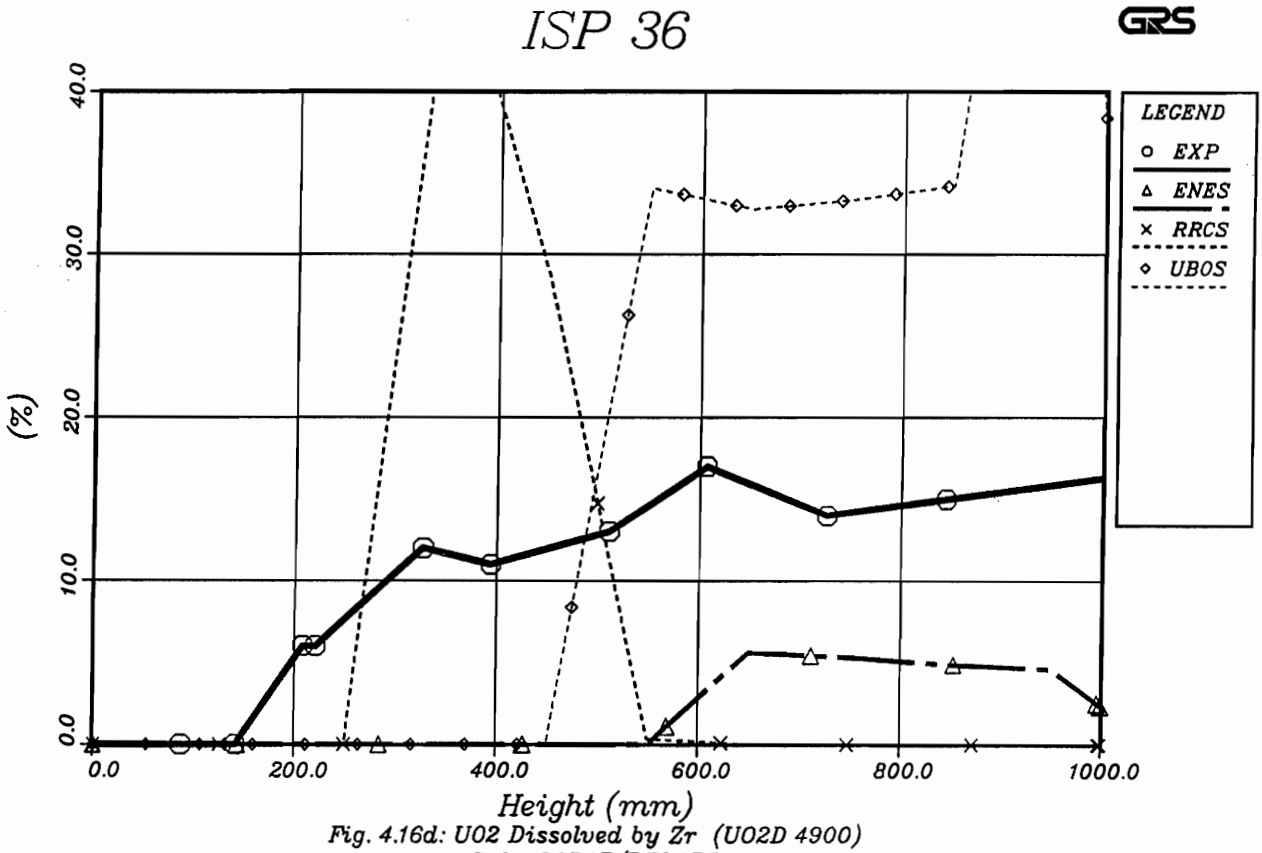

Fig. 4.16d: U02 Dissolved by Zr (U02D 4900)
Code: SCDAP/RELAP5

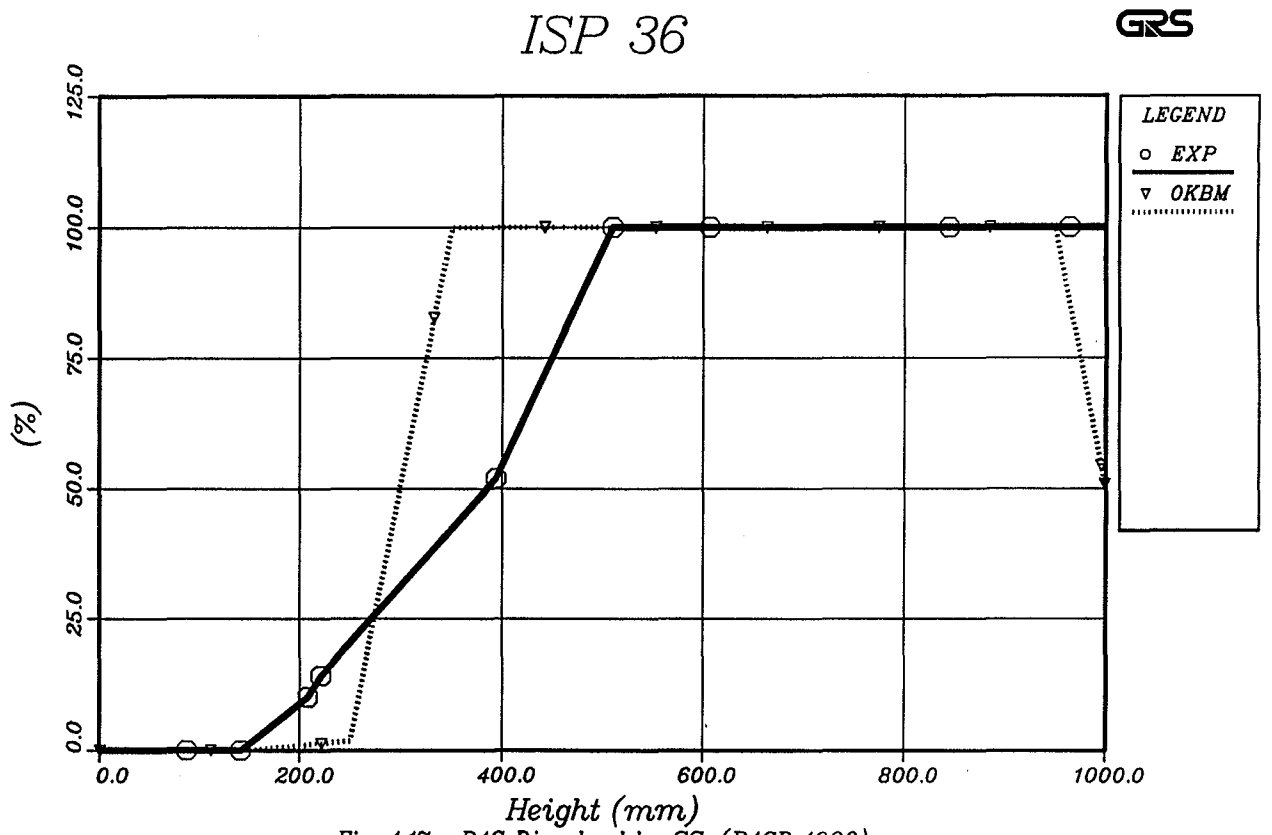

Fig. 4.17a: B4C Dissolved by SS (B4CD 4900)
Code: MELCOR

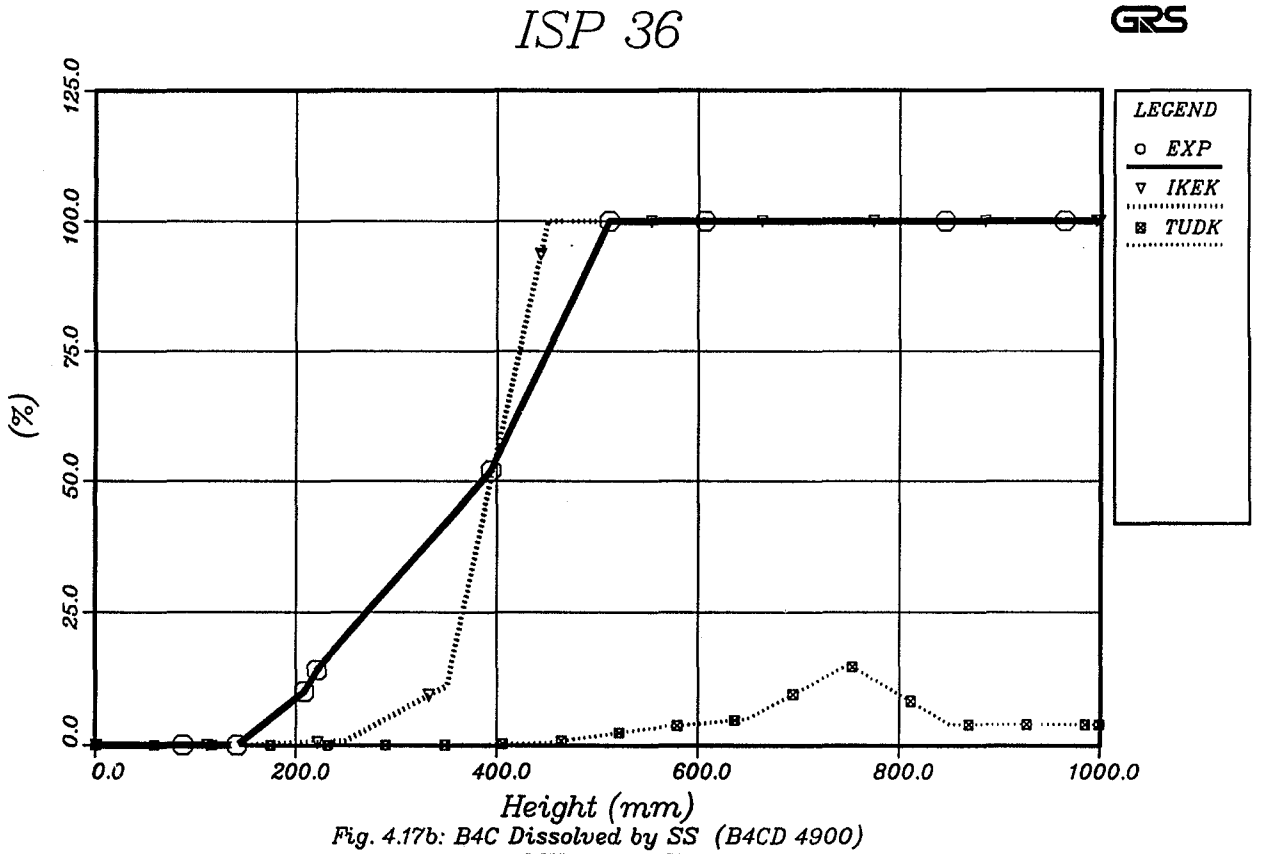

Fig. 4.17b: B4C Dissolved by SS (B4CD 4900)
Codes: ATHLET-CD, KESS III

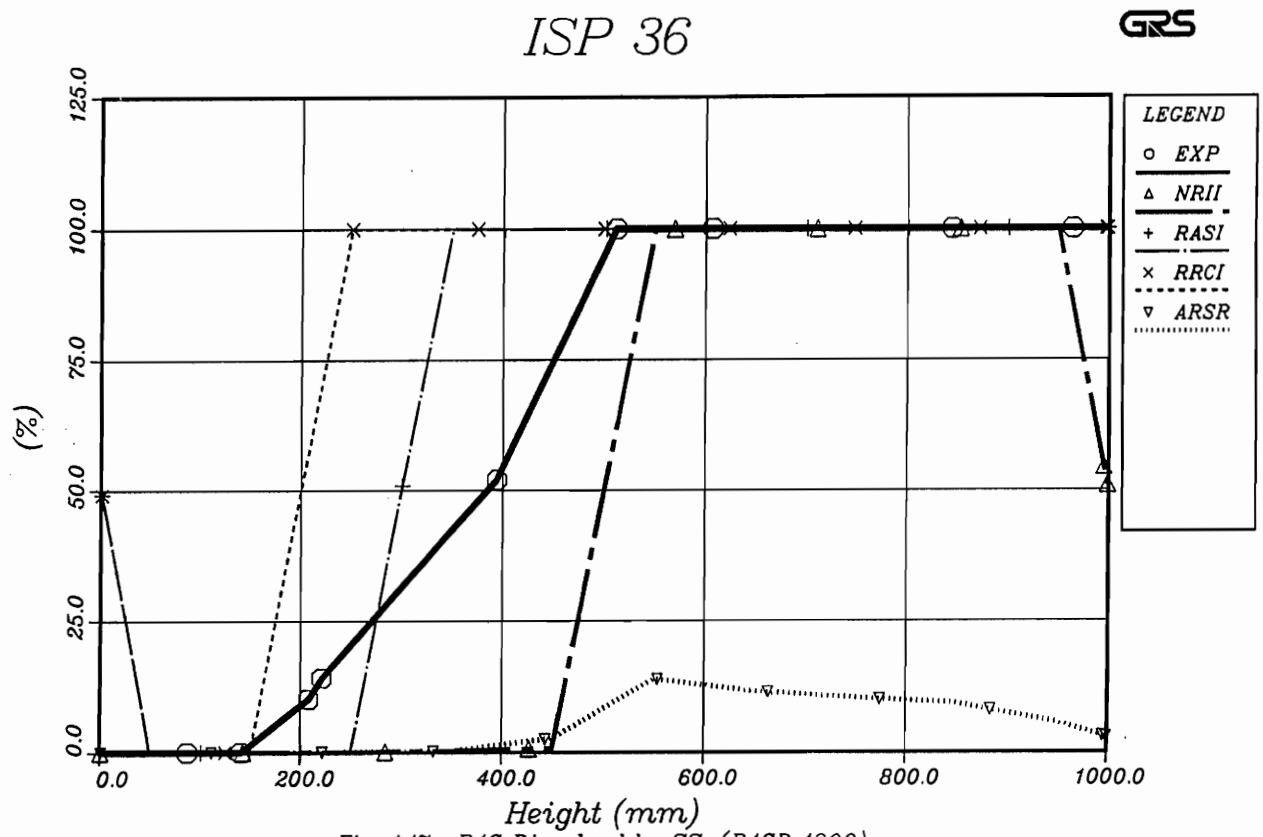

Fig. 4.17c: B4C Dissolved by SS (B4CD 4900)
Codes: ICARE2, RAPTA-SFD

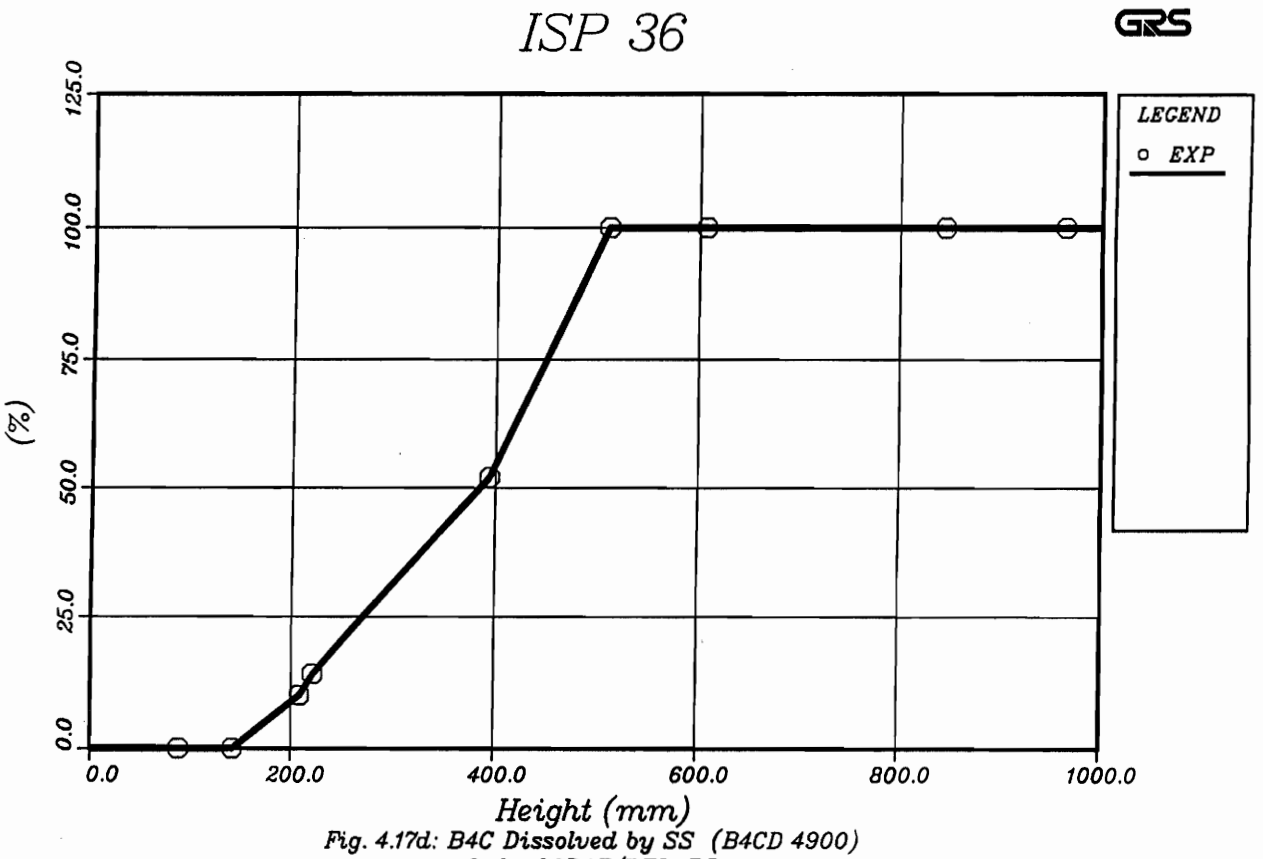

Fig. 4.17d: B4C Dissolved by SS (B4CD 4900)
Code: SCDAP/RELAP5

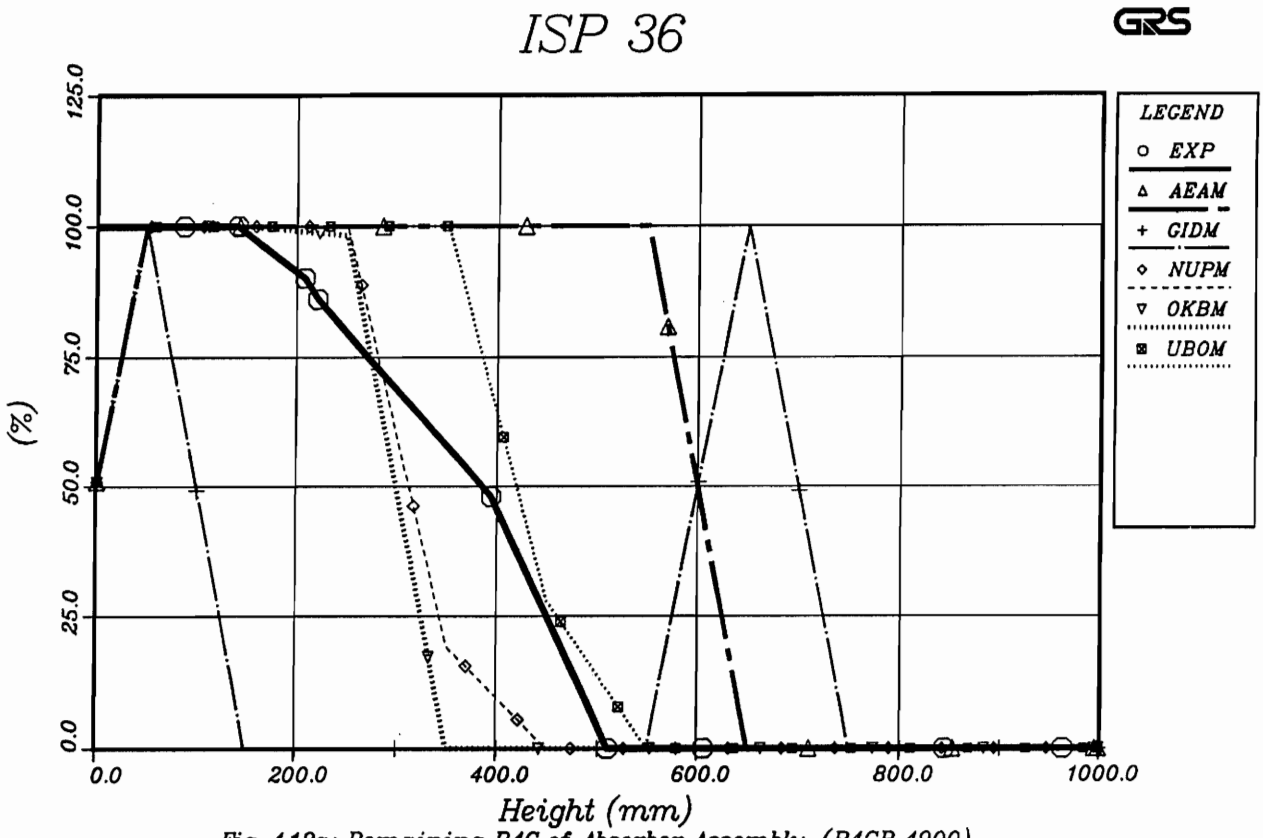

Fig. 4.18a: Remaining B4C of Absorber Assembly (B4CR 4900)
Code: MELCOR

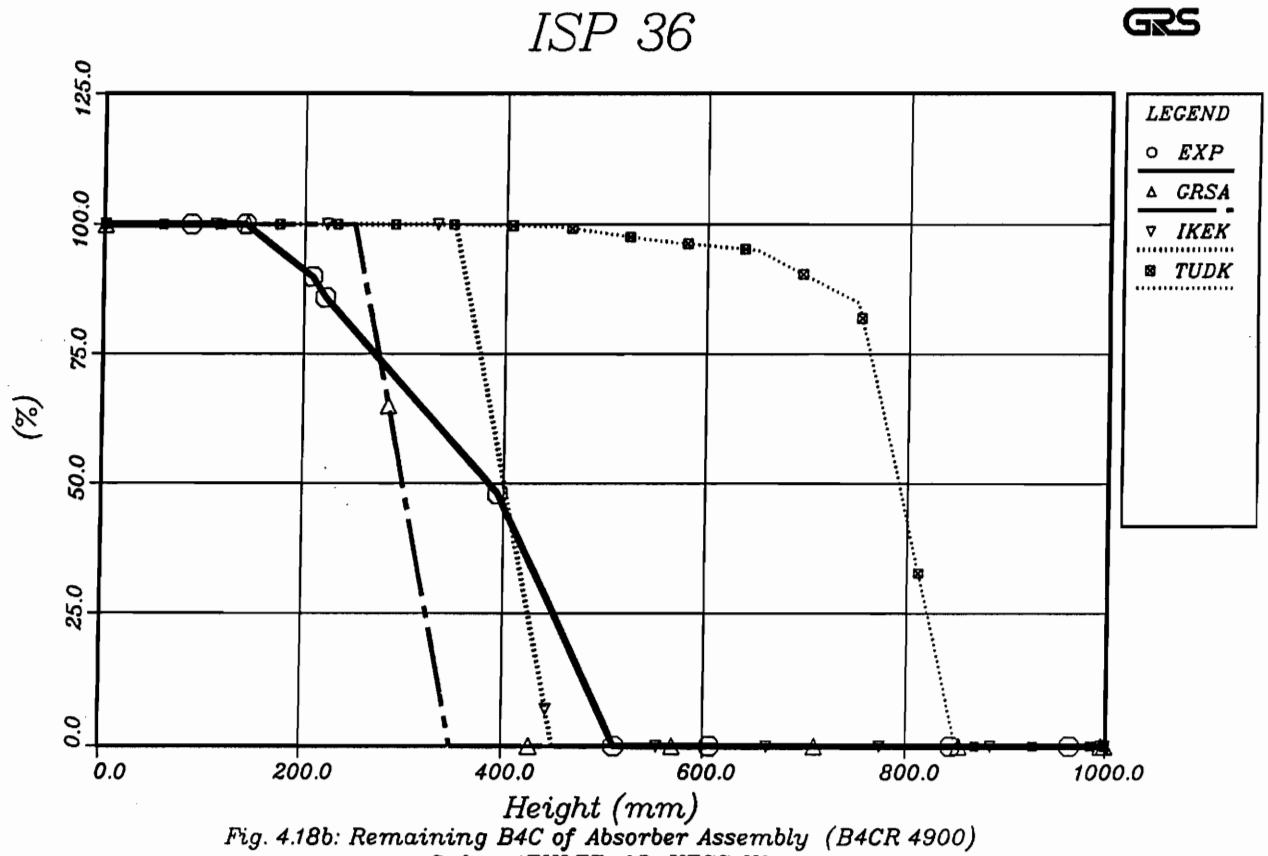

Fig. 4.18b: Remaining B4C of Absorber Assembly (B4CR 4900)
Codes: ATHLET-CD, KESS III

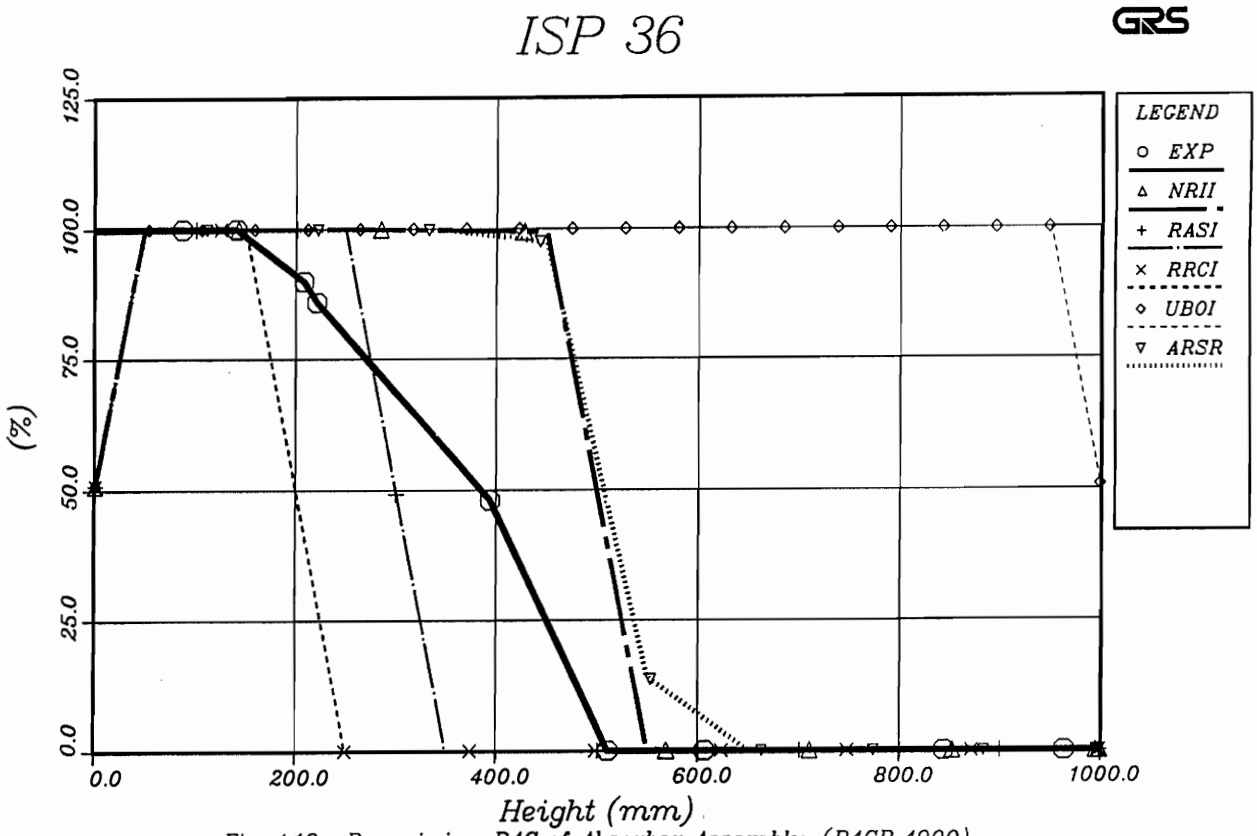

Fig. 4.18c: Remaining B4C of Absorber Assembly (B4CR 4900)
Codes: ICARE2, RAPTA–SFD

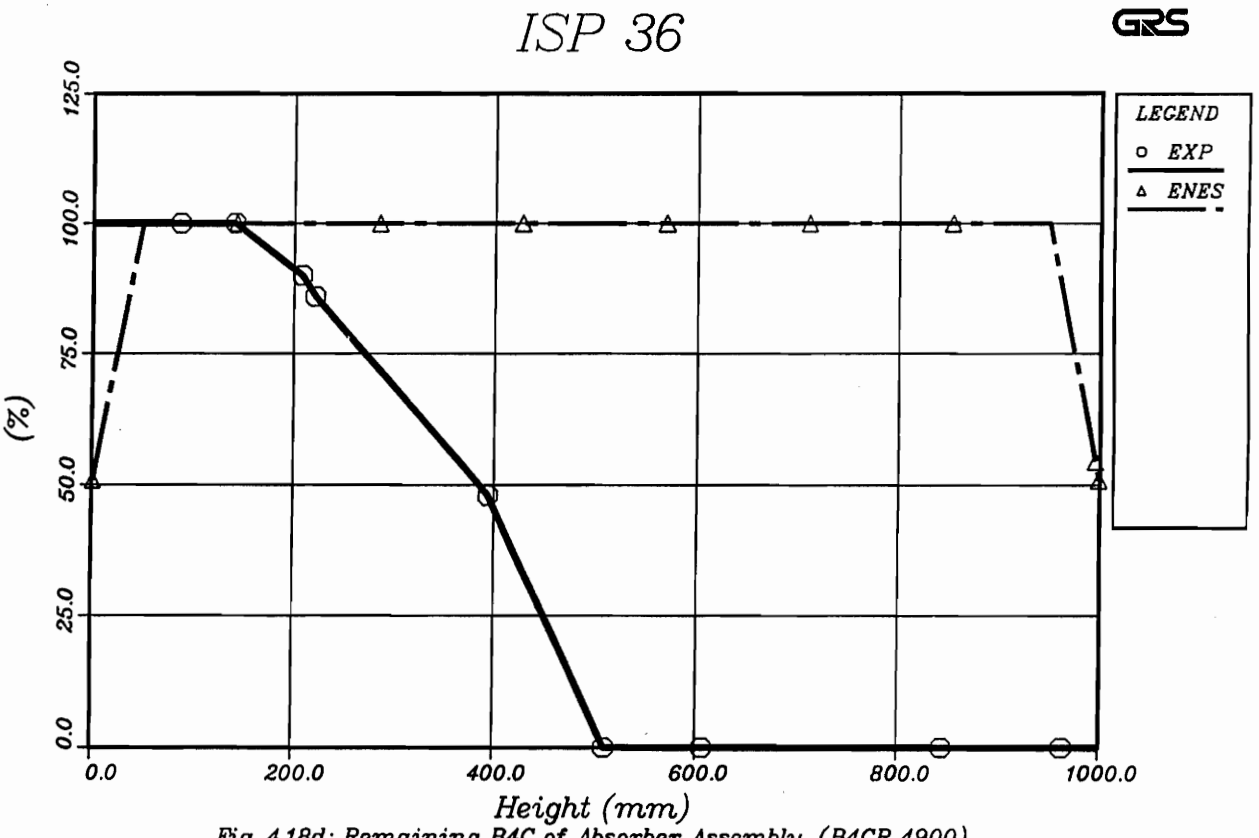

Fig. 4.18d: Remaining B4C of Absorber Assembly (B4CR 4900)
Code: SCDAP/RELAP5

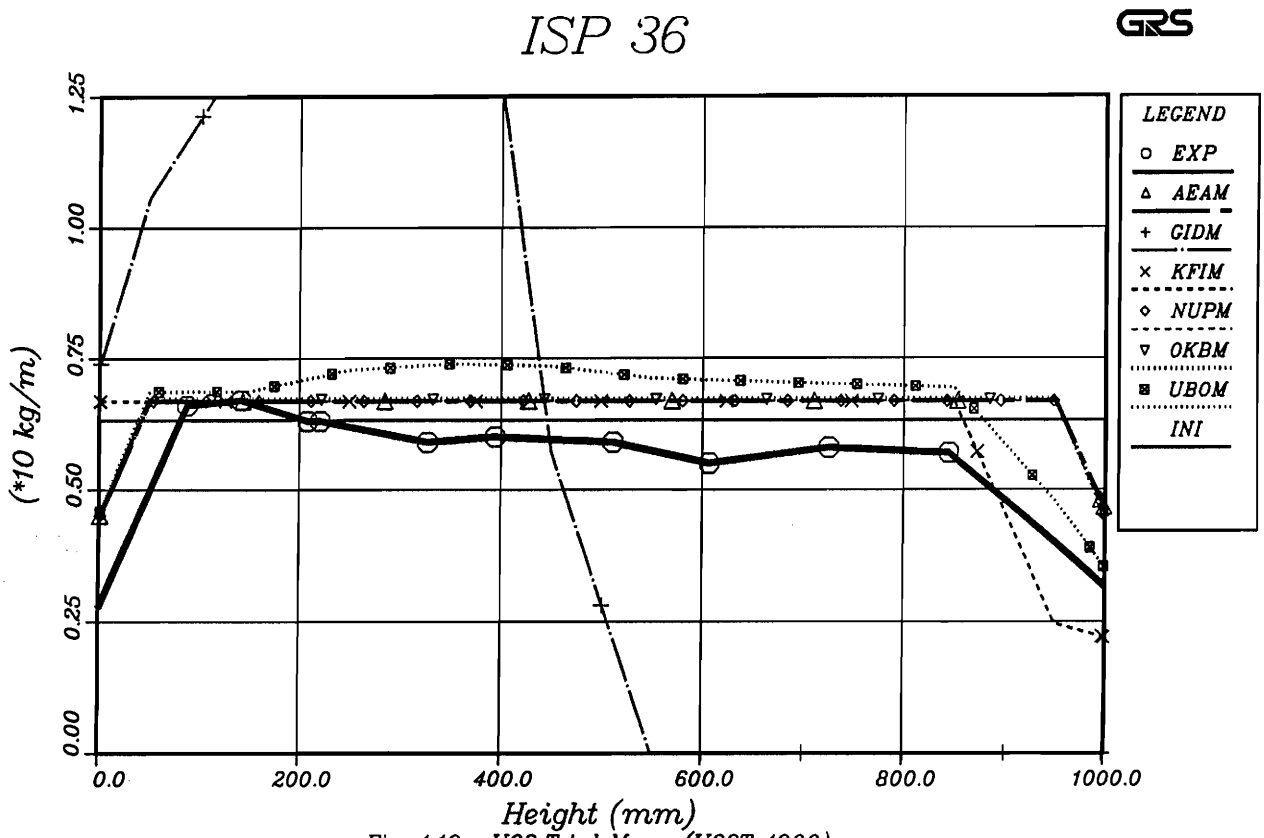

Fig. 4.19a: UO2 Total Mass (UO2T 4900)
Code: MELCOR

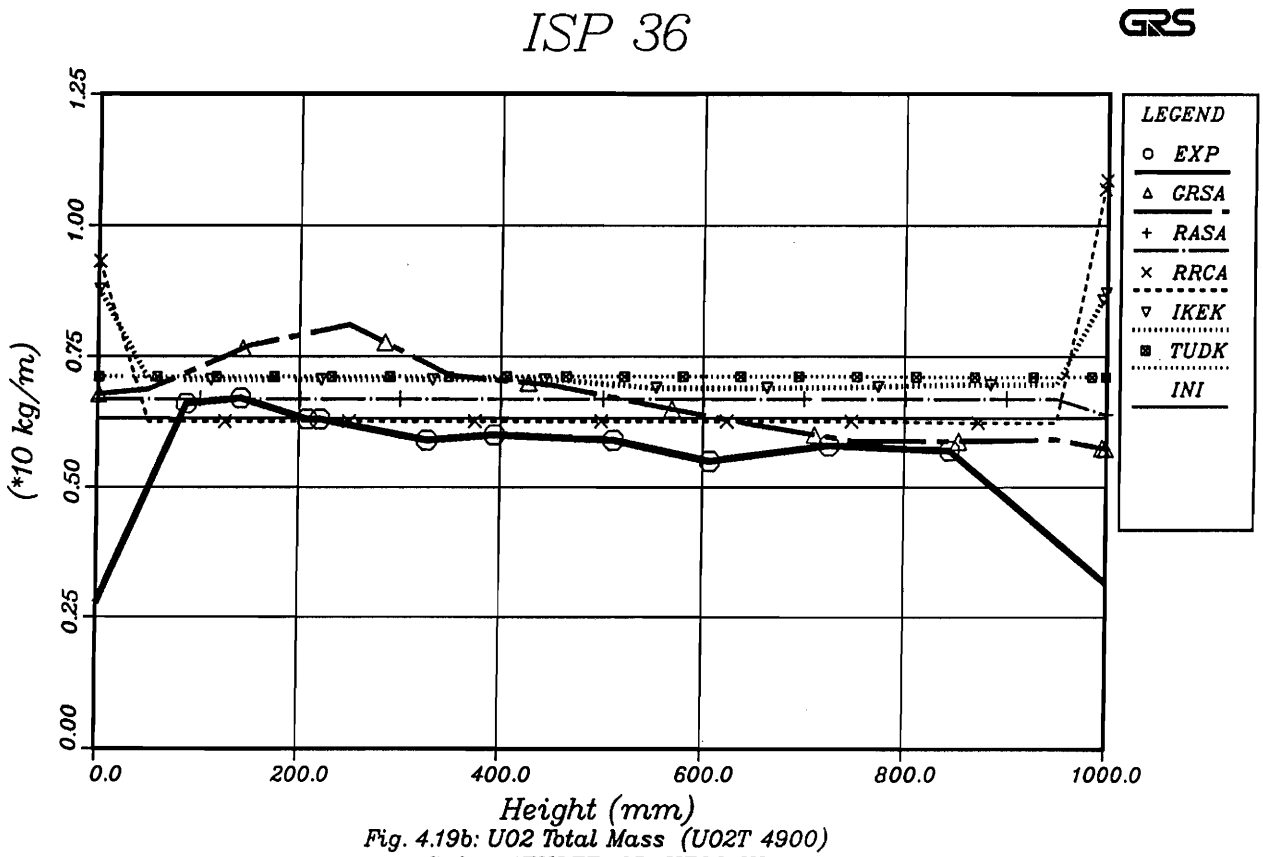

Fig. 4.19b: UO2 Total Mass (UO2T 4900)
Codes: ATHLET-CD, KESS III

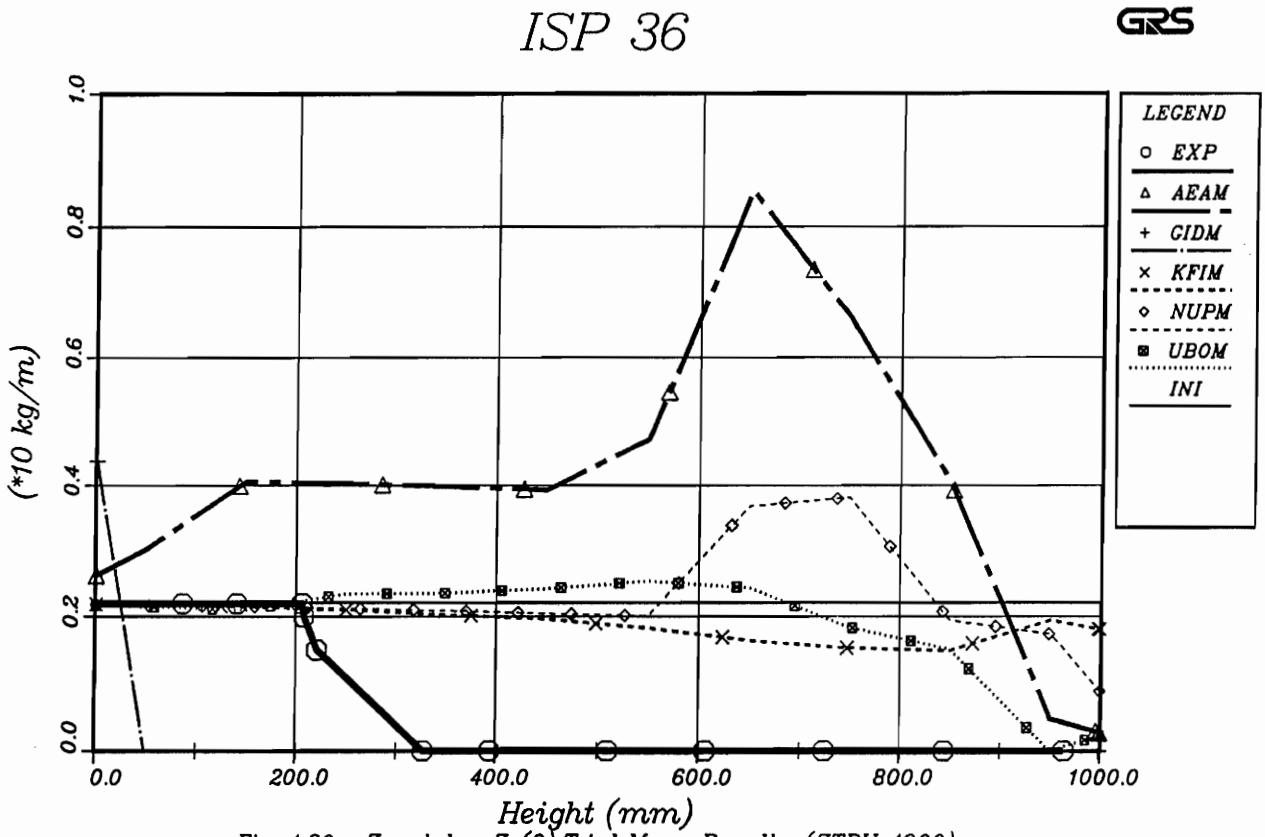

Fig. 4.20a: Zr, alpha–Zr(0) Total Mass, Bundle (ZTBU 4900)
Code: MELCOR

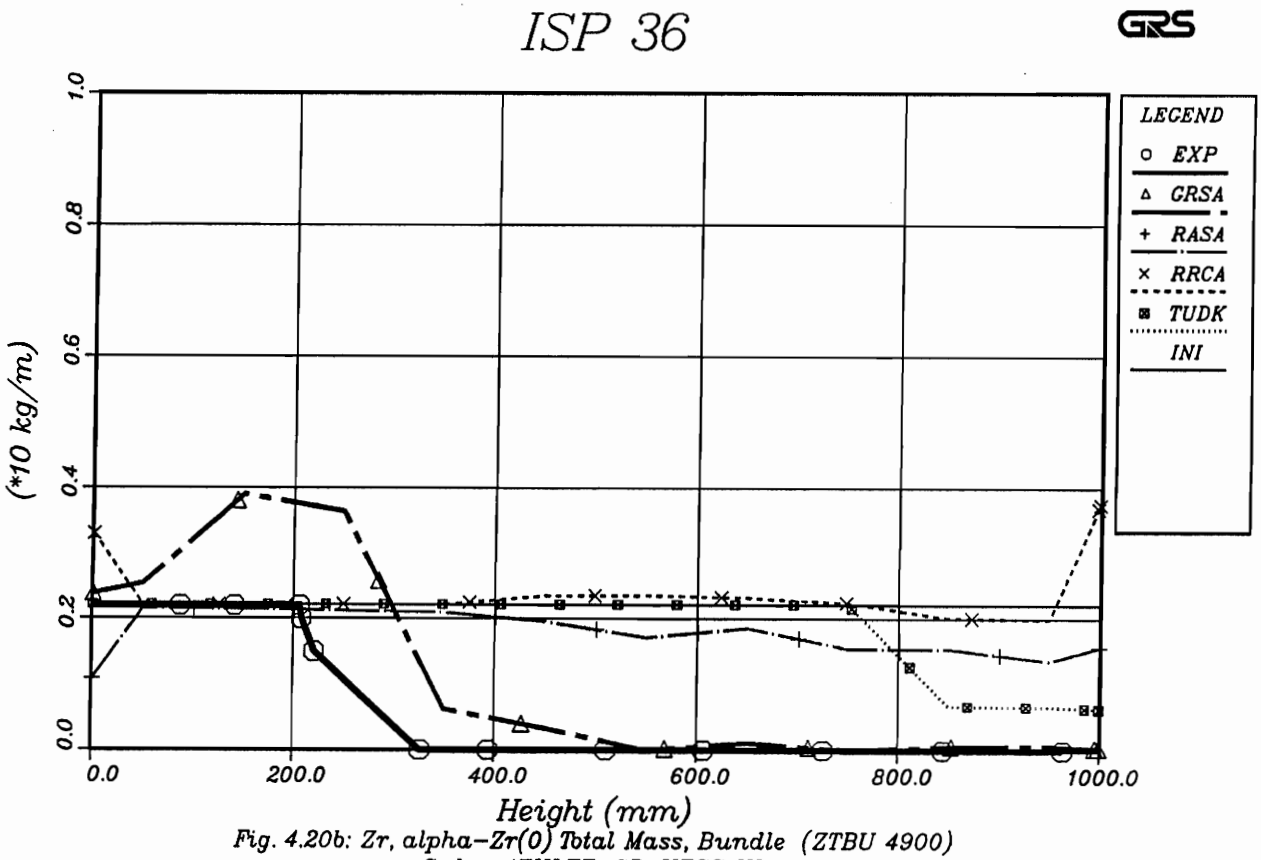

Fig. 4.20b: Zr, alpha–Zr(0) Total Mass, Bundle (ZTBU 4900)
Codes: ATHLET–CD, KESS III

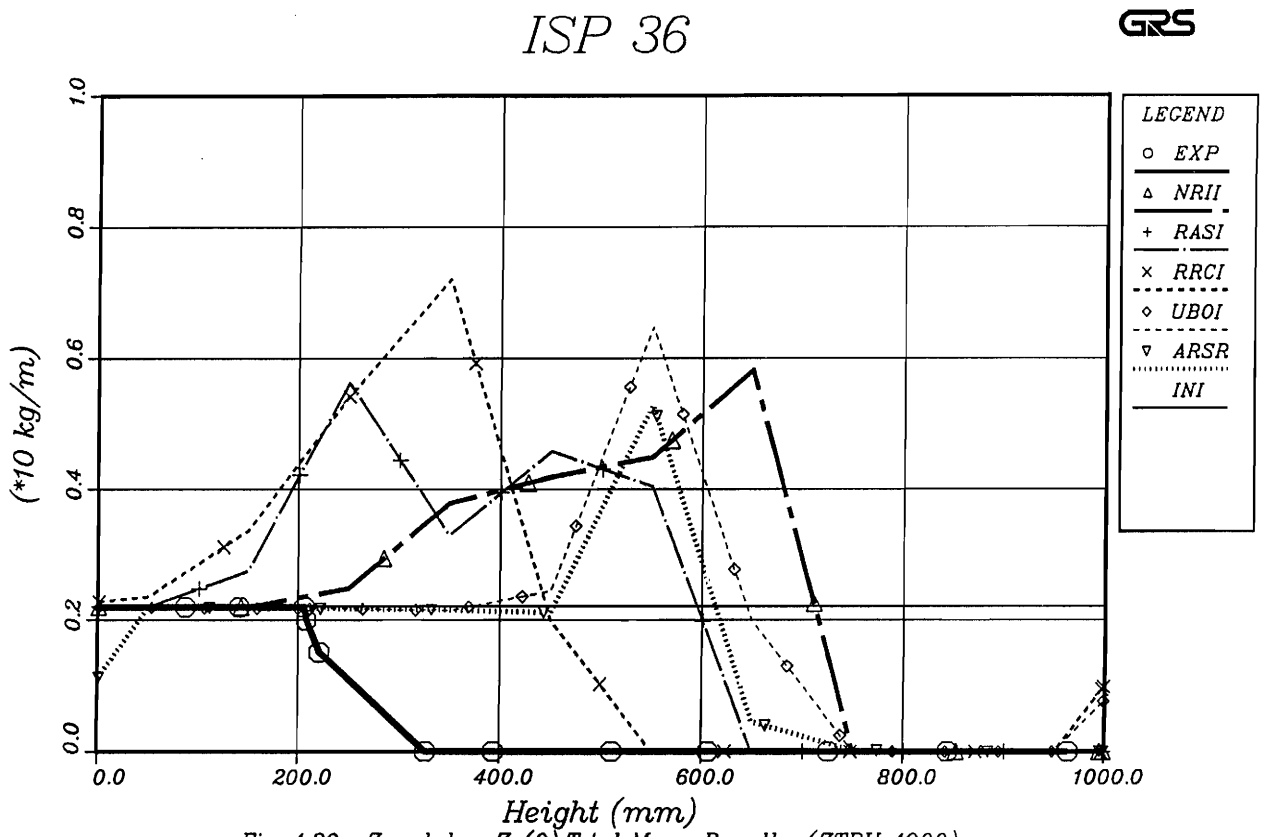

Fig. 4.20c: Zr, alpha–Zr(0) Total Mass, Bundle (ZTBU 4900)
Codes: ICARE2, RAPTA–SFD

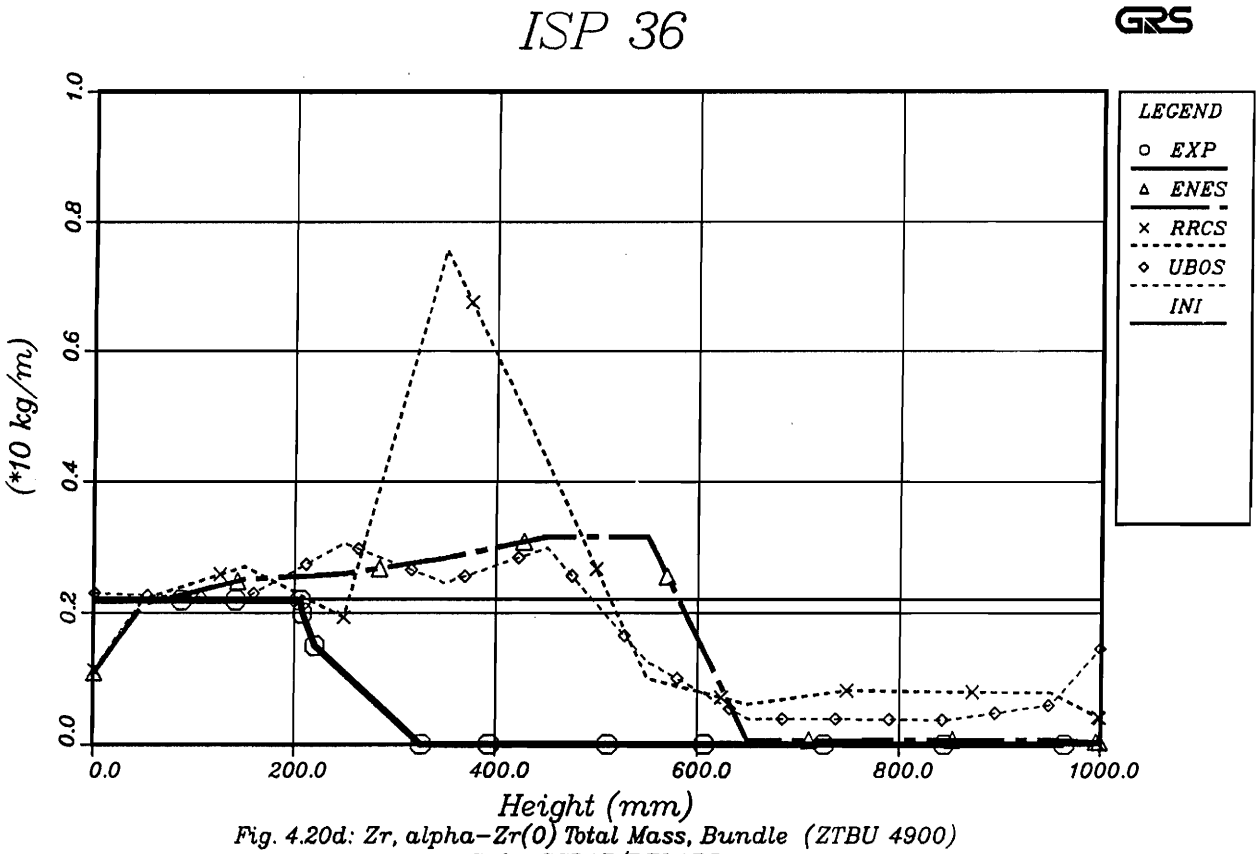

Fig. 4.20d: Zr, alpha–Zr(0) Total Mass, Bundle (ZTBU 4900)
Code: SCDAP/RELAP5

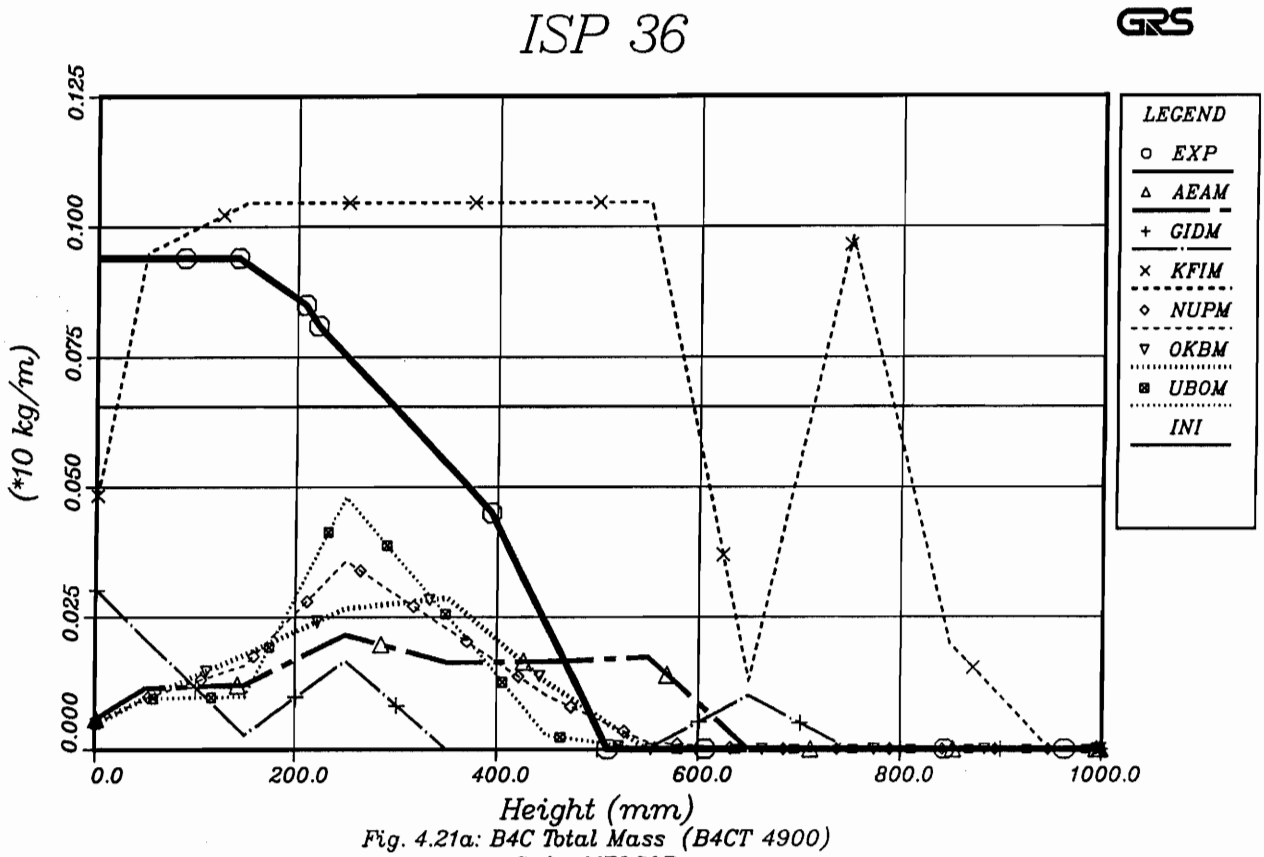

Fig. 4.21a: B4C Total Mass (B4CT 4900)
Code: MELCOR

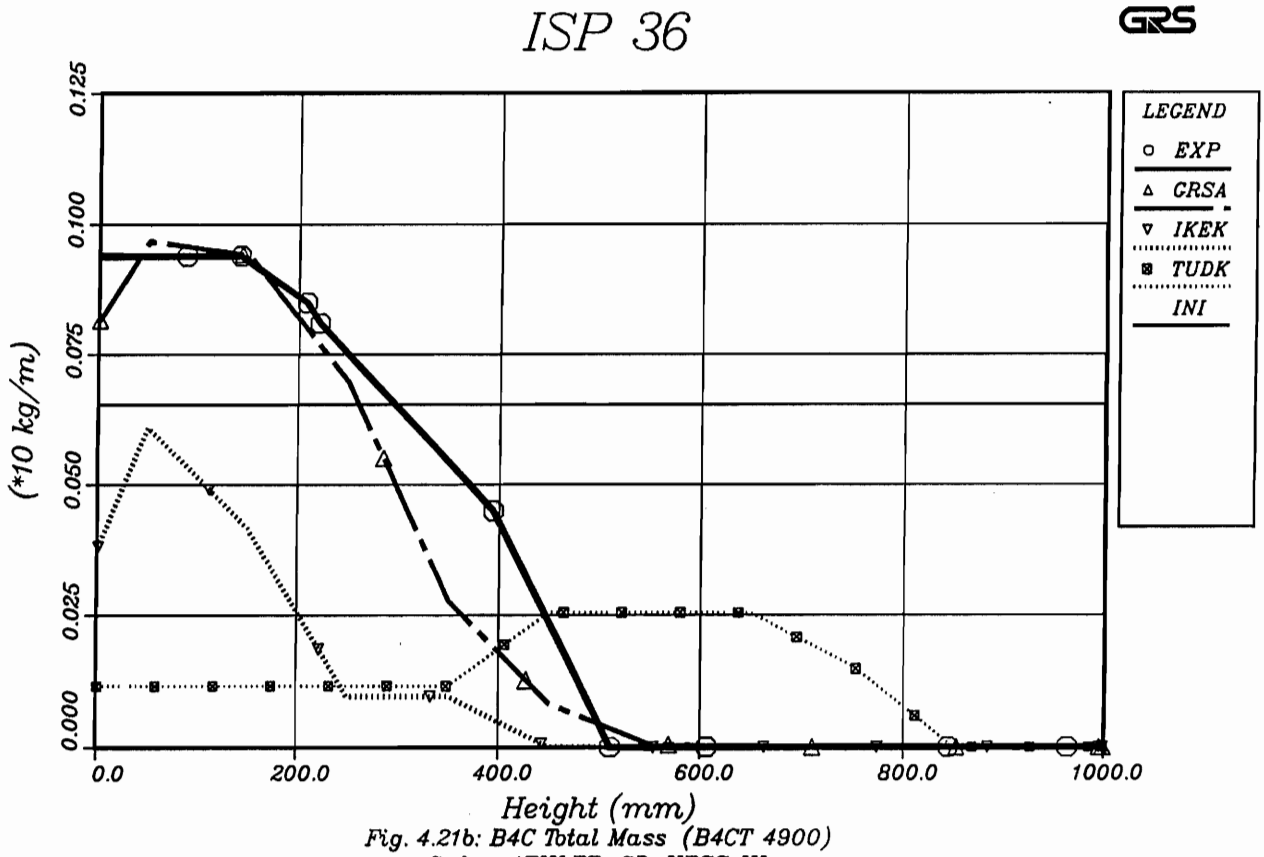

Fig. 4.21b: B4C Total Mass (B4CT 4900)
Codes: ATHLET-CD, KESS III

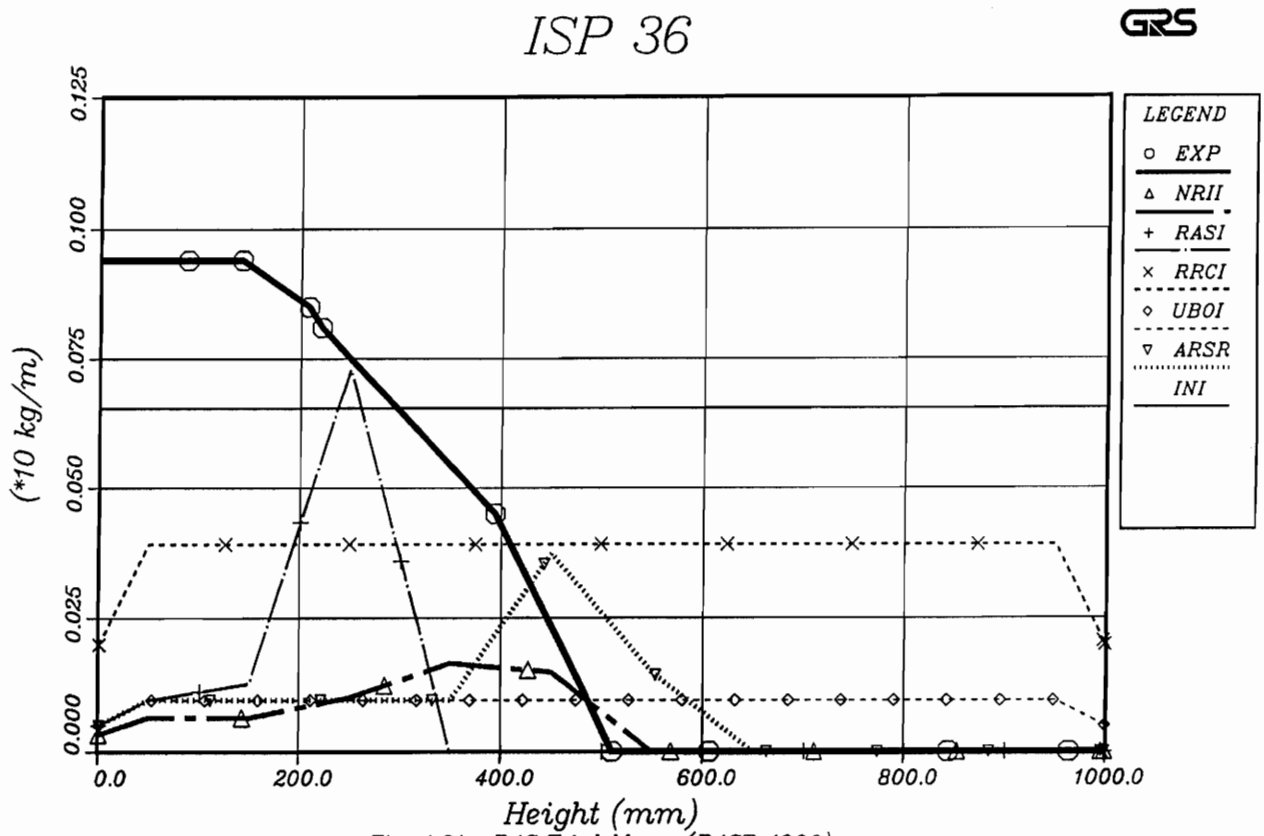

Fig. 4.21c: B4C Total Mass (B4CT 4900)
Codes: ICARE2, RAPTA–SFD

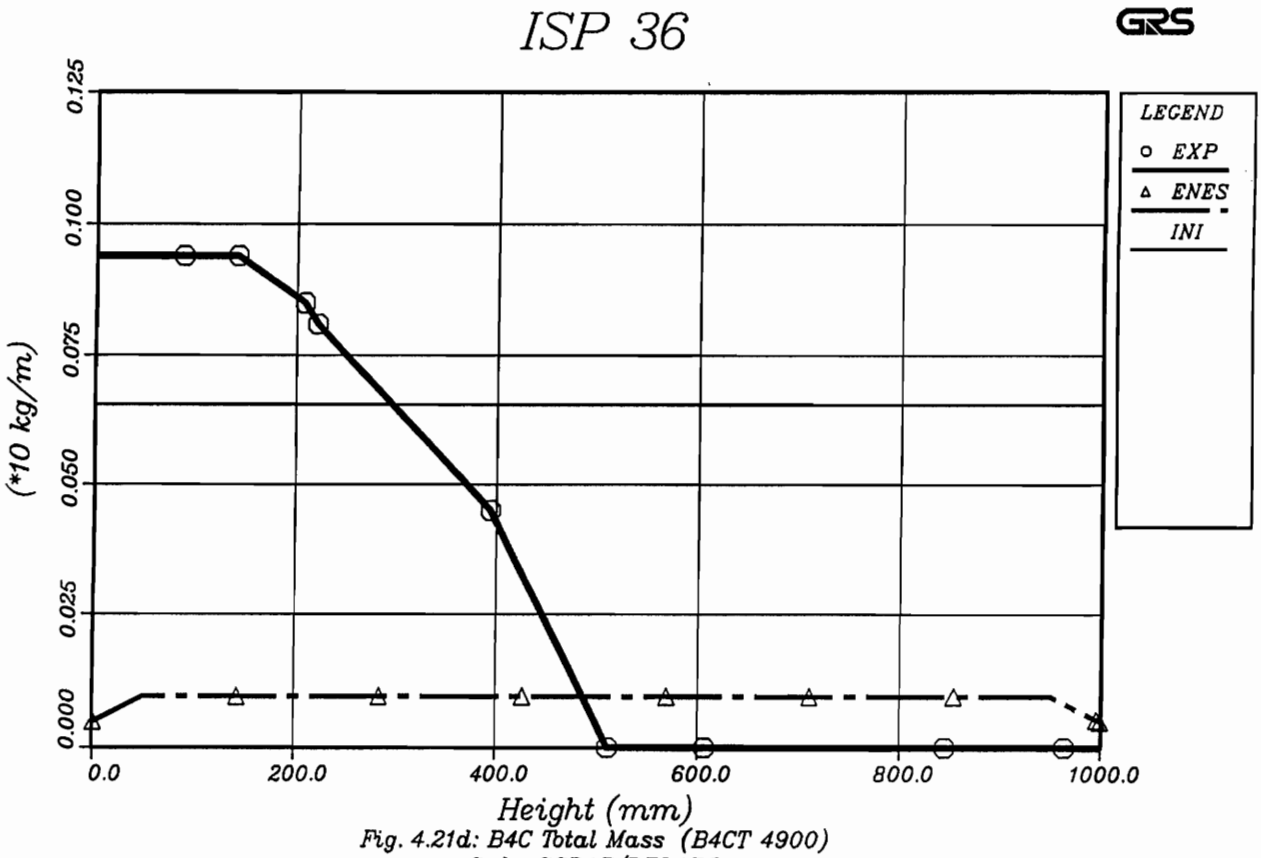

Fig. 4.21d: B4C Total Mass (B4CT 4900)
Code: SCDAP/RELAP5

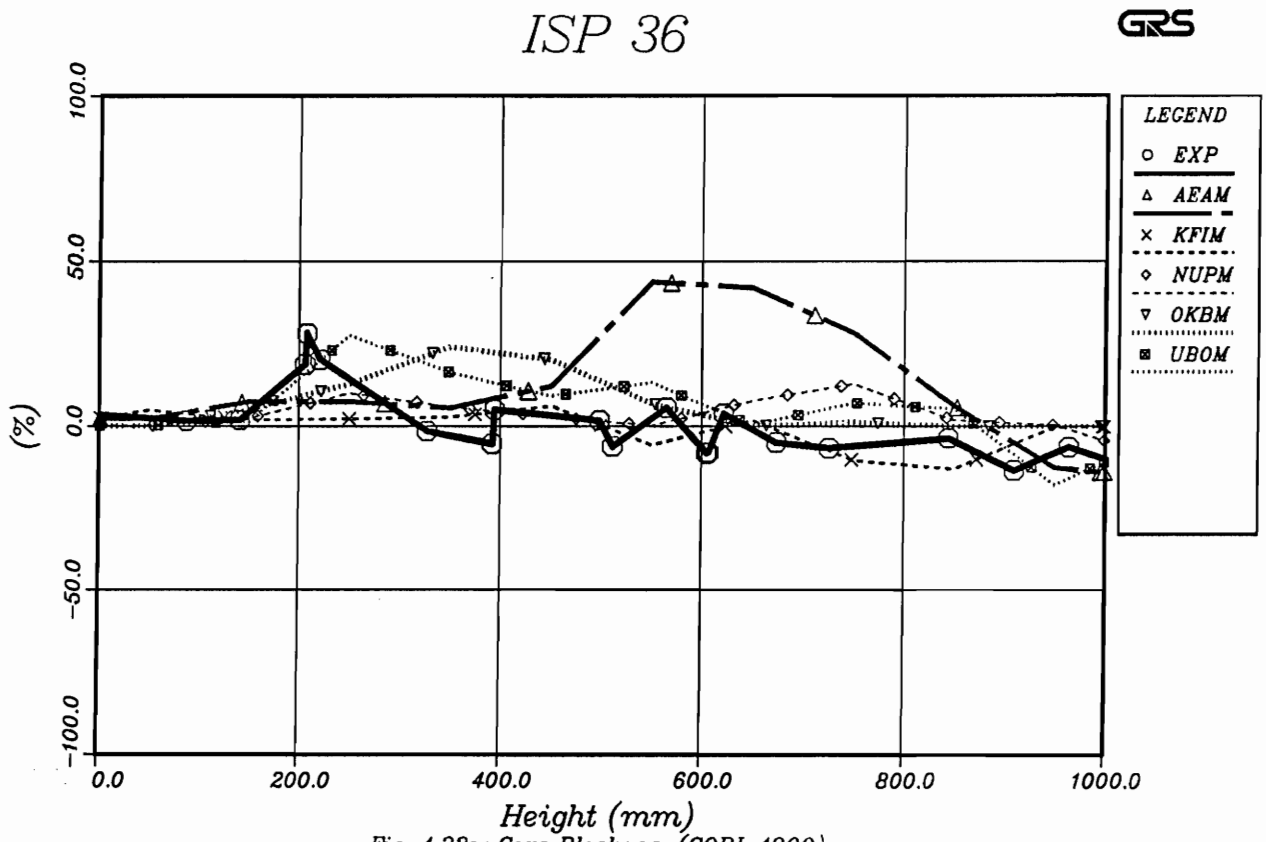

Fig. 4.22a: Core Blockage (COBL 4900)
Code: MELCOR

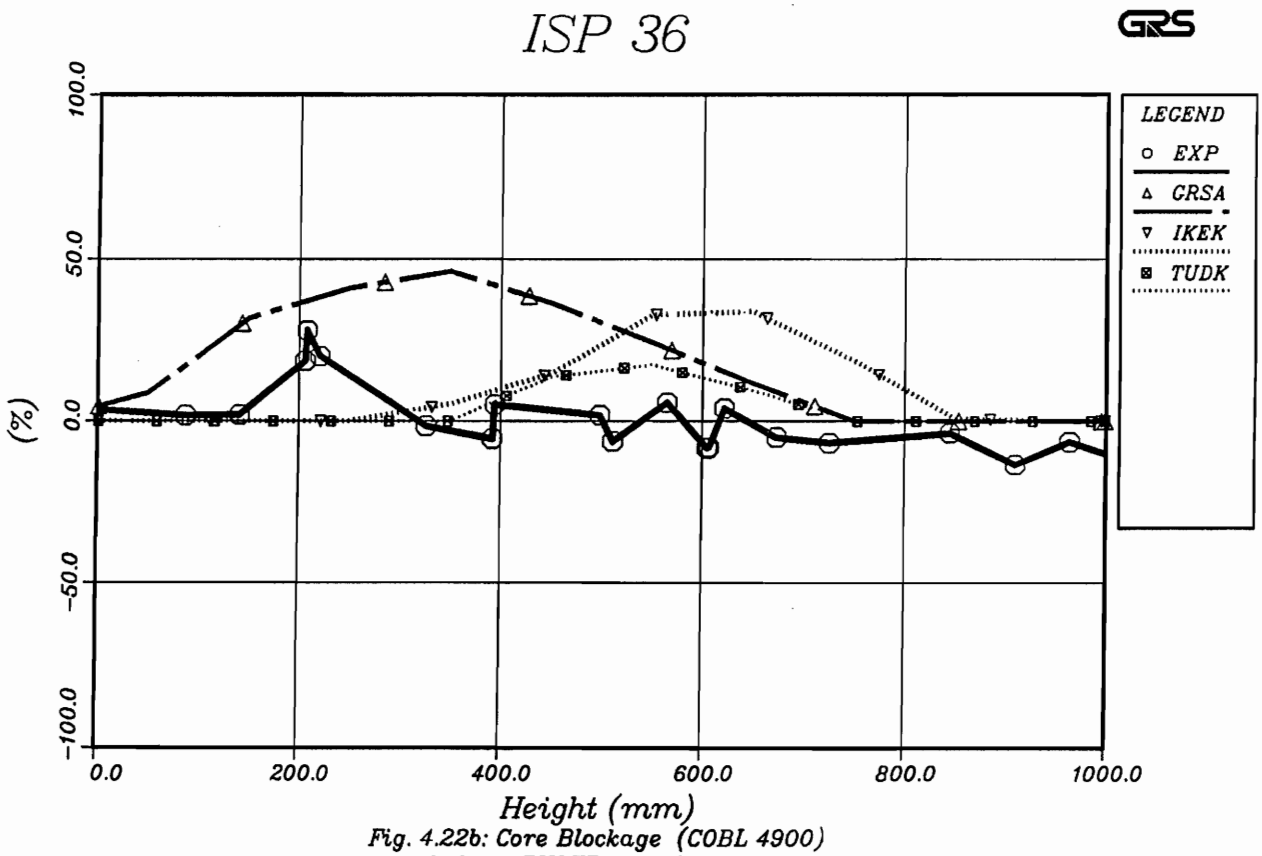

Fig. 4.22b: Core Blockage (COBL 4900)
Codes: ATHLET-CD, KESS III

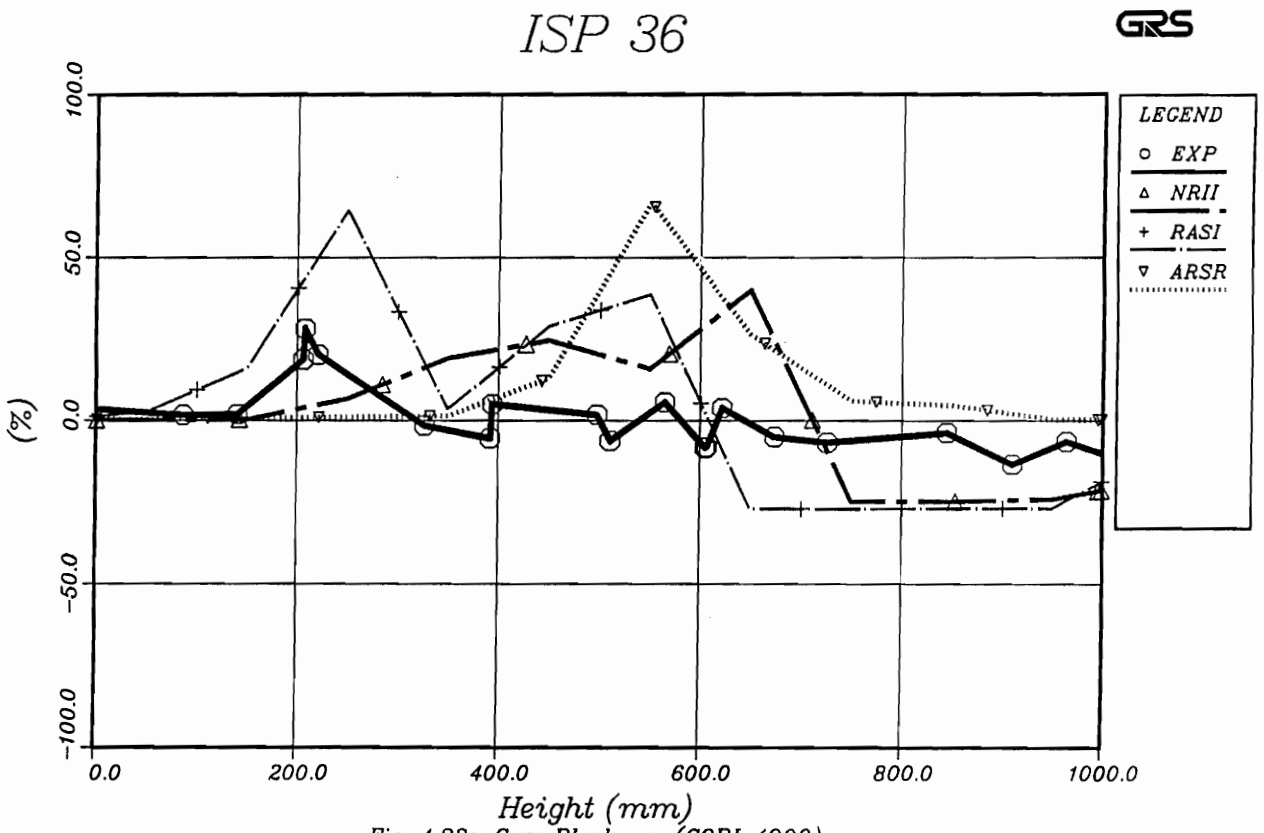

Fig. 4.22c: Core Blockage (COBL 4900)
Codes: ICARE2, RAPTA-SFD

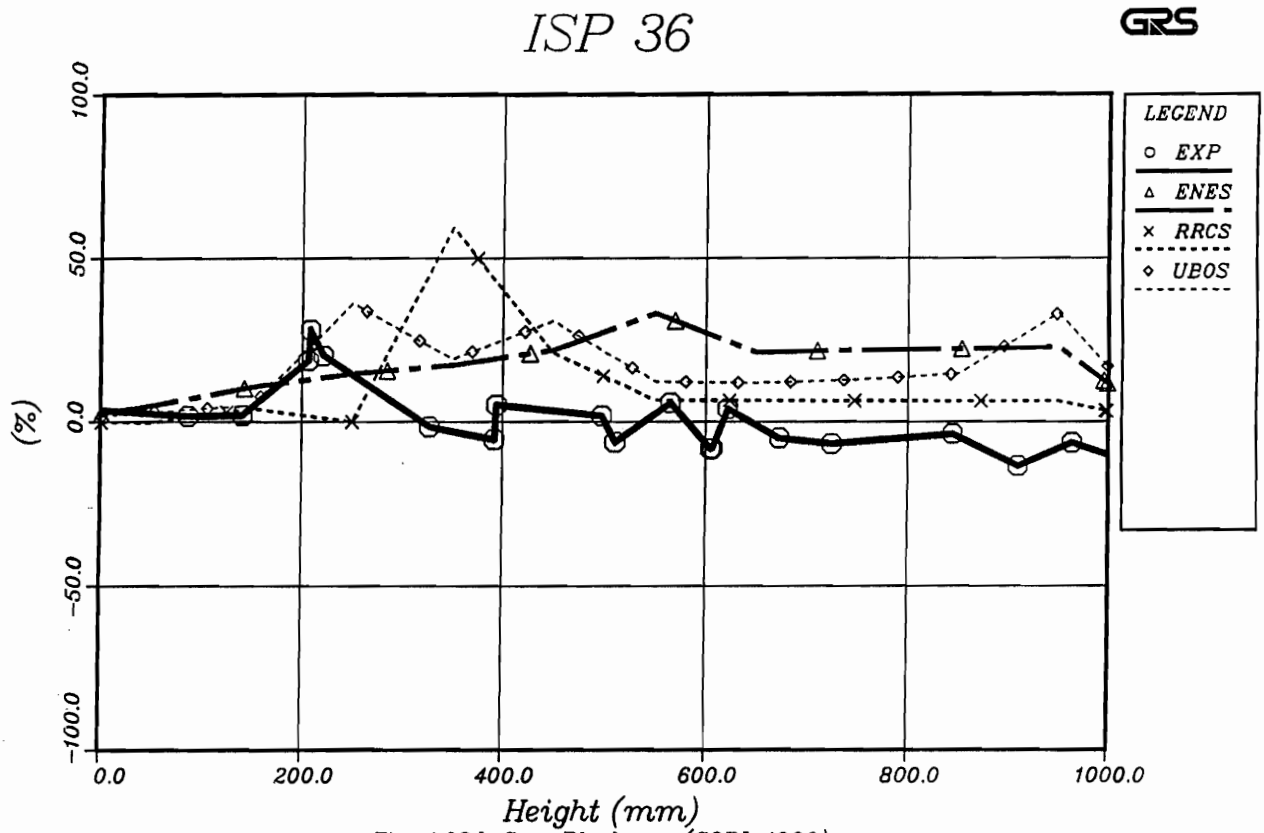

Fig. 4.22d: Core Blockage (COBL 4900)
Code: SCDAP/RELAP5

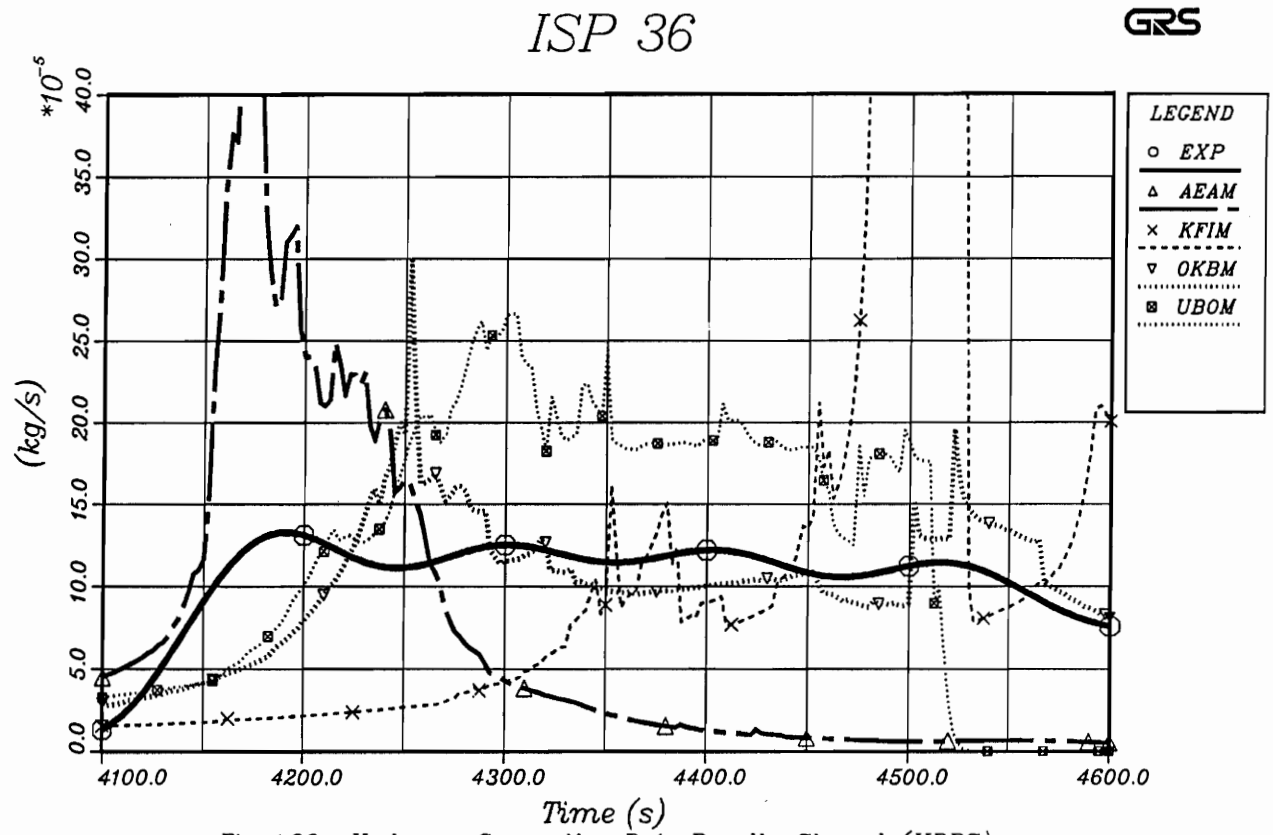

Fig. 4.23a: Hydrogen Generation Rate, Bundle+Shroud (HRBS)
Code: MELCOR

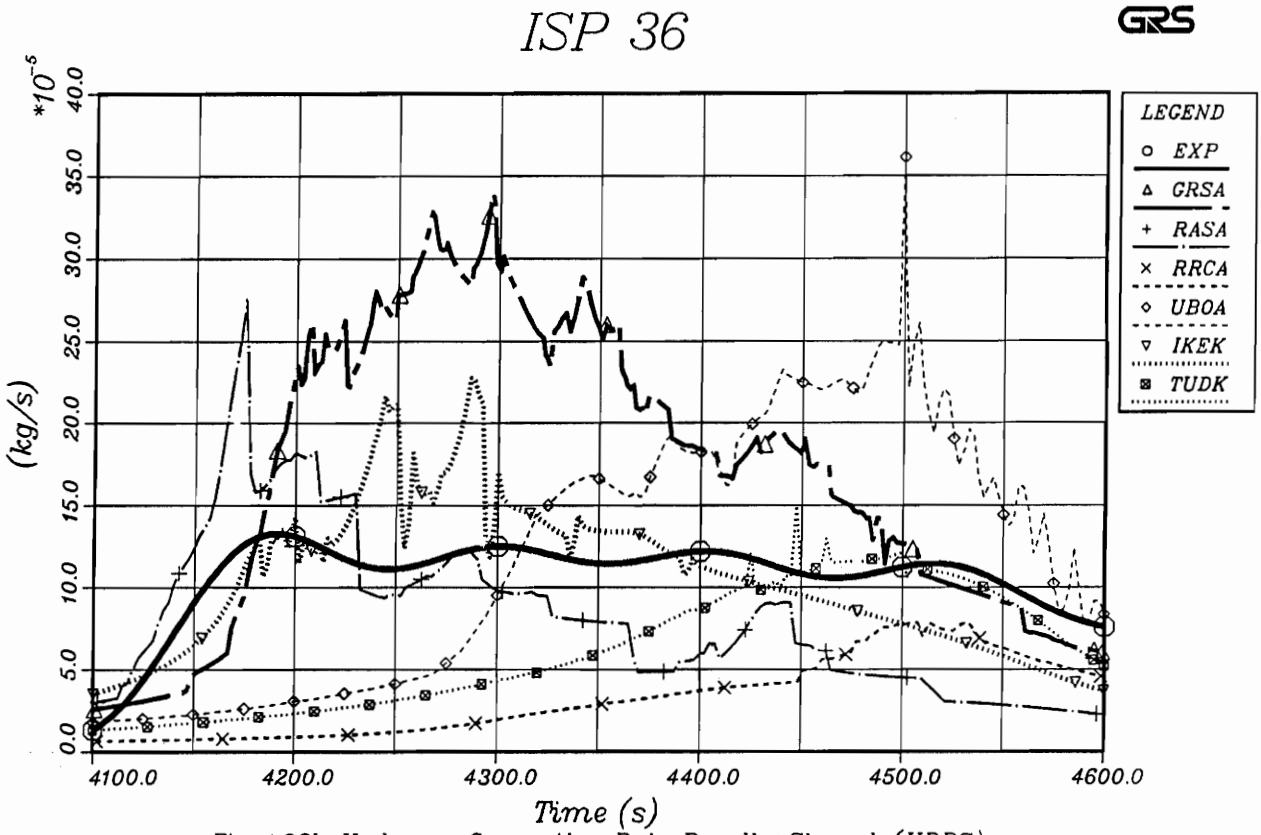

Fig. 4.23b: Hydrogen Generation Rate, Bundle+Shroud (HRBS)
Codes: ATHLET-CD, KESS III

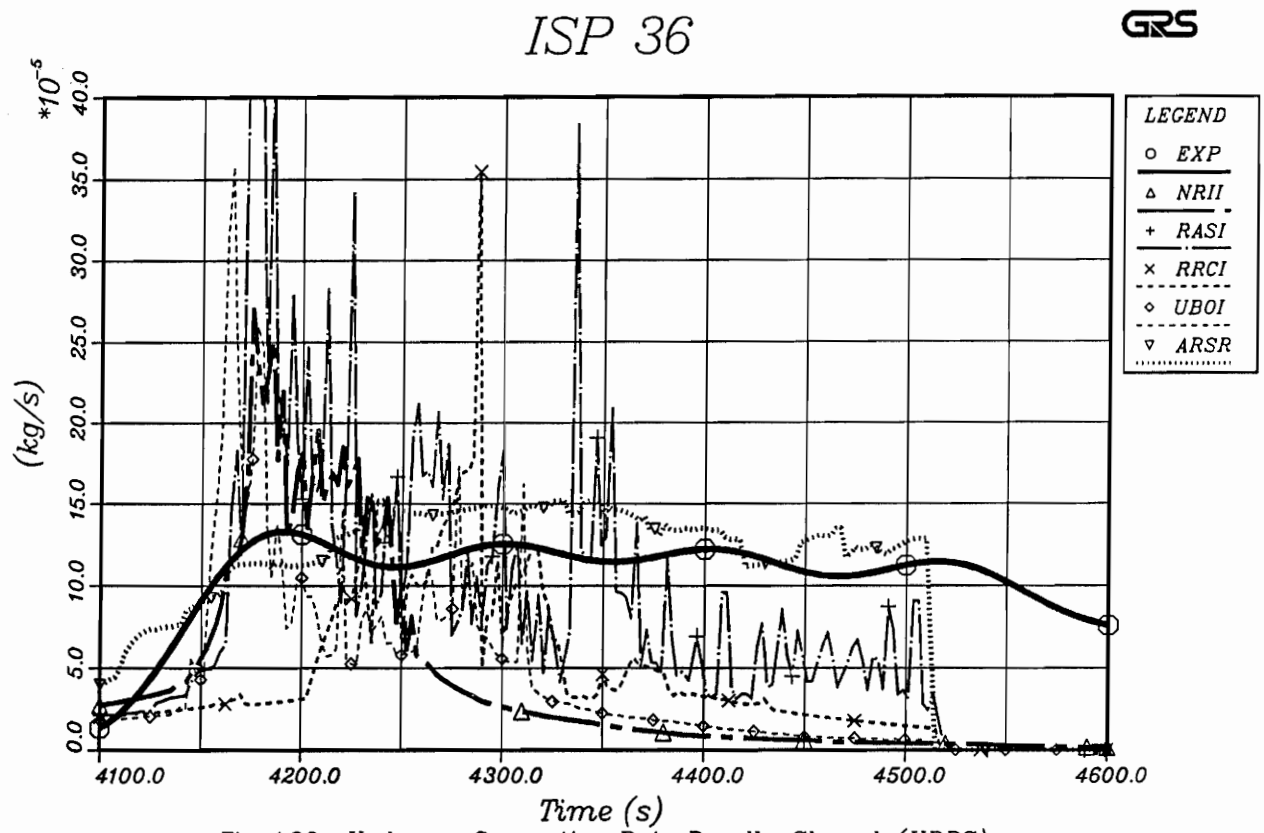

Fig. 4.23c: Hydrogen Generation Rate, Bundle+Shroud (HRBS)
Codes: ICARE2, RAPTA-SFD

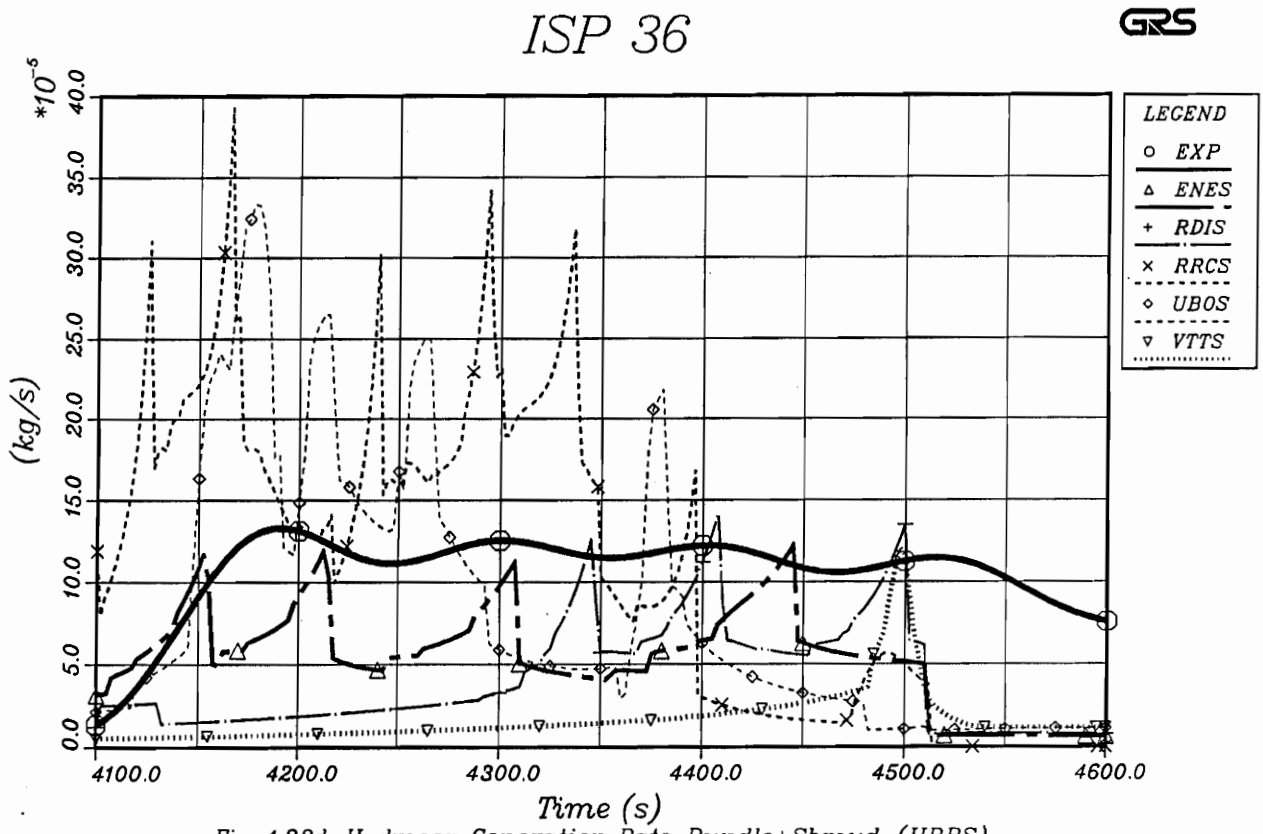

Fig. 4.23d: Hydrogen Generation Rate, Bundle+Shroud (HRBS)
Code: SCDAP/RELAP5

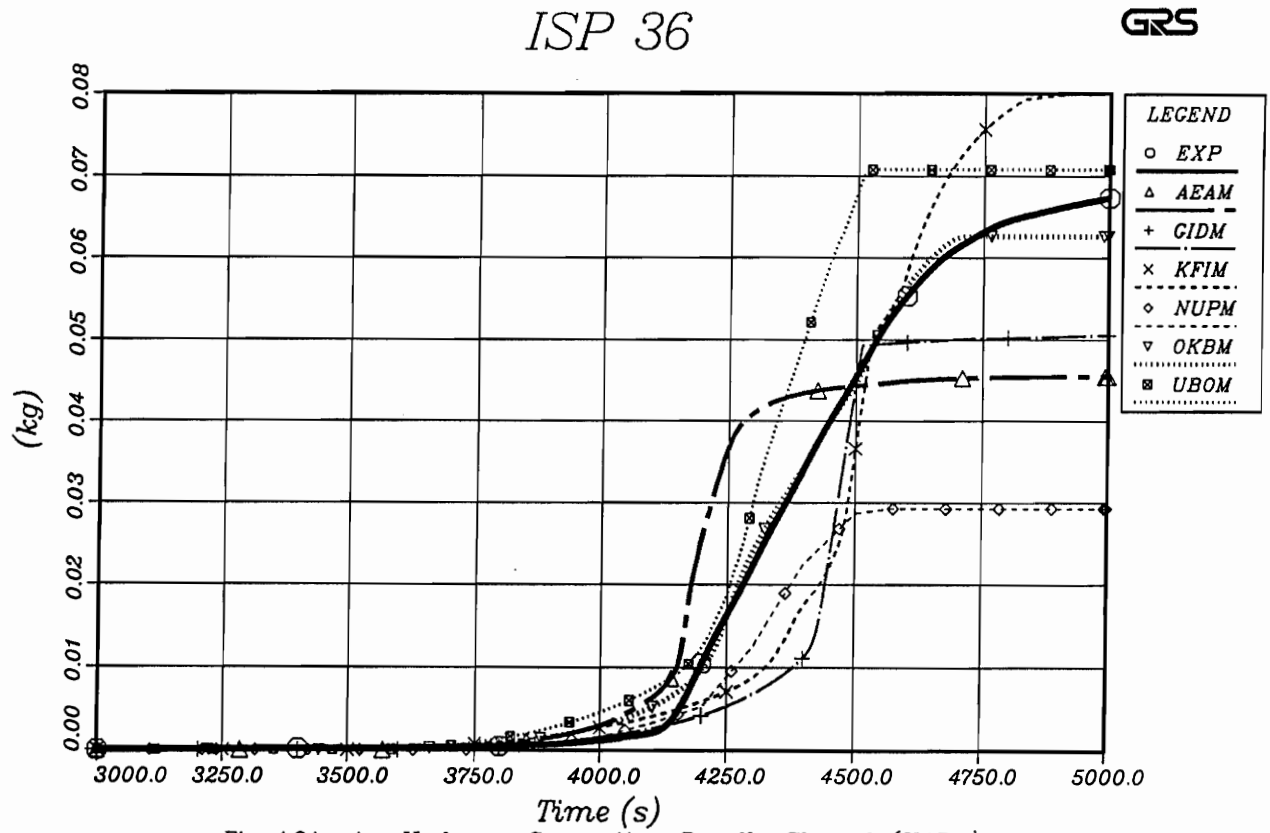

Fig. 4.24a: Acc. Hydrogen Generation, Bundle+Shroud (HABS)
Code: MELCOR

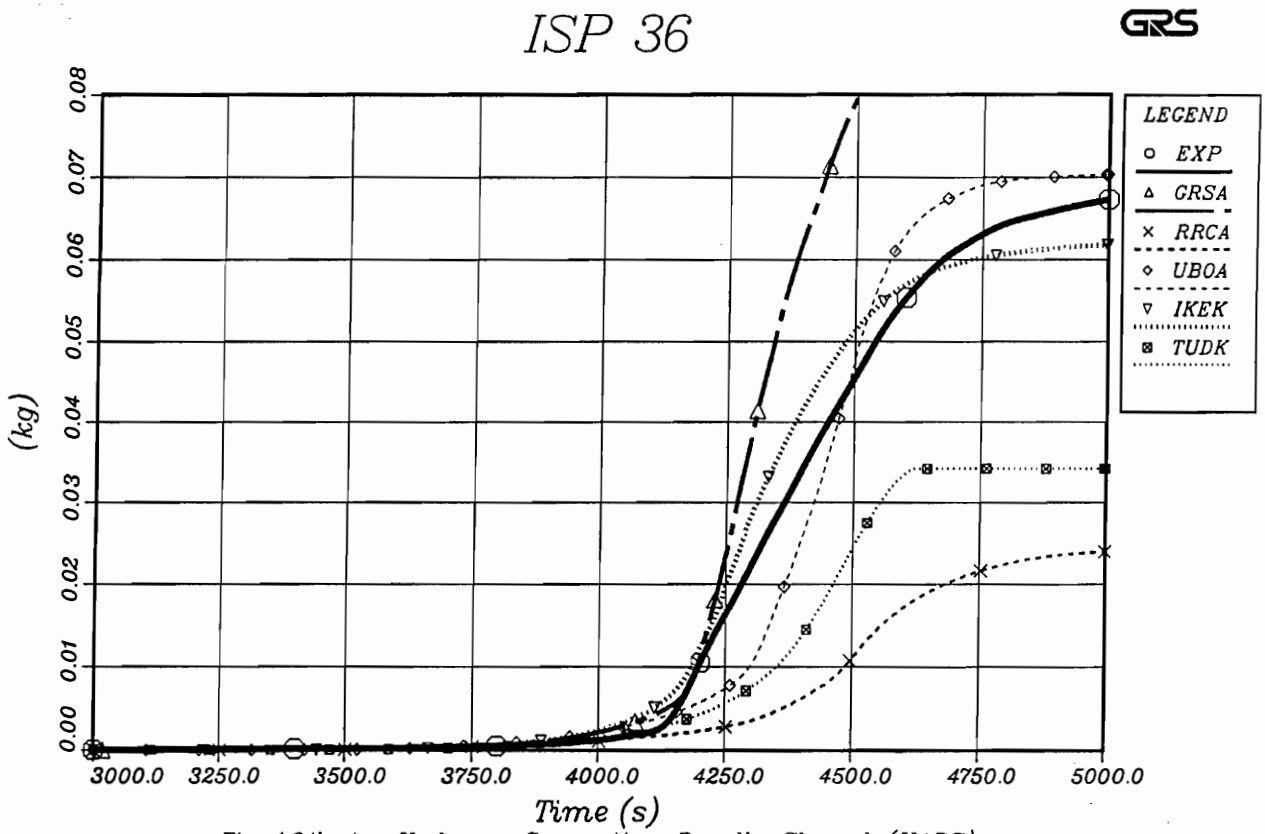

Fig. 4.24b: Acc. Hydrogen Generation, Bundle+Shroud (HABS)
Codes: ATHLET-CD, KESS III

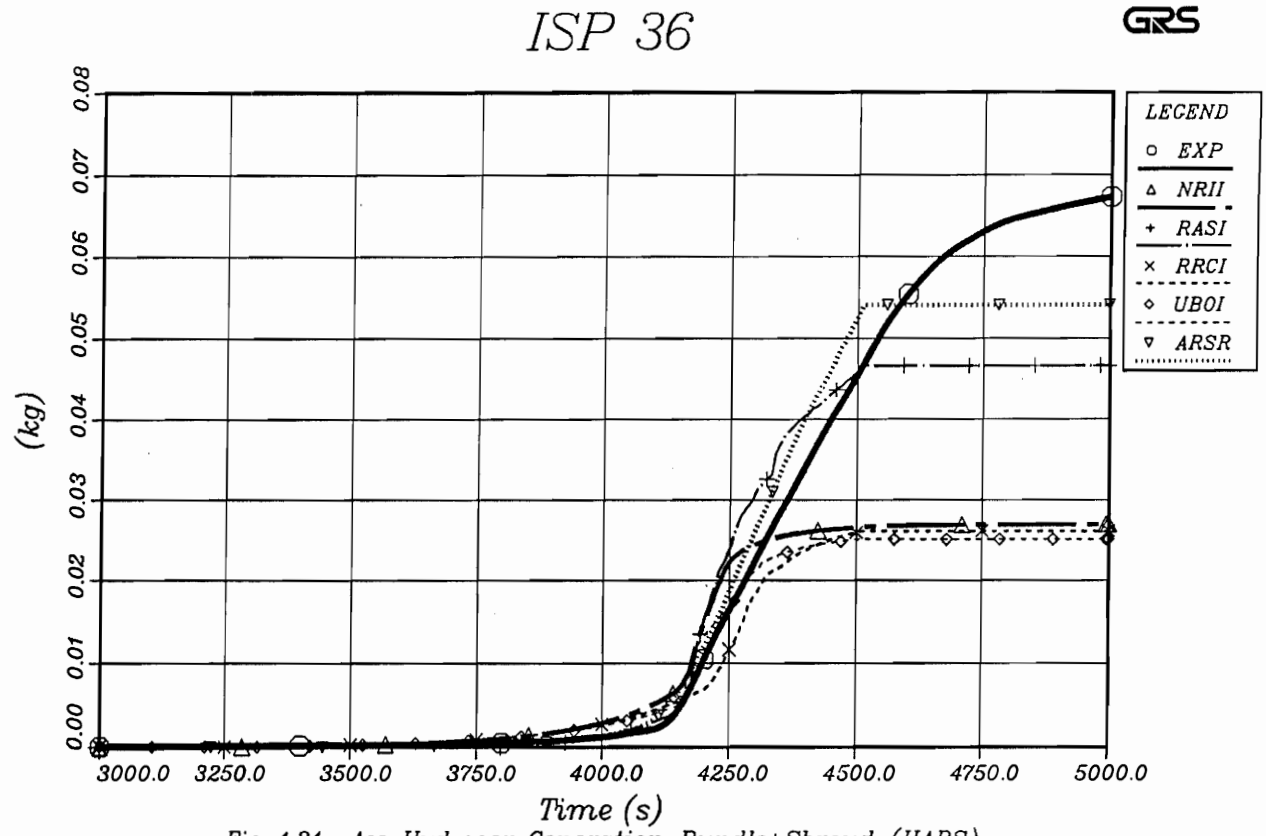

Fig. 4.24c: Acc. Hydrogen Generation, Bundle+Shroud (HABS)
Codes: ICARE2, RAPTA-SFD

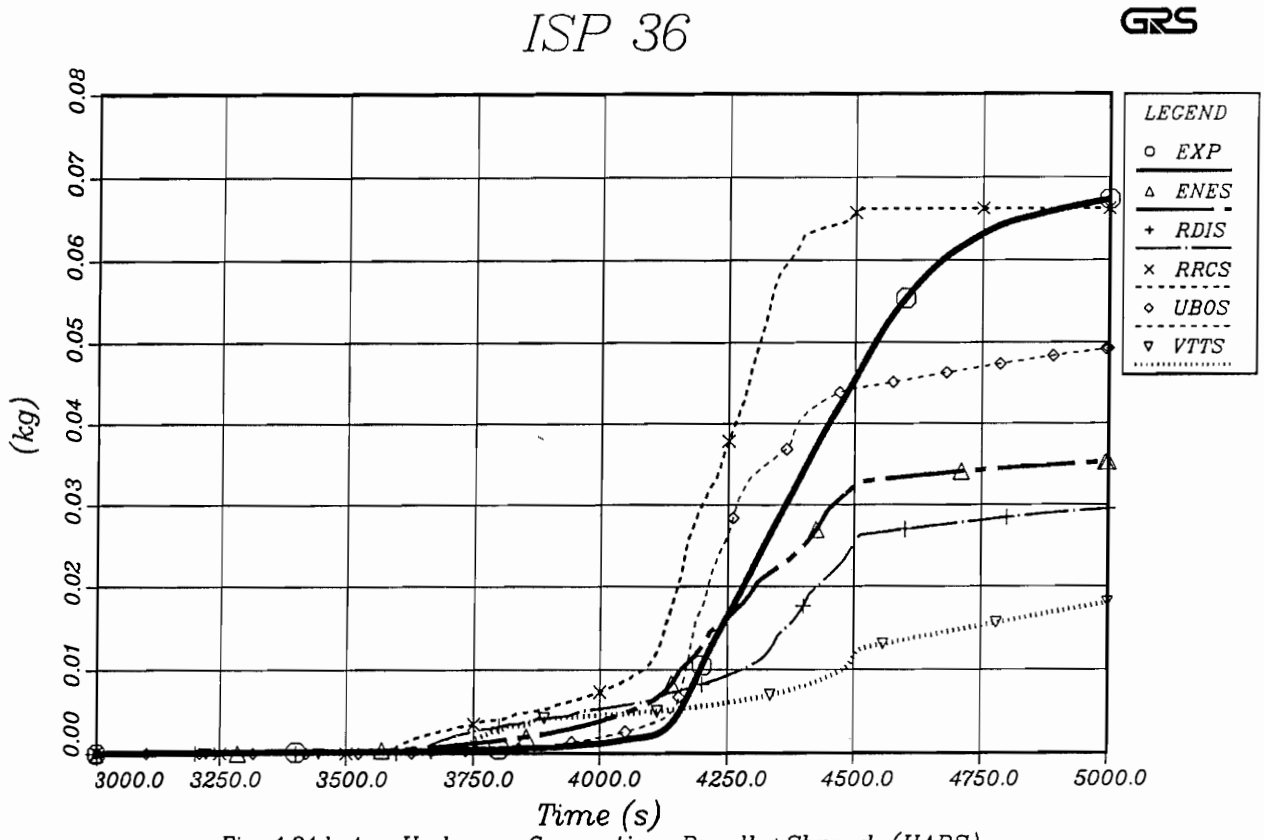

Fig. 4.24d: Acc. Hydrogen Generation, Bundle+Shroud (HABS)
Code: SCDAP/RELAP5

Gesellschaft für Anlagen- und Reaktorsicherheit (GRS) mbH

Schwertnergasse 1
50667 Köln
Telefon +49 221 2068-0
Telefax +49 221 2068-888

Forschungsinstitute
85748 Garching b. München
Telefon +49 89 32004-0
Telefax +49 89 32004-300

Kurfürstendamm 200
10719 Berlin
Telefon +49 30 88589-0
Telefax +49 30 88589-111

Theodor-Heuss-Straße 4
38122 Braunschweig
Telefon +49 531 8012-0
Telefax +49 531 8012-200

www.grs.de

ISBN 3-923875-81-9